THEORETICAL STUDIES OF NUCLEAR STRUCTURE IN VIEW OF EXOTIC NUCLEAR DECAYS

Thesis submitted to the University of Calicut
in partial fulfilment of the requirements
for the Degree of

DOCTOR OF PHILOSOPHY

IN PHYSICS

By

K.P. SANTHOSH

DEPARTMENT OF PHYSICS
UNIVERSITY OF CALICUT

2002

THEORETICAL STUDIES OF NUCLEAR STRUCTURE IN VIEW OF EXOTIC NUCLEAR DECAYS

Thesis submitted to the University of Calicut
in partial fulfilment of the requirements
for the Degree of

DOCTOR OF PHILOSOPHY

IN PHYSICS

By

K.P. SANTHOSH

DEPARTMENT OF PHYSICS
UNIVERSITY OF CALICUT

2002

DEDICATED

TO MY

TEACHERS

THEORETICAL STUDIES OF NUCLEAR STRUCTURE IN VIEW OF EXOTIC NUCLEAR DECAYS

Thesis submitted to the University of Calicut
in partial fulfilment of the requirements
for the Degree of

DOCTOR OF PHILOSOPHY

IN PHYSICS

By

K.P. SANTHOSH

DEPARTMENT OF PHYSICS
UNIVERSITY OF CALICUT

2002

DECLARATION

I hereby declare that this thesis entitled "**Theoretical studies of nuclear structure in view of exotic nuclear decays**" is a bonafide record of research work done by me and that no part of this thesis has been presented before for the award of any degree or diploma.

Calicut University

27th May 2002

K.P.SANTHOSH

THEORETICAL STUDIES OF NUCLEAR STRUCTURE IN VIEW OF EXOTIC NUCLEAR DECAYS

Thesis submitted to the University of Calicut
in partial fulfilment of the requirements
for the Degree of

DOCTOR OF PHILOSOPHY

IN PHYSICS

By

K.P. SANTHOSH

DEPARTMENT OF PHYSICS
UNIVERSITY OF CALICUT

2002

Dr.Antony Joseph
Department of Physics

University of Calicut
Dated May 2002

CERTIFICATE

This is to certify that this thesis entitled "**Theoretical studies of nuclear structure in view of exotic nuclear decays**" is a bonafide record of research work carried out by Sri. K.P.Santhosh under my supervision for the award of the Ph.D degree of University of Calicut and that no part of this thesis has been presented elsewhere for the award of any degree, diploma or other similar title.

Dr.Antony Joseph

THEORETICAL STUDIES OF NUCLEAR STRUCTURE IN VIEW OF EXOTIC NUCLEAR DECAYS

Thesis submitted to the University of Calicut
in partial fulfilment of the requirements
for the Degree of

DOCTOR OF PHILOSOPHY

IN PHYSICS

By

K.P. SANTHOSH

DEPARTMENT OF PHYSICS
UNIVERSITY OF CALICUT

2002

ACKNOWLEDGEMENT

It gives me great pleasure to express my sincere and profound gratitude to my esteemed guide Dr. Antony Joseph, Department of Physics, University of Calicut for suggesting this problem and for guiding me throughout the research work. His timely suggestions, support and encouragement made this work a reality.

I am deeply indebted to Prof. K Neelakandan, Head of the Department of Physics, University of Calicut for providing the necessary facilities and most generous encouragement.

I express my heartfelt thanks to Prof. K M Varier for going patiently through this thesis and also for the valuable discussion, suggestions and encouragement.

I owe my thanks to all members of the teaching and non-teaching staff and friends in the department for their help and cooperation.

I take this opportunity to thank Prof. R K Gupta, Punjab University, Chandigarh for his valuable suggestions and discussion when we met at Mumbai during the International Symposium on Nuclear Physics in December 2000 and Prof. S Shanmugam, Manonmanian Sundaranar University, Tirunelveli during DAE-BRNS Symposium on Nuclear Physics held at Kolkata in December 2001.

I feel it my responsibility to acknowledge the Management, Principal and Head of the Department of Physics, Payyanur College, Payyanur for deputing me to carry out and complete my research work.

I would like to express my sense of gratitude to the University Grants Commission, New Delhi for providing financial assistance in the form of fellowship under FIP (IX Plan).

Finally I express my gratitude and warmth of love to all my friends and members of my family who have inspired and supported me in this endeavour.

THEORETICAL STUDIES OF NUCLEAR STRUCTURE IN VIEW OF EXOTIC NUCLEAR DECAYS

Thesis submitted to the University of Calicut
in partial fulfilment of the requirements
for the Degree of

DOCTOR OF PHILOSOPHY

IN PHYSICS

By

K.P. SANTHOSH

DEPARTMENT OF PHYSICS
UNIVERSITY OF CALICUT

2002

CONTENTS

THEORETICAL STUDIES OF NUCLEAR STRUCTURE IN VIEW OF EXOTIC NUCLEAR DECAYS

Thesis submitted to the University of Calicut
in partial fulfilment of the requirements
for the Degree of

DOCTOR OF PHILOSOPHY

IN PHYSICS

By

K.P. SANTHOSH

DEPARTMENT OF PHYSICS
UNIVERSITY OF CALICUT

2002

CHAPTER 1

INTRODUCTION

The spontaneous decay of radioactive nuclei with the emission of clusters heavier than alpha particle, without being accompanied by neutron emission, is termed as exotic decay or cluster radioactivity. This rare, cold process is intermediate between alpha decay and spontaneous fission. The rare nature of this process stems from the fact that this process is masked by a large number of α decay events. In exotic decay the energy released as Q value is completely consumed by the kinetic energy alone of the two fragments.

The exotic decay can be treated as a case of strong asymmetric fission or an exotic process of cluster formation and tunneling through the barrier making many assaults on the barrier similar to α decay. So all theoretical attempts made so far originate either from Gamow theory of alpha decay or nuclear fission. Exotic decay was first predicted by Sandulescu et al [1] in 1980 based on the quantum mechanical fragmentation theory (QMFT). In chapter 2 we gave a brief description of QMFT and details of some theoretical models.

In the present study, we have developed a model to explain the exotic decay taking the Coulomb and proximity potential as the interacting barrier, the details of which are given in chapter 2 as the present model. The main objective in this study includes verification of the model by reproducing the available experimental data and the comparison of the present model with other models. As a part of this we have also studied the transition from cluster mode to fission mode.

A brief description of the experimental methods usually used in exotic decay studies and a short review of the experimentally observed modes of decay are given in chapter 3. In chapter 4, the present model is applied to experimentally observed decay modes and also to proton rich Xe to Gd parents in the trans-tin region emitting clusters ranging from α particle to sulphur. This region far from the β stability line can be produced in heavy ion induced reactions. These studies are extended to neutron rich Ba to Gd parents to examine the role of doubly magic ^{132}Sn daughter in these decays.

In chapter 5 an improved model incorporating ground state deformation of both parent and daughter, treating emitted cluster as sphere is given and the effect of deformation on half life time is studied in the case of experimentally observed decay modes.

In chapter 6 we studied fine structure (decay to various excited states of the daughter) for some decay modes and calculated the hindrance factor for the decay of ^{223}Ra by emitting ^{14}C cluster to various excited states of the daughter.

Within fission model, cluster formation probabilities are calculated for various clusters from some heavy nuclei and studied its variation with mass of the emitted cluster. We tried to find the transition point from the cluster mode to the fission mode in exotic decay. The details of these studies are given in chapter 7.

Exotic decay of superdeformed ^{76}Sr, ^{78}Sr and ^{80}Sr with the estimated qudrapole deformations $\beta_2 = 0.35$ to 0.44 in the ground state and decay of these nuclei produced as an excited compound system in heavy ion reaction are presented in chapter 8.

Exotic decay of 11 heavy nuclei with $Z \geq 100$ are studied with a view to look for some measurable modes of decay which in turn can lead to the production of some other new heavy or super heavy nuclei as daughter. Chapter 9 gives the details of this study.

Chapter 10 presents the summary of the present studies and the conclusions drawn there from.

THEORETICAL STUDIES OF NUCLEAR STRUCTURE IN VIEW OF EXOTIC NUCLEAR DECAYS

Thesis submitted to the University of Calicut
in partial fulfilment of the requirements
for the Degree of

DOCTOR OF PHILOSOPHY

IN PHYSICS

By

K.P. SANTHOSH

DEPARTMENT OF PHYSICS
UNIVERSITY OF CALICUT

2002

CHAPTER 2

THEORETICAL MODELS

Sandulescu et al [1] in 1980 first predicted exotic decay, the intermediate process between alpha decay and spontaneous fission on the basis of quantum mechanical fragmentation theory [2]. The first experimental evidence of this phenomena was observed by Rose and Jones [3] in 1984.There are mainly two approaches in explaining the exotic decay process: 1) the cluster model and 2) the fission model. In cluster model, the cluster is preformed in the parent nucleus before it penetrates the nuclear interacting barrier. In fission model the nucleus deforms continuously as it penetrates the nuclear barrier and reaches the scission configuration after running down the Coulomb barrier.

2.1 The Quantum Mechanical Fragmentation Theory

The Quantum Mechanical Fragmentation Theory (QMFT) is able to describe cold fusion, cold fission and exotic decay from a unified point of view [4,5,6,7]. The unifying result of this theory is the closed shell effects of one or both the reaction partners for fusion or that of the decay products for fission and exotic decay. This is achieved by treating the mass asymmetry and the length of the nucleus (or distance between the centres of fragments) as dynamical coordinates. The potential energy and dynamical

masses as functions of these variables were calculated with the asymmetric two center shell model (ATCSM), after minimising the total energy in the deformation of the fragments and the neck between them. The nuclear shape is defined [8] in terms of coordinates of relative separation R (or equivalently the length parameter $\lambda = L/R_0$ where L is the length of the nucleus and the R_0 the radius of an equivalent spherical nucleus), quadrapole deformations β_1 and β_2 of fragments, the necking-in parameter ε and the two dynamical collective coordinates of mass and charge asymmetries η and η_Z

$$\eta = \frac{A_1 - A_2}{A} \quad \text{and} \quad \eta_Z = \frac{Z_1 - Z_2}{Z} \tag{2.1}$$

where mass and charge of the parent are $A = A_1 + A_2$ and $Z = Z_1 + Z_2$ respectively. The collective Hamiltonian is

$$H = T(R, \beta_1, \beta_2, \eta, \eta_Z, \dot{R}, \dot{\beta}_1, \dot{\beta}_2, \dot{\eta}, \dot{\eta}_Z) + V(R, \beta_1, \beta_2, \eta, \eta_Z) \tag{2.2}$$

The potential V is obtained in the standard Strutinsky method [9,10] by using appropriate liquid drop model (LDM) and the single particle states of ATCSM giving the shell correction δU. The collective potential V minimized in β_1, β_2 and ε coordinates is $V(R, \eta, \eta_Z) = V_{LDM} + \delta U$ (2.3)

The mass parameter B_{ij} defining the kinetic part T in H, are the consistently calculated adiabatic cranking masses [11,12]. Assuming that the relative motion R is slow compared to the η and η_Z motions (this means that the potential is nearly independent of

R and hence R can be taken as a time independent parameter) and that the coupling between η and η_Z is weak, the Hamiltonian is quantised according to the prescription of Pauli [13] and Padolsky[14] to yield the stationary Schrodinger equation.

$$\{-\frac{\hbar^2}{2\sqrt{B_{\eta\eta}}}\frac{\partial}{\partial\eta}\frac{1}{\sqrt{B_{\eta\eta}}}\frac{\partial}{\partial\eta}+V(R,\eta)\}\Psi_R^{(\nu)}(\eta)=E_R^{(\nu)}\Psi_R^{(\nu)}(\eta) \tag{2.4}$$

Here $\Psi_R^{(\nu)}(\eta)$ are the vibrational states in the potential $V(\eta)$ and are counted by the quantum numbers $\nu=0,1,2....$ The ground state (ν=0) solution of equation (2.4) gives the probability $\left|\Psi_R^{(0)}(\eta)\right|^2$, which is proportional to the percentage mass distribution yield,

$$Y(A_2)=\left|\Psi_R^{(0)}(\eta)\right|^2\sqrt{B_{\eta\eta}(\eta)}\frac{200}{A} \tag{2.5}$$

The consequences of higher excited states $(\nu\neq 0)$ can be included through Boltzmann-like occupation function

$$\left|\Psi_R\right|^2=\sum_{\nu=0}^{\infty}\left|\Psi_R^{(\nu)}\right|^2\exp(-E_R^{(\nu)}/\theta) \tag{2.6}$$

with θ the nucleus temperature in MeV, is related to excitation energy as [15]

$$E^*=\frac{1}{9}A\theta^2-\theta \tag{2.7}$$

The excitation energy will damp the shell effect as [5]

$$V=V_{LDM}+\delta U\exp(-\frac{\theta^2}{\theta_0^2}) \tag{2.8}$$

The parameter θ_0=1.5 MeV is so chosen that the shell effect vanishes if $E^* \geq 60$ MeV [16]. Similarly mass parameter also varies with temperature but no usable prescription is available to date. A constant (averaged) mass is taken to mean a complete washing of shell effect in it [17].

2.2 Existing models

2.2.1 The fission models

2.2.1.1 Analytical Super Asymmetric Fission Model (ASAFM)

A numerical super asymmetric fission model (NSAFM) was developed by Poenaru et al [18,19,20] since 1979 by extending three variants of liquid drop model [21], finite range of nuclear forces model [22] and Yukawa plus exponential model [23] to system with charge asymmetry different from mass asymmetry and by using phenomological shell correction. Half lives computed within W K B approximation are time consuming. So an analytical relationship for half life [analytical super asymmetric fission model (ASAFM)] was developed [24] and extended to account for angular momentum and small excitation effects. In this model the potential barrier $E(R)$ for the overlapping region is approximated by a second order polynomial in R.

If time is expressed in seconds, energies in MeV and length in fermis, then the logarithm of the half life time for a system is given by

$$\log T = 0.43429(K_{ov} + K_s) - \log E_v - 20.8436 \tag{2.9}$$

here E_v is the zero point vibration energy given by

$$E_v = Q\,[0.056 + 0.039\exp[(4\text{-}A_2)/2.5]] \qquad \text{for } A_2 \geq 4 \tag{2.10}$$

The action integral K_{ov} corresponding to overlap region and K_s that for separated configuration are given by the following analytical expressions:

$$K_{ov} = 0.2196\left(E_b^0 A_1 A_2 / A\right)^{1/2}\left((b^2 - a^2)^{1/2} - \frac{a^2}{b}\ln\left(\frac{b + (b^2 - a^2)^{1/2}}{a}\right)\right) \tag{2.11}$$

$$K_s = 0.4392\left[\frac{Q' A_1 A_2}{A}\right]^{1/2} R_b \tau_{mc} \tag{2.12}$$

where $Q' = Q + E_v + E^*$, E^* being the fraction of the excitation energy concentrated in the collective mode leading to separation. The quantities a and b are defined below. The interaction energy E_i at the top of the barrier in the presence of the non-negligible angular momentum $\ell\hbar$ is given by

$$E_i = E_c + E_\ell = \frac{1.44 Z_1 Z_2}{R_t} + \frac{20.735\ell(\ell+1)A}{R_t^2 A_1 A_2} \tag{2.13}$$

The radii of parent, emitted cluster and daughter nuclei are given by $R_j = r_0 A_j^{1/3}$, where $j = 0,1,2$ and $r_0 = 1.2249$ fm. $R_i = R_0 - R_2$ is the initial separation distance, $R_t = R_1 + R_2$ is the touching separation distance and $E_b^0 = E_i - Q$ is the barrier height before correction. The outer turning point of W.K.B penetrability is given by

$$R_b = \frac{R_t E_c}{Q'}\left[\frac{1}{2}+\left[\frac{1}{4}+\frac{Q' E_\ell}{E_c^2}\right]^{1/2}\right] \tag{2.14}$$

$$a = b\left[\frac{Q'-Q}{E_b^0}\right]^{1/2} \; ; \; b = R_t - R_i \tag{2.15}$$

$$\tau_{mc} = (c+m-1)^{1/2}[r(c-r)+m]^{1/2} + \frac{c}{2}\left[\arcsin\frac{c-2r}{(c^2+4m)^{1/2}} - \arcsin\frac{c-2}{(c^2+4m)^{1/2}}\right]$$
$$+\sqrt{m}\ln\left[\frac{2\sqrt{m}[r(c-r)+m]^{1/2}+cr+2m}{r[2\sqrt{m}(c+m-1)^{1/2}+c+2m]}\right] \tag{2.16}$$

$$\text{where } r = \frac{R_t}{R_b}; \; m = \frac{r^2 E_\ell}{Q'} \; ; \; c = \frac{rE_c}{Q'} \tag{2.17}$$

2.2.1.2 Proximity potential model of Shi and Swiatecki

In this model [25], the deformation energy barrier for touching and for separated configuration consists of Coulomb repulsion between fragments and nuclear proximity potential of Blocki et al [26,27]. The deformation energy between the contact configuration and the configuration of the parent is approximated by a smooth power law interpolation. The explicit formula for deformation energy is as follows

$V(L) = -Q + Z_1 Z_2 e^2/r + V_P(z)$ for $L > L_C$ (2.18)

$V(L) = a\,(L-L_0)^{\nu}$ for $L_0 < L < L_C$ (2.19)

Here L is the major axis (overall length) of the configuration, L_0 is the diameter of the parent nucleus and L_C is the sum of fragment diameters. Q is the energy released. The parameters a and ν are determined by applying the smooth continuity condition on

potential at touching configuration. Also $r = L - C_1 - C_2$, the separation between fragment centers, z is the distance between the near surfaces of the fragments. V_P, the proximity potential is given by

$$V_P(z) = K\phi(z/b) \tag{2.20}$$

where $K = 4\pi \bar{R} \gamma b$ (2.21)

Here is ϕ is the universal nuclear proximity function [27] given as

$$\phi(\xi) \approx -4.41e^{-\xi / 0.7176} \qquad \text{for } \xi \geq 1.9475 \tag{2.22}$$

$$\phi(\xi) \approx -1.7817 + 0.9270\xi + 0.01696\xi^2 - 0.05148\xi^3 \qquad \text{for } 0 \leq \xi \leq 1.9475 \tag{2.23}$$

In the above $\xi = z / b$, b is the width (diffuseness) of nuclear surface ($b \approx 1$fm), γ is the specific nuclear surface tension given as [26]

$$\gamma = 0.9517 [1 - 1.7826 (N - Z)^2 / A^2] \qquad \text{MeV/fm}^2 \tag{2.24}$$

The reduced radius $\bar{R}$ is given by

$$\bar{R} = C_1C_2 / (C_1 + C_2) \tag{2.25}$$

where C_i is the central radii of the fragments given by

$$C_i \approx R_i - b^2 / R_i \tag{2.26}$$

The effective sharp radii R in terms of mass number A is given by [26]

$$R = 1.28A^{1/3} - 0.76 + 0.8A^{-1/3} \tag{2.27}$$

The Gamow penetrability factor G is given by

$$G = \exp\{\frac{2}{\hbar} \int_{z_0}^{z_{exit}} \sqrt{2M_r V}\, dz\} \tag{2.28}$$

here z_0 and z_{exit} are approximate zeros of the integrand and M_r is the effective mass. The absolute value of life time is given by

$$\tau = \tau_0 G \tag{2.29}$$

τ_0 is the pre exponential factor (frequency factor) taken to be 10^{-22} s for even A and 10^{-20} s for odd A parent nuclei [28]

2.2.1.3 Cubic Plus Yukawa plus exponential potential model (CYEM)

In this model [29] the potential for post scission region taken as a function of center of mass distance r of the fragments is given as

$$V(r) = Z_1 Z_2 e^2/r + V_n(r) - Q \tag{2.30}$$

Here Q is the energy released and $V_n(r)$ is the nuclear interaction energy [23] given as

$$V_n = -D\left[F + \frac{r - r_t}{a}\right]\frac{r_t}{r}\exp[(r_t - r)/a] \tag{2.31}$$

where $r_t = R_1 + R_2$ is the sum of sharp radii of fragments. The depth constant D is given by

$$D = \frac{4a^3 g_1 g_2 e^{r_t/a}[C_s(1)C_s(2)]^{1/2}}{r_0^2 r_t} \tag{2.32}$$

The constant F is given by

$$F = 4 + \frac{r_t}{a} - \frac{f_1}{g_1} - \frac{f_2}{g_2} \tag{2.33}$$

where

$$g_j = (R_j / a)\cosh(R_j / a) - \sinh(R_j / a) \tag{2.34}$$

$$f_j = (R_j / a)^2 \sinh(R_j / a) \tag{2.35}$$

$$C_s(j) = a_s(1 - K_s I_j^2) \tag{2.36}$$

$$I_j = (N_j - Z_j)/A_j \qquad (j = 1,2) \tag{2.37}$$

Here $r_0 = 1.16$ fm, $a = 0.68$ fm, $a_s = 21.13$ MeV and $K_s = 2.3$

For the overlap region the potential is approximated by a 3rd order polynomial as [29]

$$V(r) = -E_v + [V(r_t) + E_v]\left[S_1\left[\frac{r - r_i}{r_t - r_i}\right]^2 - S_2\left[\frac{r - r_i}{r_t - r_i}\right]^3\right] \tag{2.38}$$

The zero point vibration energy E_v is given by [30]

$$E_v = \frac{\pi\hbar}{2}\frac{(2Q/\mu)^{1/2}}{(C_1 + C_2)} \tag{2.39}$$

Here μ is the reduced mass. The central radii of fragments C_1 and C_2 are given by

$$C_i = 1.18A_i^{1/3} - 0.48 \qquad (i = 1,2) \tag{2.40}$$

The half life time of the system is given by the formula [31]

$$T = \frac{1.4333x10^{-21}}{E_v}[1 + \exp(K)] \tag{2.41}$$

$$\text{Where } K = \frac{2}{\hbar}\int_{r_a}^{r_t}[2B_r(r)V(r)]^{1/2}dr + \frac{2}{\hbar}\int_{r_t}^{r_b}[2B_r(r)V(r)]^{1/2}dr \tag{2.42}$$

The limits r_a and r_b are two approximate zeros of the integrand and the effective mass $B_r(r)$ is taken to be deformation dependent [32].

2.2.2 The cluster models

2.2.2.1 Microscopic model of Blendowske et al

In this model [33,34] the potential $U(R)$ used is the sum of semi empirical heavy ion potential, Coulomb potential and centrifugal potential given as

$$U(R) = V(R) + V_{Coul}(R) + V_L(R) \tag{2.43}$$

The Coulomb potential is $Z_1 Z_2 e^2 / r$ and centrifugal potential $V_L = \hbar^2 L(L+1)/2M$ where L is the angular momentum and M is the reduced mass. The semi empirical heavy ion potential [35] is given as

$$V(R) = -(50MeV/fm)\frac{R_1 R_2}{R_1 + R_2}\exp\{-(R - R_1 - R_2)/a\} \tag{2.44}$$

$$\text{with } R_j = 1.233A_j^{1/3} - 0.978A_j^{-1/3} fm \qquad (j = 1,2); a = 0.63 fm \tag{2.45}$$

The decay constant λ_0 is calculated in WKB approximation as

$$\lambda_0 = (\nu/2R_i)P \quad ; \; P = \exp\{-2\int_{R_i}^{R_o} dR[(2M/\hbar^2)(U(R) - Q)]^{1/2}\} \tag{2.46}$$

here Q is the Q value of the reaction. R_i and R_o are inner and outer turning points where $U(R) = Q$. For pre factor $(\nu/2R_i)$ Blendowske et al [33] assumed a kinetic energy $\frac{1}{2}Mv^2$ inside the barrier of 10^2 MeV for alpha particle and a scaled value

$10^2\left(\frac{14}{4}\right)$ MeV for ^{14}C cluster. In the microscopic approach the decay constant λ is given as the product

$$\lambda=\lambda_0 S \tag{2.47}$$

The spectroscopic factor S is the probability of the cluster to be preformed in the parent nuclei and is given by the overlap of nucleon states in the cluster with those of the parent nucleus [33].

2.2.2.2 Preformed cluster model (PCM)

This model [36] consists of a two steps mechanism 1) cluster formation 2) tunneling of confining nuclear interaction barrier. If P_0 is the cluster formation probability (in ground state), P the barrier penetration probability and ν the assault frequency, then decay constant λ and half life time $T_{1/2}$ are given as

$$\lambda = P_0 \nu P \tag{2.48}$$

$$T_{1/2} = \ln 2/\lambda \tag{2.49}$$

Introducing dynamical collective coordinates of mass and charge asymmetries η and η_z

$$\eta = \frac{A_1 - A_2}{A} \quad ; \eta_z = \frac{Z_1 - Z_2}{Z} \tag{2.50}$$

the quantum mechanical probability of finding fragments A_1 and A_2 (with fixed charges Z_1 and Z_2) at a relative separation R is given by the solution of the following stationary Schrodinger equation in η

$$\left[-\frac{\hbar^2}{2\sqrt{B_{\eta\eta}}}\frac{\partial}{\partial\eta}\frac{1}{\sqrt{B_{\eta\eta}}}\frac{\partial}{\partial\eta}+V(\eta,\eta_z,R)\right]\Psi(\eta)=E_{g.s}\Psi(\eta) \tag{2.51}$$

here $V(\eta,\eta_z,R)$ is the collective interaction potential energy and $B_{\eta\eta}$ is the mass parameter [37]. On proper scaling and normalization of above equation the cluster formation probability in ground state is

$$P_0(A_2)=|\Psi(\eta)|^2\sqrt{B_{\eta\eta}}\frac{2}{A} \tag{2.52}$$

The collective interaction energy is taken as the sum of experimental binding energies, the Coulomb and the nuclear proximity potential.

$$V(\eta,\eta_z,R)=-\sum_{i=1}^{2}B_i(A_i,Z_i)+\frac{Z_1Z_2e^2}{R}+V_p \tag{2.53}$$

The proximity potential V_p is given as [26]

$$V_p=4\pi\gamma b\frac{C_1C_2}{C_1+C_2}\phi\left(\frac{z}{b}\right) \tag{2.54}$$

With the nuclear surface tension coefficient

$$\gamma = 0.9517[1 - 1.7826 (N - Z)^2 / A^2] \quad MeV/fm^2 \tag{2.55}$$

ϕ, the universal proximity potential of pocket formula of Blocki et al [26]

$$\phi(\zeta) = -(1/2)(\zeta-2.54)^2-0.0852(\zeta-2.54)^3 \qquad \text{for } \zeta \le 1.2511 \tag{2.56}$$

$$\phi(\zeta) = -3.437\exp(-\zeta/0.75) \qquad \text{for } \zeta \ge 1.2511 \tag{2.57}$$

with $\zeta = (C-C_1-C_2)/b$ where width (diffuseness) of nuclear surface b $\approx$1 and Sissmann central radius C_i of fragments related to sharp radii R_i is $C_i \approx R_i - \frac{b^2}{R_i}$. The semi empirical formula R_i in terms of mass number A_i is given as

$$R_i = 1.28A_i^{1/3} - 0.76 + 0.8A_i^{-1/3} \tag{2.58}$$

The assault frequency ν is given as $\nu = (2E_2/\mu)^{1/2}/R_0$. where R_0 is the radius of parent nucleus, E_2 the kinetic energy of the emitted cluster and μ the reduced mass. The tunneling probability P consists of three contributions: 1) P_i, the penetrability from touching configuration R_t to R_i, here R_i is given by $V(R_i) = V(R_t)$ 2) W_i, the deexcitation probability at R_i and 3) the penetrability P_b from R_i to R_b. Here R_b is given by $V(R_b) = Q$.

Then tunneling probability P is given by $P = P_i W_i P_b$ (2.59)

According to Greiner and Scheid [38] the deexcitation probability vary exponentially with excitation energy, $W_i = \exp(-bE_i)$. For clusters heavier than alpha particle b = 0 ie W_i=1.

The penetrability P_i and P_b are defined as

$$P_i = \exp\{-\frac{2}{\hbar}\int_{R_t}^{R_i}[2\mu(V - V(R_i))]^{1/2}\,dR\} \tag{2.60}$$

$$P_b = \exp\{-\frac{2}{\hbar}\int_{R_i}^{R_b}[2\mu(V-Q)]^{1/2}dR\} \tag{2.61}$$

These integrals can be solved analytically [36]

2.2.2.3 Cluster model of Buck et al

The parent nucleus is viewed as consisting of a daughter nucleus core (mass A_1) and a preformed cluster (mass A_2). This model [39,40] describes the interaction between them in terms of a simple local potential $V_N(r)$ that may be obtained from a double folding integral involving their respective densities $\rho_1(r_1)$ and $\rho_2(r_2)$ and an effective nucleon-nucleon potential $U(|r_1-r_2|)$. Hence

$$V_N(r) = \iint \rho_1(r_1)\rho_2(r_2)U(|r+r_2-r_1|)d^3r_1 d^3r_2 \tag{2.62}$$

This may be approximated by a simple potential of the form

$$V_N(r) = \frac{-V_0[1+\cosh(R/a)]}{[\cosh(r/a)+\cosh(R/a)]} \tag{2.63}$$

of depth V_0 and nonzero diffuseness a. The radius R is given as

$$R = 1.04(A_1^{2/3}+A_2^{2/3})^{1/2} \tag{2.64}$$

The potential acting between cluster and core is given by

$$V(r) = V_N(r)+V_C(r)+\frac{\hbar^2}{2\mu r^2}\left(L+\frac{1}{2}\right)^2 \tag{2.65}$$

Here μ the reduced mass, $V_C(r)$ is the Coulomb potential and 3rd term represent the Langer modified centrifugal barrier. The classical turning points (r_1, r_2 and r_3 in the order of increasing distance from origin) are found by numerical solution of the equation $V(r) = Q$, where Q is the Q value of the reaction. If L is very small r_1 is close to zero and if nuclear term $V_N(r)$ is neglected in the asymptotic region, r_3 can be found by solving the resulting quadratic equation.

The decay width Γ can be calculated using the procedure of Gurvitz et al [41]

$$\Gamma = PF\frac{\hbar^2}{4\mu}\exp\left(-2\int_{r_2}^{r_3}K(r)dr\right) \tag{2.66}$$

where P is the preformation probability and semi classical wave number K(r) is given by

$$K(r) = \left[\frac{2\mu}{\hbar^2}|Q - V(r)|\right]^{1/2} \tag{2.67}$$

F is the semi classical bound state normalization factor given by

$$F\int_{r_1}^{r_2}\frac{1}{K(r)}\cos^2\left[\int_{r_1}^{r}K(r')dr' - \frac{\pi}{4}\right]dr = 1 \tag{2.68}$$

The half life time $T_{1/2}$ in terms of width Γ can be calculated using the relation

$$T_{1/2} = \hbar \ln 2/\Gamma \tag{2.69}$$

2.2.2.4 Double folded Michigan-three-Yukawa potential model

Sandulescu et al [42] studied heavy ion emission using double folded Michigan-three-Yukawa potential (M3Y) potential [43] by including deformation effect of the fragments. The nuclear plus Coulomb interaction between the fragments is given by M3Y potential as

$$V_{M3Y}(R) = \int dr_1 dr_2 \rho_1(r_1)\rho_2(r_2)v(r_{12}) \tag{2.70}$$

which contains the corresponding nucleon-nucleon interaction [44] as

$$v(r_{12}) = v_{00}(r_{12}) + \bar{J}_{00}\,\delta(r_{12}) + v_{01}(r_{12})\tau_1.\tau_2 \tag{2.71}$$

the central component of M3Y force in eqn (2.71) is

$$v_{00}(r) = \left[7999\frac{e^{-4r}}{4r} - 2134\frac{e^{-2.5r}}{2.5r}\right] \text{ MeV} \tag{2.72}$$

and isospin part has the form

$$v_{01}(r) = \left[-4885.5\frac{e^{-4r}}{4r} + 1175.5\frac{e^{-2.5r}}{2.5r}\right] \text{ MeV} \tag{2.73}$$

The second term in eqn (2.71) approximates the single nucleon exchange effects through a zero pseudopotential, $\bar{J}_{00} = -262$ MeV fm^3. The spin-spin v_{10} and spin-isospin v_{11} components are disregarded since their final contributions tend to be small [43].

The two final nuclei are viewed as coaxial spheroids ("nose to nose" configuration) with nuclear density

$$\rho(r) = \rho_0 \left\{ 1 + \exp \frac{1}{a} \left(r - \frac{R}{c} \left[1 + \beta_2 Y_2^0(\cos\theta) \right] \right) \right\}^{-1} \tag{2.74}$$

with constant ρ_0 fixed by normalizing the proton and neutron densities to proton number Z and neutron number N respectively. Here β_2 is the quadrapole deformation and c is the usual constant which ensure volume conservation condition

$$\int d^3r = \frac{4\pi}{3} R^3 \tag{2.75}$$

from which it follows

$$c(\beta_2) = \left[1 + \frac{3}{4\pi} \beta_2^2 + \frac{1}{14\pi} \sqrt{\frac{5}{4\pi}} \beta_2^3 \right]^{1/3} \tag{2.76}$$

The two parameters of fermi density are chosen as $R = 0.95A^{1/3}$ fm and a = 0.67 fm for light clusters and $R = 1.19A^{1/3}$ fm and a = 0.63 fm for heavy daughter nuclei.

The penetrability P through the double folded potential barrier is given as

$$P = \exp\left\{ -\frac{2}{\hbar} \int_{R_i}^{R_0} \sqrt{2\mu[V(R) - Q]} dR \right\} \tag{2.77}$$

where R is the distance between the fragment mass centers, μ is the reduced mass, R_i and R_0 are the inner and outer turning points defined by

$$V(R_i) = V(R_0) = Q \tag{2.78}$$

The half life time is given by $T_{1/2} = \frac{\ln 2}{\nu P_0 P}$ (2.79)

Here ν is the collision frequency and P_0 is the preformation factor.

2.3 The Present model

For the touching and for the separated configuration of the cluster and daughter we took the Coulomb and proximity potential as the interacting barrier. From the touching configuration and down to the parent central radius (overlap region), we use simple power law interpolation as done by Shi and Swiatecki [25]. Figures 2.1 and 2.2 represent potential energy barrier for the emission of ^{4}He and ^{12}C from ^{120}Nd isotope. Inclusion of the proximity potential reduces the height of the barrier, which closely agrees with experiments. Table 2.1 gives the comparison of the barrier height calculated by us taking proximity potential (present) with 1) those obtained by liquid drop model (LDM) [21] 2) by Cubic and Yukawa plus exponential potential model (CYEM) [29] and 3) experimental values obtained by the relation [18]

$$V(r) = 10.107 + 0.1021 Z_1 Z_2 - Q \qquad (2.80)$$

It is clear that LDM overestimates the barrier by about 10 MeV but as in the case of CYEM, the present model is able to reproduce experimental values, which are uncertain by about 2 MeV [45].

The proximity potential was first used by Shi and Swiatecki in an empirical manner and extensively used over a decade now by Gupta and collaborators [36] in the preformed cluster model (PCM), which is based on the "pocket formula" of Blocki et al [26]. In the present model we use another formulation of the proximity potential [27]. We

have taken the cluster formation probability as unity for all the clusters irrespective of their masses. So the present model differs from the PCM by a factor P_0, the cluster formation probability. But we have included the contribution of the overlap region in the barrier penetrability calculation. In the present model assault frequency is calculated for each parent-cluster combination which is associated with zero point vibration energy, but in Shi and Swiatecki's model it is taken as 10^{22} for even A and 10^{20} for odd A parent. For the zero point vibration energy we use semi empirical formula of Poenaru et al [24].

2.3.1 Details of the model

The interacting barrier for a parent exhibiting exotic decay is given by

$$V = Z_1 Z_2 e^2 / r + V_p(z) \qquad \text{for } z > 0 \qquad (2.81)$$

here Z_1 and Z_2 are atomic numbers of daughter and emitted cluster, r is the distance between the fragment centers, z is the distance between the near surfaces of the fragments and V_p is the proximity potential given by [26]

$$V_p(z) = 4\pi\gamma b \frac{C_1 C_2}{C_1 + C_2} \phi(\frac{z}{b}) \qquad (2.82)$$

with the nuclear surface tension coefficient,

$$\gamma = 0.9517[1 - 1.7826(N - Z)^2 / A^2] \quad \text{MeV/fm}^2 \qquad (2.83)$$

Here N, Z and A represent the neutron, proton and mass numbers of the parent respectively.

ϕ, the universal proximity potential is given as [27]

$\phi(\varepsilon) = -4.41e^{-\varepsilon/0.7176}$ for $\varepsilon \geq 1.9475$ (2.84)

$\phi(\varepsilon) = -1.7817 + 0.9270\varepsilon + 0.01696\varepsilon^2 - 0.05148\varepsilon^3$ for $0 \leq \varepsilon \leq 1.9475$ (2.85)

with $\varepsilon = z/b$, where the width (diffuseness) of nuclear surface $b \approx 1$ and Siissmann central radii C_i related to sharp radii R_i is $C_i = R_i - \frac{b^2}{R_i}$. For R_i we use the semi empirical formula in terms of the mass number A_i as [26]

$$R_i = 1.28A_i^{1/3} - 0.76 + 0.8A_i^{-1/3} \quad (2.86)$$

The barrier penetrability P is given as

$$P = \exp\{-\frac{2}{\hbar}\int_{\varepsilon_i}^{\varepsilon_f}\sqrt{2\mu(V-Q)}dz\} \quad (2.87)$$

The mass parameter is replaced by the reduced mass $\mu = mA_1A_2/A$ where m is the nucleon mass and A_1 and A_2 represent the mass numbers of the daughter and the emitted cluster respectively. The inner and the outer turning points ε_i and ε_f are defined as $V(\varepsilon_i) = V(\varepsilon_f) = Q$, where Q is the energy released.

The half life time is given by $T_{1/2} = \ln 2/\lambda = \ln 2/\nu P$ (2.88)

Here λ is the decay constant and the assault frequency, $\nu = 2E_v/h$. The empirical zero point vibration energy E_v is given as [24]

$E_v = Q\,[0.056 + 0.039\exp[(4-A_2)/2.5]]$ for $A_2 \geq 4$ (2.89)

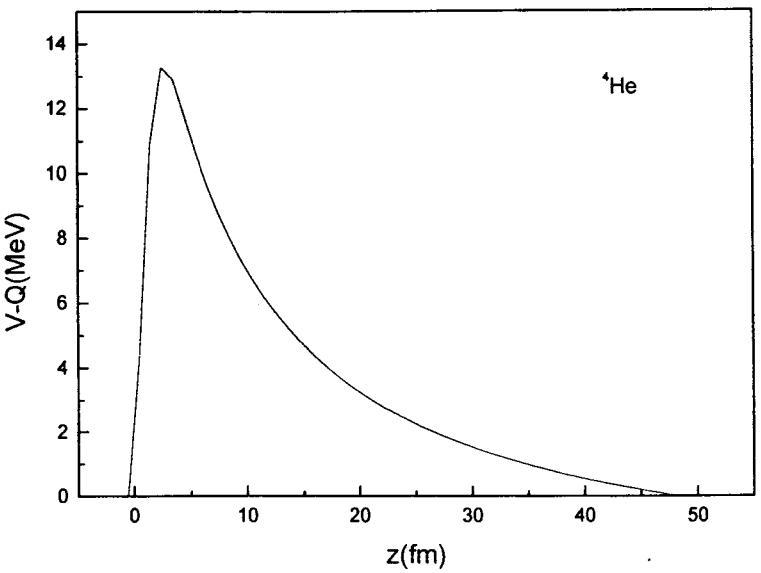

Fig. 2.1 Potential energy barrier for the emission of ^{4}He from ^{120}Nd isotope.

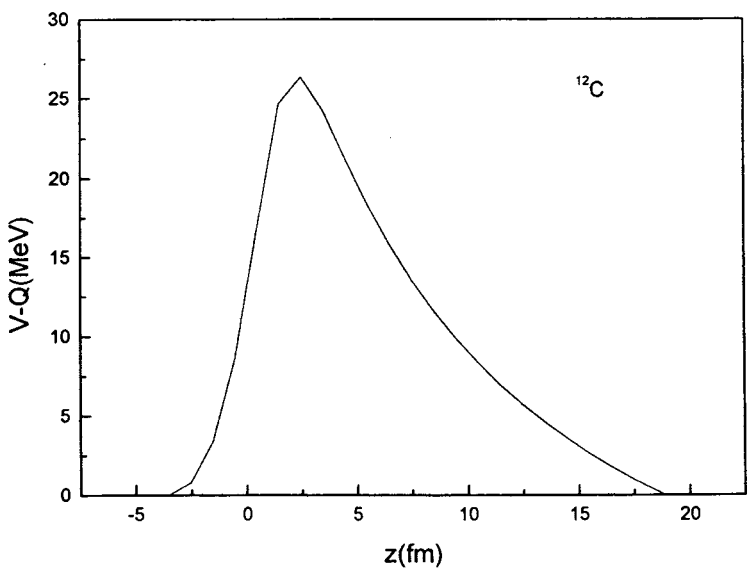

Fig. 2.2 Potential energy barrier for the emission of ^{12}C from ^{120}Nd isotope.

Table 2.1. Comparison of interacting barrier height calculated by the present model with that by other models and with experimental values.

Parent nuclei	Emitted cluster	Daughter nuclei	Q value (MeV)	Barrier height (MeV) LDM	CYEM	Present	Expt
^{221}Fr	^{14}C	^{207}Tl	31.28	37.3448	26.6349	26.7625	28.448
^{221}Ra		^{207}Pb	32.39	37.0821	26.2740	26.3948	28.270
^{222}Ra		^{208}Pb	33.05	36.3428	25.5570	25.6768	27.290
^{223}Ra		^{209}Pb	31.85	37.4639	26.7025	26.8193	28.490
^{224}Ra		^{210}Pb	30.53	38.7056	27.9625	28.0823	29.810
^{225}Ac		^{211}Bi	30.48	39.5209	28.7198	28.8144	30.473
^{226}Ra		^{212}Pb	28.21	40.8700	30.1728	30.2898	32.130
^{231}Pa	^{24}Ne	^{207}Tl	60.42	47.7894	33.6222	33.1935	32.388
^{232}U		^{208}Pb	62.31	47.1171	32.8608	32.4000	31.519
^{233}U		^{209}Pb	60.50	48.8095	34.5784	34.1189	33.329

THEORETICAL STUDIES OF NUCLEAR STRUCTURE IN VIEW OF EXOTIC NUCLEAR DECAYS

Thesis submitted to the University of Calicut
in partial fulfilment of the requirements
for the Degree of

DOCTOR OF PHILOSOPHY

IN PHYSICS

By

K.P. SANTHOSH

DEPARTMENT OF PHYSICS
UNIVERSITY OF CALICUT

2002

CHAPTER 3

EXPERIMENTAL STUDIES ON EXOTIC DECAY - A SHORT REVIEW

3.1 Experimental techniques

Rose and Jones [3] in their famous experiment using ΔE-E surface barrier silicon detectors were able to detect a few carbon events within α particle background about 10^9 times higher. They used relatively weak ^{227}Ac source containing ^{223}Ra in secular equilibrium. Gales et al [46] in their experiment used a super conducting magnetic solenoid spectrometer to suppress the intense α background. This allowed them to use intense ^{227}Ac source 60 times stronger than the one used by Rose and Jones. Kutschera et al [47] used an Enge split pole magnetic spectrograph to suppress the intense α radiation and to identify ^{14}C particle. The spectrograph was calibrated with tandem accelerated beam of ^{14}C, ^{13}C and ^{12}C.

To suppress α particle background and to increase the overall detection efficiency, solid-state nuclear track detectors (SSNTD) are now widely used which is the most sensitive technique to detect the rare decay mode, the exotic decay. Price et al [48] demonstrated that polycarbonate track detecting foils like Rodyne-P are well-suited detectors for the study of ^{14}C emission radioactivity even for ^{14}C/α branching ratio below

10^{-10}. The energy of the fragments recorded was determined via a calibrated range energy relation [49]. It is also possible to identify the nuclear charge Z by observing the ratio of etching rate along the track to the general etching rate V_t/V_g as function of the residual range [50]. The branching ratio of cluster emission with respect to alpha decay, B can be calculated as [51]

$$\rho_{cluster}(> R_{\min}) = j_\alpha(> E_{\min})|At.\Omega|4\pi B/\eta \qquad (3.1)$$

where $\rho_{cluster}(> R_{\min})$ is the density of track formed by the cluster, $j_\alpha(> E_{\min})$ is the alpha intensity, A is the source area, t is the exposure time, Ω is the solid angle and η is the detection efficiency.

Using similar plastic track detectors Barwick et al [52] detected ^{24}Ne emission from ^{232}U. In later experiments plastic detectors are replaced by phosphate glass detectors, which have better discrimination against α particle. This led to the detection of ^{20}O, ^{23}F, ^{30}Mg, and ^{32,34}Si in addition to ^{24,26}Ne. Phosphate glass BPI is more sensitive to ^{14}C, for Ne and Mg better choice would be PSK50 and for Si, LG750 glass would be more sensitive. Phosphate glass detectors are ideally suited for the detection of both heavy clusters and spontaneous fission tracks. It has now become possible to measure in the same experiment the spontaneous fission probability simultaneously with exotic decay probability [53,54].

SSNTDs are not suited for fine structure experiments where better energy resolution is required. Brillard et al [55] and Hussonnois et al [56] in their fine structure experiment used magnetic spectrometer SOLENO to focus emitted ^{14}C clusters on a single Si detector. This resulted in a high quality energy spectrum.

The decaying parent nuclei may either be a member of natural radioactive series or produced artificially (on line or off line production). ^{14}C from ^{222}Ra, ^{18}O from ^{230}U, ^{34}Si from ^{242}Cm are examples for off line production while ^{14}C from ^{221}Ra, ^{221}Fr, ^{223}Ra, ^{225}Ac performed at Isolde and ^{12}C decay of ^{114}Ba at GSI (Germany) are examples for on line production [57].

3.2 Experimentally observed decay modes

Altogether about 24 modes of exotic decay from 18 parent nuclei emitting clusters ranging from carbon to silicon have so far been confirmed and reported in the literature. The upper limit for decay rate for 16 modes were measured and one case of fine structure in the energy spectrum of ^{14}C clusters from ^{223}Ra was found. The heaviest cluster so far measured is ^{34}Si [58,59,60]. ^{14}C is the only cluster for which quite a few cases from both odd and even parent have been measured. ^{23}F is the only example for odd A cluster measured with single event using an array of $375cm^2$ of BPI plates in 2π geometry by Berkely –Livermore -Milano collaboration [61]. As for the multiple branching ratio, so far only three nuclei (^{231}Pa, ^{234}U and ^{238}Pu) are found to decay with the emission of two

heavy clusters other than α particle [53,61,62] but none with more than two.^{234}U was the first nuclide for which 4 hadronic decay modes (α, Ne, Mg and spontaneous fission) have been measured [63,64]. ^{238}Pu was the other nuclei for which 4 hadronic decay modes (α, Mg, Si and spontaneous fission) have been measured [62].

THEORETICAL STUDIES OF NUCLEAR STRUCTURE IN VIEW OF EXOTIC NUCLEAR DECAYS

Thesis submitted to the University of Calicut
in partial fulfilment of the requirements
for the Degree of

DOCTOR OF PHILOSOPHY

IN PHYSICS

By

K.P. SANTHOSH

DEPARTMENT OF PHYSICS
UNIVERSITY OF CALICUT

2002

CHAPTER 4

STUDIES ON EXOTIC DECAY

4.1 Verification of the present model with experimental data

Taking Coulomb and proximity potentials as the interacting barrier for post scission region we computed logarithm of half life time and other characteristics for the experimentally observed decay modes of parents in the trans-lead region and also of Ba isotopes which belongs to trans-tin region. The predicted half life time values are compared with the experimental result and is given in Table 4.1. Comparison of the predicted and the experimental half lives are also shown graphically in Figure 4.1. Using the present model we have calculated α decay half lives for parent nuclei from which exotic decay are observed. Fig 4.2 gives comparison of calculated α half lives with experimental value taken from [65].

The branching ratio of exotic decay with respect to alpha decay is given by

$$\text{Branching ratio, } B = \frac{\lambda_{cluster}}{\lambda_{alpha}} = \frac{T_{1/2}^{alpha}}{T_{1/2}^{cluster}} \tag{4.1}$$

Fig 4.3 gives the comparison of calculated branching ratio with experimental value. The centrifugal term $V_\ell = \frac{\hbar^2 \ell(\ell+1)}{2\mu r^2}$ is not considered for our calculation since ℓ values involved are small ($\approx 5\hbar$) and its contribution to half life time are shown to be small [24,30].

Table 4.1. Logarithm of predicted half life time and other characteristics for experimentally observed decay modes.

Parent nuclei	Daughter nuclei	Emitted cluster	Q value (MeV)	Penetrability P	Decay constant λ	$\log_{10}(T_{1/2})$ Present	Expt	Ref
^{112}Ba	^{100}Sn	^{12}C	21.46	1.92605E-25	1.15120E-04	3.78	3.75	[66]
^{114}Ba	^{102}Sn		20.75	8.04016E-27	4.64650E-06	5.17	4.23	[66]
^{221}Fr	^{207}Tl	^{14}C	31.28	1.00756E-35	8.64424E-15	13.90	14.52	[67]
^{221}Ra	^{207}Pb		32.39	2.06186E-34	1.83172E-13	12.58	13.39	[67]
^{222}Ra	^{208}Pb		33.05	6.41678E-33	5.81670E-12	11.08	11.01	[48]
^{223}Ra	^{209}Pb		31.85	1.61224E-35	1.40840E-14	13.69	15.04	[68]
^{224}Ra	^{210}Pb		30.53	1.51696E-38	1.27025E-17	16.74	15.68	[69]
^{226}Ra	^{212}Pb		28.21	2.53559E-44	1.96187E-23	22.55	21.34	[70]
^{225}Ac	^{211}Bi		30.48	7.70892E-40	6.44460E-19	18.03	17.16	[71]
^{226}Th	^{212}Po		30.67	1.49099E-40	1.25423E-19	18.74	>15.3	[72]
^{226}Th	^{208}Pb	^{18}O	45.88	2.82756E-41	3.52238E-20	19.29	>15.3	[72]
^{228}Th	^{208}Pb	^{20}O	44.72	1.23736E-43	1.50032E-22	21.66	20.72	[73]
^{231}Pa	^{208}Pb	^{23}F	51.84	2.72892E-46	3.83257E-25	24.26	26.02	[61]
^{230}U	^{208}Pb	^{22}Ne	61.59	1.03151E-44	1.72144E-23	22.60	>18.2	[72]
^{230}Th	^{206}Hg	^{24}Ne	57.78	4.45066E-48	6.96605E-27	26.00	24.61	[58]
^{232}Th	^{208}Hg		55.62	2.03030E-52	3.05897E-31	30.36	>29.2	[74]
^{231}Pa	^{207}Tl		60.42	1.16307E-44	1.90358E-23	22.56	22.88	[61]
^{230}U	^{206}Pb		61.55	1.76499E-44	2.94275E-23	22.37	>18.2	[72]
^{232}U	^{208}Pb		62.31	7.77181E-43	1.31179E-21	20.72	20.40	[75]
^{233}U	^{209}Pb		60.50	3.00812E-46	4.92987E-25	24.15	24.83	[76]
^{234}U	^{210}Pb		58.84	1.76590E-49	2.81464E-28	27.39	25.92	[63,75]
^{235}U	^{211}Pb		57.36	1.90240E-52	2.95594E-31	30.37	27.42	[64,75]
^{236}U	^{212}Pb		55.96	2.43370E-55	3.68918E-34	33.27	>25.9	[64]

Table 4.1 (continued)

Parent nuclei	Daughter nuclei	Emitted cluster	Q value (MeV)	Penetrability P	Decay constant λ	$\log_{10}(T_{1/2})$ Present	Expt	Ref
^{232}Th	^{206}Hg	^{26}Ne	55.97	1.32781E-51	2.01290E-30	29.54	>29.2	[74]
^{234}U	^{208}Pb		59.47	5.68727E-48	9.16074E-27	25.88	25.88	[64,75]
^{236}U	^{210}Pb		56.75	1.22550E-53	1.88368E-32	31.57	>25.9	[64]
^{232}U	^{204}Hg	^{28}Mg	74.32	1.33079E-49	2.67867E-28	27.41	>22.3	[54]
^{233}U	^{205}Hg		74.24	1.21732E-49	2.44763E-28	27.45	>27.5	[51]
^{234}U	^{206}Hg		74.13	9.72664E-50	1.95281E-28	27.55	27.54	[64]
^{235}U	^{207}Hg		72.20	2.65094E-53	5.18371E-32	31.13	>28.1	[64]
^{236}U	^{208}Hg		71.69	3.45938E-54	6.71677E-33	32.01	27.58	[77]
^{236}Pu	^{208}Pb		79.67	6.02919E-44	1.30094E-22	21.73	21.67	[78]
^{238}Pu	^{210}Pb		75.93	1.66739E-50	3.42889E-29	28.31	25.70	[62]
^{236}U	^{206}Hg	^{30}Mg	72.51	3.29856E-52	6.47760E-31	30.03	27.58	[77]
^{237}Np	^{207}Tl		75.02	1.56590E-49	3.18152E-28	27.34	>26.9	[58]
^{238}Pu	^{208}Pb		77.03	6.68192E-48	1.39397E-26	25.70	25.70	[62]
^{238}Pu	^{206}Hg	^{32}Si	91.21	6.24162E-51	1.54180E-29	28.65	25.27	[62]
^{240}Pu	^{206}Hg	^{34}Si	90.95	2.18591E-50	5.38418E-29	28.11	>25.5	[57]
^{241}Am	^{207}Tl		93.84	1.09336E-47	2.77866E-26	25.39	>25.3	[60]
^{242}Cm	^{208}Pb		96.53	2.01911E-45	5.27846E-24	23.12	23.24	[79]

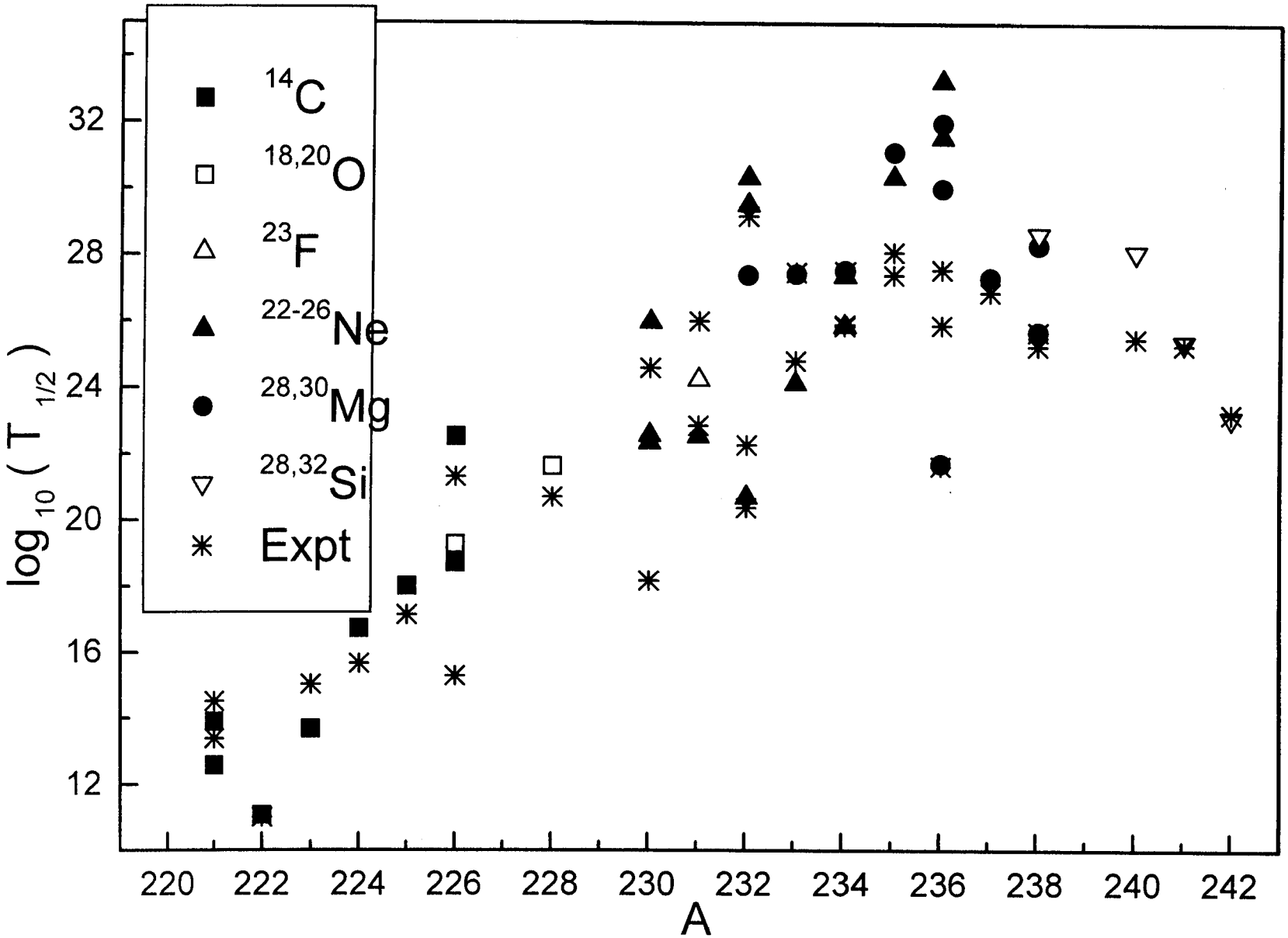

Fig. 4.1 Comparison of calculated and experimental half life time for various clusters.

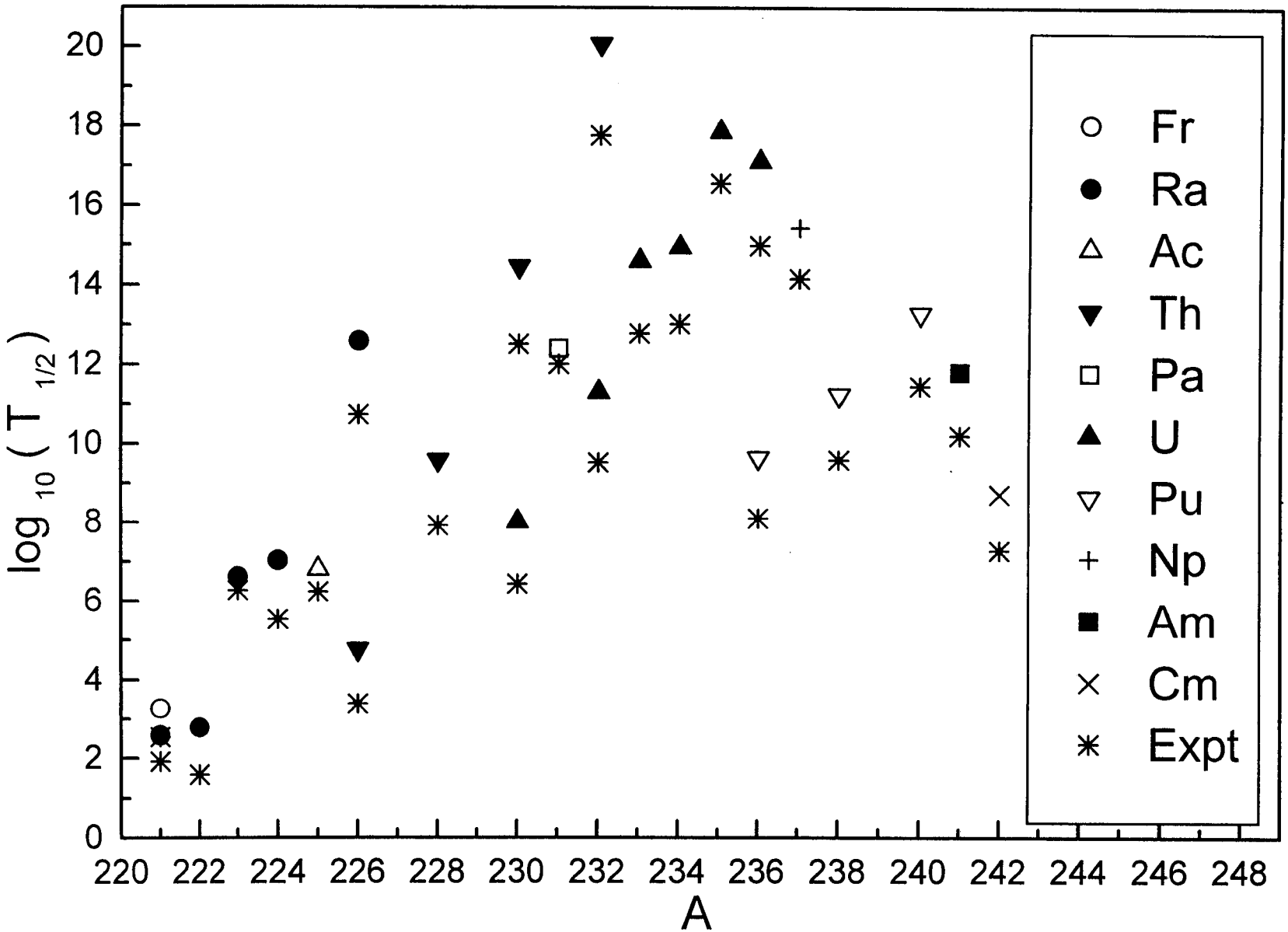

Fig. 4.2 Comparison of calculated and experimental alpha half life time as a function of parent mass number.

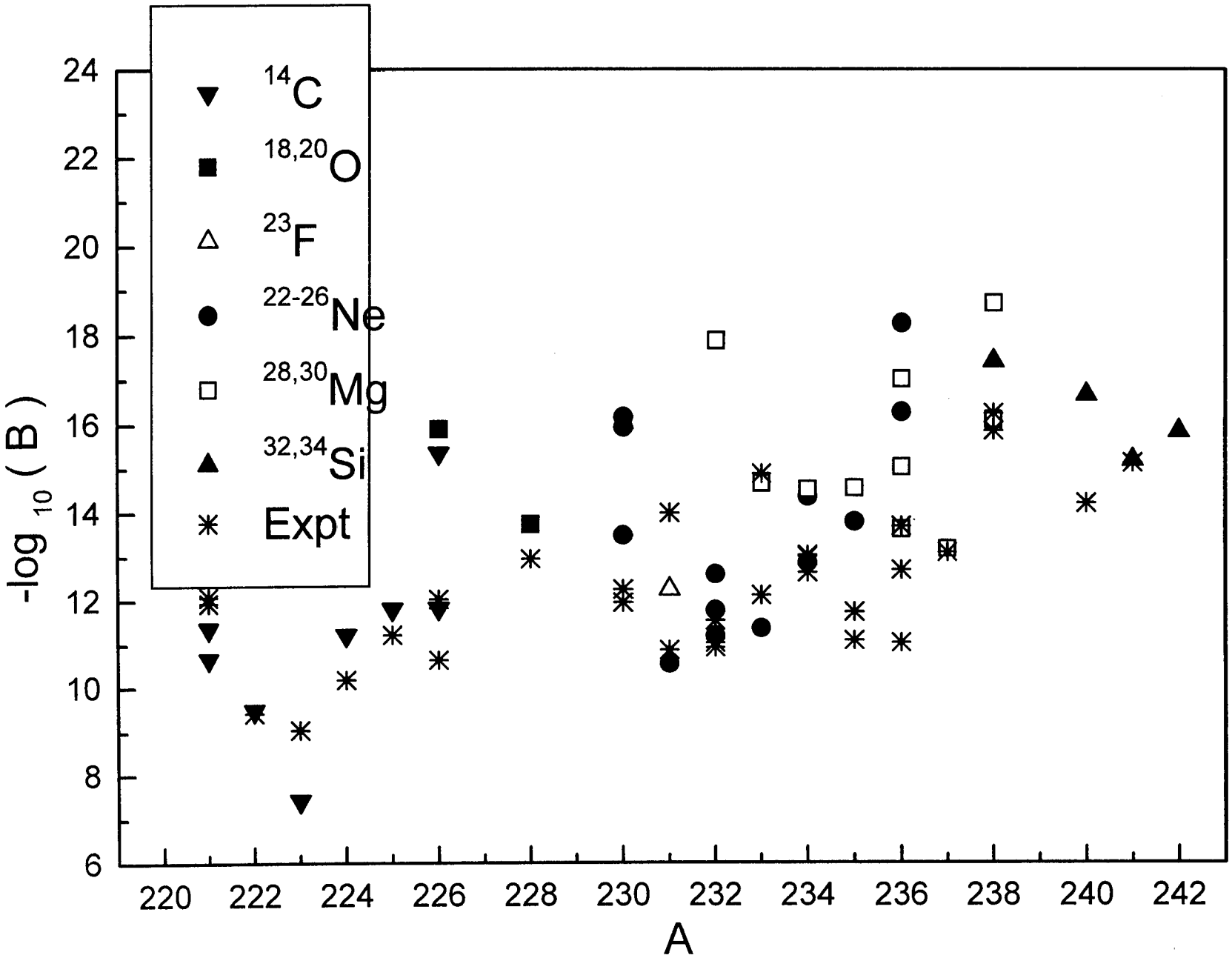

Fig. 4.3 Comparison of calculated and experimental branching ratio as a function of parent mass number.

4.2 Application of the present model to parents in trans-tin region

4.2.1 Decay leading to ^{100}Sn

The exotic decay of proton rich nuclei with Z=56-64 and N=56-72 is very interesting because the daughter nuclei in such decays are formed around the doubly magic ^{100}Sn and the estimated half lives are favourable for measurements. More over only N=Z clusters are emitted from this region and Z/A values for parent, daughter and emitted cluster are nearly equal to 0.5. These nuclei far from β stability line can be produced in reactions induced by radioactive ion beams.

The experiments to study the exotic decay of parents in this region were conducted at Dubna (Russia) [80,81] and at GSI, Darmstat (Germany) [66,82]. In all these experiments ^{114}Ba isotope (Z=56) was produced using on line mass separator by ^{58}Ni(^{58}Ni, 2n) reaction and carbon clusters were searched for by using poly carbonate track detectors in Dubna experiments and by phosphate glass detectors in GSI experiments. The experimental half life time for ^{12}C decay from ^{112}Ba was found to be 5.620×10^{3} s and that from ^{114}Ba was 1.7×10^{4} s [66]. These experiments however could not be reproduced as 1997 run [83] gave a null result and set these values as lower limit for half life time.

4.2.1.1 Xenon isotopes

Tables 4.2 and 4.3 gives the calculated half life time, branching ratio and other characteristics for ^{4}He, ^{8}Be, ^{12}C, ^{16}O, ^{20}Ne, ^{22}Ne, ^{24}Mg, ^{26}Mg and ^{28}Si emission from $^{107-116}$Xe isotopes using different mass tables. It is found that our predicted half life time values lie close to those values reported by Poenaru et al [84,85] based on ASAFM and ^{4}He, ^{8}Be, ^{12}C and ^{16}O emissions are well within the present upper limit for measurements ($T_{1/2}<10^{30}$ s). It is seen that ^{8}Be emission from ^{108}Xe ($T_{1/2} = 6.17\times10^{8}$ s) and from ^{110}Xe ($T_{1/2}=5.39\times10^{8}$ s) are the most favourable for measurements. The lowest half life time value for ^{8}Be emission from ^{108}Xe stress the role of doubly magic ^{100}Sn in cluster decay process. In the case of ^{8}Be emission from ^{110}Xe, the daughter is $^{102}_{50}Sn_{52}$ which lie close to the doubly magic N = Z = 50 shell. The most probable alpha emitter is ^{108}Xe [for Q=6.49 MeV, $\log_{10}(T_{1/2})$ = -10.2 s] since its daughter $^{104}_{52}Te_{52}$ also lies close to the doubly magic N=Z=50 shell. In the cluster radioactivity it is experimentally established that the daughter nuclei are doubly magic or near doubly magic. Experimental data available is alpha decay half life and our calculated logarithm of half life time value for ^{4}He emission from ^{110}Xe is –0.39 s which agree with the experimental value [65] which is –0.4 s.

In Tables 4.2 and 4.3, the last column gives the negative logarithm of the branching ratio, $-\log_{10}(B)$ for various clusters emitted from different Xe isotopes. The experimental half life time for respective alpha decay $T_{1/2}^{alpha}$ are taken from Royer [65]. Using presently available technique the longest measured life time is of the order of 10^{30} s

and lowest measurable branching ratio is almost 10^{-19}. The branching ratio calculations predict that ^{8}Be emissions from ^{108}Xe and from ^{110}Xe are the most favourable ones for measurements.

Figure 4.4 represent the Geiger-Nuttall plots for $\log_{10}(T_{1/2})$ vs $Q^{-1/2}$ for ^{4}He, ^{8}Be, ^{12}C, ^{16}O, ^{20}Ne, ^{24}Mg and ^{28}Si emission from various Xe isotopes. These plots are found to be linear with different slopes and intercepts. The equations for these plots are

$$\log_{10}(T_{1/2}) = \frac{X}{\sqrt{Q}} + Y \qquad (4.2)$$

The slope X and intercept Y values for various clusters are given in Table 4.4. Figures 4.5 to 4.11 represent the Geiger-Nuttall plots for $\log_{10}(T_{1/2})$ vs $-\ln P$ for ^{4}He, ^{8}Be, ^{12}C, ^{16}O, ^{20}Ne, ^{24}Mg and ^{28}Si emission from various Xe isotopes. These plots are also found to be linear.

When logarithm of the half life time for ^{8}Be emission from ^{108}Xe are compared with that from heavier isotopes up to ^{116}Xe it is found that $\log_{10}(T_{1/2})$ increases from 8.732 s (for ^{108}Xe, Q = 9.77 MeV) to 44.45 s (for ^{116}Xe, Q = 4.50 MeV). All these cases refer to the doubly or near doubly magic ^{100}Sn daughter. This points to the fact that neutron excess in the parent will slow down the cluster decay process.

Table 4.2. Logarithm of predicted half life time, branching ratio and other characteristics of ^{4}He, ^{8}Be and ^{12}C emissions from various Xe isotopes. Q values are taken from [84,85,86].

Parent nuclei	Emitted cluster	Daughter nuclei	Q-Value (MeV)	Penetrability P	Decay constant	$\log_{10}(T_{1/2})$ Present	$\log_{10}(T_{1/2})$ ASAFM	$\log_{10}(T_{1/2})$ Expt	$-\log_{10}(B)$ Present
^{107}Xe	^{4}He	^{103}Te	1.89	2.60812E-40	2.26469E-20	19.49	19.0		
^{108}Xe		^{104}Te	0.88	5.21939E-70	2.11019E-50	49.52	47.7		
			6.49	3.41605E-11	1.01856E+10	-10.2			
^{109}Xe		^{105}Te	3.99	1.47879E-20	2.71079	-0.59	-0.7		
			0.65	2.82177E-85	8.42663E-66	64.92	64.6		
^{110}Xe		^{106}Te	4.49	4.57764E-18	9.44293E+03	-3.13			
			3.88	1.02254E-20	1.82278	-0.39		-0.40	
^{112}Xe		^{108}Te	3.31	8.10013E-25	1.23179E-04	3.75			
^{114}Xe		^{110}Te	2.80	5.40006E-29	6.94664E-09	7.99	7.10		
^{115}Xe		^{111}Te	2.38	2.09757E-33	2.29356E-13	12.48	11.6		
^{116}Xe		^{112}Te	2.24	2.55514E-35	3.92084E-15	14.24			
^{107}Xe	^{8}Be	^{99}Sn	8.69	8.00462E-35	2.14872E-14	13.51	14.5		-5.98
^{108}Xe		^{100}Sn	9.77	4.25241E-30	1.28336E-09	8.732			18.90
^{110}Xe		^{102}Sn	9.71	3.74502E-30	1.12329E-09	8.790			9.19
^{112}Xe		^{104}Sn	7.95	4.55592E-38	1.11882E-17	16.79			14.28
^{113}Xe		^{105}Sn	6.20	3.68066E-49	7.04914E-29	27.99	28.7		24.09
^{114}Xe		^{106}Sn	6.18	3.04536E-49	5.81362E-29	28.08			20.09
^{115}Xe		^{107}Sn	4.76	1.86943E-62	2.74875E-42	41.40	41.3		28.92
^{116}Xe		^{108}Sn	4.50	1.77494E-65	2.46727E-45	44.45			30.21
^{107}Xe	^{12}C	^{95}Cd	16.43	2.26055E-36	1.03441E-15	14.83	16.4		-4.67
^{108}Xe		^{96}Cd	15.09	9.35528E-41	3.93175E-20	19.25	19.1		29.45
			15.45	1.75093E-39	7.53422E-19	17.96			28.16
^{109}Xe		^{97}Cd	13.85	2.37459E-45	9.15963E-25	23.88	24.8		24.47
^{110}Xe		^{98}Cd	15.93	1.43010E-37	6.34487E-17	16.04	16.3		16.44
			16.88	1.55825E-34	7.32572E-14	12.98			13.38
^{111}Xe		^{99}Cd	15.38	2.55676E-39	1.09518E-18	17.80	19.4		17.85
			15.61	1.60208E-38	6.96509E-18	16.99	18.6		17.05
^{112}Xe		^{100}Cd	14.26	2.47156E-43	9.81593E-23	21.85	21.7		19.34
			15.96	3.24729E-37	1.44343E-16	15.68			13.17
			14.43	1.12364E-42	4.51578E-22	21.19	22.5		18.68
^{113}Xe		^{101}Cd	13.56	4.77361E-46	1.80280E-25	24.58	25.6		20.68
^{114}Xe		^{102}Cd	12.70	1.01845E-49	3.60235E-29	28.28			20.29
			12.79	2.63582E-49	9.38916E-29	27.87	28.7		19.88
^{115}Xe		^{103}Cd	11.95	3.14645E-53	1.04720E-32	31.82	32.4		19.34
^{116}Xe		^{104}Cd	11.32	1.97024E-56	6.21162E-36	35.05			20.81
			10.95	1.68706E-58	5.14500E-38	37.13	37.4		22.89

Table 4.3. Logarithm of predicted half life time, branching ratio and other characteristics of ^{16}O, ^{20}Ne, ^{22}Ne, ^{24}Mg, ^{26}Mg and ^{28}Si emissions from various Xe isotopes. Q values are taken from [84,85,86].

Parent nuclei	Emitted cluster	Daughter nuclei	Q-Value (MeV)	Penetrability P	Decay constant	$\log_{10}(T_{1/2})$ Present	ASAFM	$-\log_{10}(B)$ Present
^{108}Xe	^{16}O	^{92}Pd	19.71	6.23370E-52	3.55575E-31	30.29		40.49
^{110}Xe		^{94}Pd	21.74	6.83585E-45	4.04778E-24	23.23		23.63
			18.93	2.33568E-54	1.20428E-33	32.76	32.8	33.16
^{111}Xe		^{95}Pd	20.51	1.21713E-48	6.79933E-28	27.01	27.7	27.06
^{112}Xe		^{96}Pd	22.19	3.44630E-43	2.08293E-22	21.52		19.01
			21.23	3.86029E-46	2.23221E-25	24.49	25.5	21.98
^{113}Xe		^{97}Pd	20.41	1.18551E-48	6.59041E-28	27.02	27.9	23.12
^{114}Xe		^{98}Pd	19.71	6.62807E-51	3.55827E-30	29.29		21.30
			19.13	5.46510E-53	2.84760E-32	31.39	31.9	23.40
^{115}Xe		^{99}Pd	18.26	3.79431E-56	1.88711E-35	34.56	34.8	22.08
^{116}Xe		^{100}Pd	17.35	1.20693E-59	4.85293E-39	38.15		23.91
			16.92	1.46192E-61	6.73735E-41	40.01	39.9	25.77
^{108}Xe	^{20}Ne	^{88}Ru	21.56	6.51850E-71	3.81050E-50	49.26		59.46
^{110}Xe		^{90}Ru	23.19	2.58547E-64	1.62565E-43	42.63		43.03
^{112}Xe		^{92}Ru	24.17	1.76921E-60	1.15942E-39	38.78		36.27
^{113}Xe		^{93}Ru	22.19	1.84603E-67	1.11066E-46	45.79	44.6	41.90
^{114}Xe		^{94}Ru	23.29	3.41211E-63	2.15465E-42	41.51		33.52
			22.70	2.35717E-65	1.45078E-44	43.68	42.7	35.69
^{115}Xe		^{95}Ru	21.82	1.46308E-68	8.65584E-48	46.90	45.7	34.42
^{116}Xe		^{96}Ru	20.51	8.35542E-74	4.64643E-53	52.17		37.93
^{114}Xe	^{22}Ne	^{92}Ru	17.55	2.79637E-90	1.32978E-69	68.72		60.73
^{116}Xe		^{94}Ru	17.99	1.43154E-87	6.97821E-67	66.00		51.76
^{108}Xe	^{24}Mg	^{84}Mo	26.58	2.12428E-75	1.52951E-54	53.66		63.86
^{110}Xe		^{86}Mo	28.88	4.61785E-67	3.61261E-46	45.28		45.68
^{112}Xe		^{88}Mo	29.43	7.78753E-65	6.20833E-44	43.05		40.54
^{114}Xe		^{90}Mo	27.19	7.23676E-72	5.33013E-51	50.11	48.1	42.12
^{115}Xe		^{91}Mo	27.46	1.00219E-70	7.45478E-50	48.97	47.1	36.48
^{116}Xe		^{92}Mo	27.72	1.22867E-69	9.22599E-49	47.88	46.3	33.64
^{114}Xe	^{26}Mg	^{88}Mo	24.11	7.68925E-85	5.02123E-64	63.14		55.15
^{116}Xe		^{90}Mo	23.77	5.83444E-86	3.75627E-65	64.27		50.03
^{108}Xe	^{28}Si	^{80}Zr	35.00	2.04748E-67	1.94085E-46	45.55		55.75
^{110}Xe		^{82}Zr	35.55	3.01534E-65	2.90322E-44	43.38		43.78
^{112}Xe		^{84}Zr	35.55	1.08659E-64	1.04618E-43	42.82		40.31
^{114}Xe		^{86}Zr	32.56	3.48041E-73	3.06915E-52	51.35	48.7	43.36
^{116}Xe		^{88}Zr	32.51	6.68926E-73	5.88977E-52	51.07		36.83
			32.10	3.14437E-74	2.73365E-53	52.40	49.9	38.16

Table 4.4. Slope and intercept values of Geiger-Nuttall plots for different clusters from various Xe isotopes.

Emitted cluster	Slope X	Intercept Y
^{4}He	88.5811	-44.9384
^{8}Be	236.0719	-66.8178
^{12}C	407.5291	-85.9697
^{16}O	594.7938	-104.4178
^{20}Ne	792.8314	-122.3308
^{24}Mg	1066.3716	-153.7404
^{28}Si	1034.7248	-130.3360

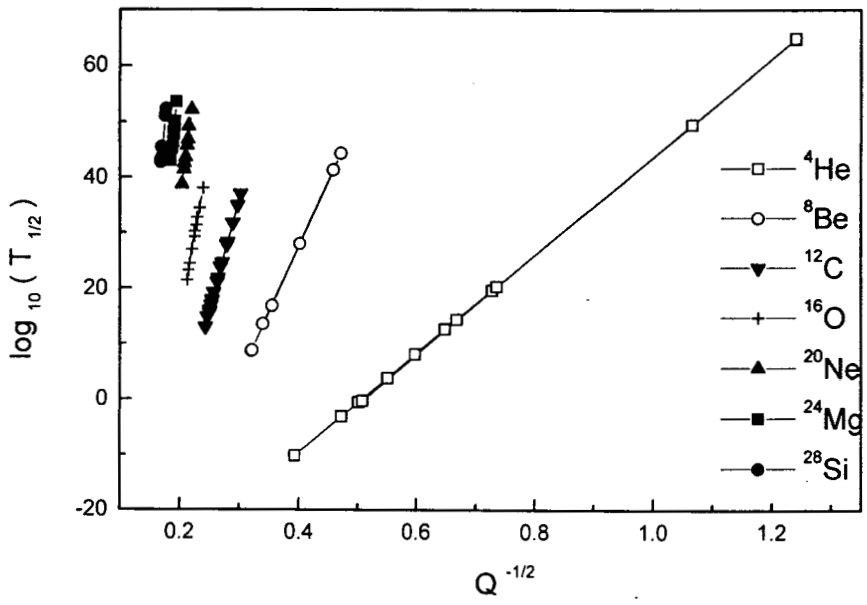

Fig. 4.4 Geiger Nuttall plot for $\log_{10}(T_{1/2})$ Vs $Q^{-1/2}$ for various clusters from different Xe isotopes.

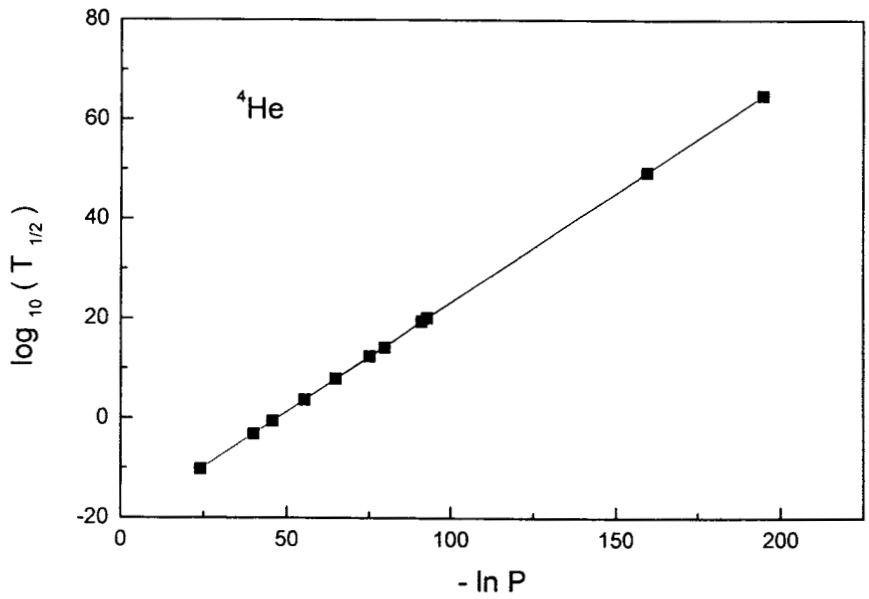

Fig. 4.5 Geiger Nuttall plot for $\log_{10}(T_{1/2})$ vs $-\ln P$ for ^4He from various Xe isotopes.

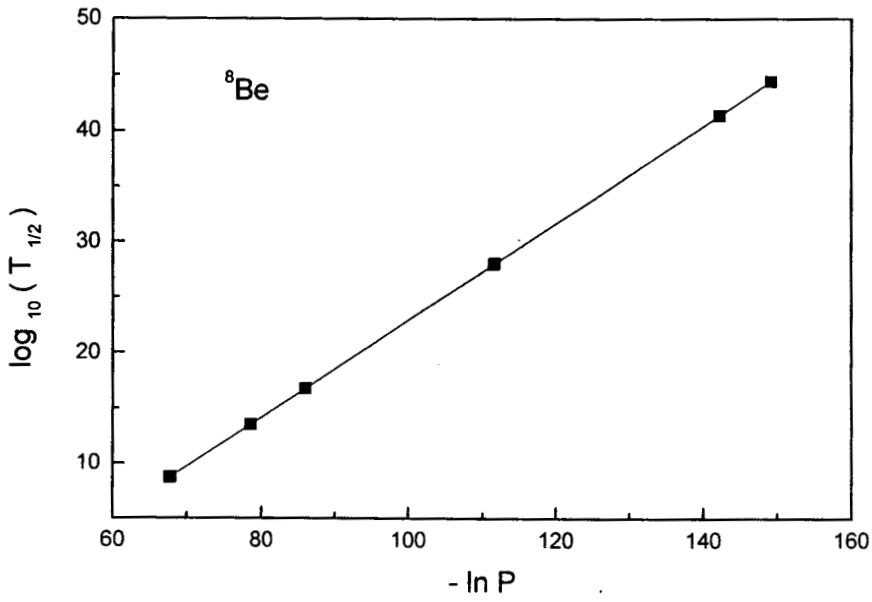

Fig. 4.6 Geiger Nuttall plot for $\log_{10}(T_{1/2})$ vs –lnP for ^{8}Be emission from various Xe isotopes.

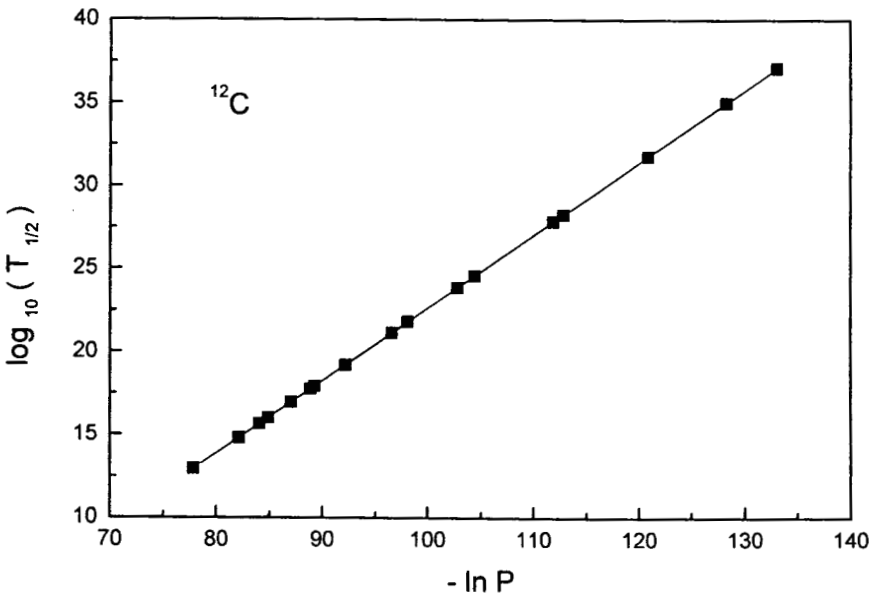

Fig. 4.7 Geiger Nuttall plot for $\log_{10}(T_{1/2})$ Vs –lnP for ^{12}C emission from various Xe isotopes.

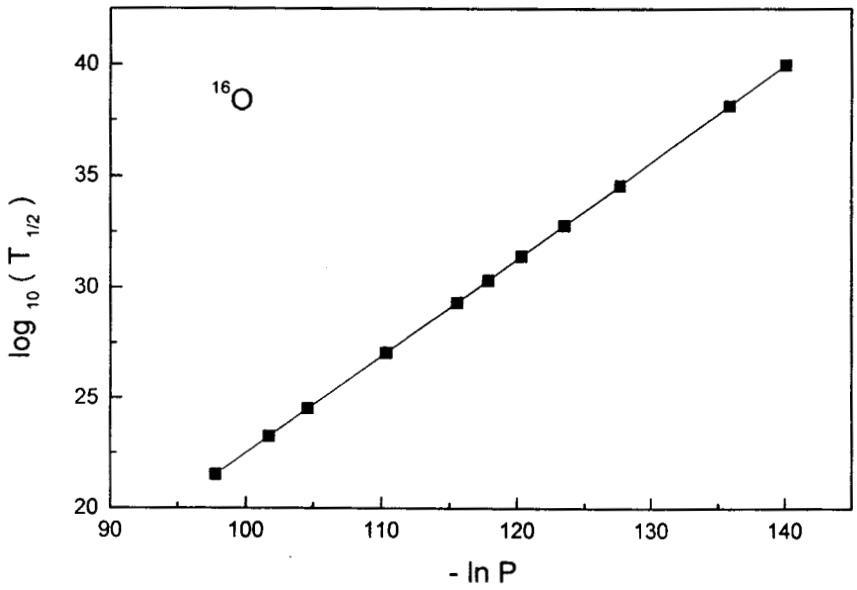

Fig. 4.8 Geiger Nuttall plot for $\log_{10}(T_{1/2})$ Vs $-\ln P$ for ^{16}O emission from various Xe isotopes.

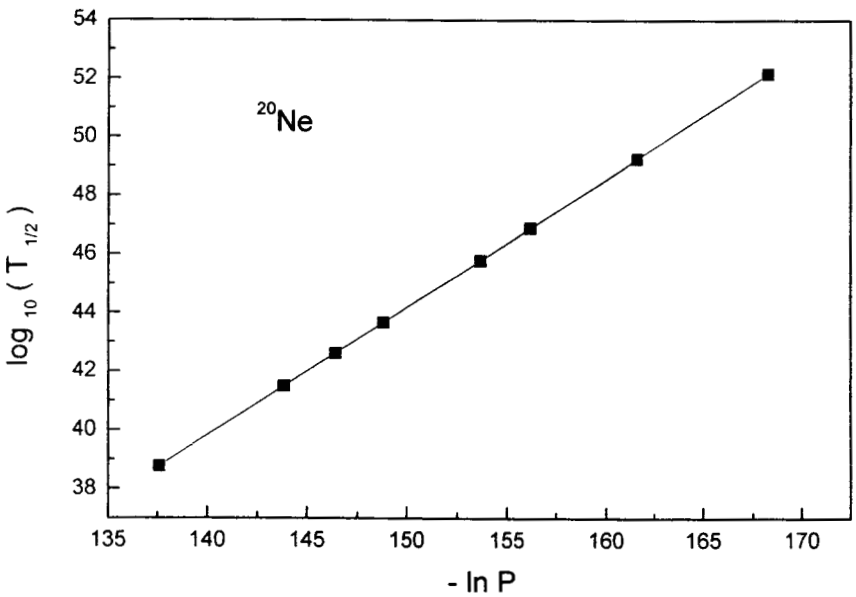

Fig. 4.9 Geiger Nuttall plot for $\log_{10}(T_{1/2})$ Vs $-\ln P$ for ^{20}Ne emission from various Xe isotopes.

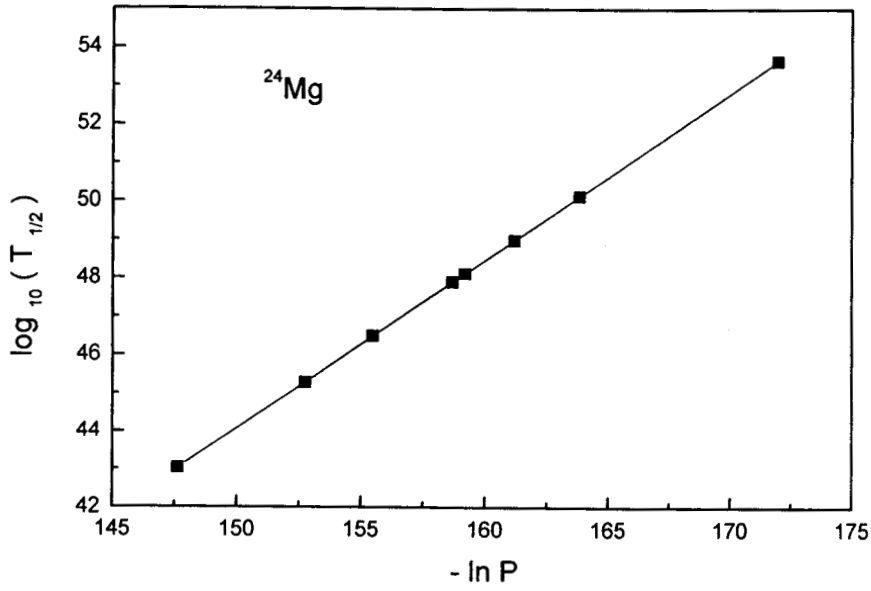

Fig. 4.10 Geiger Nuttall plot for $\log_{10}(T_{1/2})$ Vs –lnP for ^{24}Mg emission from various Xe isotopes.

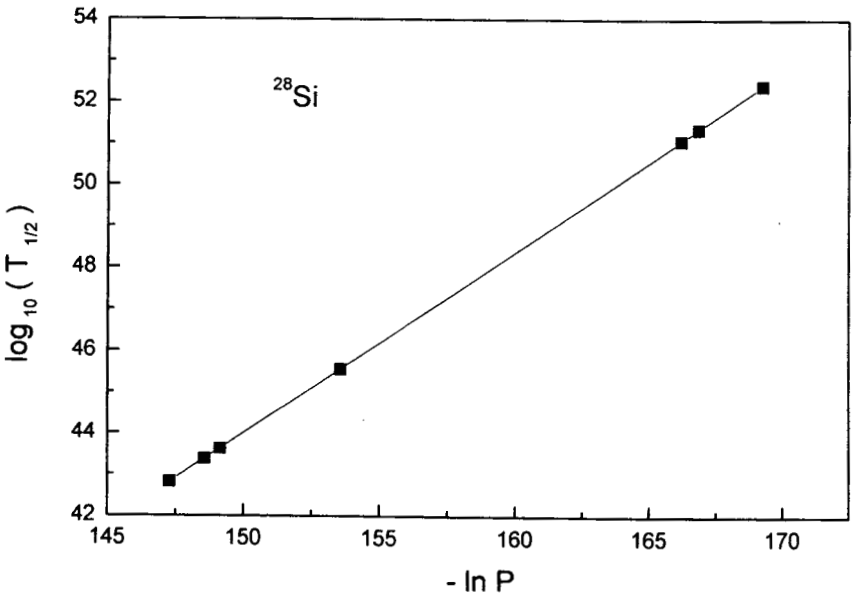

Fig. 4.11 Geiger Nuttall plot for $\log_{10}(T_{1/2})$ Vs –lnP for ^{28}Si emission from various Xe isotopes.

4.2.1.2 Barium isotopes

Table 4.5 gives the predicted half life time and other characteristics for ^{12}C and ^{4}He emission from $^{112\text{-}120}Ba$ isotopes using different mass tables and their comparison with other models. For ^{112}Ba, our calculated $T_{1/2}$ value for ^{12}C emission is 6.020×10^{3} s, which is in agreement with the experimental $T_{1/2}$ value 5.620×10^{3} s. In the case of ^{114}Ba, the experimental $\log_{10}(T_{1/2})$ value is 4.23 s which is also comparable with our value 5.17 s (for Q = 20.75 MeV). It is found that the predicted values are well with in the present upper limit for measurements and our values lie close to those values reported by CYEM [87]. It is found that ^{12}C emission from ^{112}Ba and ^{114}Ba has the lowest half life time values. The lowest $T_{1/2}$ value for ^{112}Ba stress the role of doubly magic ^{100}Sn daughter and in the case of ^{114}Ba the daughter is near doubly magic ${}^{102}_{50}Sn_{52}$ daughter. But ^{114}Ba is the best parent for ^{12}C emission with the highest decay rate since ^{112}Ba is short lived and decays by two proton emissions.

When the decay of ^{12}C from ^{112}Ba is compared with that from heavier isotopes up to ^{120}Ba, it is found that $\log_{10}(T_{1/2})$ value increases from 3.78 s (for ^{112}Ba, Q = 21.46 MeV) to 28.43 s (for ^{120}Ba, Q = 13.4 MeV). All these cases refer to doubly or near doubly magic ^{100}Sn daughter. This points to the fact that the neutron excess in the parent will slow down the cluster decay process .

Table 4.6 gives the logarithm of the half life time and other characteristics for ^{8}Be, ^{16}O, ^{20}Ne, ^{24}Mg, ^{28}Si and ^{32}S emissions from various Ba isotopes. Here most of the values are favourable for measurements. It should be noted that ^{8}Be emission from ^{112}Ba has the shortest $\log_{10}(T_{1/2})$ value, equal to 7.232 s. This may be due to the fact that its daughter $^{104}_{52}Te_{52}$ lies close to the doubly magic Z=N=50 shell.

Figure 4.12 gives the Geiger-Nuttall plots for $\log_{10}(T_{1/2})$ vs $Q^{-1/2}$ for ^{4}He, ^{8}Be, ^{12}C, ^{16}O, ^{20}Ne, ^{24}Mg, ^{28}Si and ^{32}S emission from various Ba isotopes. These are found to be linear with different slopes and intercepts. The slope and intercept values for different clusters are given in Table 4.7. Using eqn (4.2), $\log_{10}(T_{1/2})$ for ^{12}C and ^{4}He emission from various Ba isotopes are calculated using different mass tables and compared with other models which are given in Tables 4.8 and 4.9.

Fig 4.13 to 4.20 give the Geiger-Nuttall plots for $\log_{10}(T_{1/2})$ vs -lnP for ^{4}He, ^{8}Be, ^{12}C, ^{16}O, ^{20}Ne, ^{24}Mg, ^{28}Si and ^{32}S emission from various Ba isotopes. These are also found to be linear with different slopes and intercepts.

Table 4.5. Logarithm of predicted half life time and other characteristic of ^{12}C and ^{4}He emission from various Ba isotopes. Q values are taken from [88]. Table taken from [89].

Parent nuclei	Emitted cluster	Daughter nuclei	Q value (MeV)	Penetrability P	Decay Constant λ	$\log_{10}(T_{1/2})$ Present	CYEM [87]	ASAFM [90]	PCM [91]
^{112}Ba	^{12}C	^{100}Sn	21.46[f]	1.92605E-25	1.1512E-04	3.78			3.75
^{114}Ba	^{12}C	^{102}Sn	20.20[d]	3.65981E-28	2.0590E-07	6.53			5.12
			18.34[e]	4.17843E-33	2.1343E-12	11.51			9.67
			20.75[a]	8.04016E-27	4.6465E-06	5.17			
			19.97[b]	9.70947E-29	5.4003E-08	7.11			
			18.16[c]	1.27581E-33	6.4527E-13	12.01			
			19.46	4.74124E-30	2.5697E-09	8.43	8.71	9.4	
			18.91	1.61129E-31	8.4861E-11	9.91	10.12	10.6	
			19.33	2.15768E-30	1.1616E-09	8.78	9.04	9.7	
			19.40	3.29978E-30	1.7829E-09	8.59	8.86	9.5	
			20.12	2.31237E-28	1.2958E-07	6.73	7.09	7.9	
^{115}Ba	^{12}C	^{103}Sn	18.25	3.13608E-33	1.5940E-12	11.64	11.81	13.6	
			17.83	1.88045E-34	9.3380E-14	12.87	12.99	14.7	
			18.27	3.55769E-33	1.8205E-12	11.58	11.75	13.6	
			17.42	1.10089E-35	5.3411E-15	14.11	14.18	15.8	
			18.78	9.63156E-32	5.0377E-11	10.14	10.37	12.3	
^{116}Ba	^{12}C	^{104}Sn	17.63[f]	6.37407E-35	3.1298E-14	13.35			11.31
			17.40	1.27870E-35	6.1967E-15	14.05	14.15	14.4	
			17.00	7.27910E-37	3.4464E-16	15.30	15.35	15.5	
			16.64	5.08267E-38	2.3555E-17	16.47	16.47	16.6	
			17.43	1.57942E-35	7.6672E-15	13.96	14.06	14.3	
			18.95	3.76275E-31	1.9859E-10	9.54	9.84	10.4	
			16.83	2.09188E-37	9.8053E-17	15.85	15.88	16.0	
^{117}Ba	^{12}C	^{105}Sn	16.08	9.03230E-40	4.0451E-19	18.23	18.21	19.6	
^{118}Ba	^{12}C	^{106}Sn	15.44[f]	6.54238E-42	2.8133E-21	20.39			18.13
			15.10	3.65471E-43	1.5370E-22	21.65	21.54	21.3	
^{119}Ba	^{12}C	^{107}Sn	14.01	2.32280E-47	9.0634E-27	25.88	25.67	26.7	
^{120}Ba	^{12}C	^{108}Sn	13.40[f]	6.95994E-50	2.5975E-29	28.43			32.23
			13.03	1.45772E-51	5.2900E-31	30.18	29.81	29.1	
^{115}Ba	^{4}He	^{111}Xe	2.45	4.66280E-34	5.2485E-14	13.12	12.98	12.6	
^{116}Ba	^{4}He	^{112}Xe	2.32[f]	1.22770E-35	1.3086E-15	14.72			12.83
^{118}Ba	^{4}He	^{114}Xe	1.90[f]	7.14627E-42	6.2381E-22	21.05			18.59
^{119}Ba	^{4}He	^{115}Xe	1.78	4.87877E-44	3.9898E-24	23.24	23.04	22.6	
^{120}Ba	^{4}He	^{116}Xe	1.54[f]	3.75803E-49	2.6589E-29	28.46			26.17
			1.60	9.31120E-48	6.8445E-28	27.01	26.78	26.0	

Masses are taken from [a] [92], [b] [93], [c] [94], [d] [95], [e] [96], [f] [97].

Table 4.6. Logarithm of predicted half life time for the emission of clusters like ^{8}Be, ^{16}O, ^{20}Ne, ^{24}Mg, ^{28}Si and ^{32}S from different Ba isotopes and comparison with other models. Q values are taken from [84,91]. Table taken from [98].

Parent nuclei	Emitted cluster	Daughter nuclei	Q value (MeV)	Penetrability P	Decay constant λ	$\log_{10}(T_{1/2})$ Present	PCM [91]	ASAFM [84]
^{112}Ba	^{8}Be	^{104}Te	10.72	1.22672E-28	4.06218E-08	7.232	5.84	
^{114}Ba		^{106}Te	7.52	3.19109E-43	7.4127E-23	21.97	18.14	
^{116}Ba		^{108}Te	5.50	2.63679E-58	4.47979E-38	37.19	32.11	
^{118}Ba		^{110}Te	5.35	1.26600E-59	2.09222E-39	38.52	32.83	
^{120}Ba		^{112}Te	2.92	5.02270E-97	4.53043E-77	76.18	68.45	
^{112}Ba	^{16}O	^{96}Cd	26.94	5.08764E-35	3.73318E-14	13.27	13.36	
^{114}Ba		^{98}Cd	27.17	4.33417E-34	3.20746E-13	12.34	11.36	
			25.96	4.94650E-37	3.49758E-16	15.30		16.00
^{115}Ba		^{99}Cd	25.41	2.98419E-38	2.06537E-17	16.53		18.70
			25.22	9.59602E-39	6.59176E-18	17.02		19.10
^{116}Ba		^{100}Cd	25.44	5.29599E-38	3.66969E-17	16.28	14.92	
			24.02	8.32167E-42	5.44438E-21	20.10		20.30
			24.21	2.79584E-41	1.84363E-20	19.58		19.80
^{118}Ba		^{102}Cd	21.76	3.17244E-48	1.88026E-27	26.57	25.27	
			22.11	4.04041E-47	2.43321E-26	25.45		25.10
^{120}Ba		^{104}Cd	20.10	1.52625E-53	8.35578E-33	31.92	41.29	
^{112}Ba	^{20}Ne	^{92}Pd	28.77	2.68092E-52	2.09127E-31	30.52	31.03	
^{114}Ba		^{94}Pd	29.60	1.47910E-49	1.18706E-28	27.77	26.82	
^{116}Ba		^{96}Pd	29.24	4.15618E-50	3.29502E-29	28.32	27.10	
^{118}Ba		^{98}Pd	26.34	2.88188E-58	2.05815E-37	36.53	35.93	
^{120}Ba		^{100}Pd	23.60	2.74306E-67	1.75523E-46	45.60	58.61	
^{112}Ba	^{24}Mg	^{88}Ru	35.19	1.67909E-55	1.60059E-34	33.64	34.29	
^{114}Ba		^{90}Ru	35.62	7.64084E-54	7.37258E-33	31.97	31.14	
^{116}Ba		^{92}Ru	35.79	6.75663E-53	6.55053E-32	31.02	29.98	
^{118}Ba		^{94}Ru	34.49	8.17166E-56	7.63463E-35	33.98	33.39	
^{120}Ba		^{96}Ru	31.40	3.48850E-64	2.96724E-43	42.37	61.60	
^{112}Ba	^{28}Si	^{84}Mo	40.89	1.01505E-58	1.12411E-37	36.79	37.23	
^{114}Ba		^{86}Mo	41.99	2.07491E-55	2.35965E-34	33.47	32.08	
^{116}Ba		^{88}Mo	41.73	1.95936E-55	2.21445E-34	33.50	32.05	
^{118}Ba		^{90}Mo	39.65	4.41221E-60	4.73808E-39	38.67	36.84	
^{120}Ba		^{92}Mo	39.80	3.38394E-59	3.64762E-38	37.28	56.77	
^{112}Ba	^{32}S	^{80}Zr	46.28	9.94975E-61	1.24708E-39	38.75	38.52	
^{114}Ba		^{82}Zr	45.63	1.49281E-61	1.84478E-40	39.57	37.91	
^{116}Ba		^{84}Zr	44.82	7.27928E-63	8.83583E-42	40.89	39.10	
^{118}Ba		^{86}Zr	43.94	1.83439E-64	2.18293E-43	42.50	40.81	
^{120}Ba		^{88}Zr	41.00	9.90037E-72	1.09932E-50	49.80	67.45	

Table 4.7. Slope and intercept values of Geiger-Nuttall plots for different clusters from various Ba isotopes.

Cluster	Slope X	Intercept Y
^{4}He	91.62	-45.42
^{8}Be	246.28	-67.91
^{12}C	431.93	-89.49
^{20}Ne	804.91	-120.13
^{24}Mg	960.93	-129.15
^{28}Si	1017.52	-123.47
^{32}S	1225.68	-141.90

Table 4.8. Logarithm of predicted half life time for ^{12}C emission from various Ba isotopes using equation (4.2) and comparison with other models. Q values are taken from [88]. Table taken from [89].

Parent nuclei	Emitted cluster	Daughter nuclei	Q value (MeV)	$\log_{10}(T_{1/2})$ Present	[87]	[90]	[91]
^{112}Ba	^{12}C	^{100}Sn	21.46[c]	3.75			3.75
^{114}Ba	^{12}C	^{102}Sn	20.20[a]	6.16			5.12
			18.34[b]	11.37	11.65	12.10	9.67
^{115}Ba	^{12}C	^{103}Sn	18.25	11.62	11.81	13.60	
			18.78	10.18	10.37	12.30	
^{116}Ba	^{12}C	^{104}Sn	17.40	14.00	14.15	14.40	
			17.00	15.27	15.35	15.50	
^{117}Ba	^{12}C	^{105}Sn	16.08	18.22	18.21	19.60	
^{118}Ba	^{12}C	^{106}Sn	15.10	21.66	21.54	21.30	
			17.63[c]	13.38			11.31
^{119}Ba	^{12}C	^{107}Sn	14.01	25.91	25.67	26.70	
^{120}Ba	^{12}C	^{108}Sn	13.03	30.17	29.81	29.10	
			13.40[c]	28.50			32.23

Masses are taken from [a] [95], [b] [96], [c] [97].

Table 4.9. Logarithm of predicted half life time for ^{4}He emission from various Ba isotopes using equation (4.2) and comparison with other models. Q values are taken from [88]. Table taken from [89].

Parent nuclei	Emitted cluster	Daughter nuclei	Q value (MeV)	$\log_{10}(T_{1/2})$ Present	[87]	[90]	[91]	[99]
^{112}Ba	^{4}He	^{108}Xe	4.33[f]	-1.39			-2.91	
^{114}Ba	^{4}He	^{110}Xe	3.13[f]	6.37			4.96	
			3.99	0.44	0.29	0.00		
			3.43	4.04	3.91	3.40		
			3.85	1.27	1.12	0.80		
			3.93	0.79	0.64	0.40		
			2.87	8.66	8.54	8.00		
			4.65	-2.93	-3.11	-3.10		
			3.035[b]	7.16				6.52
			3.125[d]	6.41				5.78
			3.155[e]	6.16				5.54
			3.465[a]	3.79				3.26
			3.475[c]	3.73				3.19
^{115}Ba	^{4}He	^{111}Xe	3.28	5.16	5.00	4.80		
			2.86	8.75	8.60	8.30		
			2.67	10.65	10.51	10.10		
			3.30	5.01	4.84	4.60		
			2.45	13.11	12.98	12.60		
			3.81	1.52	1.33	1.20		
^{116}Ba	^{4}He	^{112}Xe	2.32[f]	14.73			12.83	
			3.35	4.64	4.43	4.00		
			2.96	7.83	7.64	7.20		
			2.60	11.39	11.23	10.60		
			3.38	4.41	4.21	3.80		
			4.90	-4.03	-4.28	-4.20		
			2.78	9.53	9.35	8.70		
			3.39	4.34	4.13	3.70		
^{117}Ba	^{4}He	^{113}Xe	2.50	12.52	12.33	11.9		
^{118}Ba	^{4}He	^{114}Xe	1.90[f]	21.05			18.59	
			2.40	13.72	13.50	12.80		
^{119}Ba	^{4}He	^{115}Xe	1.78	23.25	23.04	22.60		
^{120}Ba	^{4}He	^{116}Xe	1.54[f]	28.41			26.17	
			1.60	27.00	26.78	26.00		

Masses are taken from [a] [92], [b] [93], [c] [94], [d] [95], [e] [96], [f] [97].

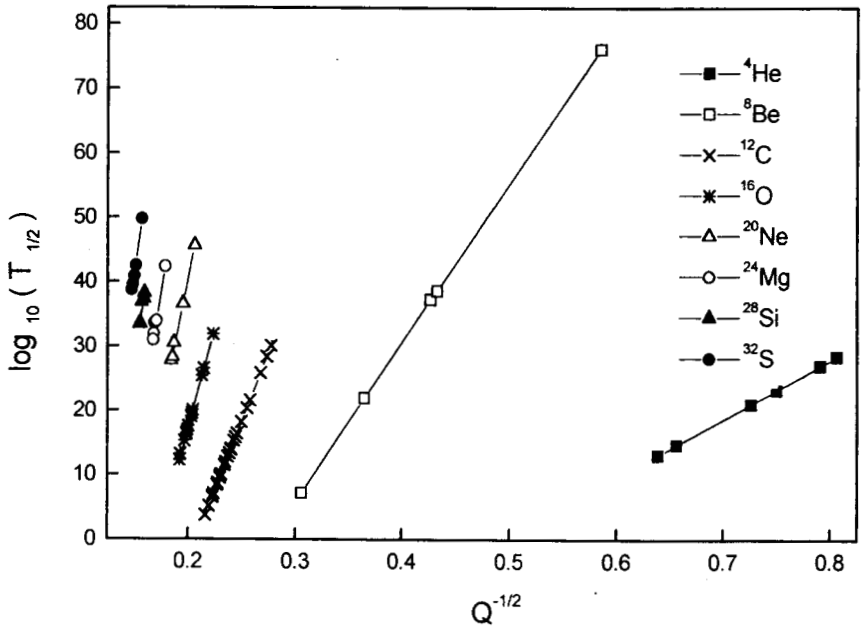

Fig. 4.12 Geiger Nuttall plot for $\log_{10}(T_{1/2})$ Vs $Q^{-1/2}$ for various clusters from different Ba isotopes.

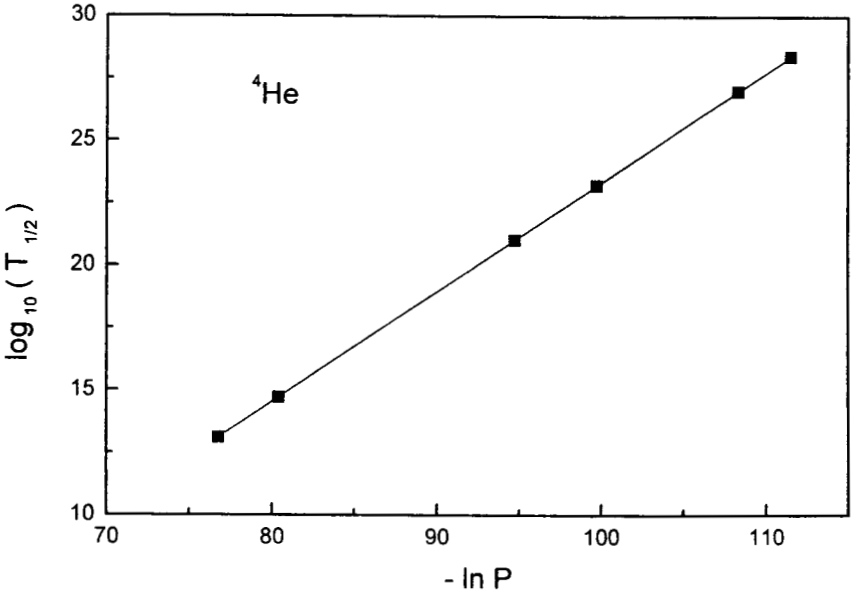

Fig. 4.13 Geiger Nuttall plot for $\log_{10}(T_{1/2})$ vs $-\ln P$ for ^4He emission from various Ba isotopes.

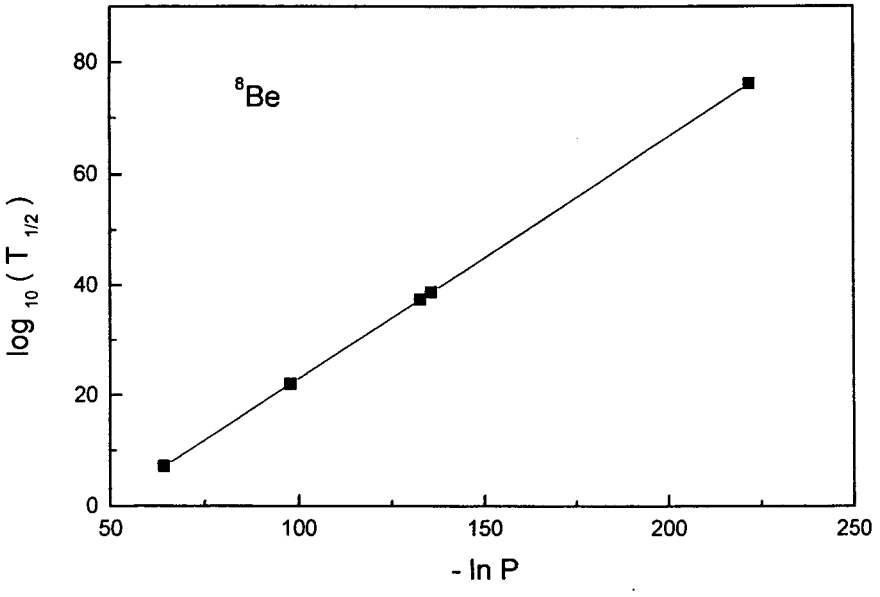

Fig. 4.14 Geiger Nuttall plot for $\log_{10}(T_{1/2})$ vs –lnP for ^{8}Be emission from various Ba isotopes.

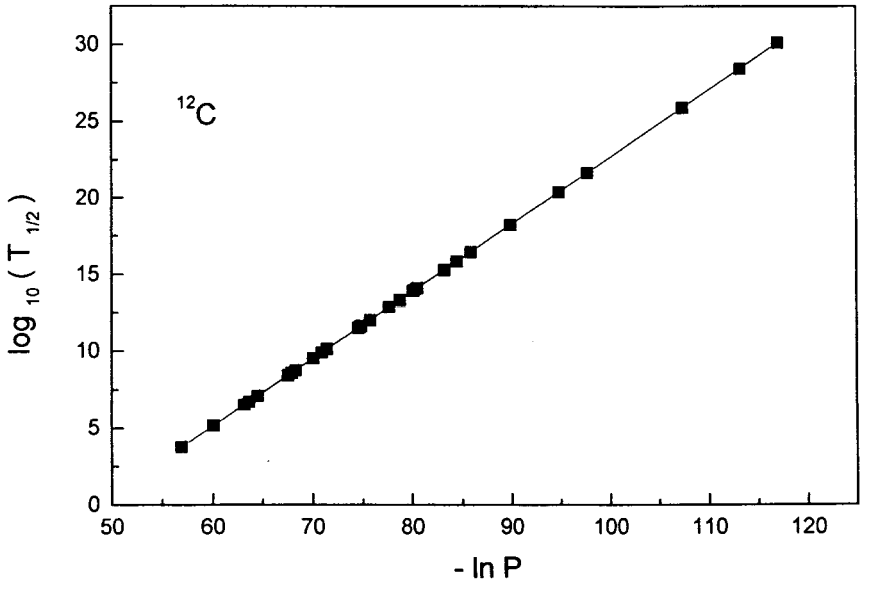

Fig. 4.15 Geiger Nuttall plot for $\log_{10}(T_{1/2})$ vs –lnP for ^{12}C emission from various Ba isotopes.

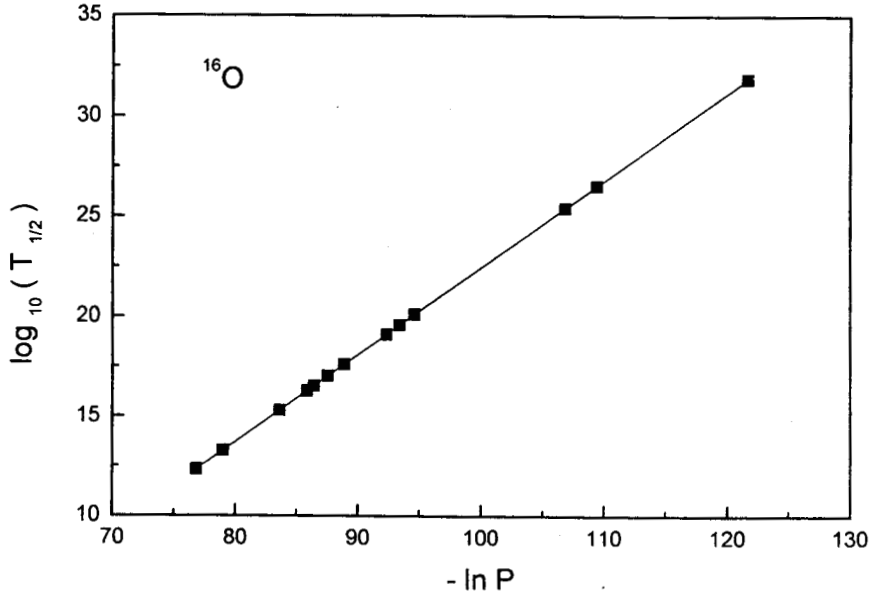

Fig. 4.16 Geiger Nuttall plot for $\log_{10}(T_{1/2})$ vs $-\ln P$ for ^{16}O emission from various Ba isotopes.

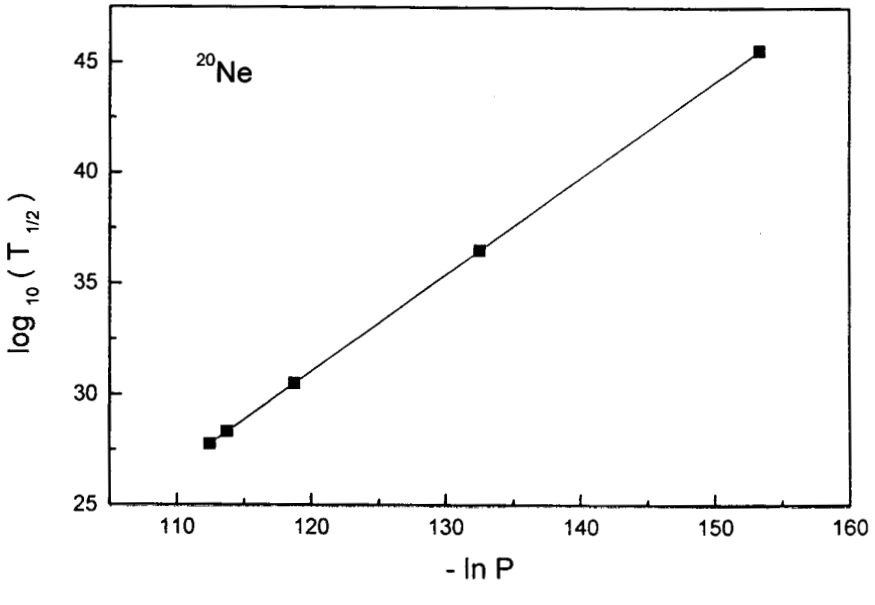

Fig. 4.17 Geiger Nuttall plot for $\log_{10}(T_{1/2})$ vs $-\ln P$ for ^{20}Ne emission from various Ba isotopes.

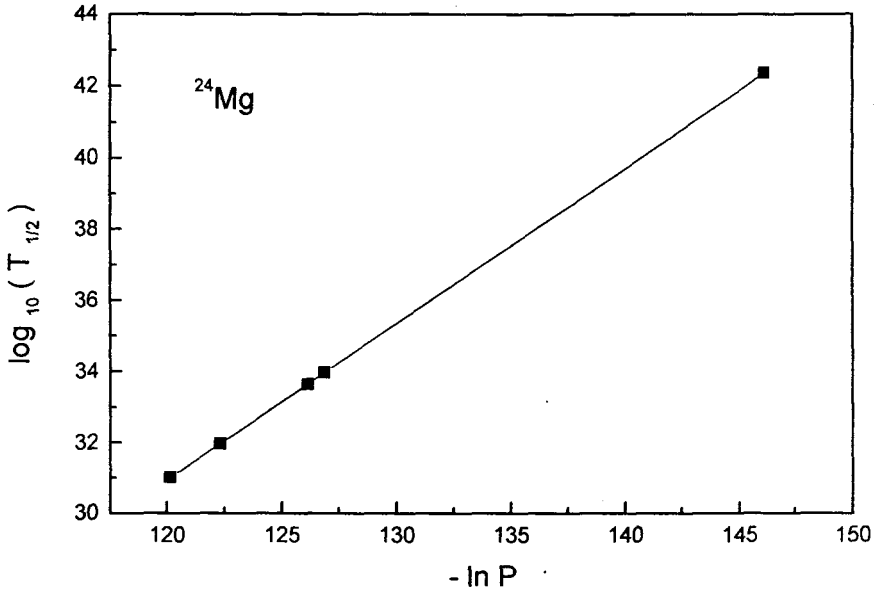

Fig. 4.18 Geiger Nuttall plot for $\log_{10}(T_{1/2})$ Vs –lnP for ^{24}Mg emission from various Ba isotopes.

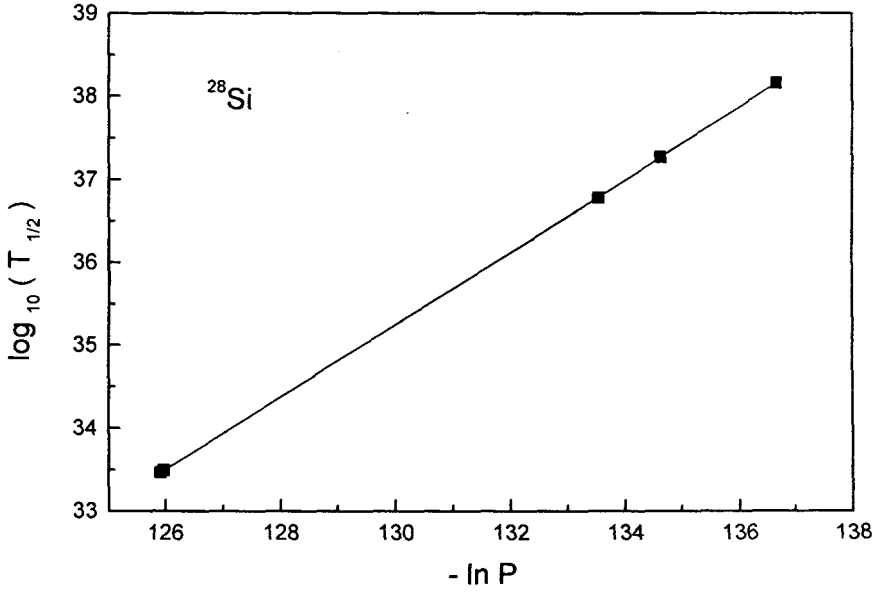

Fig. 4.19 Geiger Nuttall plot for $\log_{10}(T_{1/2})$ Vs –lnP for ^{28}Si emission from various Ba isotopes.

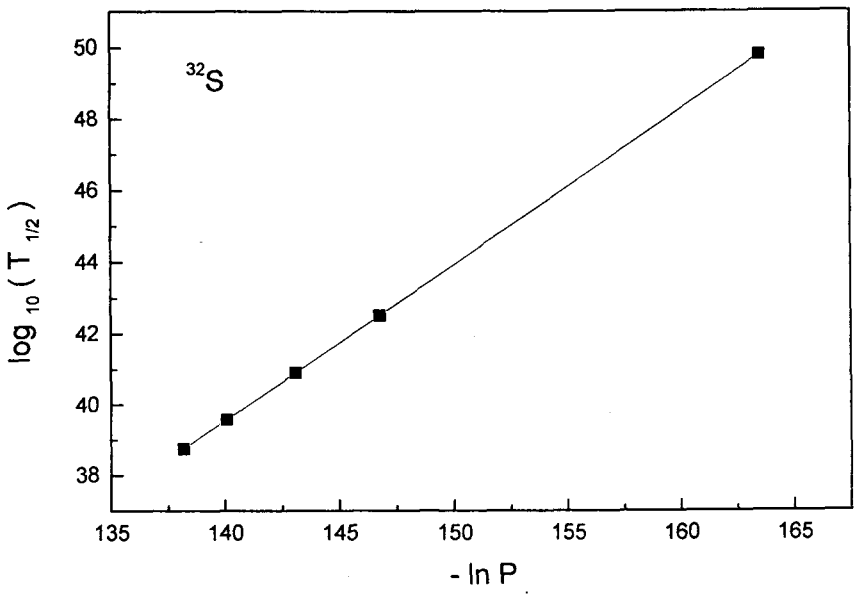

Fig. 4.20 Geiger Nuttall plot for $\log_{10}(T_{1/2})$ Vs –lnP for ^{32}S emission from various Ba isotopes.

4.2.1.3 Cerium isotopes

Tables 4.10 and 4.11 give the logarithm of the predicted half life time and other characteristics for ^{4}He and ^{16}O emission from $^{116\text{-}124}$Ce isotopes using different mass tables and their comparison with other models. Our predicted values are below the present upper limit for measurements and these values lie close to those reported by CYEM [87]. It is found that ^{16}O emission from ^{116}Ce (Q = 31.71 MeV, $T_{1/2}$ =1.30965x10^{6} s) and from ^{118}Ce (for Q = 29.94 MeV, $T_{1/2}$ =2.71757x10^{9} s and for Q = 29.97 MeV, $T_{1/2}$ =2.33921x10^{9} s) are the most favourable cases for measurements. Out of this ^{16}O emission from ^{116}Ce has the lowest $T_{1/2}$ value, which stresses the role of doubly magic ^{100}Sn daughter. For ^{16}O decay from ^{118}Ce the daughter is $^{102}_{50}Sn_{52}$ which lies close to the doubly magic Z = N = 50 shell. Table 4.12 gives the predicted half life time and other characteristics for ^{8}Be, ^{12}C, ^{20}Ne, ^{22}Ne, ^{24}Mg, ^{26}Mg and ^{28}Si emission from various Ce isotopes. Most of them are favourable for measurements. Here ^{12}C from ^{116}Ce (for Q = 21.17 MeV, $T_{1/2}$ =9.94412x10^{6} s) is the most favourable one for measurements since its daughter is $^{104}_{52}Te_{52}$ which lies close to the doubly magic N = Z = 50 shell.

Figure 4.21 gives the Geiger-Nuttall plot for $\log_{10}(T_{1/2})$ vs $Q^{-1/2}$ for different clusters from various Ce isotopes. These plots are also found to be linear with different slopes and intercepts. The slope and intercepts values for different clusters are given in Table 4.13. From the observed variation in slopes and intercepts of the Geiger-Nuttall

plots with proton number (Z_2) of the emitted cluster, we arrived at a general equation for the half life time which is applicable for all clusters from various Ce isotopes. The equation is

$$Log_{10}(T_{1/2}) = \frac{X(Z_2)}{\sqrt{Q}} + Y(Z_2) \tag{4.3}$$

where

$$X(Z_2) = -0.39712Z_2^3 + 9.04574Z_2^2 + 36.32311Z_2 - 10.14493 \tag{4.4}$$

$$Y(Z_2) = 0.02872Z_2^3 - 0.28315Z_2^2 - 10.20002Z_2 - 24.9127 \tag{4.5}$$

Using the above equations, we have calculated the half lifetime for all possible clusters from various Ce isotopes and are given in Table 4.12 as Cal II.

Figures 4.22 to 4.28 give the Geiger-Nuttall plots for $\log_{10}(T_{1/2})$ vs -lnP for ^{4}He, ^{8}Be, ^{12}C, ^{16}O, ^{20}Ne, ^{24}Mg and ^{28}Si emission from various Ce isotopes. These are also found to be linear.

When the half life times for different clusters from ^{116}Ce are compared with that from other heavier Ce isotopes up to ^{124}Ce, the $\log_{10}(T_{1/2})$ values are found to increase. For example the $\log_{10}(T_{1/2})$ value for ^{16}O emission increases from 6.12 s (for ^{116}Ce, Q = 31.7 1MeV) to 27.65 s (for ^{124}Ce, Q = 22.59 MeV) . All these cases refer to the doubly magic or near doubly magic Sn nuclei. From this it is clear that the presence of the neutron excess in the parent nuclei will slow down the exotic decay process.

When the emission of ^{22}Ne and ^{20}Ne from the same parent (either ^{122}Ce or ^{124}Ce) are compared, it is found that ^{20}Ne has lowest $T_{1/2}$ value. Also when emission of ^{26}Mg and ^{24}Mg from the same parent (either ^{122}Ce or ^{124}Ce) are compared it is found that ^{24}Mg has the lowest $T_{1/2}$ value. This points to the fact that clusters with N = Z are most probable for decay [100].

Table 4.10. Logarithm of predicted half life time and other characteristic of ^{4}He emission from various Ce isotopes. Q values are taken from [88]. Table taken from [100].

Parent nuclei	Emitted cluster	Daughter nuclei	Q value (MeV)	Penetrability P	Decay Constant λ	$\log_{10}(T_{1/2})$ Present	CYEM [87]	ASAFM [90]	PCM [86]
^{116}Ce	^{4}He	^{112}Ba	3.09[a]	2.94866E-29	4.186E-09	8.219			6.15
^{118}Ce	^{4}He	^{114}Ba	2.58[a]	2.84922E-34	3.377E-14	13.31			11.04
			3.18	2.48935E-28	3.637E-08	7.28	7.25	6.60	
			1.48	3.48632E-53	2.371E-33	32.47	32.16	31.20	
			3.40	1.37099E-26	2.141E-06	5.51	5.49	5.00	
			3.57	2.32192E-25	3.808E-05	4.26	4.24	3.80	
			2.46	1.07345E-35	1.213E-15	14.76	14.58	13.70	
^{120}Ce	^{4}He	^{116}Ba	2.33[a]	2.77794E-37	2.974E-17	16.37			12.98
			3.16	1.69366E-28	2.459E-08	7.45	7.35	6.80	
			2.71	9.29767E-33	1.158E-12	11.78	11.64	11.00	
			1.21	2.30783E-61	1.283E-41	40.73	40.39	39.20	
			2.57	2.67839E-34	3.092E-14	13.35	13.20	12.50	
			2.26	3.07880E-38	3.197E-18	17.34	17.15	16.40	
^{121}Ce	^{4}He	^{117}Ba	2.91	1.07187E-30	1.433E-10	9.68	9.58	9.40	
			2.24	1.75322E-38	1.804E-18	17.58	17.40	17.20	
			2.37	1.01686E-36	1.107E-16	15.80	15.63	15.50	
			4.24	2.95902E-21	5.764E-01	0.08	-0.02	0.10	
			1.88	2.75865E-44	2.383E-24	23.46	23.24	23.10	
			2.26	3.34953E-38	3.478E-18	17.30	17.12	16.80	
^{122}Ce	^{4}He	^{118}Ba	2.09[a]	1.10523E-40	1.061E-20	19.81			14.74
			2.87	4.78737E-31	6.312E-11	10.04	9.94	9.50	
			2.18	2.58513E-39	2.589E-19	18.43	18.25	17.70	
			2.46	1.51690E-35	1.714E-15	14.61	14.46	13.80	
			1.70	8.04444E-48	6.283E-28	27.04	26.80	26.20	
			2.26	3.63247E-38	3.772E-18	17.26	17.09	16.50	
^{123}Ce	^{4}He	^{119}Ba	2.43	6.96022E-36	7.770E-16	14.95	14.80	14.60	
			1.86	1.37411E-44	1.174E-24	23.77	23.56	23.50	
			2.03	1.30122E-41	1.214E-21	20.76	20.56	20.50	
			1.54	1.79278E-51	1.268E-31	30.74	30.48	30.50	
			2.04	1.89568E-41	1.777E-21	20.59	20.40	20.20	
^{124}Ce	^{4}He	^{120}Ba	1.73[a]	4.01922E-47	3.195E-27	26.34			21.48
			1.70	9.34546E-48	7.299E-28	26.98	26.75	26.20	
			2.12	3.76460E-40	3.667E-20	19.28	19.10	18.60	
			1.38	9.47770E-56	6.009E-36	35.06	34.78	34.00	
			2.02	9.59652E-42	9.806E-22	20.89	20.70	20.10	

[a] Q values are taken from Ref [86].

Table 4.11. Logarithm of predicted half life time and other characteristic of ^{16}O emission from various Ce isotopes. Q values are taken from [88]. Table taken from [100].

Parent nuclei	Emitted cluster	Daughter nuclei	Q value (MeV)	Penetrability P	Decay Constant λ	$\log_{10}(T_{1/2})$ Present	CYEM [87]	ASAFM [90]	PCM [86]
^{116}Ce	^{16}O	^{100}Sn	31.71[a]	6.12654E-28	5.292E-07	6.12			6.14
^{118}Ce	^{16}O	^{102}Sn	29.94[a]	3.12705E-31	2.551E-10	9.43			10.79
			29.26	1.01470E-32	8.087E-12	10.93	10.97	11.90	
			27.97	1.13475E-35	8.645E-15	13.90	13.74	14.50	
			29.97	3.62921E-31	2.983E-10	9.37	9.51	10.60	
			29.08	4.02489E-33	3.188E-12	11.34	11.34	12.30	
			29.75	1.21218E-31	9.823E-11	9.85	9.96	11.00	
^{120}Ce	^{16}O	^{104}Sn	27.12[a]	2.30664E-37	1.704E-16	15.61			16.79
			27.73	6.90985E-36	5.219E-15	14.12	14.05	14.80	
			26.88	5.88827E-38	4.311E-17	16.21	16.00	16.60	
			25.02	8.34774E-43	5.689E-22	21.09	20.60	20.80	
			27.19	3.42476E-37	2.536E-16	15.44	15.28	15.90	
			26.87	5.56068E-38	4.069E-17	16.23	16.03	16.60	
^{121}Ce	^{16}O	^{105}Sn	26.16	1.29644E-39	9.238E-19	17.88	17.62	19.70	
			25.48	2.13035E-41	1.478E-20	19.67	19.31	21.30	
			25.61	4.72578E-41	3.296E-20	19.32	18.99	21.00	
			27.48	2.54666E-36	1.906E-15	14.56	14.51	16.90	
			25.12	2.27876E-42	1.559E-21	20.65	20.24	22.20	
			25.51	2.56161E-41	1.780E-20	19.59	19.24	21.20	
^{122}Ce	^{16}O	^{106}Sn	24.69[a]	2.13691E-43	1.437E-22	21.68			28.07
			25.13	3.48409E-42	2.385E-21	20.46	20.11	20.40	
			24.44	4.24473E-44	2.826E-23	22.39	21.93	22.10	
			24.73	2.76185E-43	1.860E-22	21.57	21.16	21.40	
			23.96	1.78793E-45	1.167E-24	23.77	23.25	23.30	
			24.52	7.13718E-44	4.767E-23	22.16	21.72	21.90	
^{123}Ce	^{16}O	^{107}Sn	23.61	2.36815E-46	1.523E-25	24.66	24.13	25.80	
			23.03	4.21602E-48	2.645E-27	26.42	25.81	27.40	
			23.20	1.39287E-47	8.802E-27	25.90	25.31	26.90	
			22.71	4.30003E-49	2.660E-28	27.42	26.76	28.30	
			23.22	1.60187E-47	1.013E-26	25.84	25.25	26.90	
^{124}Ce	^{16}O	^{108}Sn	22.26[a]	2.22455E-50	1.349E-29	28.71			37.39
			22.59	2.50263E-49	1.540E-28	27.65	27.02	26.90	
			21.89	1.38886E-51	8.281E-31	29.92	29.19	28.90	
			21.58	1.29239E-52	7.596E-32	30.96	30.18	29.80	
			22.22	1.65334E-50	1.001E-29	28.84	28.16	27.90	

[a] Q values are taken from Ref [86].

Table 4.12. Logarithm of predicted half life time and other characteristic for ^{8}Be, ^{12}C, ^{20}Ne, ^{22}Ne, ^{24}Mg, ^{26}Mg, and ^{28}Si emission from various Ce isotopes and comparison with PCM. Q values are taken from [86]. Table taken from [100].

Parent nuclei	Emitted cluster	Daughter nuclei	Q value (MeV)	Penetrability P	Decay constant	$\log_{10}(T_{1/2})$ Present Cal I	Present Cal II	PCM [86]
^{116}Ce	^{8}Be	^{108}Xe	7.32	2.74101E-47	6.198E-27	26.05	25.68	23.52
^{118}Ce		^{110}Xe	5.61	1.35520E-60	2.348E-40	39.47	39.07	35.48
^{120}Ce		^{112}Xe	4.55	2.39877E-72	3.371E-52	51.31	50.94	49.01
^{122}Ce		^{114}Xe	3.89	5.86879E-82	7.052E-62	60.99	60.66	55.36
^{124}Ce		^{116}Xe	3.17	9.19393E-96	9.002E-76	74.89	74.57	66.03
^{116}Ce	^{12}C	^{104}Te	21.17	1.18197E-28	6.969E-08	6.998	7.214	6.200
^{118}Ce		^{106}Te	17.46	1.29786E-38	6.311E-18	17.04	17.06	16.47
^{120}Ce		^{108}Te	15.19	2.83273E-46	1.198E-25	24.76	24.78	25.08
^{122}Ce		^{110}Te	14.80	1.41766E-47	5.844E-27	26.07	26.28	30.57
^{124}Ce		^{112}Te	12.77	2.13625E-56	7.598E-36	34.96	35.19	40.77
^{116}Ce	^{20}Ne	^{96}Cd	34.76	8.04943E-42	7.586E-21	19.96	19.47	19.68
^{118}Ce		^{98}Cd	34.48	5.58809E-42	5.224E-21	20.12	20.06	22.36
^{120}Ce		^{100}Cd	32.50	2.87741E-46	2.536E-25	24.44	24.46	26.82
^{122}Ce		^{102}Cd	28.58	1.82296E-56	1.413E-35	34.69	34.48	41.15
^{124}Ce		^{104}Cd	26.53	1.78461E-62	1.284E-41	40.73	40.58	50.11
^{122}Ce	^{22}Ne	^{100}Cd	26.38	3.07499E-64	2.198E-43	42.50	41.06	49.98
^{124}Ce		^{102}Cd	26.10	7.51923E-65	5.318E-44	43.12	41.95	53.86
^{116}Ce	^{24}Mg	^{92}Pd	41.16	1.00526E-46	1.121E-25	24.79	23.99	25.81
^{118}Ce		^{94}Pd	41.53	2.48944E-45	2.801E-24	23.39	23.36	26.39
^{120}Ce		^{96}Pd	40.87	2.96583E-46	3.283E-25	24.32	24.56	26.50
^{122}Ce		^{98}Pd	37.73	3.74020E-53	3.823E-32	31.26	31.21	40.43
^{124}Ce		^{100}Pd	34.65	8.83675E-61	8.294E-40	38.92	38.59	45.89
^{122}Ce	^{26}Mg	^{96}Pd	34.89	5.74934E-61	5.433E-40	39.11	37.98	46.79
^{124}Ce		^{98}Pd	33.01	4.63836E-66	4.147E-45	44.22	42.94	46.95
^{116}Ce	^{28}Si	^{88}Ru	48.26	2.41571E-48	3.157E-27	26.34	25.71	27.68
^{118}Ce		^{90}Ru	48.18	7.89775E-48	1.031E-26	25.83	25.85	28.50
^{120}Ce		^{92}Ru	48.10	2.29684E-47	2.992E-26	25.37	25.99	27.50
^{122}Ce		^{94}Ru	46.56	4.10641E-50	5.178E-29	28.13	28.79	37.28
^{124}Ce		^{96}Ru	43.06	1.08941E-57	1.270E-36	35.74	35.69	41.69

Table 4.13. Slope and intercept values of Geiger-Nuttall plots for different clusters from various Ce isotopes.

Emitted cluster	Slope X	Intercept Y
^{4}He	95.79888	-46.43929
^{8}Be	254.20336	-67.87994
^{12}C	446.96278	-90.04361
^{16}O	659.11292	-110.94215
^{20}Ne	857.25478	-125.71802
^{24}Mg	1043.9027	-138.51576
^{28}Si	1181.4194	-144.47783

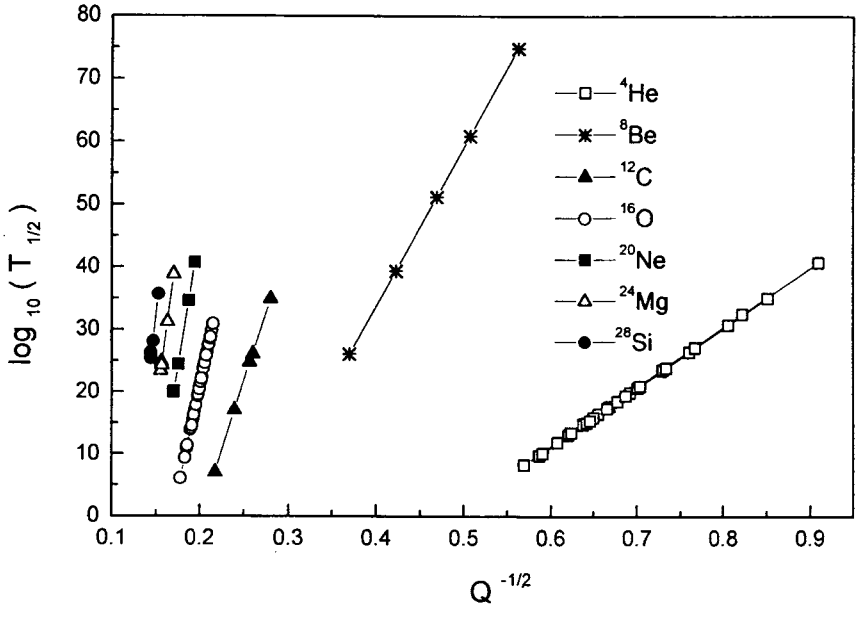

Fig. 4.21 Geiger Nuttall plot for $\log_{10}(T_{1/2})$ Vs $Q^{-1/2}$ for various clusters from different Ce isotopes.

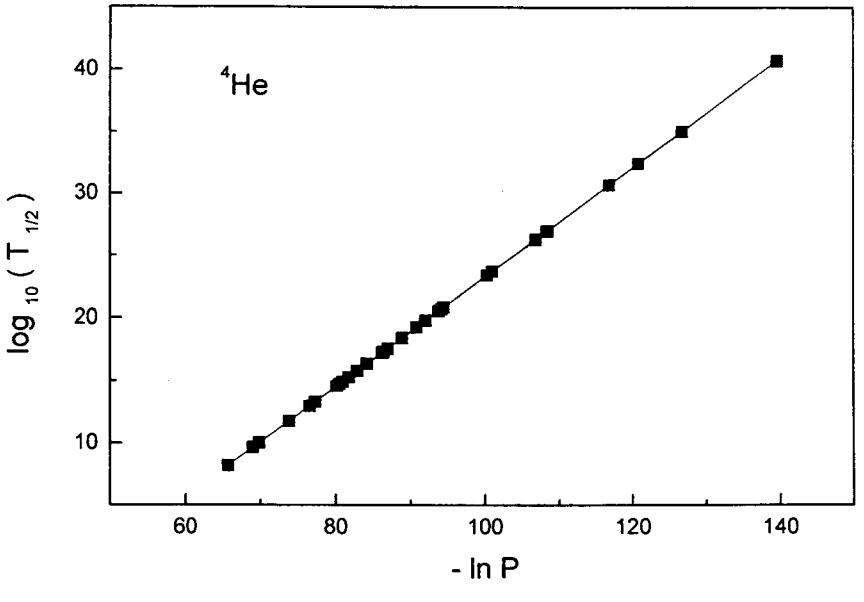

Fig. 4.22 Geiger Nuttall plot for $\log_{10}(T_{1/2})$ vs –lnP for ^{4}He emission from various Ce isotopes.

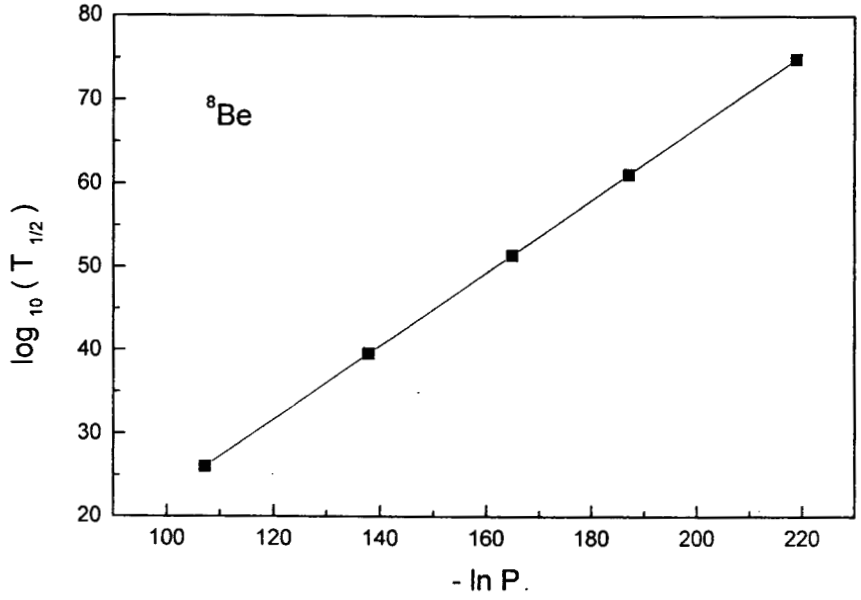

Fig. 4.23 Geiger Nuttall plot for $\log_{10}(T_{1/2})$ vs –lnP for ^{8}Be emission from various Ce isotopes.

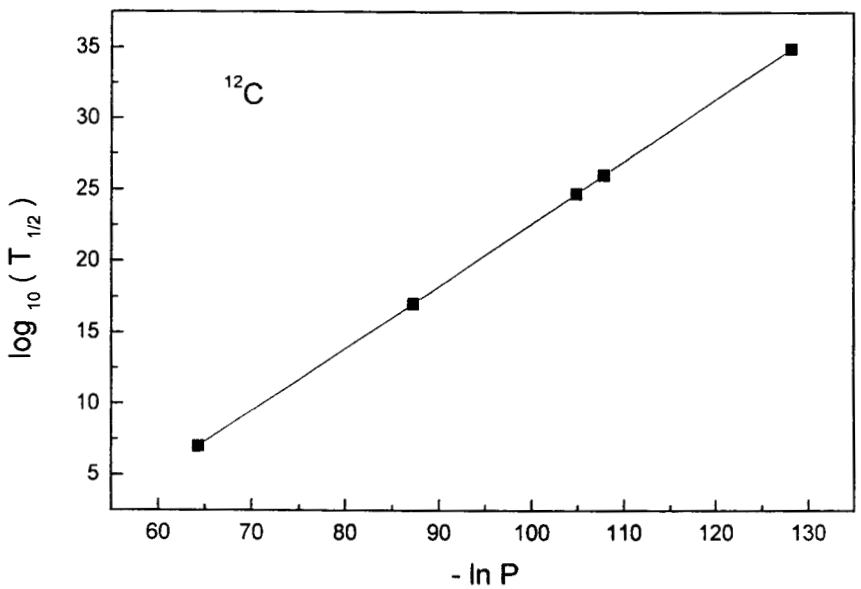

Fig. 4.24 Geiger Nuttall plot for $\log_{10}(T_{1/2})$ vs –lnP for ^{12}C emission from various Ce isotopes.

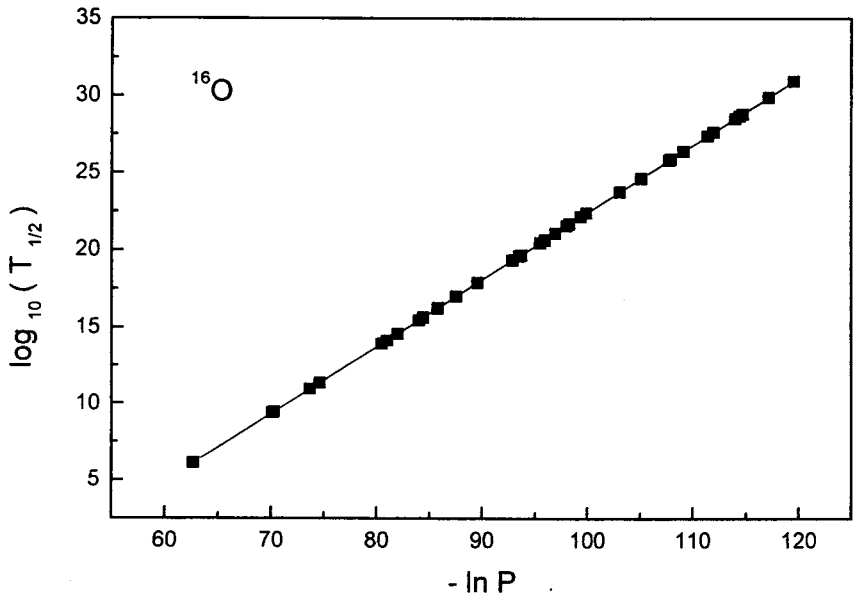

Fig. 4.25 Geiger Nuttall plot for $\log_{10}(T_{1/2})$ vs $-\ln P$ for ^{16}O emission from various Ce isotopes.

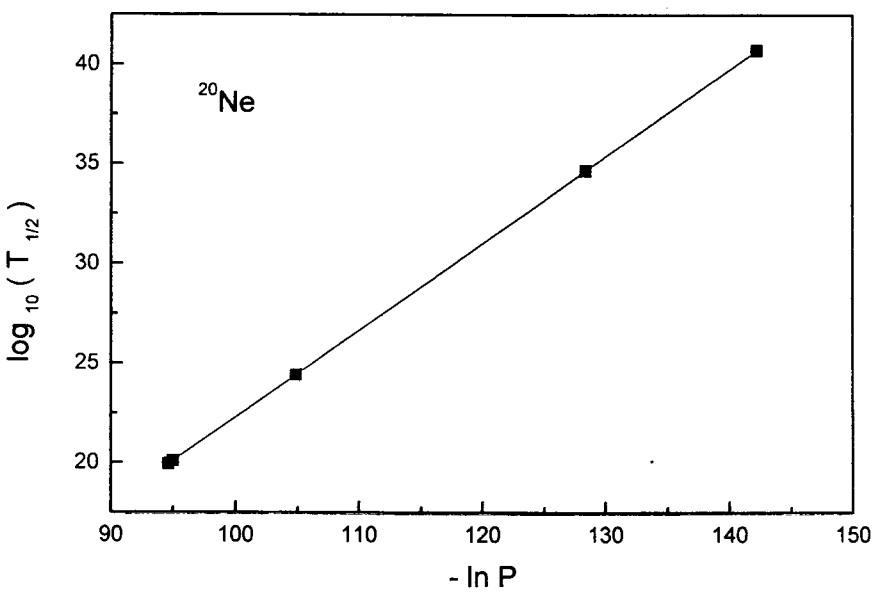

Fig. 4.26 Geiger Nuttall plot for $\log_{10}(T_{1/2})$ vs $-\ln P$ for ^{20}Ne emission from various Ce isotopes.

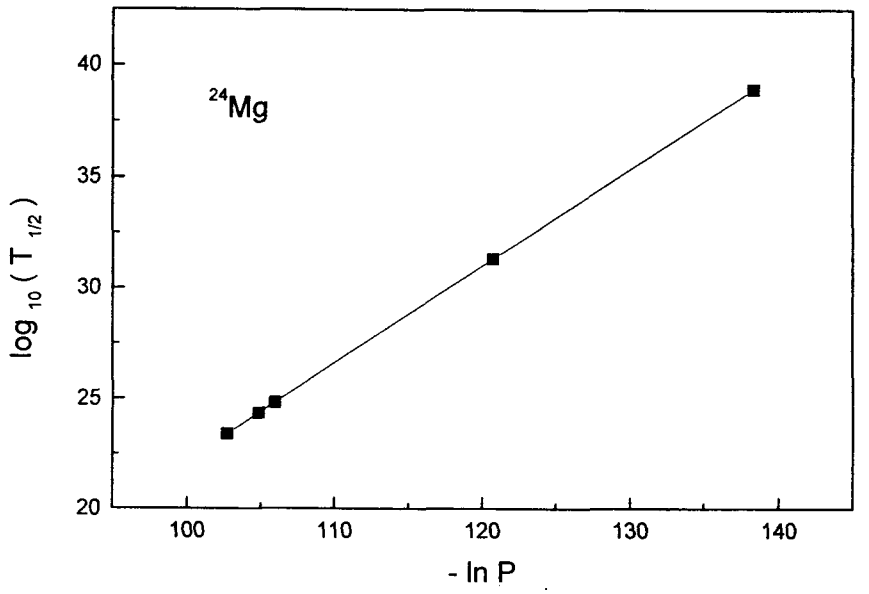

Fig. 4.27 Geiger Nuttall plot for $\log_{10}(T_{1/2})$ Vs –lnP for ^{24}Mg emission from various Ce isotopes.

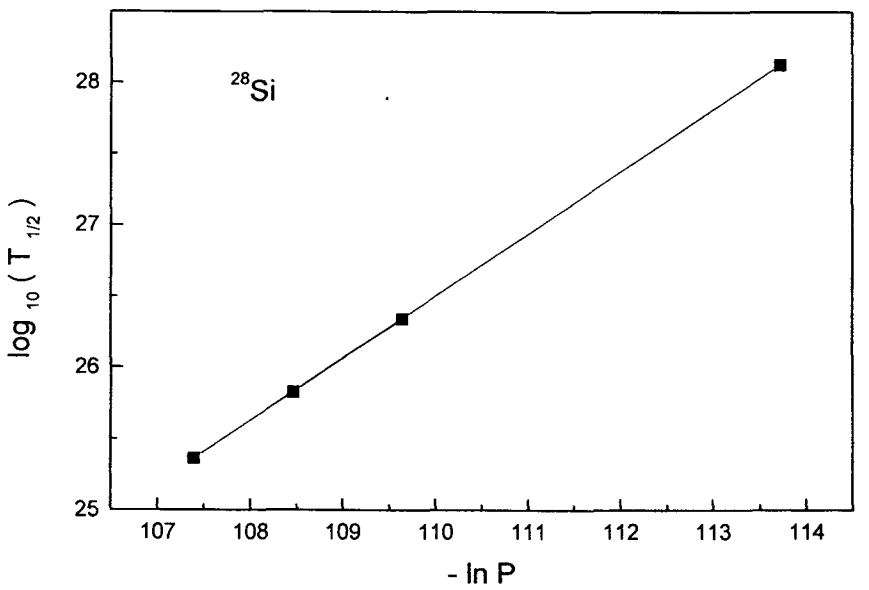

Fig. 4.28 Geiger Nuttall plot for $\log_{10}(T_{1/2})$ Vs –lnP for ^{28}Si emission from various Ce isotopes.

4.2.1.4 Neodymium isotopes

Tables 4.14 to 4.19 give the logarithm of predicted half life time for the emission of ^{4}He, ^{8}Be, ^{12}C, ^{16}O, ^{20}Ne, ^{24}Mg, ^{28}Si and ^{29}Si clusters from $^{120\text{-}128}$Nd isotopes using different mass tables and their comparison with other models. The half life time predicted for ^{12}C, ^{16}O, ^{20}Ne, ^{24}Mg, ^{28}Si and ^{29}Si from various Nd isotopes are below the present upper limit for measurements ($T_{1/2} < 10^{30}$ s). It is to be noted that ^{16}O and ^{20}Ne emissions from ^{120}Nd have the smallest half life values ($T_{1/2} < 10^{14}$ s). The ^{16}O emission from ^{120}Nd refers to the near doubly magic $^{104}_{52}Te_{52}$ with N = Z = 52 but ^{20}Ne from ^{120}Nd refers to the doubly magic ^{100}Sn daughter. This points to the role of doubly magic ^{100}Sn daughter in exotic decay processes.

Figures 4.29 to 4.35 give the Geiger-Nuttall plots of predicted $\log_{10}(T_{1/2})$ vs $Q^{-1/2}$ for ^{4}He, ^{8}Be, ^{12}C, ^{16}O, ^{20}Ne, ^{24}Mg and ^{28}Si from various Nd isotopes. We notice that the Geiger-Nuttall plots for all clusters are linear with different slope and intercepts. The values of slope X and intercept Y for different clusters are given in Table 4.20.

Figures 4.36 to 4.42 give the Geiger-Nuttall plot of predicted $\log_{10}(T_{1/2})$ vs $-\ln P$ for ^{4}He, ^{8}Be, ^{12}C, ^{16}O, ^{20}Ne, ^{24}Mg and ^{28}Si from various Nd isotopes. These plots are also found to be linear.

When decay of ^{20}Ne from ^{120}Nd is compared with that from heavier isotopes up to ^{126}Nd it is found that $\log_{10}(T_{1/2})$ value increases from 14.13 s (for ^{120}Nd, Q = 39.41 MeV) to 30.63 s (for ^{126}Nd, Q = 31.72 MeV). All these cases refer to the doubly magic or near doubly magic daughter Sn nuclei. This point to the fact that the neutron excesses in the parent nuclei slows down the exotic decay process.

Table 4.14. Logarithm of predicted half life time and other characteristics of ^{4}He emission from various Nd isotopes and comparison with other models. Q values are taken from [84,85].

Parent nuclei	Emitted cluster	Daughter nuclei	Q value (MeV)	Penetrability P	Decay Constant λ	$\log_{10}(T_{1/2})$ Present	CYEM [87]	ASAFM [84]	PCM [86]
^{120}Nd	^{4}He	^{116}Ce	3.03[a]	2.7218E-31	3.7889E-11	10.26			6.69
^{121}Nd	^{4}He	^{117}Ce	1.77	1.1399E-48	9.2696E-29	27.87		27.10	
^{122}Nd	^{4}He	^{118}Ce	2.55	2.6815E-36	3.1415E-16	15.34	15.15	14.30	
			1.74	2.9086E-49	2.3252E-29	28.47	28.17	27.10	
			2.53	1.5324E-36	1.7812E-16	15.59	15.39	14.60	
			2.32	2.8012E-39	2.9857E-19	18.36	18.14	17.30	
			2.95[a]	5.7269E-32	7.7618E-12	10.95			7.56
^{123}Nd	^{4}He	^{119}Ce	3.10	1.5906E-30	2.2653E-10	9.49	9.36	9.30	
			2.21	7.9415E-41	8.0633E-21	19.93	19.71	19.60	
			1.69	2.5641E-50	1.9909E-30	29.54	29.24	28.90	
			2.19	3.9679E-41	3.9923E-21	20.24	20.01	19.70	
			2.01	4.8703E-44	4.4975E-24	23.19	22.93	22.80	
			2.64	3.3693E-35	4.0866E-15	14.23	14.05	13.90	
			2.72	2.6588E-34	3.3226E-14	13.32		12.90	
^{124}Nd	^{4}He	^{120}Ce	2.81[a]	2.6692E-33	3.4459E-13	12.30			8.71
			2.93	4.3766E-32	5.8914E-12	11.07		10.30	
			1.95	4.6443E-45	4.1608E-25	24.22		23.10	
			1.70	4.6682E-50	3.6460E-30	29.28		28.10	
			2.19	4.3331E-41	4.3598E-21	20.20		19.20	
			1.83	2.4871E-47	2.0910E-27	26.52		25.40	
			2.81	2.6692E-33	3.4459E-13	12.30		11.60	
^{125}Nd	^{4}He	^{121}Ce	2.90	2.4077E-32	3.2079E-12	11.33	11.20	11.10	
			1.88	2.5402E-46	2.1939E-26	25.50	25.24	25.20	
			1.90	6.0701E-46	5.2987E-26	25.17	24.86	24.80	
			3.58	1.1085E-26	1.8232E-06	5.56	5.39	5.40	
			2.60	1.3772E-35	1.6451E-15	14.62	14.46	14.50	
			2.66	6.7779E-35	8.2832E-15	13.92		13.70	
^{126}Nd	^{4}He	^{122}Ce	2.85	8.1778E-33	1.0708E-12	11.81		11.30	
			1.79	4.5676E-48	3.7563E-28	27.27		26.40	
			1.93	2.3704E-45	2.1018E-25	24.52		23.70	
			3.36	3.3509E-28	5.1728E-08	7.12		6.70	
			2.46	2.9011E-37	3.2788E-17	16.33		15.50	
			2.54	2.8724E-36	3.3519E-16	15.32		14.60	
^{127}Nd	^{4}He	^{123}Ce	2.82	4.3437E-33	5.6277E-13	12.09		12.10	
			3.18	1.1396E-29	1.6649E-09	8.62		8.70	
^{128}Nd	^{4}He	^{124}Ce	2.76	1.0903E-33	1.3825E-13	12.70		12.10	
			3.68	6.7558E-26	1.1422E-05	4.78		4.30	

[a] Q values are taken from [86].

Table 4.15. Logarithm of predicted half life time and other characteristics of ^{8}Be and ^{12}C emission from various Nd isotopes and comparison with other models. Q values are taken from [84,85].

Parent nuclei	Emitted cluster	Daughter nuclei	Q value (MeV)	Penetrability P	Decay Constant λ	$\log_{10}(T_{1/2})$ Present	ASAFM [84]	PCM [86]
^{120}Nd	^{8}Be	^{112}Ba	6.02[a]	4.6768E-60	8.6969E-40	38.90		35.08
^{122}Nd	^{8}Be	^{114}Ba	5.43[a]	1.2999E-65	2.1804E-45	44.50		39.70
^{124}Nd	^{8}Be	^{116}Ba	5.04[a]	8.8320E-70	1.3750E-49	48.70		43.76
^{127}Nd	^{8}Be	^{119}Ba	7.72	8.1407E-47	1.9413E-26	25.55	25.50	
^{128}Nd	^{8}Be	^{120}Ba	7.99	4.1656E-45	1.0281E-24	23.83	22.70	
^{120}Nd	^{12}C	^{108}Xe	17.71[a]	5.1825E-41	2.5562E-20	19.43		20.83
^{122}Nd	^{12}C	^{110}Xe	15.92[a]	6.2252E-47	2.7602E-26	25.40		25.58
			16.45	5.3391E-45	2.4461E-24	23.45	22.20	
			17.14	1.3057E-42	6.2331E-22	21.05	20.00	
^{124}Nd	^{12}C	^{112}Xe	14.72[a]	2.0051E-51	8.2202E-31	29.93		32.71
			16.73	9.2349E-44	4.3029E-23	22.21	21.20	
			16.46	1.0336E-44	4.7381E-24	23.17	22.10	
^{125}Nd	^{12}C	^{113}Xe	17.60	1.0188E-40	4.9939E-20	19.14	20.00	
^{126}Nd	^{12}C	^{114}Xe	15.39	1.7594E-48	7.5412E-28	26.96	25.60	
			17.89	1.1316E-39	5.6383E-19	18.09	17.60	
			14.65	1.7243E-51	7.0354E-31	29.99	28.40	
^{127}Nd	^{12}C	^{115}Xe	16.87	6.2397E-43	2.9317E-22	21.37	22.10	
^{128}Nd	^{12}C	^{116}Xe	16.96	1.6255E-42	7.6778E-22	20.96	20.20	

[a] Q values are taken from [86].

Table 4.16. Logarithm of predicted half life time and other characteristics of ^{16}O emission from various Nd isotopes and comparison with other models. Q values are taken from [84,85].

Parent nuclei	Emitted cluster	Daughter nuclei	Q value (MeV)	Penetrability P	Decay Constant λ	$\log_{10}(T_{1/2})$ Present	CYEM [87]	ASAFM [84]	PCM [86]
^{120}Nd	^{16}O	^{104}Te	31.36[a]	7.6626E-32	6.5451E-11	10.02			11.90
^{121}Nd	^{16}O	^{105}Te	24.68	5.0070E-48	3.3658E-27	26.31		26.60	
^{122}Nd	^{16}O	^{106}Te	22.57[a]	2.5608E-54	1.5742E-33	32.64			20.12
			27.49	2.5910E-40	1.9401E-19	18.55	17.99	18.20	
			25.39	7.7388E-46	5.3518E-25	24.11	23.23	23.00	
			28.18	1.2806E-38	9.8289E-18	16.85	16.40	16.70	
			27.08	2.3992E-41	1.7696E-20	19.59	18.97	19.10	
^{123}Nd	^{16}O	^{107}Te	28.01	7.4767E-39	5.7041E-18	17.08	16.67	18.60	
			26.24	2.3561E-43	1.6840E-22	21.91	20.93	22.60	
			23.83	3.4639E-50	2.2483E-29	28.49	27.44	28.30	
			26.50	1.1440E-42	8.2575E-22	20.92	20.28	22.00	
			25.74	1.0628E-44	7.4513E-24	22.97	22.21	23.80	
			26.95	1.6792E-41	1.2326E-20	19.75	19.18	20.90	
^{124}Nd	^{16}O	^{108}Te	25.16[a]	3.8756E-46	2.6559E-25	24.42			28.49
			25.40	1.8168E-45	1.2569E-24	23.74		22.80	
			23.29	1.1027E-51	6.9952E-31	29.99		28.40	
			25.95	5.8220E-44	4.1150E-23	22.23		21.50	
			26.96	2.6387E-41	1.9376E-20	19.55		19.20	
			24.85	5.1131E-47	3.4608E-26	25.30		24.20	
			26.55	2.2878E-42	1.6545E-21	20.62		20.10	
^{125}Nd	^{16}O	^{109}Te	25.87	5.1482E-44	3.6276E-23	22.28		23.30	
			24.17	7.6866E-49	5.0602E-28	27.14		27.60	
			24.32	2.1377E-48	1.4161E-27	26.69		27.20	
			27.87	7.3975E-39	5.6155E-18	17.09		18.80	
			23.82	6.8286E-50	4.4304E-29	28.19		28.60	
			25.22	8.2946E-46	5.6978E-25	24.09		24.90	
^{126}Nd	^{16}O	^{110}Te	25.25	1.4423E-45	9.9192E-25	23.84		23.00	
			23.50	1.0175E-50	6.5124E-30	29.03		27.60	
			23.93	2.0943E-49	1.3650E-28	27.71		26.50	
			27.75	5.4108E-39	4.0897E-18	17.23		17.30	
			23.17	9.4786E-52	5.9819E-31	30.06		28.60	
			24.26	2.0289E-48	1.3406E-27	26.71		25.60	
^{127}Nd	^{16}O	^{111}Te	23.86	1.8104E-49	1.1766E-28	27.77		28.30	
			26.41	2.9207E-42	2.1009E-21	20.52		21.90	
^{128}Nd	^{16}O	^{112}Te	23.00	5.3244E-52	3.3355E-31	30.32		28.90	
			25.92	2.0036E-43	1.4145E-22	21.69		21.30	

[a] Q values are taken from [86].

Table 4.17. Logarithm of predicted half life time and other characteristics of ^{20}Ne emission from various Nd isotopes and comparison with other models. Q values are taken from [84,85].

Parent nuclei	Emitted cluster	Daughter nuclei	Q value (MeV)	Penetrability P	Decay Constant λ	$\log_{10}(T_{1/2})$ Present	ASAFM [84]	PCM [86]
^{120}Nd	^{20}Ne	^{100}Sn	39.41[a]	4.8049E-36	5.1342E-15	14.13		17.04
^{122}Nd	^{20}Ne	^{102}Sn	37.62[a]	2.8752E-39	2.9327E-18	17.37		18.69
			36.55	1.3622E-41	1.3499E-20	19.71	19.60	
			37.24	4.3911E-40	4.4337E-19	18.19	18.30	
			36.14	1.6641E-42	1.6307E-21	20.63	20.40	
^{123}Nd	^{20}Ne	^{103}Sn	36.73	5.7403E-41	5.7167E-20	19.08	20.70	
			34.96	5.5433E-45	5.2544E-24	23.12	24.10	
			35.22	2.2355E-44	2.1348E-23	22.51	23.60	
			34.46	3.6550E-46	3.4150E-25	24.31	25.20	
			35.67	2.4229E-43	2.3433E-22	21.47	22.70	
			36.13	2.6637E-42	2.6094E-21	20.42	21.80	
^{124}Nd	^{20}Ne	^{104}Sn	34.66[a]	1.7929E-45	1.6849E-24	23.61		28.07
			33.57	4.1608E-48	3.7872E-27	26.26	25.40	
			34.12	9.1612E-47	8.4751E-26	24.91	24.20	
			33.02	1.7688E-49	1.5836E-28	27.64	26.50	
			34.33	2.9331E-46	2.7302E-25	24.40	23.80	
			34.72	2.4859E-45	2.3402E-24	23.47	23.00	
^{126}Nd	^{20}Ne	^{106}Sn	31.72	1.9072E-52	1.6403E-31	30.63	29.30	

[a] Q values are taken from [86].

Table 4.18. Logarithm of predicted half life time and other characteristics of ^{24}Mg emission from various Nd isotopes and comparison with other models. Q values are taken from [84,85].

Parent nuclei	Emitted cluster	Daughter nuclei	Q value (MeV)	Penetrability P	Decay Constant λ	$\log_{10}(T_{1/2})$ Present	ASAFM [84]	PCM [86]
^{120}Nd	^{24}Mg	^{96}Cd	47.09[a]	1.8939E-39	2.4159E-18	17.46		20.83
^{122}Nd	^{24}Mg	^{98}Cd	46.76[a]	1.6905E-39	2.1412E-18	17.51		18.78
			46.31	2.1650E-40	2.7160E-19	18.41	19.00	
			44.21	1.0865E-44	1.3011E-23	22.73	22.60	
			47.00	5.0133E-39	6.3827E-18	17.04	17.90	
			45.90	3.2640E-41	4.0583E-20	19.23	19.70	
^{123}Nd	^{24}Mg	^{99}Cd	46.45	7.8735E-40	9.9069E-19	17.84	20.10	
			44.68	1.9777E-43	2.3936E-22	21.46	23.00	
			42.27	1.3132E-48	1.5037E-27	26.66	27.30	
			44.94	6.8406E-43	8.3275E-22	20.92	22.60	
			44.18	1.7759E-44	2.1253E-23	22.51	23.90	
			45.39	5.7471E-42	7.0664E-21	19.99	21.80	
			45.85	4.9383E-41	6.1334E-20	19.05	21.10	
^{124}Nd	^{24}Mg	^{100}Cd	44.61[a]	2.6190E-43	3.1649E-22	21.34		25.63
			44.92	1.1540E-42	1.4042E-21	20.69	21.10	
			43.09	1.5223E-46	1.7768E-25	24.59	24.40	
			40.98	2.8659E-51	3.1814E-30	29.34	28.30	
			43.64	2.3367E-45	2.7622E-24	23.39	23.40	
			44.65	3.1735E-43	3.8383E-22	21.26	21.60	
			42.54	9.5103E-48	1.0959E-26	25.80	25.40	
			43.85	6.5586E-45	7.7905E-24	22.95	23.00	
			44.26	4.8381E-44	5.8006E-23	22.08	22.30	
^{125}Nd	^{24}Mg	^{101}Cd	43.10	2.8762E-46	3.3580E-25	24.32	25.60	
			41.40	4.6920E-50	5.2619E-29	28.12	28.80	
			41.55	1.0306E-49	1.1599E-28	27.78	28.50	
			45.10	4.9337E-42	6.0274E-21	20.06	22.10	
			41.05	7.3804E-51	8.2068E-30	28.93	29.50	
			42.14	2.2015E-48	2.5131E-27	26.44	27.40	
			42.45	1.0773E-47	1.2388E-26	25.75	26.80	
^{126}Nd	^{24}Mg	^{102}Cd	41.86	9.0606E-49	1.0274E-27	26.83	26.40	
			40.11	8.0580E-53	8.7551E-32	30.89	29.90	
			40.54	8.3476E-52	9.1671E-31	29.88	29.00	
			40.87	4.9176E-51	5.4443E-30	29.11	28.40	
			41.12	1.8627E-50	2.0748E-29	28.52	27.90	

[a] Q values are taken from [86].

Table 4.19. Logarithm of predicted half life time and other characteristics of ^{28}Si and ^{29}Si emission from various Nd isotopes and comparison with other models. Q values are taken from [84,85].

Parent nuclei	Emitted cluster	Daughter nuclei	Q value (MeV)	Penetrability P	Decay Constant λ	$\log_{10}(T_{1/2})$ Present	CYEM [87]	ASAFM [84]	PCM [86]
^{120}Nd	^{28}Si	^{92}Pd	54.17[a]	2.2041E-42	3.2336E-21	20.33			23.76
^{122}Nd	^{28}Si	^{94}Pd	54.41[a]	3.2349E-41	4.7671E-20	19.16			20.00
^{123}Nd	^{28}Si	^{95}Pd	52.50	1.3348E-44	1.8979E-23	22.56		24.30	
			50.09	1.6539E-49	2.2437E-28	27.49		28.30	
			52.76	4.3661E-44	6.2388E-23	22.05		23.90	
			52.00	1.3424E-45	1.8906E-24	23.56		25.10	
			53.21	3.3464E-43	4.8225E-22	21.16		23.20	
			53.67	2.6340E-42	3.8287E-21	20.26		22.50	
^{124}Nd	^{28}Si	^{96}Pd	53.66[a]	5.2821E-42	7.6765E-21	19.96			23.87
			54.34	1.0841E-40	1.5955E-19	18.64		20.10	
			52.51	2.9069E-44	4.1340E-23	22.22		22.90	
			50.40	1.4986E-48	2.0456E-27	26.53		26.40	
			53.06	3.5519E-43	5.1042E-22	21.13		22.10	
			54.07	3.2815E-41	4.8054E-20	19.16		20.50	
			51.96	2.3128E-45	3.2547E-24	23.33		23.80	
			53.27	9.1698E-43	1.3230E-21	20.72		21.70	
			53.66	5.2821E-42	7.6765E-21	19.96		21.10	
^{125}Nd	^{28}Si	^{97}Pd	52.80	2.2180E-43	3.1718E-22	21.34	19.91	23.30	
			51.10	8.3653E-47	1.1577E-25	24.78	22.97	26.40	
			51.25	1.6963E-46	2.3546E-25	24.47	22.70	26.10	
			54.80	1.6850E-39	2.5008E-18	17.44	16.45	18.80	
			50.75	1.5929E-47	2.1894E-26	25.50	23.62	27.00	
			51.84	2.6772E-45	3.7588E-24	23.26	21.62	25.20	
^{126}Nd	^{28}Si	^{98}Pd	51.00	1.0215E-46	1.4109E-25	24.69		25.20	
			49.25	2.1752E-50	2.9013E-29	28.38		28.20	
			49.68	1.7914E-49	2.4104E-28	27.46		27.40	
			53.50	1.0483E-41	1.5189E-20	19.67		21.20	
			48.92	4.2512E-51	5.6325E-30	29.09		28.20	
			50.01	8.9096E-49	1.2068E-27	26.76		26.10	
			50.26	2.9798E-48	4.0561E-27	26.23		26.40	
^{127}Nd	^{28}Si	^{99}Pd	49.33	6.1027E-50	8.1534E-29	27.93		29.20	
			51.88	1.2227E-44	1.7180E-23	22.61		24.90	
^{125}Nd	^{29}Si	^{96}Pd	51.58	1.0878E-45	1.5195E-24	23.66		26.20	
			49.88	2.9618E-49	4.0011E-28	27.24		29.10	
			50.04	6.4990E-49	8.8077E-28	26.90		28.90	
			49.54	5.5230E-50	7.4102E-29	27.97		29.70	
			50.63	1.1503E-47	1.5773E-26	25.64		27.80	
			50.93	4.8880E-47	6.7422E-26	25.01		27.30	

[a] Q values are taken from [86].

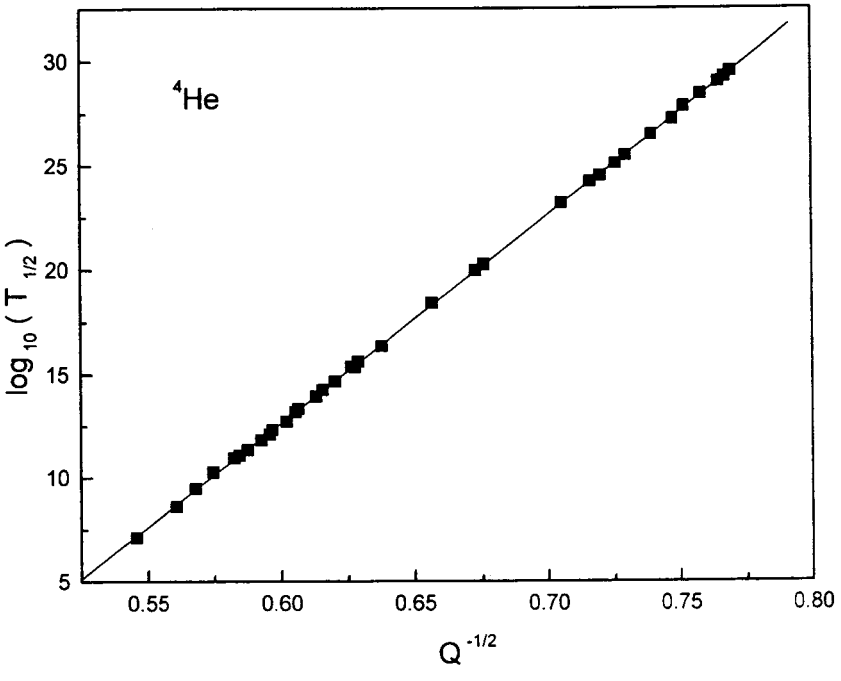

Fig. 4.29 Geiger Nuttall plot for $\log_{10}(T_{1/2})$ Vs $Q^{-1/2}$ for ^{4}He emission from various Nd isotopes.

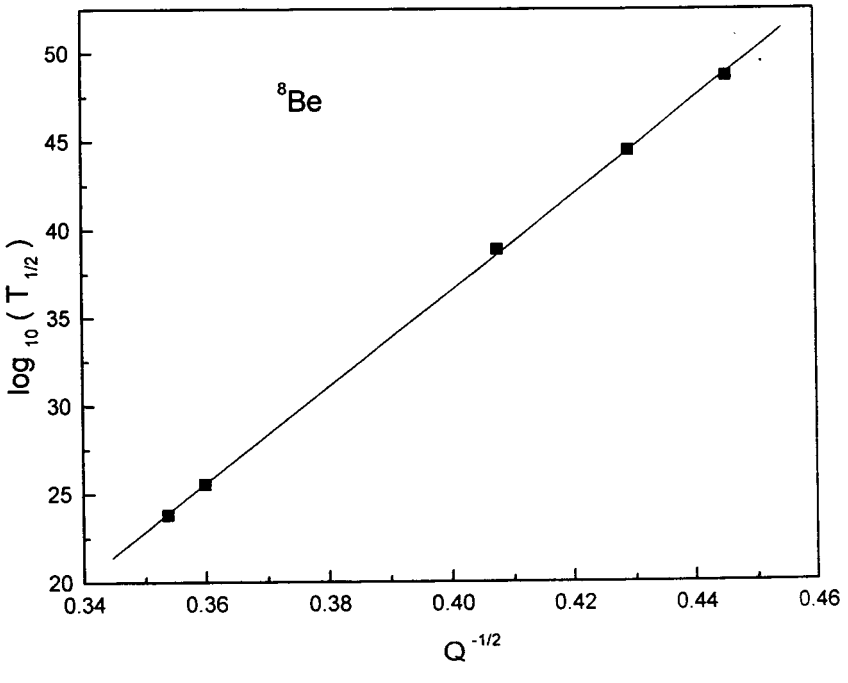

Fig. 4.30 Geiger Nuttall plot for $\log_{10}(T_{1/2})$ Vs $Q^{-1/2}$ for ^{8}Be emission from various Nd isotopes.

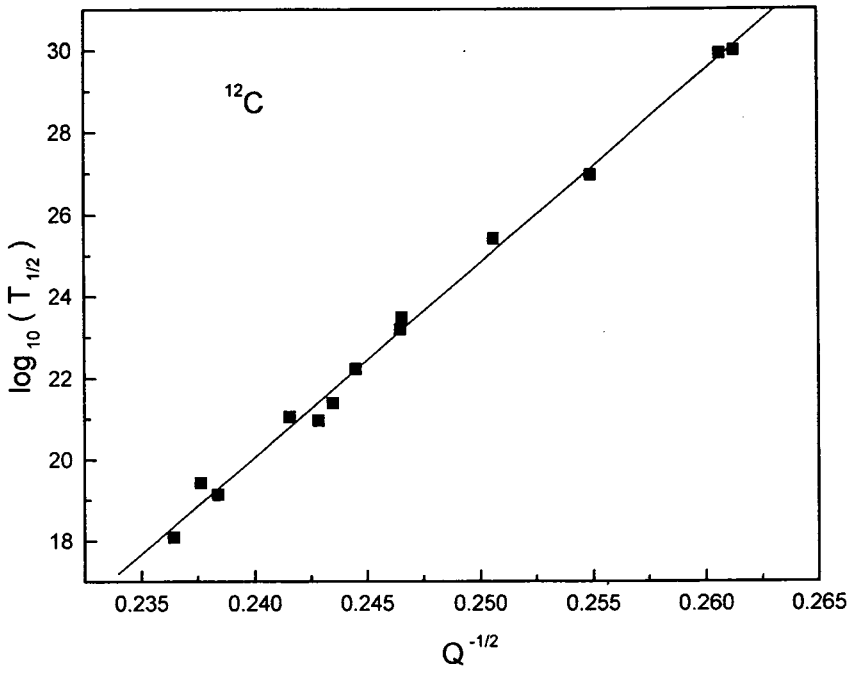

Fig. 4.31 Geiger Nuttall plot for $\log_{10}(T_{1/2})$ Vs $Q^{-1/2}$ for ^{12}C emission from various Nd isotopes.

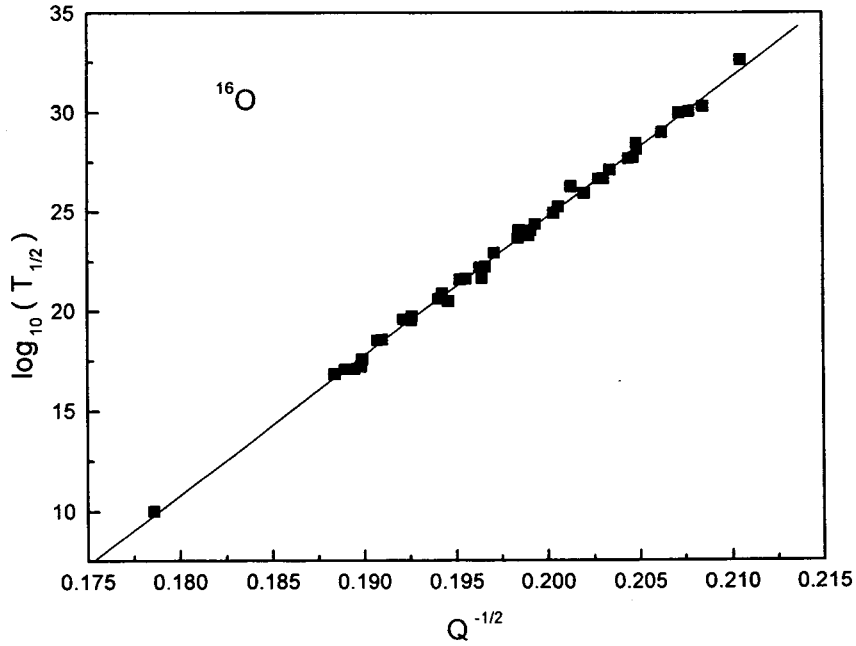

Fig. 4.32 Geiger Nuttall plot for $\log_{10}(T_{1/2})$ Vs $Q^{-1/2}$ for ^{16}O emission from various Nd isotopes.

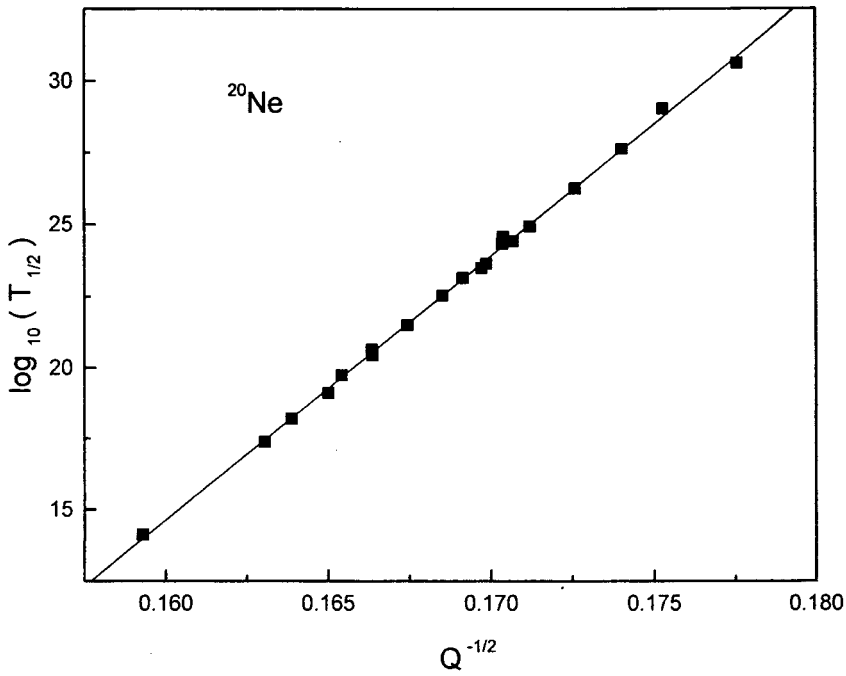

Fig. 4.33 Geiger Nuttall plot for $\log_{10}(T_{1/2})$ Vs $Q^{-1/2}$ for ^{20}Ne emission from various Nd isotopes.

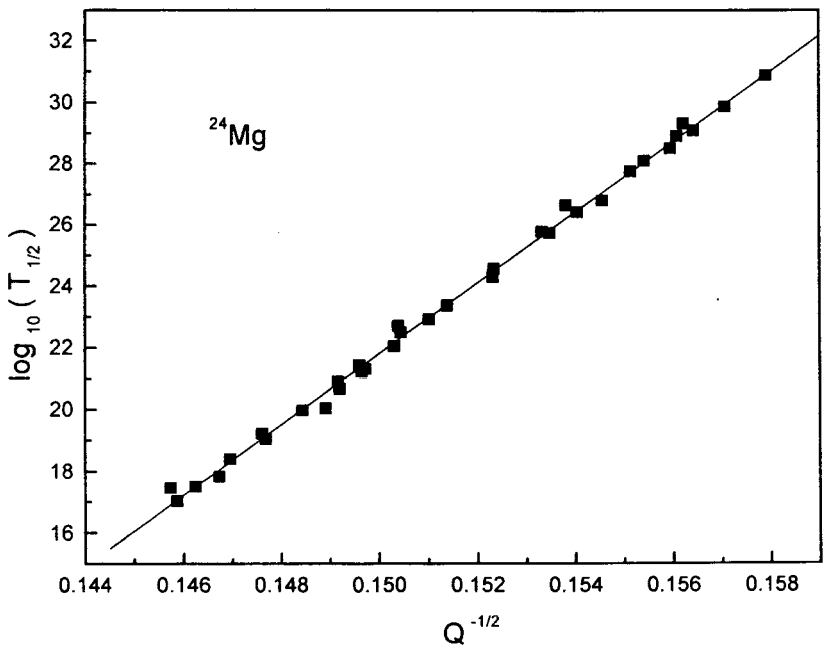

Fig. 4.34 Geiger Nuttall plot for $\log_{10}(T_{1/2})$ Vs $Q^{-1/2}$ for ^{24}Mg emission from various Nd isotopes.

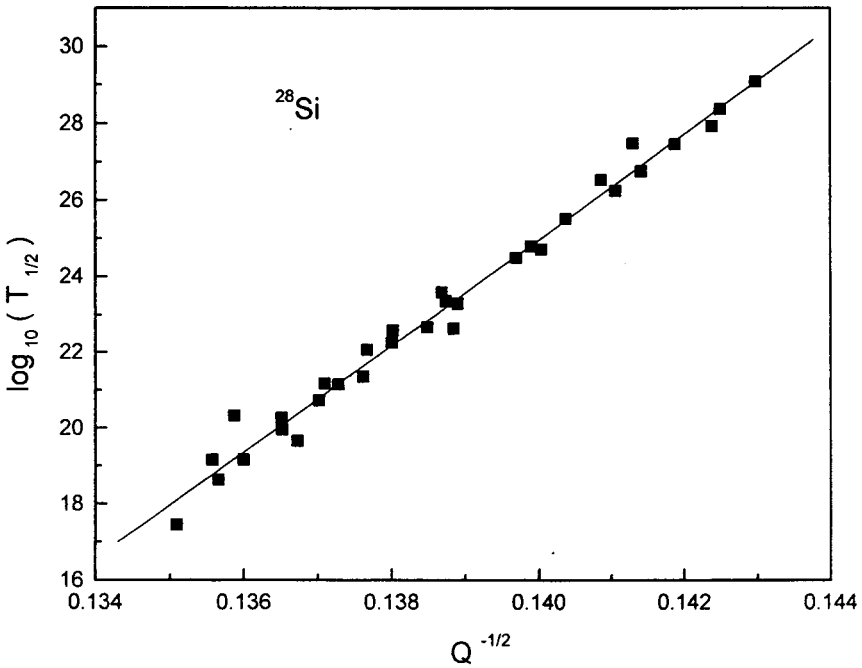

Fig. 4.35 Geiger Nuttall plot for $\log_{10}(T_{1/2})$ vs $Q^{-1/2}$ for ^{28}Si emission from various Nd isotopes.

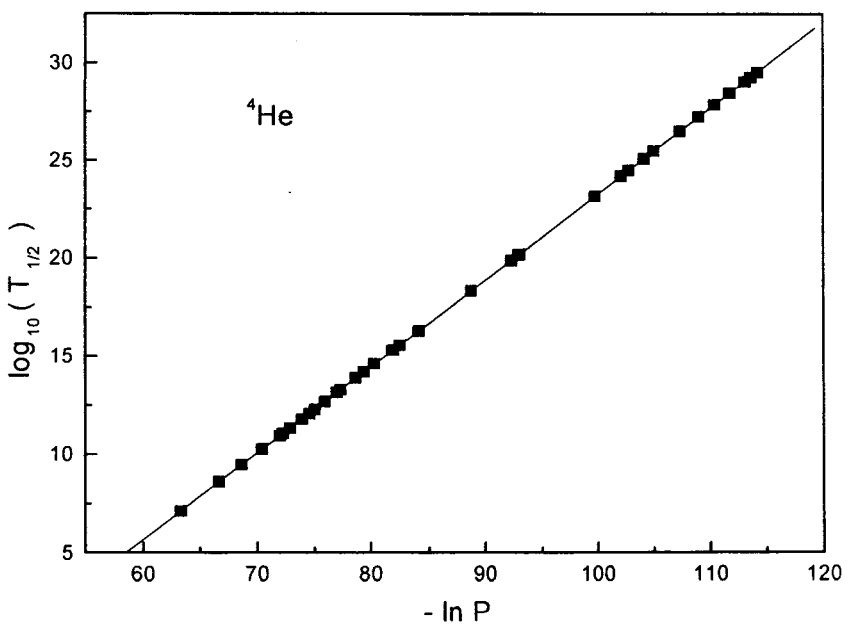

Fig. 4.36 Geiger Nuttall plot for $\log_{10}(T_{1/2})$ vs $-\ln P$ for ^{4}He emission from various Nd isotopes.

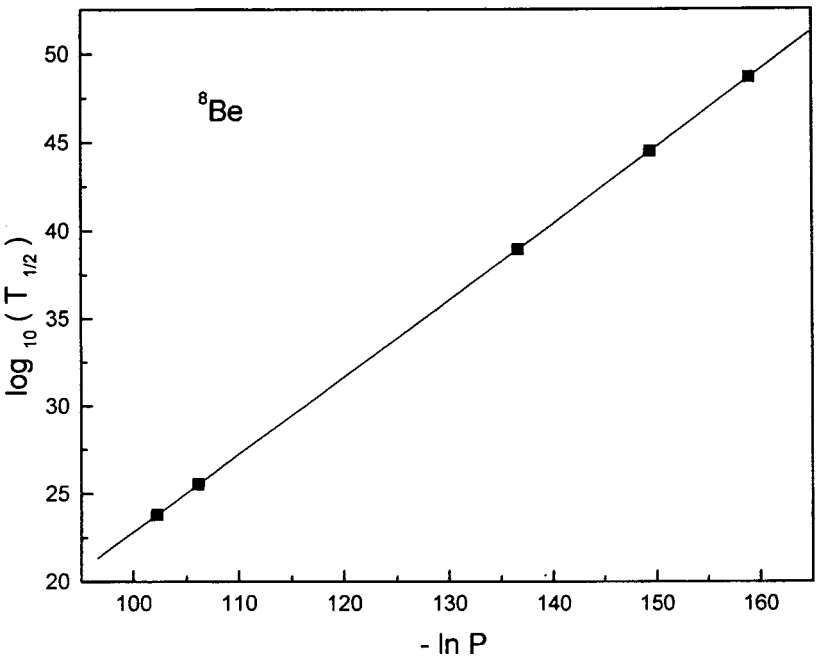

Fig. 4.37 Geiger Nuttall plot for $\log_{10}(T_{1/2})$ vs –lnP for ^{8}Be emission from various Nd isotopes.

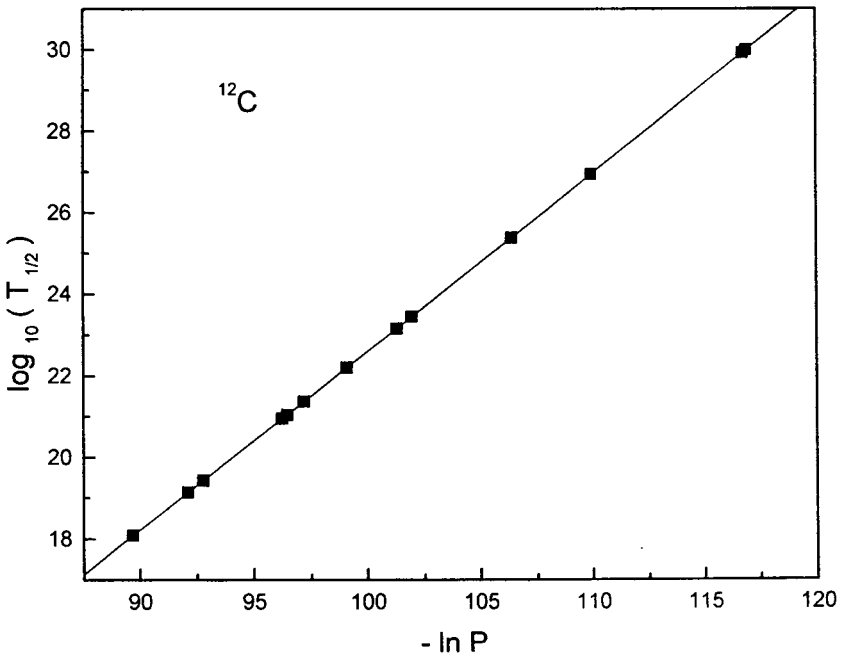

Fig. 4.38 Geiger Nuttall plot for $\log_{10}(T_{1/2})$ vs –lnP for ^{12}C emission from various Nd isotopes.

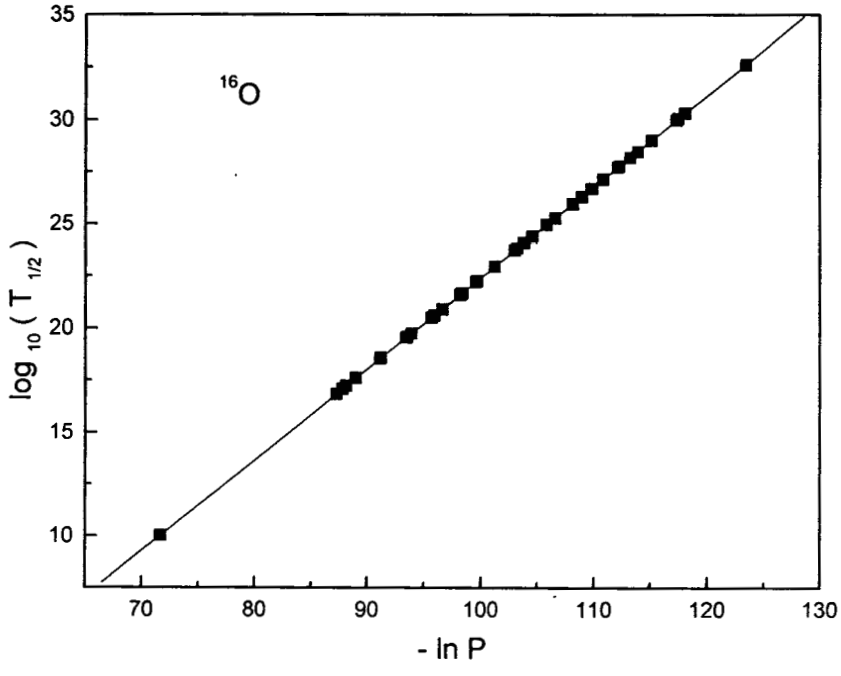

Fig. 4.39 Geiger Nuttall plot for $\log_{10}(T_{1/2})$ vs $-\ln P$ for ^{16}O emission from various Nd isotopes.

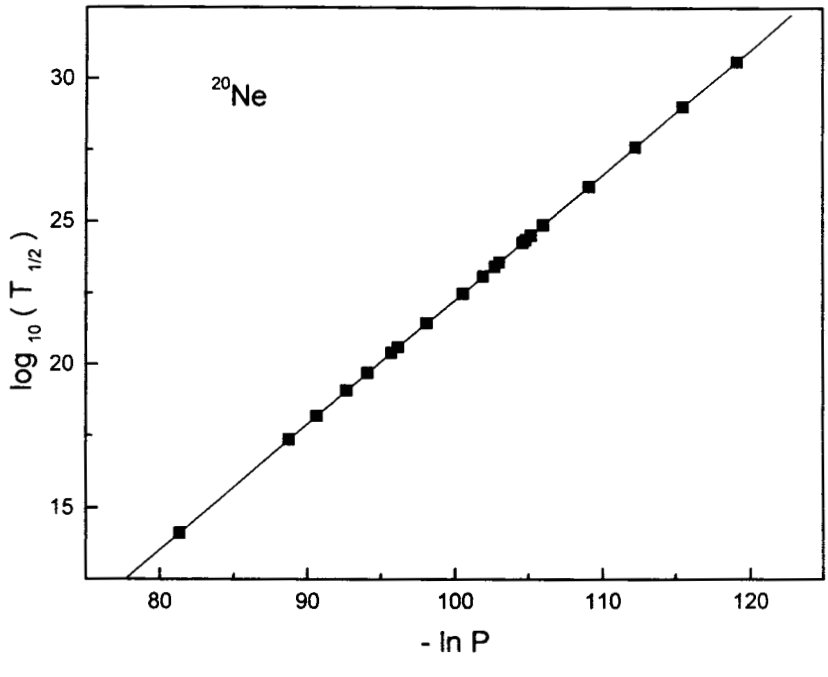

Fig. 4.40 Geiger Nuttall plot for $\log_{10}(T_{1/2})$ vs $-\ln P$ for ^{20}Ne emission from various Nd isotopes.

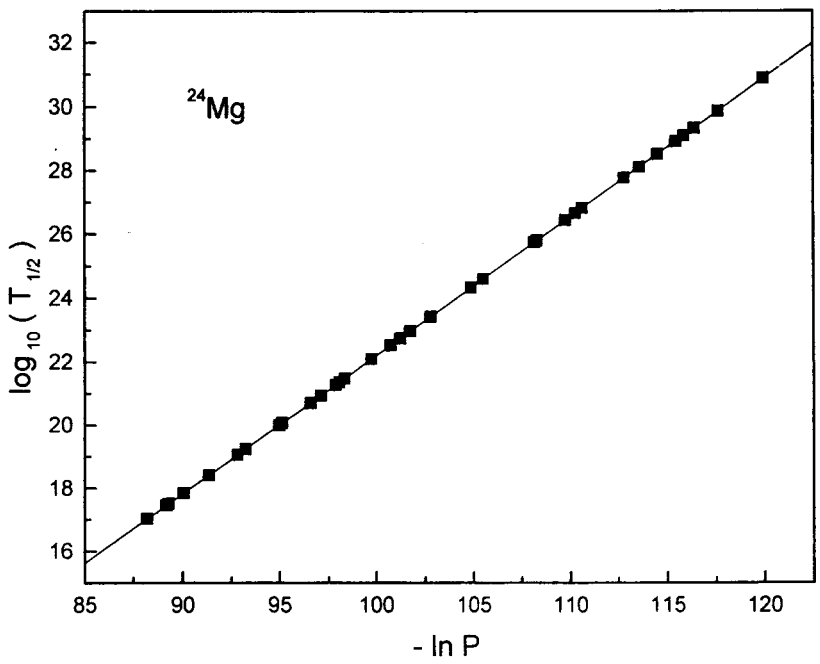

Fig. 4.41 Geiger Nuttall plot for $\log_{10}(T_{1/2})$ vs –lnP for ^{24}Mg emission from various Nd isotopes.

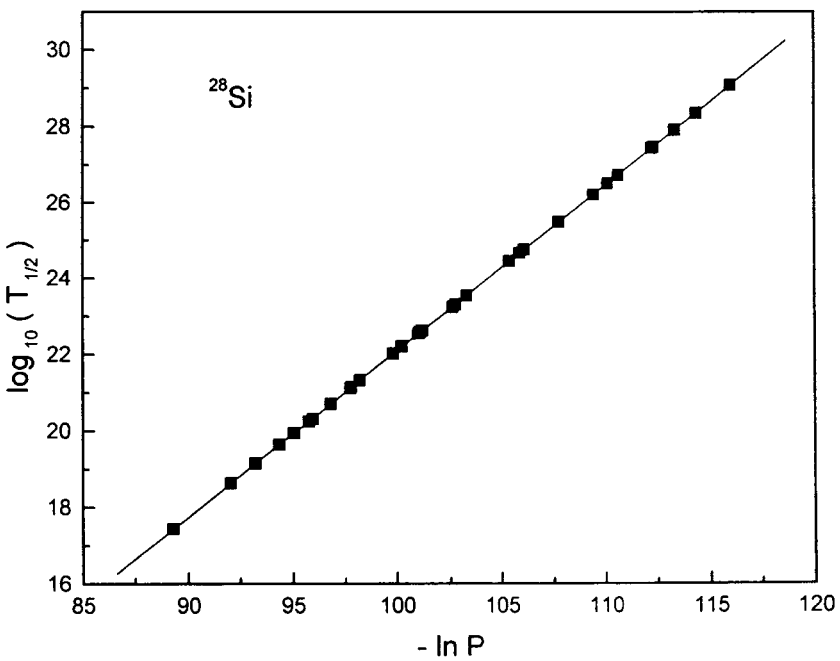

Fig. 4.42 Geiger Nuttall plot for $\log_{10}(T_{1/2})$ vs –lnP for ^{28}Si emission from various Nd isotopes.

Table 4.20. Slope and intercept values of Geiger-Nuttall plots for different clusters emitted from various Nd isotopes.

Emitted cluster	Intercept Y	Slope X
^{4}He	- 47.2312	99.7807
^{8}Be	- 72.5167	272.6039
^{12}C	- 93.6219	473.6761
^{16}O	-114.8198	697.9871
^{20}Ne	-133.0517	923.1437
^{24}Mg	-150.0555	1151.0555
^{28}Si	-170.0863	1393.0632

4.2.1.5 Samarium isotopes

Tables 4.21 to 4.24 give the logarithm of predicted half life time for ^{4}He, ^{8}Be, ^{12}C, ^{16}O, ^{20}Ne, ^{24}Mg, ^{28}Si, ^{29}Si and ^{32}S clusters from $^{124-132}Sm$ isotopes using different mass tables and their comparison with other models. It is found that most of the predicted half life time values are below the present upper limit for measurements ($T_{1/2} < 10^{30}$s). It is found that our values lie close to those values reported by ASAFM [84]. It is also seen that ^{24}Mg emission from ^{124}Sm and ^{28}Si emission from ^{130}Sm are the most favourable ones for measurements with the smallest half life values ($T_{1/2} \leq 10^{17}$s). The lowest $T_{1/2}$ value for ^{24}Mg emission from ^{124}Sm stresses the role of doubly magic ^{100}Sn daughter in exotic decay process and in the case of ^{28}Si from ^{130}Sm, the daughter is $^{102}_{48}Cd_{52}$ which lies close to N = Z = 50 shell.

When decay of ^{24}Mg from ^{124}Sm is compared with that from heavier isotopes up to ^{130}Sm it is found that $\log_{10}(T_{1/2})$ value increases from 17.19 s (for ^{124}Sm, Q = 49.70 MeV) to 29.11 s (for ^{130}Sm, Q = 43.14 MeV). All these cases refer to the doubly magic or near doubly magic daughter Sn nuclei. This point to the fact that the neutron excesses in the parent nuclei slows down the exotic decay process.

Figure 4.43 gives the Geiger-Nuttall plots of predicted $\log_{10}(T_{1/2})$ vs $Q^{-1/2}$ for ^{4}He, ^{8}Be, ^{12}C, ^{16}O, ^{20}Ne, ^{24}Mg and ^{28}Si from various Sm isotopes. We notice that the Geiger-Nuttall plots for all clusters are linear with different slopes and intercepts. The values of slope X and intercept Y for different clusters are given in Table 4.25.

Figures 4.44 to 4.52 give the Geiger-Nuttall plot of predicted $\log_{10}(T_{1/2})$ vs $-\ln P$ for ^{4}He, ^{8}Be, ^{12}C, ^{16}O, ^{20}Ne, ^{24}Mg, ^{28}Si, ^{29}Si and ^{32}Si from various Sm isotopes. These plots are also found to be linear.

Table 4.21. Logarithm of predicted half life time and other characteristic of ^{4}He and ^{8}Be emission from various Sm isotopes. Q values are taken from [84].

Parent nuclei	Emitted cluster	Daughter nuclei	Q value (MeV)	Penetrability P	Decay Constant λ	$\log_{10}(T_{1/2})$ Present	CYEM [87]	ASAFM [84]	PCM [86]
^{124}Sm	^{4}He	^{120}Nd	2.89[a]	3.34834E-34	4.44576E-14	13.19			6.64
^{126}Sm		^{122}Nd	2.46	3.83833E-39	4.33807E-19	18.20		17.20	
			2.65[a]	9.01616E-37	1.09771E-16	15.80			8.74
^{127}Sm		^{123}Nd	2.72	6.39008E-36	7.98535E-16	14.94	14.74	14.70	
			2.51	1.87953E-38	2.16742E-18	17.50	17.28	17.40	
			2.49	1.03857E-38	1.18810E-18	17.77	17.54	17.50	
			3.01	7.19018E-33	9.94318E-13	11.84	11.68	11.60	
^{128}Sm		^{124}Nd	3.22[a]	6.96850E-31	1.03089E-10	9.83			5.52
			2.84	1.45631E-34	1.90016E-14	13.56	13.39	12.90	
			2.57	1.16799E-37	1.37908E-17	16.70	16.49	15.80	
			2.54	4.93602E-38	5.76010E-18	17.08	16.78	16.30	
			3.21	5.68511E-31	8.38422E-11	9.92	9.78	9.30	
^{129}Sm		^{125}Nd	3.95	2.53276E-25	4.59631E-05	4.18		4.40	
			2.91	8.55367E-34	1.14357E-13	12.78		12.80	
			2.62	5.17417E-37	6.22817E-17	16.05		16.20	
			2.36	2.18137E-40	2.36515E-20	19.47		19.50	
			3.99	4.61325E-25	8.45665E-05	3.91		4.20	
			3.19	4.11145E-31	6.02566E-11	10.06		10.10	
^{130}Sm		^{126}Nd	3.95	2.77314E-25	5.03255E-05	4.14		3.80	
			2.88	4.54875E-34	6.01871E-14	13.06		12.40	
			2.67	2.19691E-36	2.69490E-16	15.41		14.80	
			2.52	3.26172E-38	3.77629E-18	17.26		16.50	
			3.59	8.38654E-28	1.38324E-07	6.70		6.30	
			3.20	5.48570E-31	8.06493E-11	9.93		9.40	
^{131}Sm		^{127}Nd	3.71	6.86893E-27	1.17080E-06	5.77		6.20	
			2.89	6.26071E-34	8.31266E-14	12.92		13.20	
			2.94	2.03455E-33	2.74811E-13	12.40		12.70	
			2.74	1.50678E-35	1.89678E-15	14.56		15.00	
			2.82	1.14113E-34	1.47844E-14	13.67		14.00	
^{132}Sm		^{128}Nd	3.57	6.94595E-28	1.13925E-07	6.78		6.40	
			2.79	5.82895E-35	7.47160E-15	13.97		13.40	
^{124}Sm	^{8}Be	^{116}Ce	5.99[a]	2.21426E-63	4.09708E-43	42.23			37.63
^{126}Sm		^{118}Ce	4.52[a]	3.52969E-80	4.92826E-60	59.15			53.58
^{128}Sm		^{120}Ce	4.47[a]	9.42090E-81	1.30083E-60	59.73			54.32

[a] Q values are taken from [86].

Table 4.22. Logarithm of predicted half life time and other characteristic of ^{12}C, ^{16}O, ^{20}Ne and ^{24}Mg emission from various Sm isotopes. Q values are taken from [84].

Parent nuclei	Emitted cluster	Daughter nuclei	Q value (MeV)	Penetrability P	Decay Constant λ	$\log_{10}(T_{1/2})$ Present	ASAFM [84]	PCM [86]
^{124}Sm	^{12}C	^{112}Ba	17.87[a]	2.11475E-43	1.05250E-22	21.82		21.33
^{126}Sm		^{114}Ba	15.92[a]	4.51688E-50	2.00264E-29	28.54		31.91
^{128}Sm		^{116}Ba	14.87[a]	4.31866E-54	1.78855E-33	32.59		37.77
^{129}Sm		^{117}Ba	19.08	5.78898E-39	3.07624E-18	17.35	18.20	
^{130}Sm		^{118}Ba	16.94	8.12929E-46	3.83536E-25	24.26	22.90	
			19.08	7.57082E-39	4.02310E-18	17.24	16.60	
^{132}Sm		^{120}Ba	16.01	4.94117E-49	2.20324E-28	27.50	25.90	
^{124}Sm	^{16}O	^{108}Xe	28.45[a]	8.82223E-42	6.83637E-21	20.01		20.78
^{126}Sm		^{110}Xe	26.65[a]	4.84379E-46	3.51599E-25	24.29		30.03
^{128}Sm		^{112}Xe	24.83[a]	7.68967E-51	5.20055E-30	29.12		41.85
^{129}Sm		^{113}Xe	28.75	3.69460E-40	2.89315E-19	18.38	19.60	
^{130}Sm		^{114}Xe	26.51	9.29497E-46	6.71155E-25	24.01	22.90	
			23.76	8.41556E-54	5.44621E-33	32.10	30.00	
			28.65	3.04066E-40	2.37278E-19	18.47	18.00	
^{124}Sm	^{20}Ne	^{104}Te	36.77[a]	8.68948E-46	8.66309E-25	23.90		25.01
^{126}Sm		^{106}Te	34.69[a]	3.31706E-50	3.11991E-29	28.35		34.26
^{128}Sm		^{108}Te	33.04[a]	6.14727E-54	5.50691E-33	32.10		47.01
^{124}Sm	^{24}Mg	^{100}Sn	49.70[a]	3.36335E-39	4.52807E-18	17.18		17.32
^{126}Sm		^{102}Sn	47.66[a]	1.45177E-42	1.87429E-21	20.57		25.66
^{127}Sm		^{103}Sn	46.99	1.24963E-43	1.59064E-22	21.64	22.80	
			47.02	1.43708E-43	1.83040E-22	21.58	22.70	
			46.78	4.68431E-44	5.93595E-23	22.07	23.10	
^{128}Sm		^{104}Sn	45.71	5.37875E-46	6.66005E-25	24.02	23.40	
			45.96	1.78649E-45	2.22416E-24	23.49	23.00	
			45.54	2.36745E-46	2.92051E-25	24.38	23.70	
			46.12[a]	3.83636E-45	4.79284E-24	23.16		36.66
^{129}Sm		^{105}Sn	44.32	1.05520E-48	1.26683E-27	26.74	27.20	
			43.92	1.41181E-49	1.67966E-28	27.62	28.00	
			44.25	7.43268E-49	8.90930E-28	26.89	27.40	
^{130}Sm		^{106}Sn	43.15	4.81996E-51	5.63390E-30	29.09	27.90	
			43.22	6.91984E-51	8.10150E-30	28.93	27.70	
			43.14	4.57702E-51	5.34869E-30	29.11	27.90	

[a] Q values are taken from [86].

Table 4.23. Logarithm of predicted half life time and other characteristic of ^{28}Si and ^{29}Si emission from various Sm isotopes. Q values are taken from [84,85,86].

Parent nuclei	Emitted cluster	Daughter nuclei	Q value (MeV)	Penetrability P	Decay Constant λ	$\log_{10}(T_{1/2})$ Present	CYEM [87]	ASAFM [84]	PCM [86]
^{124}Sm	^{28}Si	^{96}Cd	56.23	4.14107E-44	6.30644E-23	22.04			21.73
^{126}Sm		^{98}Cd	56.66	1.36533E-42	2.09516E-21	20.52		20.8	
			56.95	4.78844E-42	7.38570E-21	19.97			24.12
^{127}Sm		^{99}Cd	57.39	6.91158E-41	1.07428E-19	18.81	17.26	20.9	
			54.76	6.65112E-46	9.86420E-25	23.85	21.70	24.9	
			57.42	7.86055E-41	1.22242E-19	18.75	17.21	20.8	
			57.18	2.80310E-41	4.34097E-20	19.20	17.60	21.2	
^{128}Sm		^{100}Cd	54.91	2.72170E-45	4.04758E-24	23.23			36.00
			55.91	2.33513E-43	3.53594E-22	21.29	19.55	21.7	
			53.54	5.30611E-48	7.69411E-27	25.95	23.69	25.4	
			56.16	7.01610E-43	1.06715E-21	20.81	19.13	21.3	
			55.74	1.10195E-43	1.66354E-22	21.62	19.84	22.0	
^{129}Sm		^{101}Cd	57.03	6.40364E-41	9.89085E-20	18.85		21.2	
			54.30	3.49851E-46	5.14501E-25	24.13		25.4	
			51.72	2.01470E-51	2.82210E-30	29.39		29.7	
			53.90	5.61771E-47	8.20071E-26	24.93		26.0	
			59.07	3.76627E-37	6.25350E-16	15.06		18.3	
			54.23	2.54290E-46	3.73485E-25	24.27		25.5	
^{130}Sm		^{102}Cd	55.80	5.87362E-43	8.87654E-22	20.89		21.7	
			52.98	1.55163E-48	2.22641E-27	26.49		26.1	
			50.84	5.44832E-53	7.50190E-32	30.97		29.8	
			53.05	2.15323E-48	3.09371E-27	26.35		26.0	
			57.94	6.45554E-39	1.01301E-17	16.84		18.5	
			52.97	1.48062E-48	2.12411E-27	26.51		26.2	
^{131}Sm		^{103}Cd	53.92	2.34584E-46	3.42573E-25	24.31		25.8	
			51.57	3.61415E-51	5.04786E-30	29.14		29.7	
			51.47	2.22757E-51	3.10520E-30	29.35		29.9	
			52.05	3.63479E-50	5.12393E-29	28.13		28.9	
			52.32	1.31771E-49	1.86720E-28	27.57		28.4	
^{132}Sm		^{104}Cd	50.76	1.28650E-52	1.76862E-31	30.59		29.7	
^{127}Sm	^{29}Si	^{98}Cd	55.80	1.04883E-43	1.58502E-22	21.64		23.9	
			53.18	6.22548E-49	8.96640E-28	26.89		28.1	
			55.83	1.19961E-43	1.81386E-22	21.58		23.8	
			55.60	4.27525E-44	6.43774E-23	22.03		24.2	
^{129}Sm		^{100}Cd	56.10	1.76105E-42	2.67567E-21	20.41		23.2	
			53.37	6.45210E-48	9.32599E-27	25.87		27.6	
			52.97	9.73087E-49	1.39598E-27	26.70		28.2	
			53.30	4.63893E-48	6.69641E-27	26.01		27.7	
^{131}Sm		^{102}Cd	51.79	1.26087E-50	1.76853E-29	28.59		30.0	

Table 4.24. Logarithm of predicted half life time and other characteristic of ^{32}S emission from various Sm isotopes. Q values are taken from [84,85].

Parent nuclei	Emitted cluster	Daughter nuclei	Q value (MeV)	Penetrability P	Decay Constant λ	$\log_{10}(T_{1/2})$ Present	$\log_{10}(T_{1/2})$ ASAFM [84,85]
^{128}Sm	^{32}S	^{96}Pd	62.30	1.30212E-46	2.19699E-25	24.50	24.70
			59.93	3.35784E-51	5.44994E-30	29.10	28.30
			62.55	3.87842E-46	6.57006E-25	24.02	24.30
			62.13	6.18422E-47	1.04058E-25	24.82	25.00
^{129}Sm		^{97}Pd	63.70	1.28667E-43	2.21969E-22	21.49	23.60
			60.97	8.22100E-49	1.35746E-27	26.71	27.70
			60.57	1.36390E-49	2.23731E-28	27.49	28.30
			60.90	6.00856E-49	9.91003E-28	26.84	27.80
^{130}Sm		^{98}Pd	59.09	3.44264E-52	5.50926E-31	30.10	29.50
			59.16	4.75959E-52	7.62580E-31	29.96	29.40

Table 4.25. Slope and intercept values of Geiger-Nuttall plots for different clusters emitted from various Sm isotopes.

Emitted cluster	Intercept Y	Slope X
^{4}He	- 48.1744	103.9625
^{8}Be	- 69.2035	272.7304
^{12}C	- 96.6007	498.1507
^{16}O	-117.3339	729.1777
^{20}Ne	-125.3007	904.8134
^{24}Mg	-147.3472	1158.8367
^{28}Si	-174.8798	1466.4289
^{32}S	-198.4671	1758.5892

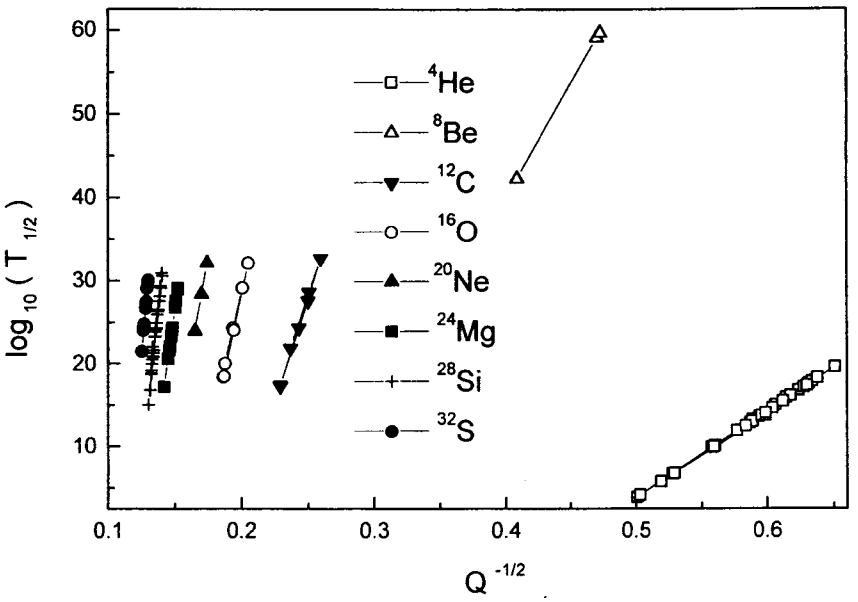

Fig. 4.43 Geiger Nuttall plot for $\log_{10}(T_{1/2})$ Vs $Q^{-1/2}$ for various clusters from different Sm isotopes.

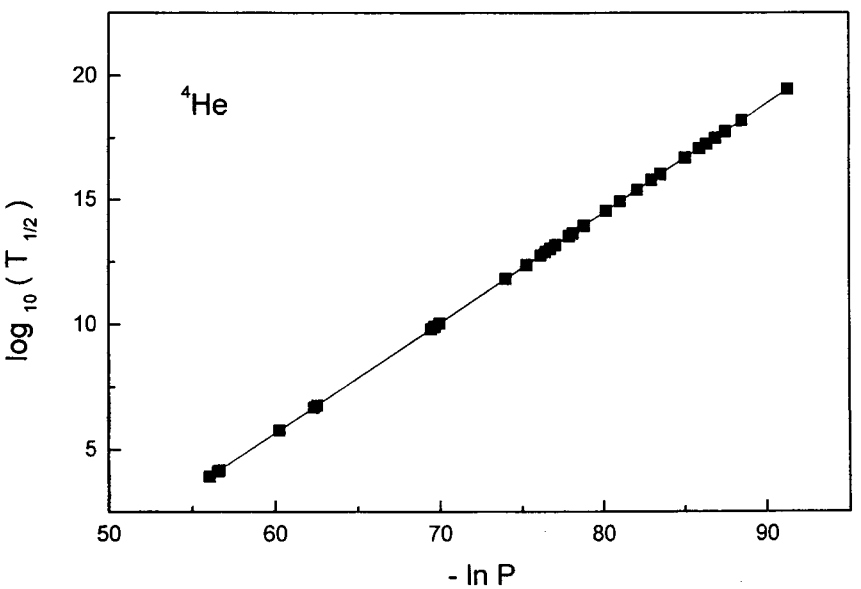

Fig. 4.44 Geiger Nuttall plot for $\log_{10}(T_{1/2})$ vs –lnP for ^{4}He emission from various Sm isotopes.

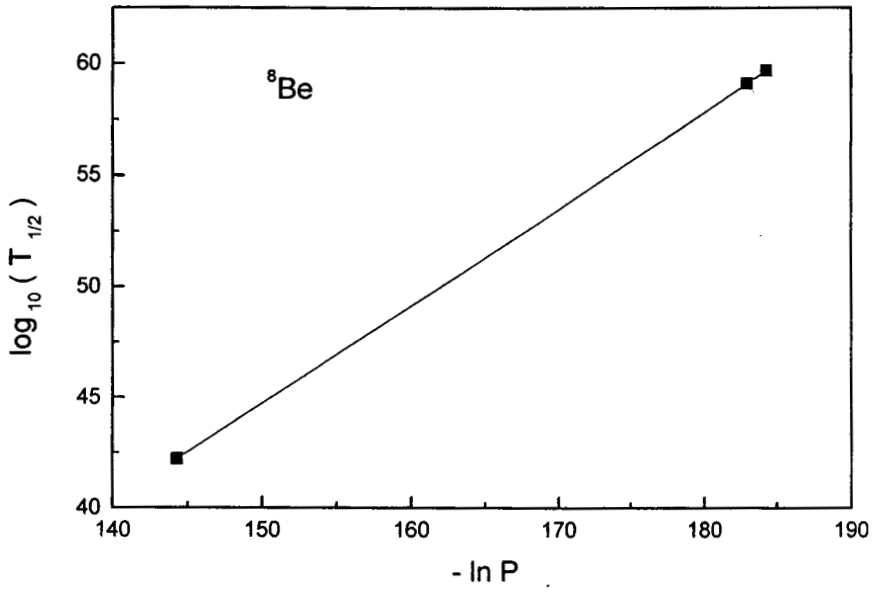

Fig. 4.45 Geiger Nuttall plot for $\log_{10}(T_{1/2})$ vs –lnP for ^{8}Be emission from various Sm isotopes.

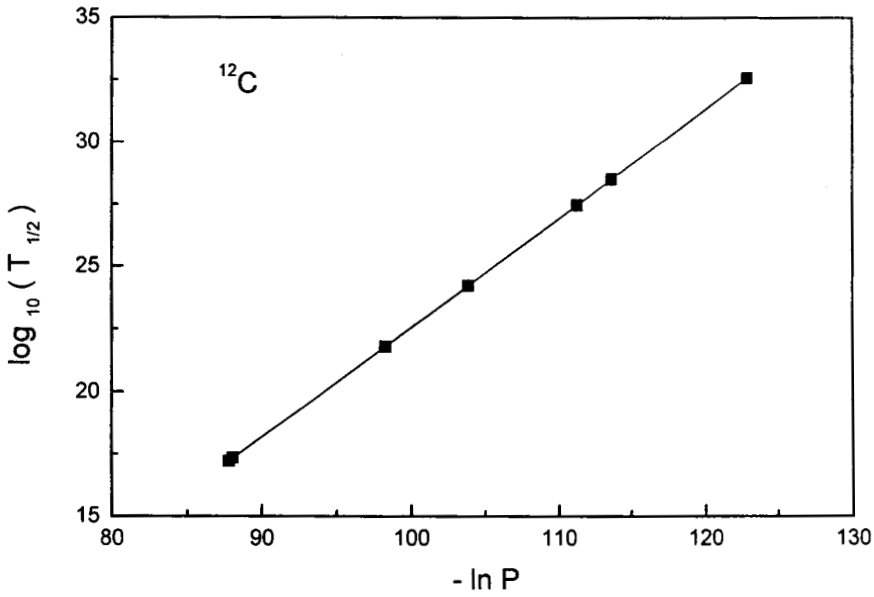

Fig. 4.46 Geiger Nuttall plot for $\log_{10}(T_{1/2})$ vs –lnP for ^{12}C emission from various Sm isotopes.

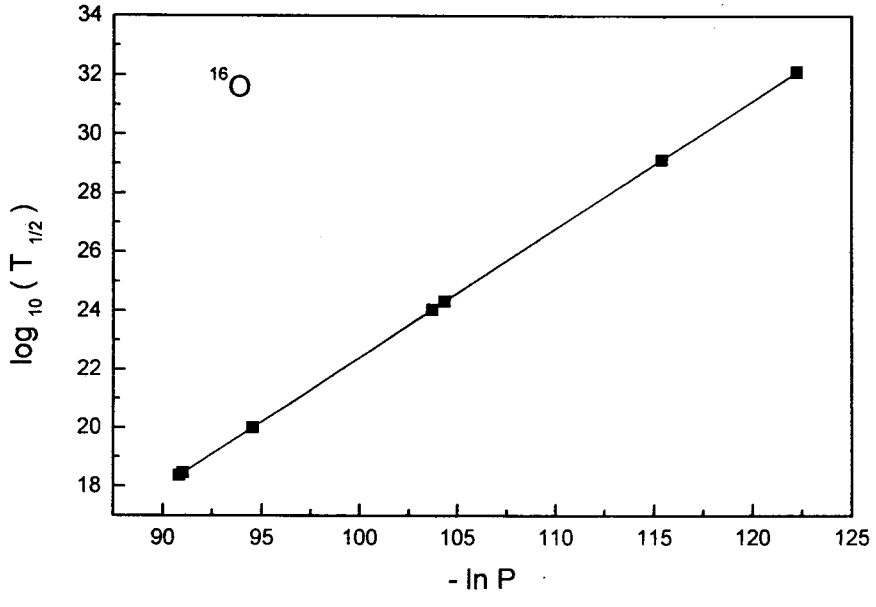

Fig. 4.47 Geiger Nuttall plot for $\log_{10}(T_{1/2})$ vs –lnP for ^{16}O emission from various Sm isotopes.

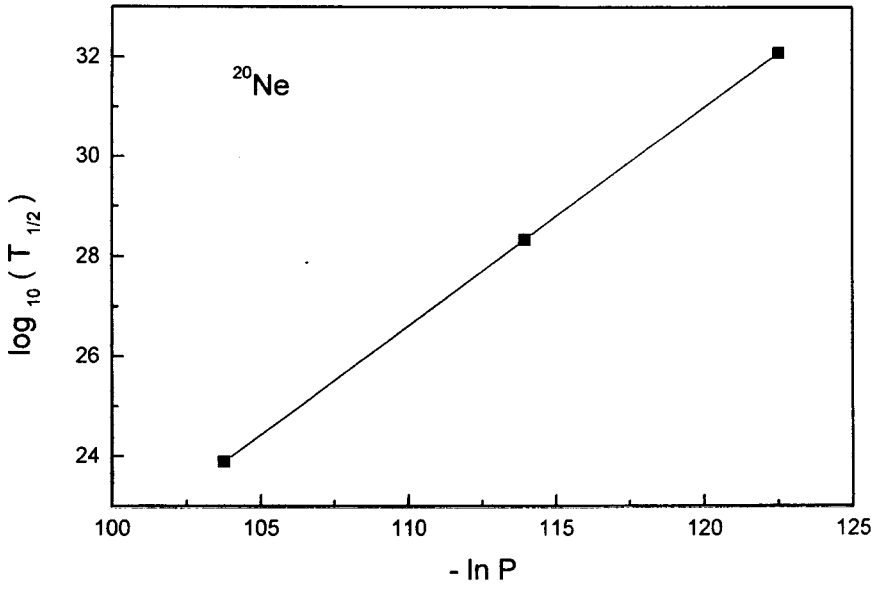

Fig. 4.48 Geiger Nuttall plot for $\log_{10}(T_{1/2})$ vs –lnP for ^{20}Ne emission from various Sm isotopes.

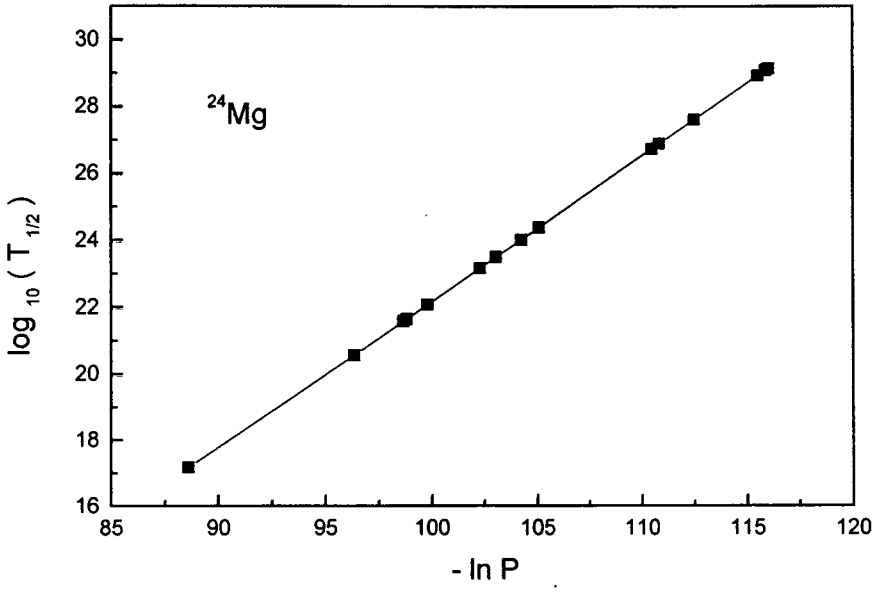

Fig. 4.49 Geiger Nuttall plot for $\log_{10}(T_{1/2})$ vs $-\ln P$ for ^{24}Mg emission from various Sm isotopes.

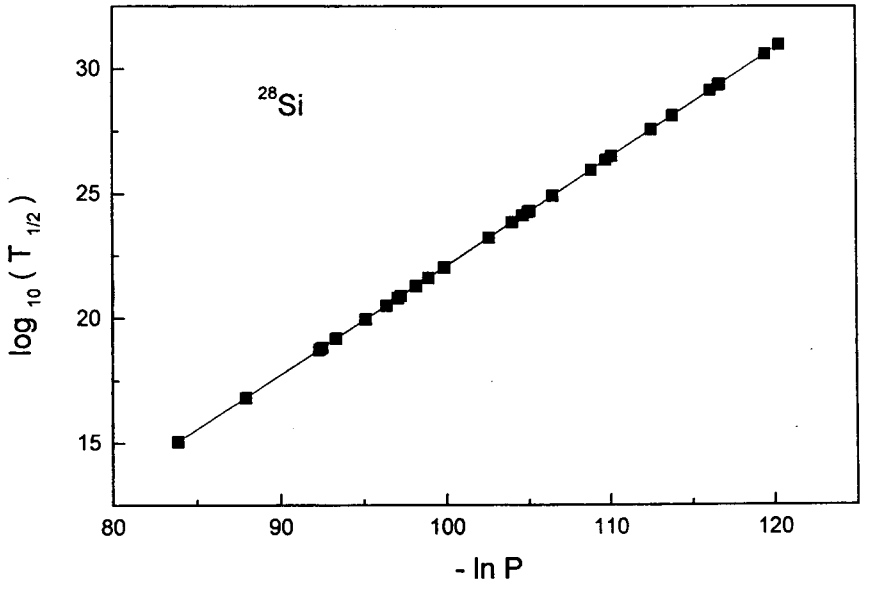

Fig. 4.50 Geiger Nuttall plot for $\log_{10}(T_{1/2})$ vs $-\ln P$ for ^{28}Si emission from various Sm isotopes.

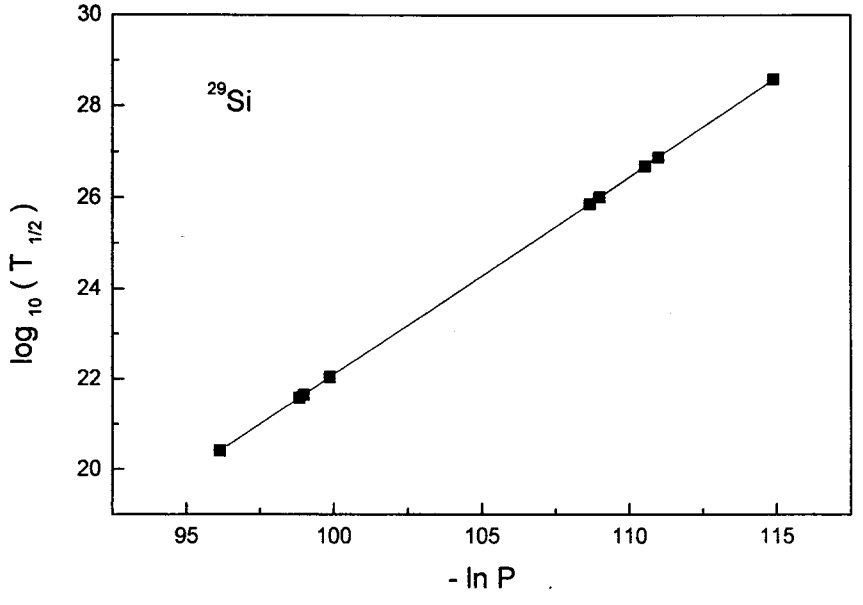

Fig. 4.51 Geiger Nuttall plot for $\log_{10}(T_{1/2})$ vs –lnP emission for ^{29}Si from various Xe isotopes.

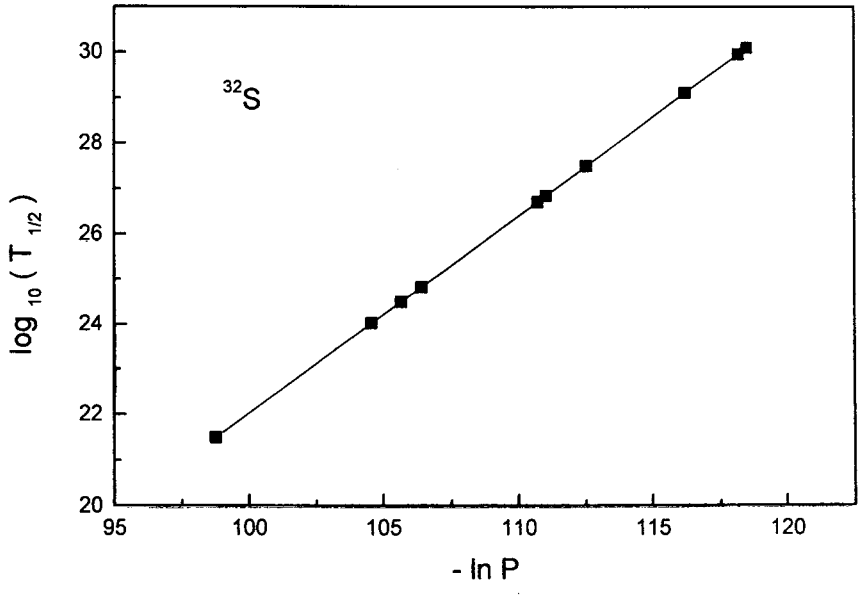

Fig. 4.52 Geiger Nuttall plot for $\log_{10}(T_{1/2})$ Vs –lnP emission for ^{32}S from various Xe isotopes.

4.2.1.6 Gadolinium isotopes

Tables 4.26 and 4.27 give the logarithm of predicted half life time for ^{4}He, ^{8}Be, ^{12}C, ^{16}O, ^{20}Ne, ^{24}Mg, ^{28}Si, ^{29}Si and ^{32}S clusters from $^{128\text{-}137}$Gd isotopes using different mass tables and their comparison with other models. It is found that most of the values are below the present upper limit for measurements ($T_{1/2} < 10^{30}$ s) and our values lie close to those values reported by ASAFM [84]. It is found that ^{28}Si emission from ^{128}Gd and ^{130}Gd are most favourable for measurements with the smallest half life values ($T_{1/2} \leq 10^{17}$ s). The lowest $T_{1/2}$ value for ^{28}Si emission from ^{128}Gd indicates the role of doubly magic ^{100}Sn daughter in exotic decay process and in the case of ^{28}Si from ^{130}Gd, the daughter is $^{102}_{50}Sn_{52}$ which lie close to N = Z = 50 shell.

When decay of ^{28}Si from ^{128}Gd is compared with that from heavier isotopes up to ^{136}Nd it is found that $\log_{10}(T_{1/2})$ value increases from 15.12 s (for ^{128}Gd, Q = 63.03 MeV) to 28.62 s (for ^{136}Gd, Q = 54.50 MeV). All these cases refer to the doubly magic or near doubly magic daughter Sn nuclei. This point to the fact that the neutron excesses in the parent nuclei slows down the exotic decay process.

Figure 4.53 gives the Geiger-Nuttall plots of predicted $\log_{10}(T_{1/2})$ vs $Q^{-1/2}$ for ^{4}He, ^{8}Be, ^{12}C, ^{16}O, ^{20}Ne, ^{24}Mg and ^{28}Si from various Gd isotopes. We notice that the Geiger-Nuttall plots for all clusters are linear with different slope and intercepts. The values of slope X and intercept Y for different clusters are given in Table 4.28.

Figures 4.54 to 4.62 give the Geiger-Nuttall plot of predicted $\log_{10}(T_{1/2})$ vs $-\ln P$ for ^{4}He, ^{8}Be, ^{12}C, ^{16}O, ^{20}Ne, ^{24}Mg, ^{28}Si, ^{29}Si and ^{32}S from various Gd isotopes. These plots are also found to be linear.

Table 4.26. Logarithm of predicted half life time and other characteristic of ^{4}He, ^{8}Be, ^{12}C and ^{16}O emission from various Gd isotopes. Q values are taken from [84].

Parent nuclei	Emitted cluster	Daughter nuclei	Q value (MeV)	Penetrability P	Decay Constant λ	$\log_{10}(T_{1/2})$ Present	ASAFM [84]	PCM [86]
^{128}Gd	^{4}He	^{124}Sm	3.70[a]	1.46710E-28	2.49398E-08	7.44		3.28
^{130}Gd		^{126}Sm	4.16[a]	2.35368E-25	4.49842E-05	4.19		1.55
^{132}Gd		^{128}Sm	3.90[a]	5.67556E-27	1.01693E-06	5.83	5.40	3.76
			3.58	2.62155E-29	4.31181E-09	8.21	7.60	
			3.70	2.13665E-28	3.63206E-08	7.28	6.80	
^{133}Gd		^{129}Sm	3.85	2.79050E-27	4.93584E-07	6.15	6.60	
			3.82	1.71812E-27	3.01533E-07	6.36	6.70	
^{134}Gd		^{130}Sm	3.80	1.34702E-27	2.35167E-07	6.47	6.10	
			3.87	4.17679E-27	7.42630E-07	5.97	5.70	
			3.96	1.71214E-26	3.11497E-06	5.35	5.00	
^{135}Gd		^{131}Sm	3.67	1.63935E-28	2.76412E-08	7.40	8.10	
			3.57	2.81323E-29	4.61415E-09	8.18	8.80	
			3.70	2.74314E-28	4.66304E-08	7.17	7.90	
^{136}Gd		^{132}Sm	4.37	7.18171E-24	1.44188E-03	2.68	2.50	
			3.46	4.00956E-30	6.37370E-10	9.04	8.70	
			3.57	3.04137E-29	4.98834E-09	8.14	7.90	
^{137}Gd		^{133}Sm	3.83	2.77436E-27	4.88181E-07	6.15	7.10	
^{128}Gd	^{8}Be	^{120}Nd	6.12[a]	3.34317E-65	6.32017E-45	44.04		30.54
^{130}Gd		^{122}Nd	6.37[a]	9.34989E-63	1.83978E-42	41.58		26.99
^{132}Gd		^{124}Nd	6.65[a]	3.38552E-60	6.95449E-40	39.00		25.47
^{137}Gd		^{129}Nd	8.94	1.41574E-44	3.90968E-24	23.25	23.00	
^{128}Gd	^{12}C	^{116}Ce	17.51[a]	1.49974E-47	7.31378E-27	25.98		14.65
^{130}Gd		^{118}Ce	16.50[a]	5.81143E-51	2.67059E-30	29.41		17.66
^{132}Gd		^{120}Ce	16.19[a]	6.53563E-52	2.94696E-31	30.37		18.16
^{136}Gd		^{124}Ce	17.99	6.12881E-45	3.07077E-24	23.35	21.90	
^{137}Gd		^{125}Ce	17.09	5.60214E-48	2.66646E-27	26.41	26.30	
^{128}Gd	^{16}O	^{112}Ba	28.67[a]	1.13841E-44	8.88979E-24	22.89		14.63
^{130}Gd		^{114}Ba	27.18[a]	3.42900E-48	2.53853E-27	26.44		16.96
^{132}Gd		^{116}Ba	25.84[a]	1.31151E-51	9.23056E-31	29.88		19.20

[a] Q values are taken from [86].

Table 4.27. Logarithm of predicted half life time and other characteristic of ^{20}Ne, ^{24}Mg, ^{28}Si, ^{29}Si and ^{32}S emission from various Gd isotopes. Q values are taken from [84].

Parent nuclei	Emitted cluster	Daughter nuclei	Q value (MeV)	Penetrability P	Decay Constant λ	$\log_{10}(T_{1/2})$ Present	ASAFM [84]	PCM [86]
^{128}Gd	^{20}Ne	^{108}Xe	36.78[a]	5.59138E-50	5.57592E-29	28.09		21.37
^{130}Gd		^{110}Xe	35.44[a]	1.00906E-52	9.69607E-32	30.85		23.20
^{132}Gd		^{112}Xe	33.36[a]	1.30941E-57	1.18437E-36	35.77		26.40
^{128}Gd	^{24}Mg	^{104}Te	50.02[a]	2.70440E-43	3.66437E-22	21.28		18.99
^{130}Gd		^{106}Te	48.48[a]	9.64976E-46	1.26725E-24	23.74		21.54
^{132}Gd		^{108}Te	46.57[a]	3.94055E-49	4.97105E-28	27.14		24.31
^{128}Gd	^{28}Si	^{100}Sn	63.03[a]	3.08642E-37	5.26874E-16	15.12		12.01
^{130}Gd		^{102}Sn	61.42[a]	2.37762E-39	3.95508E-18	17.24		15.08
^{132}Gd		^{104}Sn	59.62[a]	6.01395E-42	9.71081E-21	19.85		17.95
			59.28	1.41485E-42	2.27156E-21	20.48	20.60	
			59.42	2.56986E-42	4.13567E-21	20.22	20.40	
^{133}Gd		^{105}Sn	58.15	2.22859E-44	3.50981E-23	22.30	23.50	
			57.75	3.87680E-45	6.06357E-24	23.06	24.10	
			58.06	1.50520E-44	2.36687E-23	22.47	23.60	
^{134}Gd		^{106}Sn	56.94	2.14900E-46	3.31404E-25	24.32	23.90	
			57.07	3.83414E-46	5.92624E-25	24.07	23.70	
			57.09	4.19080E-46	6.47978E-25	24.03	23.70	
^{135}Gd		^{107}Sn	55.48	5.63828E-49	8.47201E-28	26.91	27.40	
			55.87	3.35451E-48	5.07588E-27	26.14	26.80	
^{136}Gd		^{108}Sn	54.50	1.12710E-50	1.66366E-29	28.62	27.60	
			54.82	5.02524E-50	7.46105E-29	27.97	27.10	
^{133}Gd	^{29}Si	^{104}Sn	56.99	1.97105E-46	3.04223E-25	24.36	25.90	
			56.60	3.36389E-47	5.15650E-26	25.13	26.50	
			56.90	1.31217E-46	2.02209E-25	24.53	26.00	
^{135}Gd		^{106}Sn	55.26	2.70270E-49	4.04488E-28	27.23	28.50	
			55.65	1.66589E-48	2.51078E-27	26.44	27.80	
^{132}Gd	^{32}S	^{100}Cd	66.45	2.55341E-45	4.59518E-24	23.18	23.10	
			64.19	1.57270E-49	2.73401E-28	27.40	26.40	
			66.59	4.60883E-45	8.31164E-24	22.92	22.90	
^{133}Gd		^{101}Cd	65.10	1.85621E-47	3.27261E-26	25.33	26.00	
			64.70	3.32931E-48	5.77020E-27	26.08	26.60	
			65.01	1.25900E-47	2.21663E-26	25.50	26.20	

[a] Q values are taken from [86].

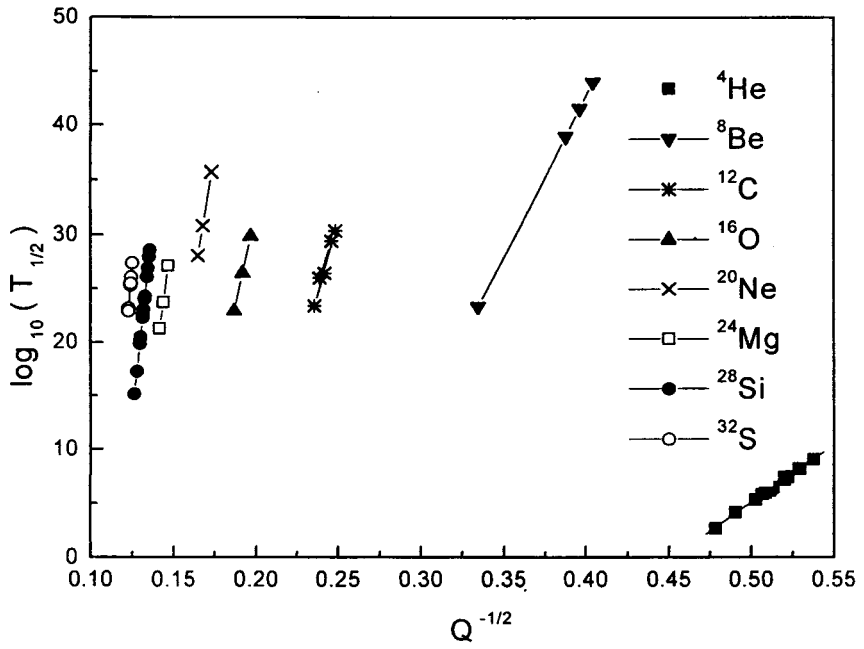

Fig. 4.53 Geiger Nuttall plot for $\log_{10}(T_{1/2})$ Vs $Q^{-1/2}$ for various clusters from different Gd isotopes.

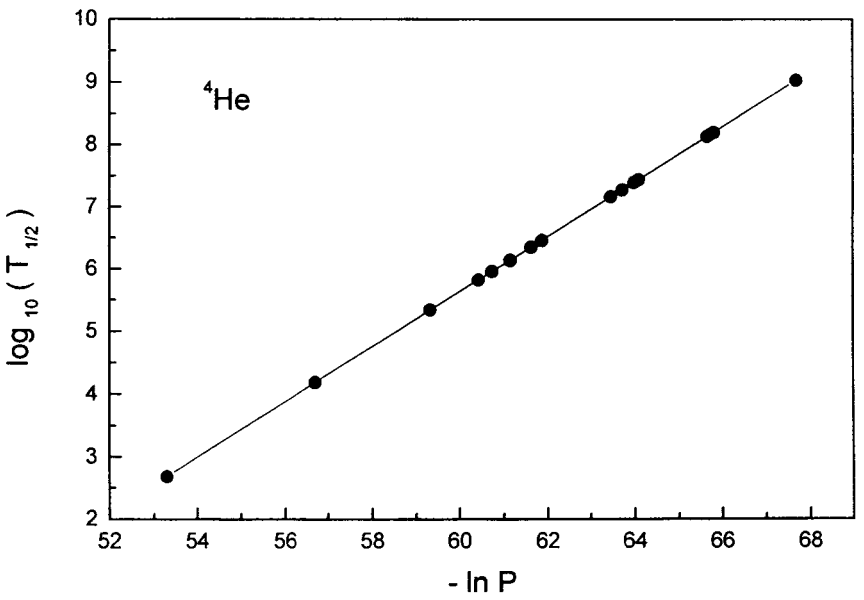

Fig. 4.54 Geiger Nuttall plot for $\log_{10}(T_{1/2})$ vs $-\ln P$ for ^4He emission from various Gd isotopes.

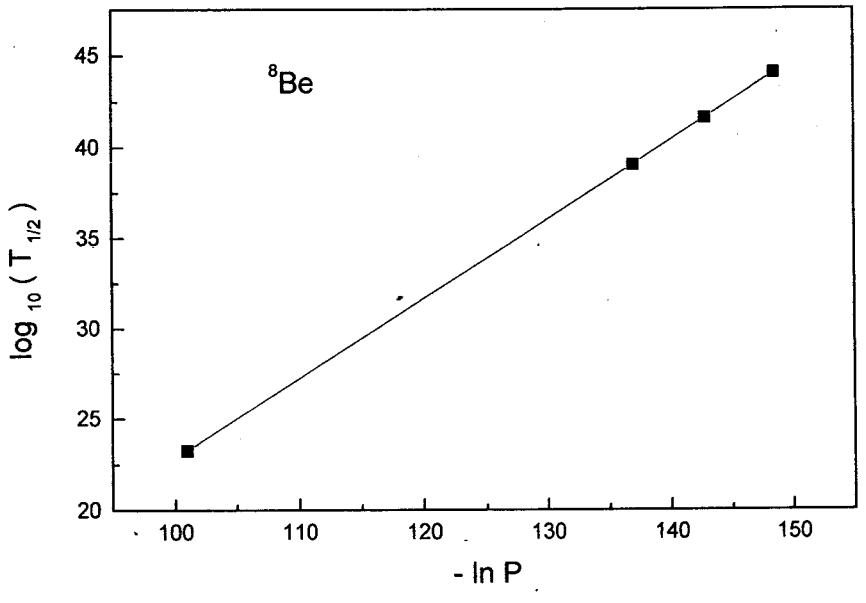

Fig. 4.55 Geiger Nuttall plot for $\log_{10}(T_{1/2})$ vs $-\ln P$ for ^{8}Be emission from various Gd isotopes.

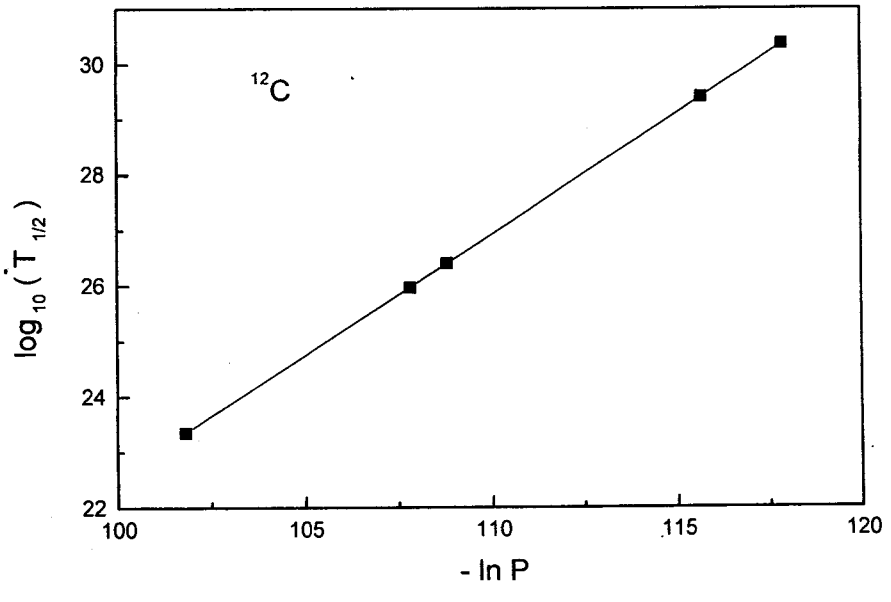

Fig. 4.56 Geiger Nuttall plot for $\log_{10}(T_{1/2})$ vs $-\ln P$ for ^{12}C emission from various Gd isotopes.

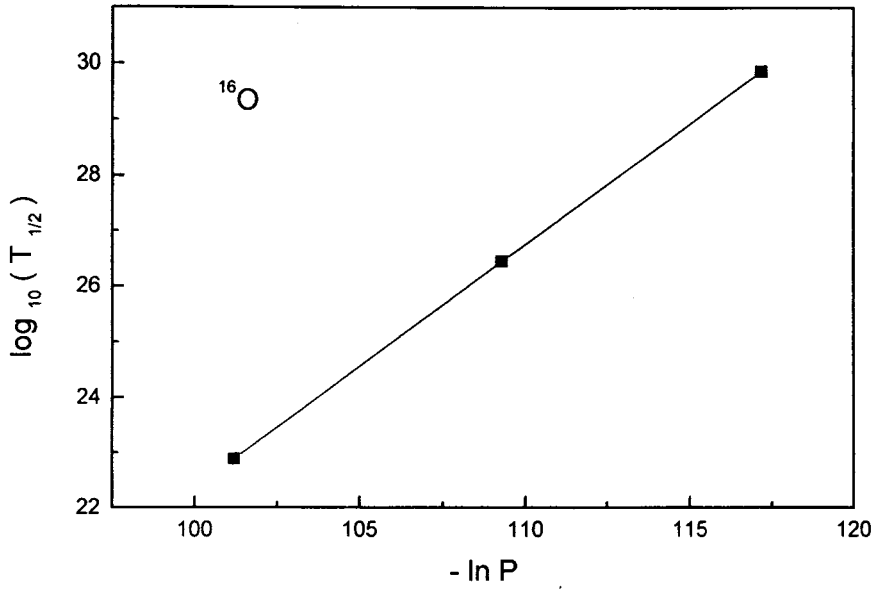

Fig. 4.57 Geiger Nuttall plot for $\log_{10}(T_{1/2})$ vs –lnP for ^{16}O emission from various Gd isotopes.

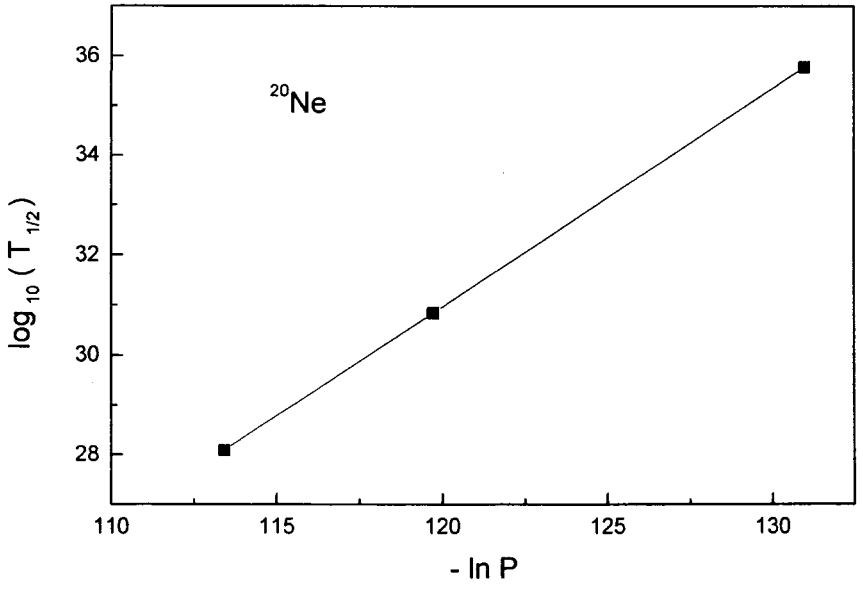

Fig. 4.58 Geiger Nuttall plot for $\log_{10}(T_{1/2})$ vs –lnP for ^{20}Ne emission from various Gd isotopes.

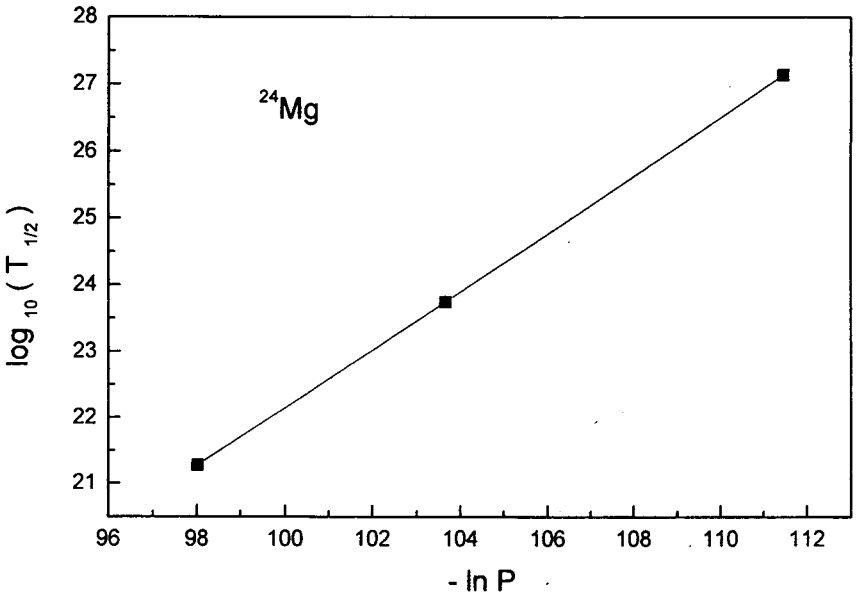

Fig. 4.59 Geiger Nuttall plot for $\log_{10}(T_{1/2})$ vs –lnP for ^{24}Mg emission from various Gd isotopes.

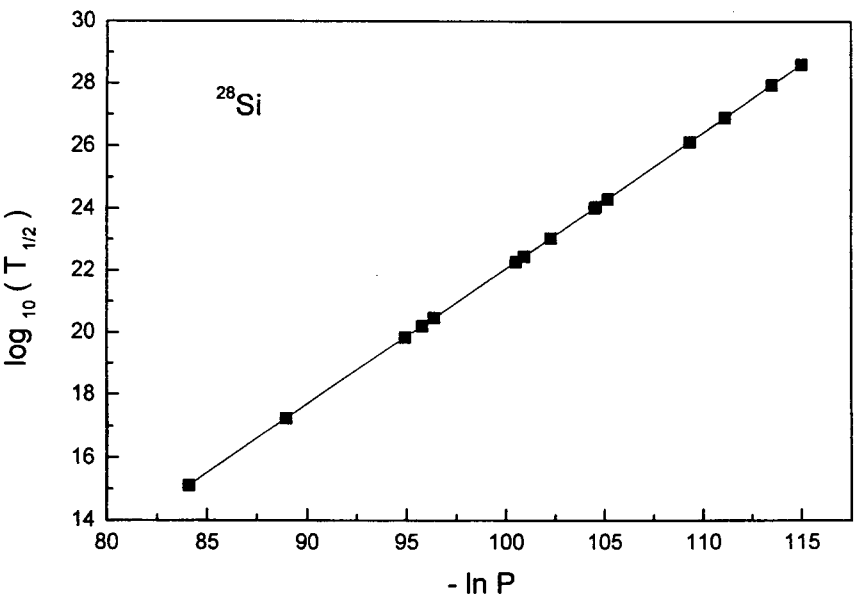

Fig. 4.60 Geiger Nuttall plot for $\log_{10}(T_{1/2})$ vs –lnP for ^{28}Si emission from various Gd isotopes.

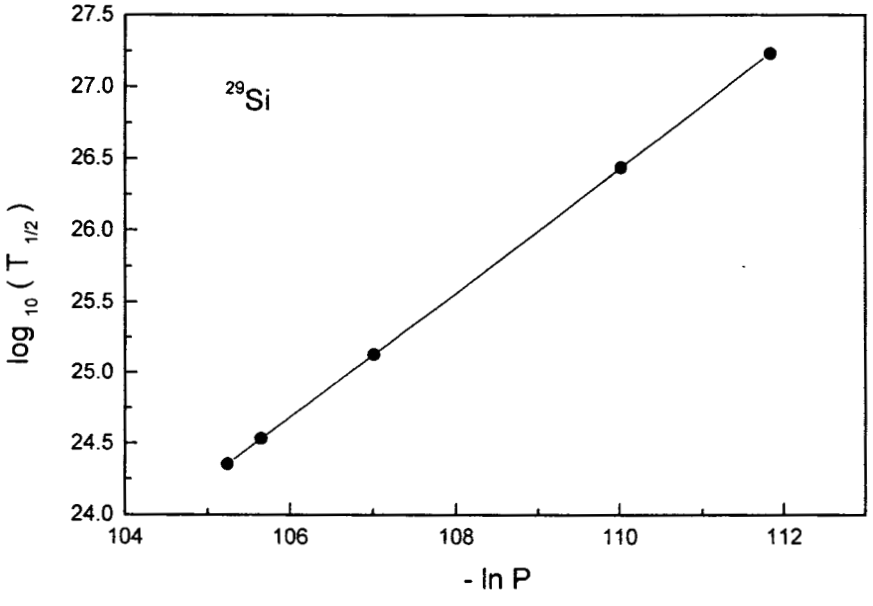

Fig. 4.61 Geiger Nuttall plot for $\log_{10}(T_{1/2})$ vs –lnP for ^{29}Si emission from various Gd isotopes.

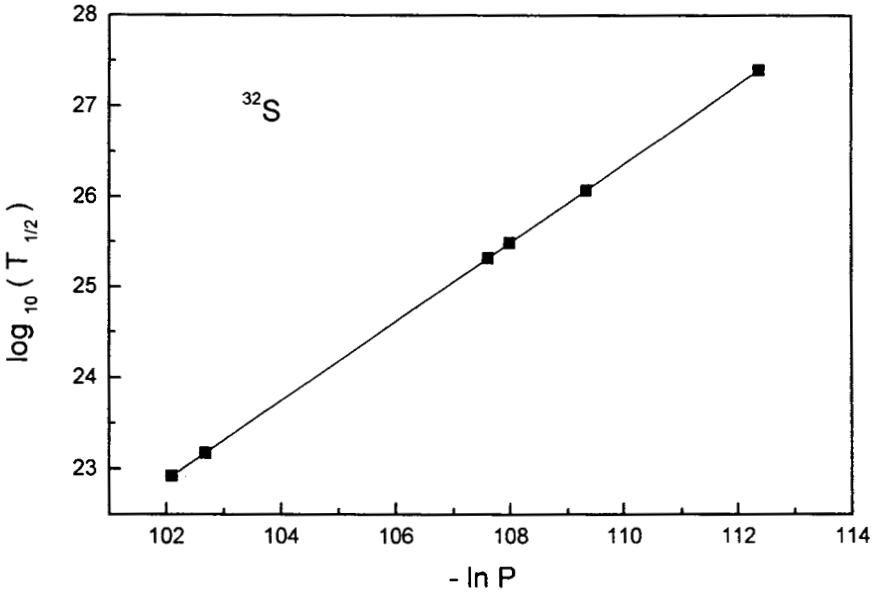

Fig. 4.62 Geiger Nuttall plot for $\log_{10}(T_{1/2})$ vs –lnP for ^{32}S emission from various Gd isotopes.

Table 4.28. Slope and intercept values of Geiger-Nuttall plots for different clusters emitted from various Gd isotopes.

Emitted cluster	Intercept Y	Slope X
^{4}He	- 48.1053	106.4218
^{8}Be	- 76.1826	297.2352
^{12}C	-102.9657	536.8863
^{16}O	-108.0414	701.0794
^{20}Ne	-125.7557	932.7649
^{24}Mg	-140.2352	1142.0761
^{28}Si	-165.7883	1434.5761
^{32}S	-207.5100	1879.8672

4.2.1.7 Conclusion

From the observed nature of Geiger-Nuttall plots for all clusters ranging from ^{4}He to ^{32}S emitted from various Ba to Gd parents, it is found that inclusion of proximity potential will not produce significant deviation to the linear nature of these plots. Nuclear structure effects (presence of nuclear proximity potential) and shell effects (through Q value) are evident from the observed variation in slopes and intercepts of Geiger-Nuttall plot for different clusters [89,98,100].

4.2.2 Decay leading to ^{132}Sn

In order to examine the role of doubly magic ^{132}Sn in exotic decay process, the exotic decay of $^{144\text{-}152}$Ba, $^{148\text{-}156}$Ce, $^{152\text{-}160}$Nd, $^{156\text{-}164}$Sm and $^{160\text{-}168}$Gd parents emitting clusters ranging from ^{4}He to ^{32}Si are studied. The Q value estimates show that these parents are stable against ^{4}He, ^{8}Be and ^{10}Be emissions (Q < 0). For ^{4}He emission ^{144,146}Ba, ^{148,150}Ce, ^{152}Nd, ^{156,158}Sm, ^{162,164,166}Gd isotopes have positive Q value but $T_{1/2}$ values show that these nuclei are stable against ^{4}He decay ($T_{1/2} > 10^{40} s$). Figures 4.63 to 4.67 represent the plots for $\log_{10}(T_{1/2})$ vs A, the mass of the parent nuclei, for various clusters from neutron rich Ba, Ce, Nd, Sm and Gd parents respectively. From these plots it is clear that the decays of ^{14}C from ^{146}Ba, ^{20}O from ^{152}Ce, ^{24}Ne from ^{156}Nd, ^{28}Mg from ^{160}Sm and ^{32}Si from ^{164}Gd have the lowest $T_{1/2}$ value compared with the decay from neighbouring ones. All these decays lead to doubly magic ^{132}Sn daughter. Table 4.29 gives the logarithm of the predicted half life time and other characteristics of neutron rich parents which decay to ^{132}Sn daughter and Table 4.30 gives that for parents which decay to the doubly magic ^{100}Sn daughter.

When results of Table 4.29 are compared with that of Table 4.30 it is found that carbon emission from ^{144}Ba and ^{146}Ba have the largest $T_{1/2}$ values than that from ^{112}Ba. Here both the cases refer to doubly magic ^{132}Sn and ^{100}Sn daughter respectively. Same is the case for oxygen emission from Ce isotopes, Ne emission from Nd isotopes, Mg

emission from Sm isotopes and Si emission from Gd isotopes. It is evident that the decay leading to ^{100}Sn is most probable for measurements $(T_{1/2} < 10^{30} s)$. The neutron proton asymmetry in parent and daughter nuclei is responsible for the reduced decay rate in the case of decays leading to ^{132}Sn. The preference of non alpha like structure in decays leading to ^{132}Sn and alpha like structure in the decays leading to ^{100}Sn point out the importance of asymmetry and symmetry of proton neutron in the two cases.

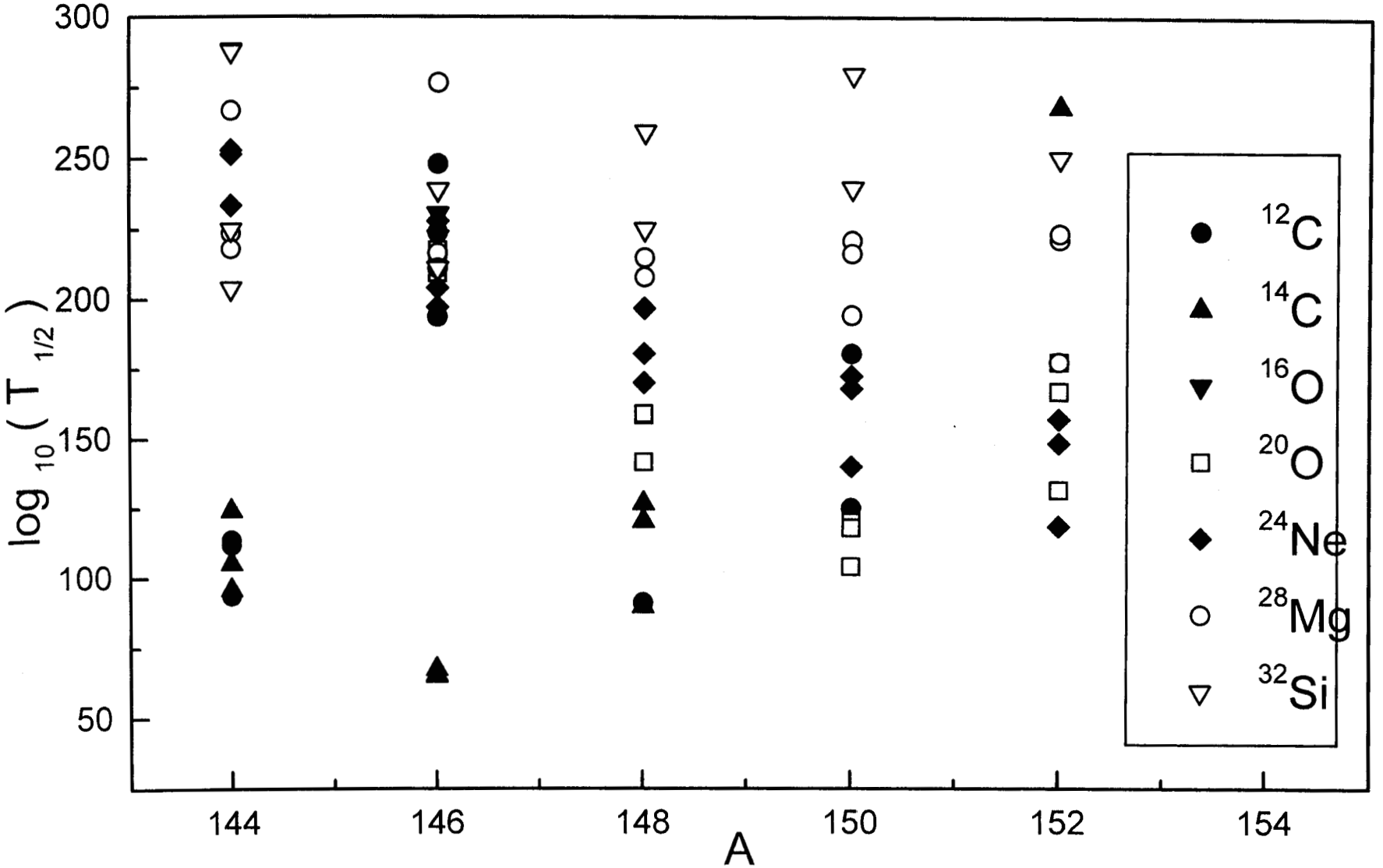

Fig. 4.63 Plot for $\log_{10}(T_{1/2})$ Vs A for various clusters from $^{144\text{-}154}$Ba isotopes.

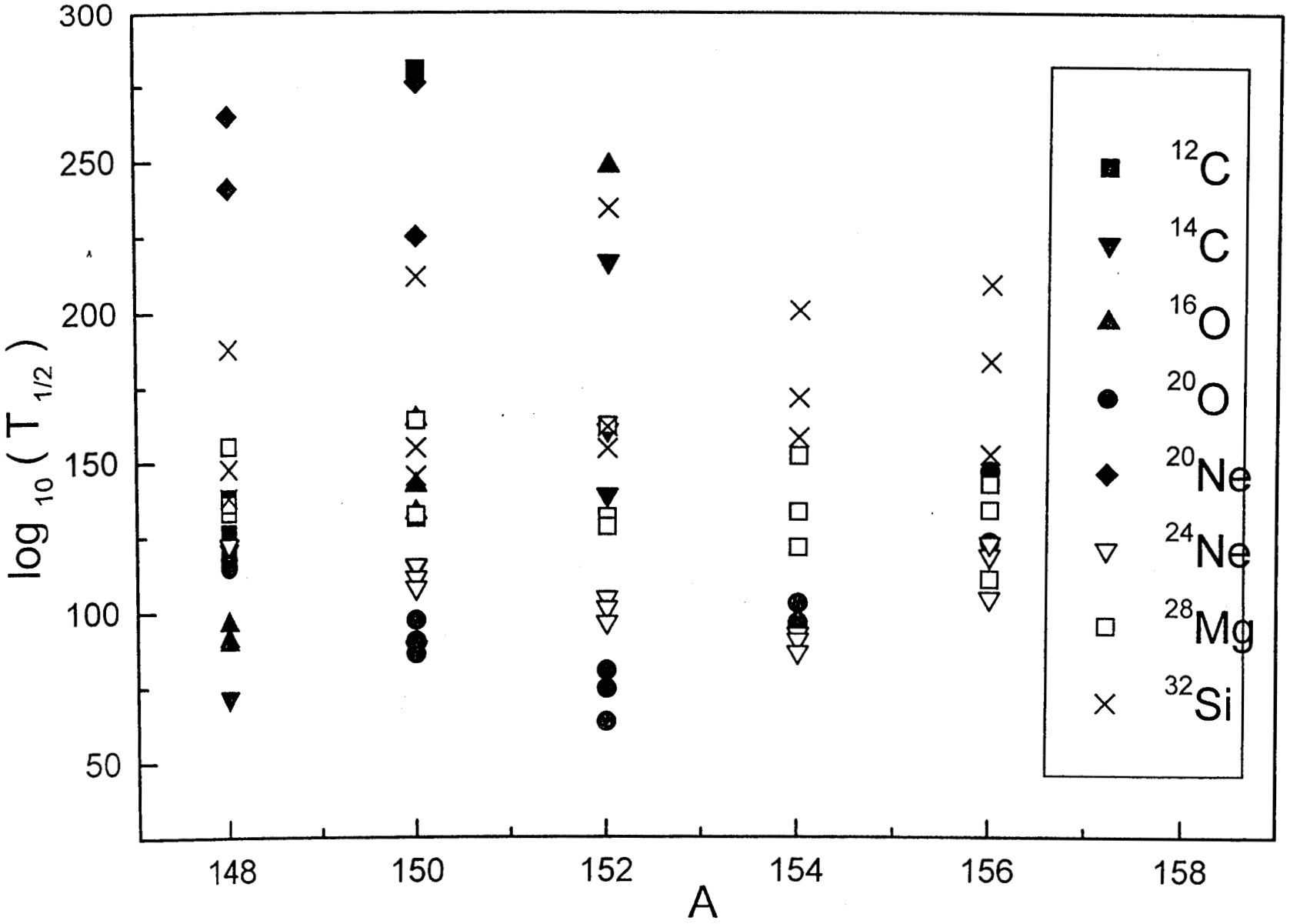

Fig. 4.64 Plot for $\log_{10}(T_{1/2})$ Vs A for various clusters from $^{148\text{-}156}$Ce isotopes.

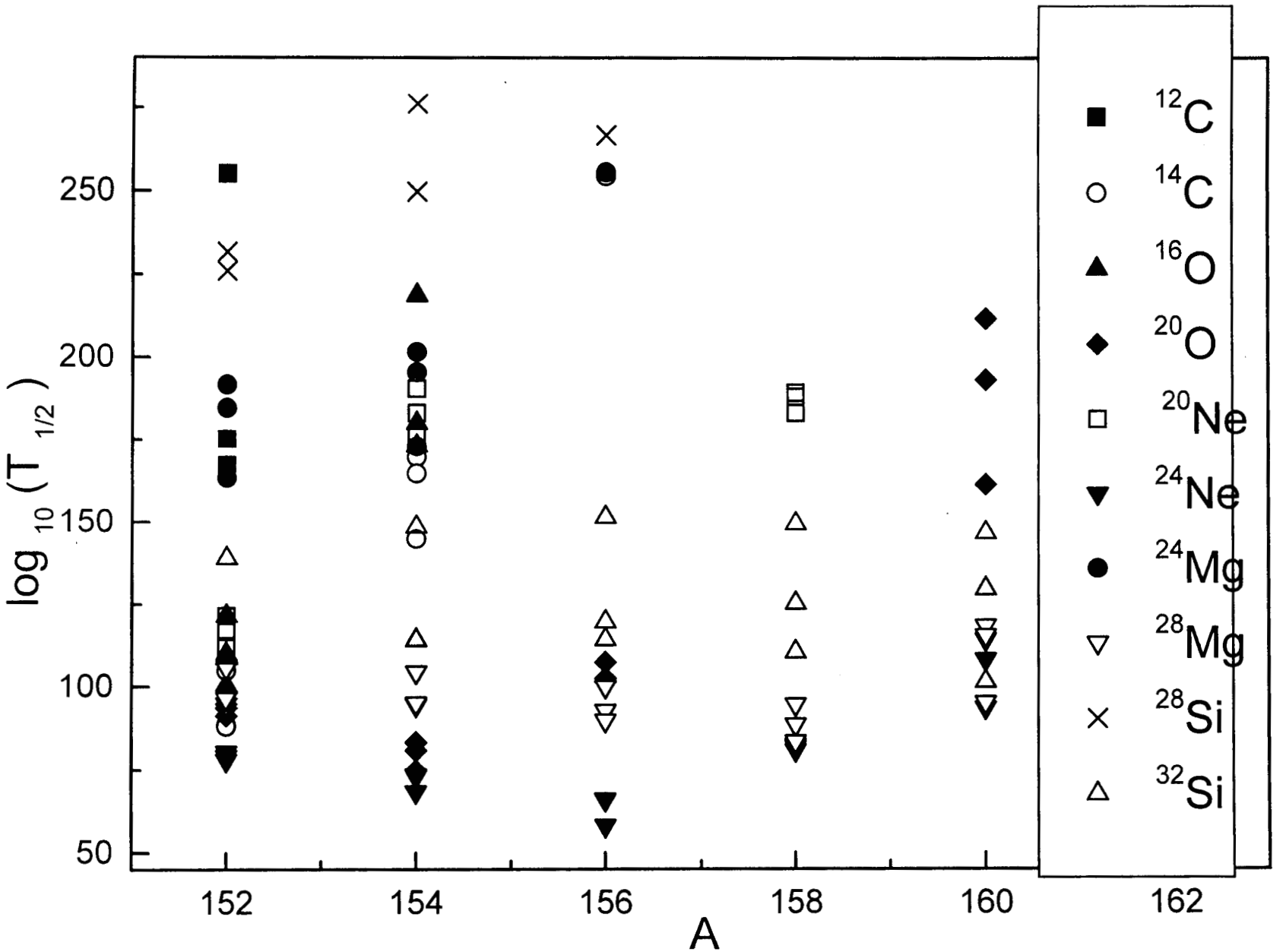

Fig. 4.65 Plot for $\log_{10}(T_{1/2})$ Vs A for various clusters from $^{152\text{-}160}$Nd isotopes.

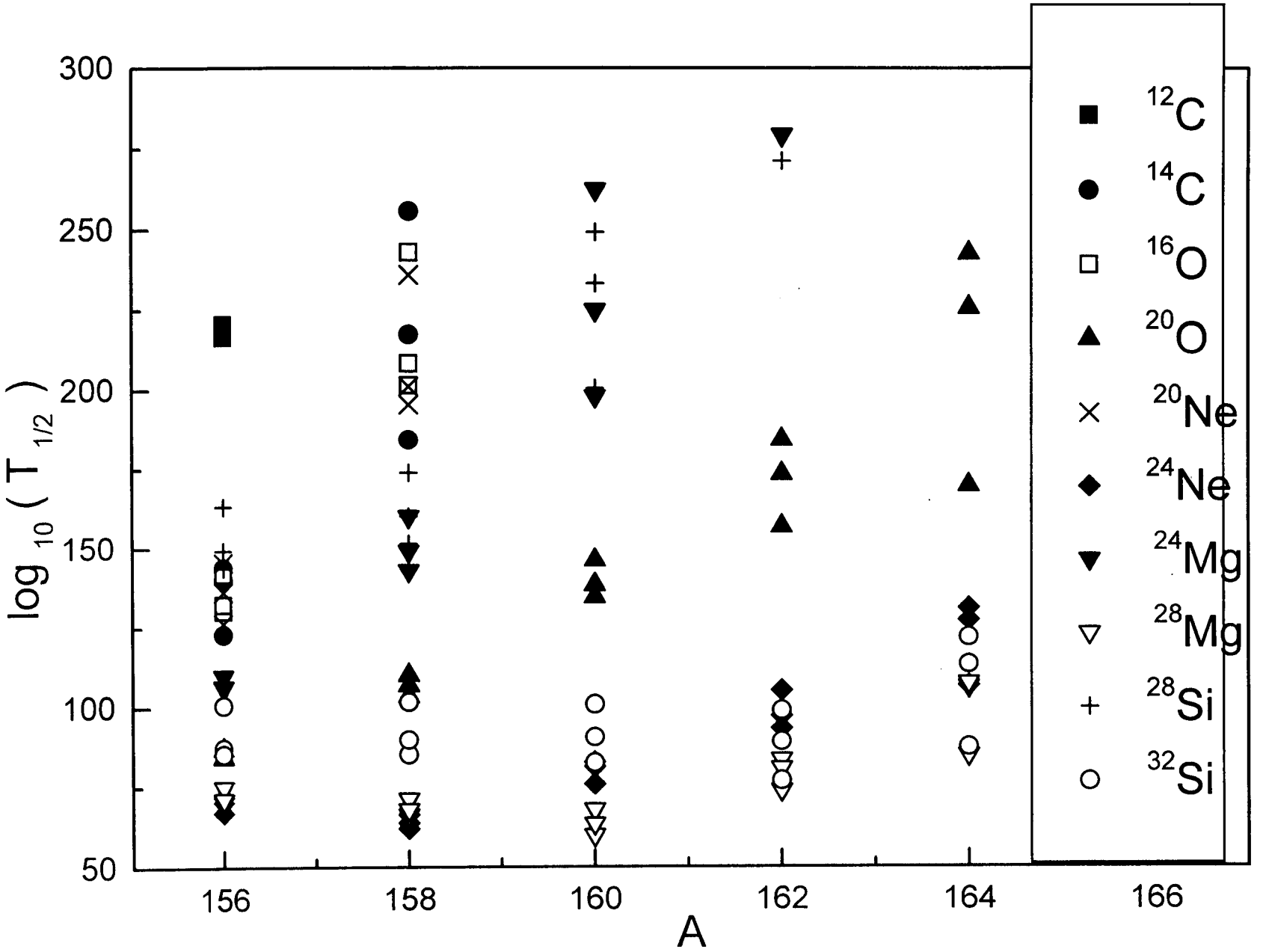

Fig. 4.66 Plot for $\log_{10}(T_{1/2})$ Vs A for various clusters from $^{156\text{-}164}$Sm isotopes.

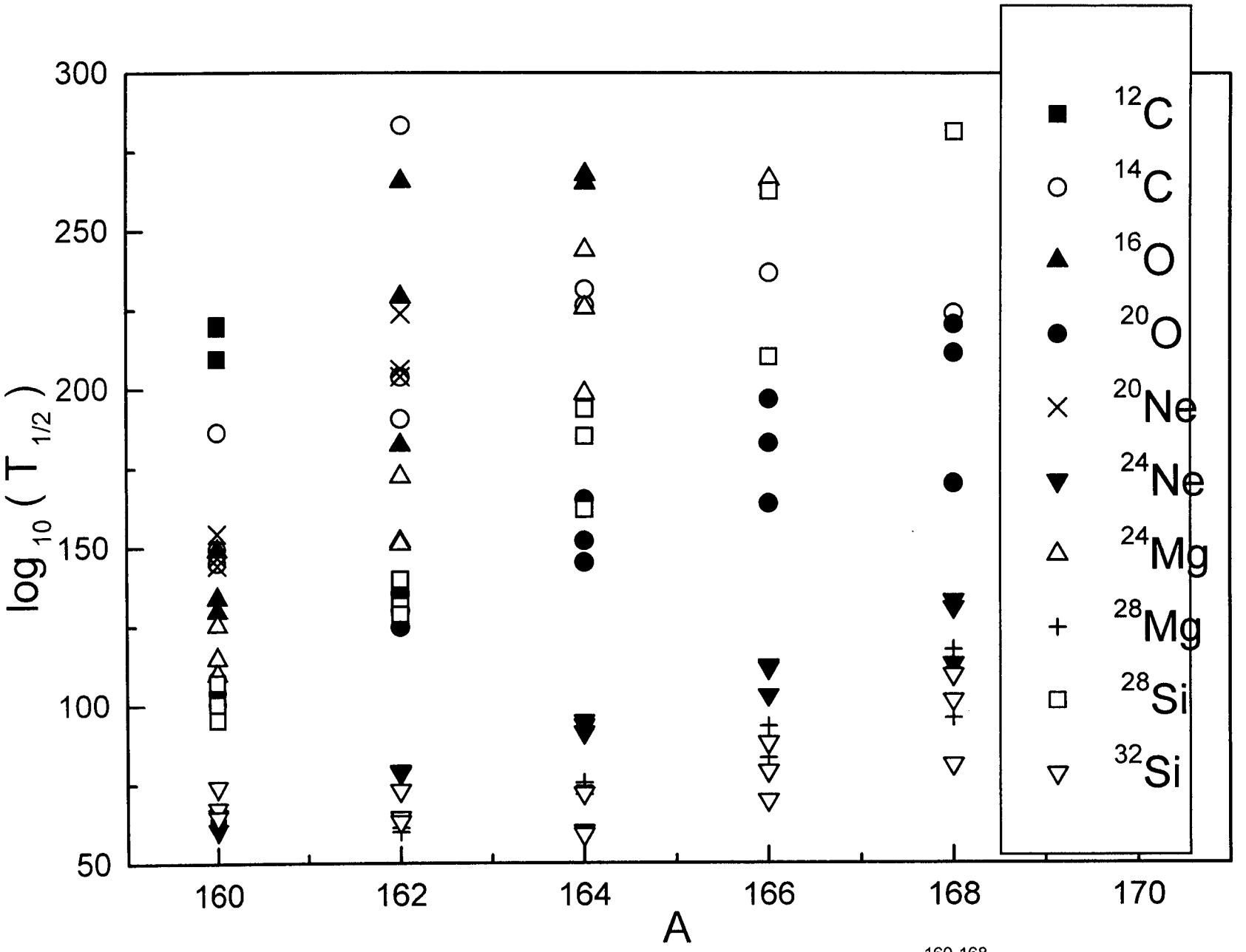

Fig. 4.67 Plot for $\log_{10}(T_{1/2})$ Vs A for various clusters from $^{160\text{-}168}$Gd isotopes.

Table 4.29. Logarithm of predicted half life time and other characteristics of parent nuclei which decays to ^{132}Sn daughter. For Q value masses are taken from [93,95,101]. Table taken from [102].

Parent nuclei	Emitted cluster	Q value (MeV)	Penetrability P	Decay constant λ	$\log_{10}(T_{1/2})$ Present
^{144}Ba	^{12}C	4.55	7.0074E-133	8.8799E-113	111.89
		5.49	7.7577E-115	1.1862E-94	93.77
		4.47	1.1304E-134	1.4073E-114	113.69
^{146}Ba	^{14}C	8.09	1.2946E-84	2.8726E-66	65.38
		7.89	1.1441E-88	2.4758E-68	67.45
		8.13	3.2649E-86	7.2803E-66	64.98
^{148}Ce	^{16}O	10.00	1.6875E-117	4.5964E-97	96.18
		10.66	5.6769E-111	1.6483E-90	89.62
		10.59	1.2318E-111	3.5530E-91	90.92
^{152}Ce	^{20}O	12.49	5.4296E-102	1.8387E-81	80.58
		14.81	4.3078E-85	1.7298E-64	63.60
		13.24	4.6722E-96	1.6772E-75	74.62
^{152}Nd	^{20}Ne	12.85	7.6972E-143	2.6818E-122	121.41
		13.83	1.0210E-133	3.8287E-113	112.26
		13.35	4.6175E-138	1.6714E-117	116.62
^{156}Nd	^{24}Ne	21.65	9.6577E-88	5.6639E-67	66.09
		23.34	9.2285E-80	5.8347E-59	58.07
		21.69	1.5273E-87	8.9734E-67	65.89
^{156}Sm	^{24}Mg	20.40	2.1438E-131	1.1847E-110	109.77
		20.93	4.7732E-128	2.7062E-107	106.41
		20.96	7.3216E-128	4.1570E-107	106.22
^{160}Sm	^{28}Mg	29.35	1.2402E-89	9.8581E-69	67.85
		31.41	1.3768E-81	1.1712E-60	59.77
		30.47	3.6406E-85	3.0043E-64	63.36
^{160}Gd	^{28}Si	28.02	5.6536E-129	4.2904E-108	107.21
		30.55	4.9152E-117	4.0669E-96	95.23
		29.42	3.4710E-122	2.7658E-101	100.40
^{164}Gd	^{32}Si	36.95	6.4111E-94	6.4156E-73	72.03
		40.50	7.2271E-82	7.9269E-61	59.94
		40.80	6.4931E-81	7.1746E-60	58.98

Table 4.30. Logarithm of predicted half life time and other characteristics of parents which decays to ^{100}Sn and comparison with PCM [86,91]. Table taken from [103].

Parent nuclei	Emitted cluster	Q value (MeV)	Penetrability P	Decay constant λ	$\log_{10}(T_{1/2})$ Present	PCM
^{112}Ba	^{12}C	21.46	1.92605E-25	1.15120E-04	3.78	3.75
^{116}Ce	^{16}O	31.71	6.12654E-28	5.29147E-07	6.12	6.14
^{120}Nd	^{20}Ne	39.41	4.80487E-36	5.13421E-15	14.13	17.04
^{124}Sm	^{24}Mg	49.70	3.36335E-39	4.52807E-18	17.18	17.32
^{128}Gd	^{28}Si	63.03	3.08642E-37	5.26874E-16	15.12	12.01

THEORETICAL STUDIES OF NUCLEAR STRUCTURE IN VIEW OF EXOTIC NUCLEAR DECAYS

Thesis submitted to the University of Calicut
in partial fulfilment of the requirements
for the Degree of

DOCTOR OF PHILOSOPHY

IN PHYSICS

By

K.P. SANTHOSH

DEPARTMENT OF PHYSICS
UNIVERSITY OF CALICUT

2002

CHAPTER 5

EFFECT OF DEFORMATION

Exotic decay of various parents emitting different clusters, which we have so far studied are treating parents and fragments as spheres. In this chapter an improved model is given incorporating ground state deformation of both parent and daughter. We studied the effect of deformation of parent and daughter on half life time treating emitted cluster as spherical.

5.1.Details of the model

Here the emitted cluster is assumed to be spherical but the parent and daughter nuclei may have axially symmetric deformation. The potential energy barrier will depend on the polar angle θ between the axis of symmetry of the parent or daughter and the direction of the emitted cluster.

If the nuclei have spheroidal shape, the radius vector $R_i(\theta)$ making an angle θ with the axis of symmetry locating sharp surface of deformed nuclei is given by [23]

$$R_i(\theta) = R_i[1 + \sum_{n=0}^{\infty} \sum_{m=-n}^{n} \beta_{nm} Y_{nm}(\theta)] \tag{5.1}$$

If we consider spheroidal deformation β_2 then

$$R_i(\theta) = R_i[1 + \beta_2\left(\frac{5}{4\pi}\right)^{1/2}\left(\frac{3}{2}\cos^2\theta - \frac{1}{2}\right)] \tag{5.2}$$

and if Nilssion hexadecapole deformation β_4 is also included in the deformation then equation (5.2) becomes

$$R_i(\theta) = R_i[1 + \beta_2\left(\frac{5}{4\pi}\right)^{1/2}\left(\frac{3}{2}\cos^2\theta - \frac{1}{2}\right) + \beta_4\left(\frac{9}{4\pi}\right)^{1/2}\frac{1}{8}(35\cos^4\theta - 30\cos^2\theta + 3)] \tag{5.3}$$

The central Siissmann radius vector $C_i(\theta)$ specifying the parent and daughter surfaces related to $R_i(\theta)$ as [28]

$$C_i(\theta) = R_i(\theta) - \frac{1}{2}kb^2 \tag{5.4}$$

where k is the total curvature of the surface at the point in consideration and b $\approx$1 is the width (diffuseness) of the nuclear surface.

The Siissmann central radius C_2 of emitted cluster is $C_2 = R_2 - \frac{b^2}{R_2}$ (5.5)

The Coulomb potential between the spherical emitted cluster and the spheroidal daughter nucleus is given by $V_c = \frac{Z_1 Z_2 e^2}{r}$. Here Z_1 and Z_2 are the atomic numbers of the daughter and the emitted cluster and $r = z + C_1(\theta) + C_2$, is the distance between the fragment centers. The proximity potential V_p now becomes, as given by [26]

$$V_p(z) = 4\pi\gamma b\frac{C_1(\theta)C_2}{C_1(\theta) + C_2}\phi\left(\frac{z}{b}\right) \tag{5.6}$$

With these modifications, we have calculated the barrier penetrability and half life time using equations 2.87 and 2.88

5.2 Effect of deformation on half life time

We studied the effect of deformation of parent and daughter on half life time treating emitted cluster as spherical. The deformation parameters β_2 and β_4 are taken from [104]. In Table 5.1, (a) gives half life time without considering deformation, (b) gives the values when considering both parent and daughter deformation, (c) gives those when daughter deformation alone is considered and (d) gives the half life time when parent deformation alone is considered.

Figures 5.1 and 5.2 give the plot for logarithm of ratio of experimental branching ratio to calculated (theoretical) branching ratio, $\log_{10}(B_{EX}/B_{TH})$ vs A, mass number of the parent for ^{14}C emission and ^{24}Ne emission respectively. Here (a) represents plot for the case without considering deformation, (b) for the case of parent and daughter deformation, (c) for the case of daughter deformation and (d) for the case of parent deformation respectively. The experimental half life time for respective alpha decay $T_{1/2}^{alpha}$ are taken from [65].

5.3 Results and discussion

When deformation effects are included, half life time value is found to decrease slightly. When logarithm of predicted half life time obtained treating parent and fragments as spherical are compared with that for deformed parent and daughter it is found that deviation (change) in half life time value increases with increase in mass of the parent and also with increase in mass of the cluster. When deformation of parent alone is taken there is appreciably no deviation in half life time value. This is because parent deformation affects relatively small pre scission part of the barrier but it will not affect the barrier corresponding to separated fragments. In asymmetric disintegration most of the barrier corresponding to separated fragments.

Table 5.1. Comparison of calculated values of logarithm of half life time for the case with out deformation (a), with parent and daughter deformation (b), with daughter deformation (c), with parent deformation (d), with experimental values.

Parent nuclei	Daughter nuclei	Emitted cluster	Q value (MeV)	Deformation Parent β_2	daughter β_4	daughter β_2	$\log_{10}(T_{1/2})$ (a)	(b)	(c)	(d)	Expt.
^{221}Fr	^{207}Tl	^{14}C	31.28	0.098	-0.060	0.003	13.90	13.73	13.79	13.85	14.52
^{221}Ra	^{207}Pb		32.39	0.098	-0.060	0.003	12.58	12.41	12.46	12.52	13.39
^{222}Ra	^{208}Pb		33.05	0.104	-0.060	0.003	11.07	10.90	10.96	11.01	11.01
^{223}Ra	^{209}Pb		31.85	0.138	-0.075	0.003	13.69	13.45	13.58	13.56	15.04
^{224}Ra	^{210}Pb		30.53	0.144	-0.075	0.003	16.74	16.45	16.62	16.55	15.68
^{225}Ac	^{211}Bi		30.48	0.151	-0.080	0.003	18.03	17.72	17.92	17.83	17.16
^{226}Ra	^{212}Pb		28.21	0.151	-0.080	0.003	22.55	22.21	22.44	22.31	21.34
^{230}Th	^{206}Hg	^{24}Ne	57.78	0.185	-0.075	-0.003	26.00	25.34	26.19	25.17	24.61
^{231}Pa	^{207}Tl		60.42	0.185	-0.080	0.003	22.56	21.70	22.36	21.87	22.88
^{232}U	^{208}Pb		62.31	0.192	-0.080	0.003	20.72	19.83	20.52	20.01	20.40
^{233}U	^{209}Pb		60.50	0.192	-0.080	0.003	24.15	23.16	23.95	23.34	24.84
^{234}U	^{210}Pb		58.84	0.198	-0.075	0.003	27.39	26.16	27.20	26.33	25.92
^{232}Th	^{206}Hg	^{26}Ne	55.97	0.192	-0.070	-0.003	29.54	28.81	29.74	28.63	>29.2
^{234}U	^{208}Pb		59.47	0.196	-0.075	0.003	25.88	24.87	25.67	25.05	25.88
^{234}U	^{206}Hg	^{28}Mg	74.13	0.198	-0.075	-0.003	27.55	26.47	27.78	26.27	27.54
^{238}Pu	^{210}Pb		75.93	0.205	-0.060	0.003	28.31	26.32	28.07	26.58	25.70
^{237}Np	^{207}Tl	^{30}Mg	75.02	0.198	-0.070	0.003	27.34	25.92	27.09	26.14	>26.9
^{238}Pu	^{208}Pb		77.03	0.025	-0.060	0.003	25.70	24.07	25.45	24.29	25.70
^{238}Pu	^{206}Hg	^{32}Si	91.21	0.205	-0.060	-0.003	28.65	26.82	28.94	26.58	25.27
^{241}Am	^{207}Tl	^{34}Si	93.84	0.212	-0.050	0.003	25.40	23.16	25.10	23.41	>25.3

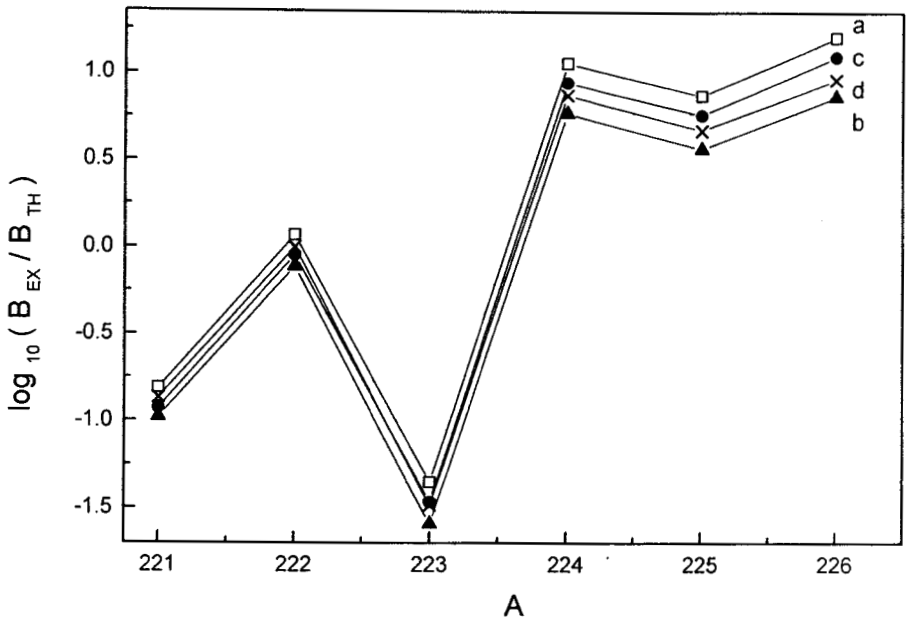

Fig. 5.1 Plot of $\log_{10}(B_{EX}/B_{TH})$ Vs A for ^{14}C emission from various parents.

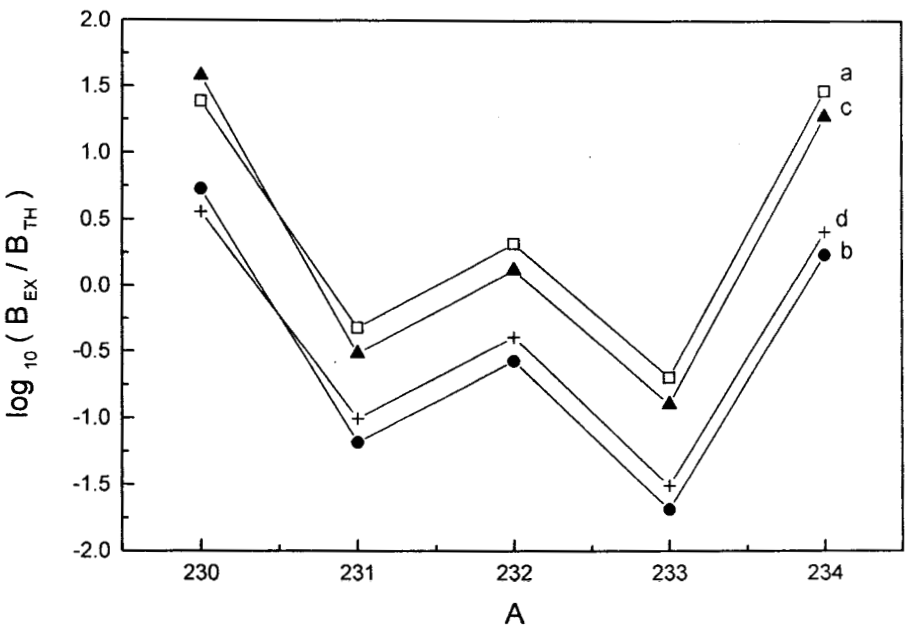

Fig. 5.2 Plot of $\log_{10}(B_{EX}/B_{TH})$ Vs A for ^{24}Ne emission from various parents.

THEORETICAL STUDIES OF NUCLEAR STRUCTURE IN VIEW OF EXOTIC NUCLEAR DECAYS

Thesis submitted to the University of Calicut
in partial fulfilment of the requirements
for the Degree of

DOCTOR OF PHILOSOPHY

IN PHYSICS

By

K.P. SANTHOSH

DEPARTMENT OF PHYSICS
UNIVERSITY OF CALICUT

2002

CHAPTER 6

FINE STRUCTURE

Greiner and Schied [38] in 1986 anticipated the fine structure (decay to excited states of daughter) in exotic decay and Brillard et al [55] in 1989 observed this phenomenon experimentally in the ^{14}C emission from ^{223}Ra. This phenomenon is rather similar to the fine structure of α decay observed by Rosenblum [105].

The measurements done by Brillard et al [55], Hussonnois et al [56] and by Hourani et al [69] revealed a fine structure spectrum involving an intense ^{14}C branch to an excited state of ^{209}Pb daughter. The low hindrance factor (HF) values deduced for the first ^{209}Pb excited state is due to the existence of common shell model configuration describing the odd neutron in both parent and daughter nuclei. In a recent experiment, with maximum resolution of ^{14}C ion [90 KeV full width at half maximum (FWHM)] and with no alpha particle background done in 1995 by Hourani et al [68], a total number of 899 ^{14}C events were recorded, 130 events for transition to ground state of ^{209}Pb, 768 events leading to 1^{st} excited state and a solitary event at the location of 4^{th} excited state. No event was detected at the location of 2^{nd} and 3^{rd} excited states. The relative intensities of transition to ground state and 1^{st} excited state are 18% and 82% respectively. The decay scheme for ^{14}C fine structure from ^{223}Ra is shown in Fig 6.1

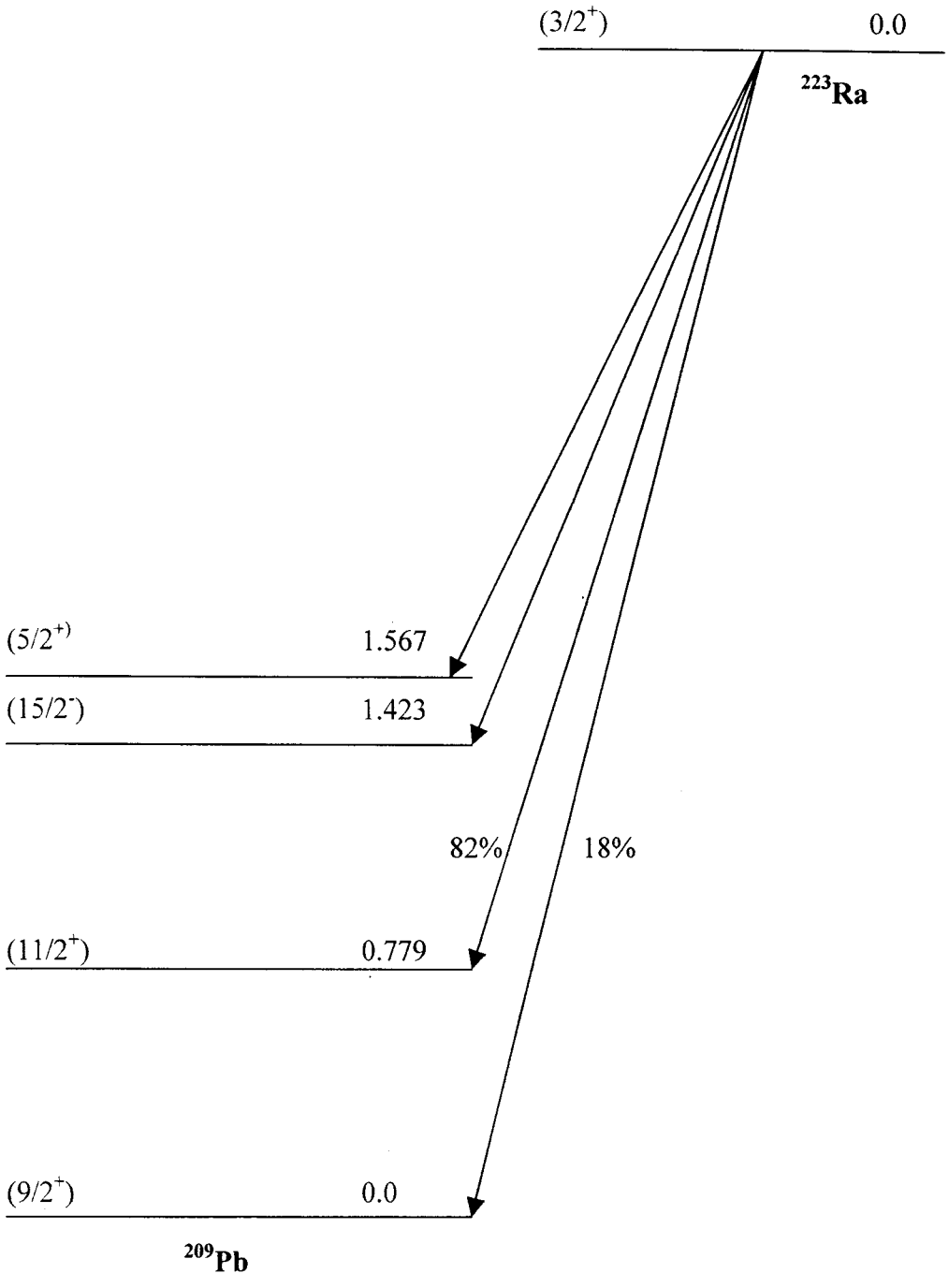

Fig. 6.1. ^{14}C Decay scheme for ^{223}Ra

6.1 Hindrance Factor

There are different definitions for Hindrance factor (HF), some of them are related to model dependent parameter (eg. reduced width) [68,106,107] In analogy to the barrier penetration theory of alpha decay, all transitions other than ground state to ground state transition of even-even nuclei are observed to be slower than the theoretical predictions and are said to be hindered. This odd-even effect of parent nuclei is denoted by a quantity called hindrance factor (HF), simply a ratio between calculated (theoretical) and measured decay constant or ratio between experimental half life time and theoretical half life time [72]. Conventionally a transition is favoured if hindrance factor is low close to 1 and is hindered if it is greater than 5.

$$\mathrm{HF} = \frac{\lambda_{cal}}{\lambda_{expt}} = \frac{T_{1/2}^{expt}}{T_{1/2}^{cal}} \tag{6.1}$$

For fine structure studies we included centrifugal term $V_\ell = \frac{\hbar^2 \ell(\ell+1)}{2\mu r^2}$ in the interacting potential barrier. The angular momentum ℓ is determined from the spin and parity conservation

$$| J_f - J_i | \leq \ell \leq J_f + J_i \tag{6.2}$$

$$\pi_i \pi_f (-1)^\ell = 1 \tag{6.3}$$

6.2 ^{14}C fine structure in ^{223}Ra isotope

Table 6.1 gives calculated logarithm of half life time and hindrance factor for ^{14}C transition from ^{223}Ra (g.s $3/2^{+}$) to various excited states of ^{209}Pb. Here effective Q value is $Q_{eff} = Q - E^{*}$, where E^{*} is the excitation energy and J^{π} represent the spin and parity. Experimental half life time values are taken from Hourani et al [68]

6.3 Fine structure in the exotic decay of other isotopes

Logarithm of half life time and other characteristics for ^{14}C fine structure from ^{221}Fr, ^{225}Ac are given in Table 6.2 and Table 6.3 respectively. Tables 6.4 and 6.5 show ^{24}Ne fine structure from ^{231}Pa, ^{233}U respectively.

Table 6.1. Logarithm of half life time and Hindrance factor for ^{14}C transition from ^{223}Ra (g.s $3/2^{+)}$ to various excited states of ^{209}Pb. Table taken from Ref [108]

E* (MeV)	J^{π}	Q_{eff} (MeV)	ℓ	Penetrability P	Decay constant λ	$\log_{10}(T_{1/2})$ Present	Expt.	Hindrance factor
0	$9/2^{+}$	31.850	0	1.61224E-35	1.40840E-14	13.69	15.79	125.31
			4	9.25069E-36	8.08111E-15	13.93		71.895
			6	5.04396E-36	4.40624E-15	14.20		39.201
0.779	$11/2^{+}$	31.071	0	2.59232E-37	2.20918E-16	15.50	15.13	0.430
			4	1.49779E-39	1.27642E-16	15.73		0.248
			6	8.22911E-38	7.01287E-17	15.99		0.137
1.423	$15/2^{-}$	30.427	0	7.65952E-39	6.39217E-18	17.04	>18.08	>11.09
			7	1.69161E-39	1.41172E-18	17.69		>2.449
1.567	$5/2^{+}$	30.283	0	3.43699E-39	2.85473E-18	17.39	>18.09	>5.068
			2	2.92035E-39	2.42562E-18	17.46		>4.306
			4	1.99967E-39	1.66091E-18	17.62		>2.948

Table 6.2. Logarithm of half life time and other characteristics of ^{14}C transition from ^{221}Fr (g.s $5/2^-$) to various excited states of ^{207}Tl. ['?' symbol shows one of the two spins is unknown].

E* (MeV)	J^π	Q_{eff} (MeV)	ℓ	Penetrability P	Decay constant λ	$\log_{10}(T_{1/2})$ Present
0	$1/2^+$	31.280	0	1.00756E-35	8.64424E-15	13.90
			3	7.20308E-36	8.47631E-15	13.91
0.351	$3/2^+$	30.929	0	1.55369E-36	1.31801E-15	14.72
			1	1.46949E-36	1.71951E-15	14.61
			3	1.11283E-36	1.30217E-15	14.73
1.340	$11/2^-$	29.940	0	6.83666E-39	5.61414E-18	17.09
			4	3.95773E-39	4.55646E-18	17.18
			6	2.17911E-39	2.50877E-18	17.44
			8	9.73159E-40	1.12038E-18	17.94
1.670	$5/2^+$	29.610	0	1.05887E-39	8.59944E-19	17.90
			1	1.00266E-39	1.14796E-18	17.78
			3	7.63761E-40	8.74445E-19	17.90
			5	4.69112E-40	5.37095E-19	18.11
2.690	?	28.590	0	2.76048E-42	2.16465E-21	20.51

Table 6.3. Logarithm of half life time and other characteristics of ^{14}C transition from ^{225}Ac (g.s $3/2^-$) to various excited states of ^{211}Bi. ['?' symbol shows one of the two spins is unknown].

E* (MeV)	J^π	Q_{eff} (MeV)	ℓ	Penetrability P	Decay constant λ	$\log_{10}(T_{1/2})$ Present
0	$9/2^-$	30.480	0	7.70892E-40	6.44460E-19	18.03
			4	4.51307E-40	3.77289E-19	18.26
			6	2.51544E-40	2.10289E-19	18.52
0.404	$7/2^-$	30.075	0	7.84694E-41	6.47287E-20	19.03
			2	6.68692E-41	5.51598E-20	19.09
			4	4.60997E-41	3.80272E-20	19.26
0.766	?	29.714	0	9.84008E-42	8.01942E-21	19.94
0.832	$9/2^-$	29.648	0	6.72995E-42	5.47265E-21	20.10
			4	3.96824E-42	3.22689E-21	20.33
			6	2.22910E-42	1.81266E-21	20.58
0.951	?	29.529	0	3.36104E-42	2.72214E-21	20.46

Table 6.4. Logarithm of half life time and other characteristics of ^{24}Ne transition from ^{231}Pa (g.s $3/2^-$) to various excited states of ^{207}Tl. ['?' symbol shows one of the two spins is unknown]. Table taken from [109].

E* (MeV)	J^π	Q_{eff} (MeV)	ℓ	Penetrability P	Decay constant λ	$\log_{10}(T_{1/2})$ Present
0	$1/2^+$	60.420	0	1.16307E-44	1.90358E-23	22.56
			1	1.11848E-44	1.83060E-23	22.58
0.351	$3/2^+$	60.069	0	2.38432E-45	3.87972E-24	23.25
			1	2.29338E-45	3.73174E-24	23.27
			3	1.88852E-45	3.07295E-24	23.35
1.340	$11/2^-$	59.080	0	2.59046E-47	4.14574E-26	25.22
			4	1.76675E-47	2.82749E-26	25.39
			6	1.16141E-47	1.85871E-26	25.57
1.670	$5/2^+$	58.750	0	5.61932E-48	8.94286E-27	25.89
			1	5.40902E-48	8.60818E-27	25.91
			3	4.47068E-48	7.11485E-27	25.99
2.690	?	57.730	0	4.68492E-50	7.32636E-29	27.98

Table 6.5. Logarithm of half life time and other characteristics of ^{24}Ne transition from ^{233}U (g.s $5/2^+$) to various excited states of ^{209}Pb

E* (MeV)	J^π	Q_{eff} (MeV)	ℓ	Penetrability P	Decay constant λ	$\log_{10}(T_{1/2})$ Present
0	$9/2^+$	60.500	0	3.00812E-46	4.92987E-25	24.15
			2	2.68093E-46	4.39365E-25	24.20
			4	2.05016E-46	3.35991E-25	24.31
			6	1.34668E-46	2.20701E-25	24.50
0.779	$11/2^+$	59.721	0	8.59018E-48	1.38968E-26	25.70
			4	5.88001E-48	9.51239E-27	25.86
			6	3.88073E-48	6.27806E-27	26.04
			8	2.20734E-48	3.57093E-27	26.29
1.423	$15/2^-$	59.077	0	4.36364E-49	6.98316E-28	27.00
			5	2.48539E-49	3.97739E-28	27.24
			7	1.52931E-49	2.44737E-28	27.45
			9	8.12915E-50	1.30091E-28	27.73
1.567	$5/2^+$	58.933	0	2.22971E-49	3.55952E-28	27.29
			2	1.99234E-49	3.18058E-28	27.33
			4	1.53279E-49	2.44696E-28	27.45
2.032	$1/2^+$	58.468	0	2.51738E-50	3.98706E-29	28.24
			2	2.25106E-50	3.56525E-29	28.29
2.152	$1/2^-$	58.348	0	1.42910E-50	2.25877E-29	28.49
			3	1.14327E-50	1.80701E-29	28.58

6.4 Results and discussion

Table.6.1 gives hindrance factor values for ^{14}C transition from $3/2^+$ ground state of ^{223}Ra to various final states of ^{209}Pb. It is found that the transition to ground state $9/2^+$ (HF=125, for $\ell = 0$) is strongly hindered, while the one to the first excited state $11/2^+$ (HF=0.43, for $\ell = 0$) is favoured. The transition to 2^{nd} and 3^{rd} excited state $15/2^-$ and $5/2^+$ (HF>11 and HF>5 respectively, for $\ell = 0$) are also hindered [108]. Same is the case when centrifugal term (angular momentum) is included in the interacting potential. These findings are in good agreement with experiments done by Hourani et al [68].

Hindrance factor pattern observed in ^{14}C decay of ^{223}Ra is similar to hindrance factor pattern observed in alpha decay of ^{227}Th, where both the parents have reflection asymmetric deformed shape [110]. This pattern results because ground state of the parent is parity mixed state, very different from the ground state ($9/2^+$) of daughter but very similar to the parity mixed excited state ($11/2^+$state) of daughter. ^{223}Ra Nilsson deformed wave function contains large components arising from the spherical $i_{11/2}$ neutron shell model orbit but none from the $g_{9/2}$ state, the ground state configuration of ^{209}Pb. The fine structure from ^{223}Ra gives direct evidence on the presence of spherical component in the deformed parent nucleus [108].

THEORETICAL STUDIES OF NUCLEAR STRUCTURE IN VIEW OF EXOTIC NUCLEAR DECAYS

Thesis submitted to the University of Calicut
in partial fulfilment of the requirements
for the Degree of

DOCTOR OF PHILOSOPHY

IN PHYSICS

By

K.P. SANTHOSH

DEPARTMENT OF PHYSICS
UNIVERSITY OF CALICUT

2002

CHAPTER 7

TRANSITION FROM CLUSTER MODE TO FISSION MODE

As mentioned in chapter 2, for studying exotic decay two types of models are used; namely, the cluster model and the fission model. In the cluster model the cluster of nucleons is assumed to be formed initially within the parent nucleus, which then penetrate the nuclear interacting barrier. In fission model the parent nuclei is considered to deform continuously as it penetrates the nuclear barrier and reach the scission or saddle shape after running down the Coulomb barrier where mass and charge distributions are decided. In the study of exotic decay of parent nuclei cluster like shapes are preferred for very high asymmetric mass splitting and fissioning shapes are more suitable for less asymmetric and symmetric mass splitting. The present chapter is to study the cluster formation probability (within fission model) in some heavy nuclei with $Z \geq 100$ and to find the transition point from cluster mode to fission mode.

7.1 The theory

According to the theory developed by Poenaru et al [99] the cluster formation probability, S can be calculated within fission model as penetrability of internal part (overlap region) of the barrier given as

$$S = \exp(-K_{ov}) \tag{7.1}$$

$$\text{where, } K_{ov} = \frac{2}{\hbar}\int_{\varepsilon_i}^{0}\sqrt{2\mu(V-Q)}dz \tag{7.2}$$

Here $z = 0$ represent the touching configuration and ε_i is inner turning point of W K B penetrability defined as $V(\varepsilon_i) = Q$.

7.2 Decay of heavy nuclei

Table 7.1 to 7.8 give cluster formation probability for various clusters ranging from ^{4}He to ^{24}Ne for the decay of ^{246}Fm, ^{254}No, ^{256}No, ^{274}Rf, ^{262}Sg, ^{270}110, ^{272}110 and ^{278}112 respectively. For Q value the masses are taken from Moller and Nix [95], Moller et al [93] and Wapstra et al [101]. Figures 7.1 to 7.8 give plots for $-\log_{10}(S)$ vs A_2, mass of the emitted cluster for ^{246}Fm, ^{254}No, ^{256}No, ^{274}Rf, ^{262}Sg, ^{270}110, ^{272}110 and ^{278}112 respectively.

Table 7.1. Calculated Q value and cluster formation probability for the decay of ^{246}Fm emitting various clusters.

Parent nuclei	Emitted cluster	Daughter nuclei	Q value (MeV)	Cluster formation probability, S
^{246}Fm	^{4}He	^{242}Cf	8.506	2.30552E-01
			8.206	2.04860E-01
			8.376	2.19033E-01
	^{8}Be	^{238}Cm	16.14	4.51125E-05
			15.59	3.41123E-05
			15.78	3.79406E-05
	^{10}Be	^{236}Cm	10.09	5.15128E-06
			9.693	4.09377E-06
			9.643	3.97824E-06
	^{12}C	^{234}Pu	30.51	1.19773E-08
			29.76	7.39360E-09
			27.96	2.37644E-09
	^{14}C	^{232}Pu	29.30	1.77529E-08
			28.66	1.10772E-08
			27.08	3.51837E-09
	^{16}C	^{230}Pu	19.92	4.98900E-11
			19.43	3.46974E-11
			18.04	1.25216E-11
	^{16}O	^{230}U	44.74	7.55606E-13
			42.23	1.15990E-13
			43.26	2.47782E-13
	^{18}O	^{228}U	44.42	1.87884E-12
			42.62	4.12259E-13
			41.69	1.91326E-13
	^{20}O	^{226}U	39.28	7.26093E-14
			38.00	2.36278E-14
			39.15	6.49656E-14
	^{20}Ne	^{226}Th	54.91	7.43256E-19
			53.08	1.69157E-19
			53.98	3.50042E-19
	^{22}Ne	^{224}Th	59.05	7.59302E-17
			57.58	1.90097E-17
			58.17	3.29493E-17
	^{24}Ne	^{222}Th	59.16	3.40373E-16
			57.84	8.78578E-17
			58.89	2.57049E-16

Table 7.2. Calculated Q value and cluster formation probability for the decay of ^{254}No emitting various clusters.

Parent nuclei	Emitted cluster	Daughter nuclei	Q value (MeV)	Cluster formation probability, S
^{254}No	^{4}He	^{250}Fm	8.336	1.799E-01
			8.230	1.718E-01
			8.240	1.725E-01
	^{8}Be	^{246}Cf	15.98	2.615E-05
	^{10}Be	^{244}Cf	10.91	4.856E-06
	^{12}C	^{242}Cm	30.47	4.943E-09
	^{14}C	^{240}Cm	30.30	1.409E-08
	^{16}O	^{238}Pu	45.15	2.697E-13
	^{18}O	^{236}Pu	45.70	1.277E-12
	^{20}O	^{234}Pu	41.34	9.711E-14
	^{20}Ne	^{234}U	55.39	1.747E-19
	^{22}Ne	^{232}U	59.96	2.292E-17
	^{24}Ne	^{230}U	59.97	8.744E-17

Table 7.3. Calculated Q value and cluster formation probability for the decay of ^{256}No emitting various clusters.

Parent nuclei	Emitted cluster	Daughter nuclei	Q value (MeV)	Cluster formation probability, S
^{256}No	^{4}He	^{252}Fm	8.286	1.745E-01
			8.580	1.959E-01
			8.550	1.936E-01
	^{8}Be	^{248}Cf	15.64	2.200E-05
	^{10}Be	^{246}Cf	11.06	5.225E-06
	^{12}C	^{244}Cm	29.79	3.262E-09
	^{14}C	^{242}Cm	30.20	1.325E-08
	^{16}O	^{240}Pu	44.07	1.256E-13
	^{18}O	^{238}Pu	45.31	9.553E-13
	^{20}O	^{236}Pu	41.58	1.244E-13
	^{20}Ne	^{236}U	53.99	6.069E-20
	^{22}Ne	^{234}U	59.35	1.395E-17
	^{24}Ne	^{232}U	60.09	1.073E-16

Table 7.4. Cluster formation probability for various clusters emitting from ^{274}Rf. Table taken from [111]. Q values are taken from [112].

Parent nuclei	Emitted cluster	Daughter nuclei	Q value (MeV)	Cluster formation probability, S
^{274}Rf	^{4}He	^{270}No	10.82	3.78910E-01
	^{10}Be	^{264}Fm	26.98	7.70463E-02
	^{12}Be	^{262}Fm	21.95	1.93522E-02
	^{14}C	^{260}Cf	42.91	1.39952E-04
	^{16}C	^{258}Cf	40.26	1.26988E-04
	^{18}C	^{256}Cf	35.78	1.53795E-05
	^{20}O	^{254}Cm	58.16	3.56559E-07
	^{22}O	^{252}Cm	57.83	2.54031E-06

Table 7.5. Calculated Q value and cluster formation probability for the decay of ^{262}Sg emitting various clusters.

Parent nuclei	Emitted cluster	Daughter nuclei	Q value (MeV)	Cluster formation probability, S
^{262}Sg	^{4}He	^{258}Rf	9.646	2.118E-01
			9.610	2.087E-01
			9.700	2.163E-01
	^{8}Be	^{254}No	18.70	4.110E-05
			18.81	4.352E-05
	^{10}Be	^{252}No	12.84	5.357E-06
	^{12}C	^{250}Fm	34.40	1.028E-08
	^{14}C	^{248}Fm	33.55	2.128E-08
	^{16}O	^{246}Cf	50.27	7.416E-13
	^{18}O	^{244}Cf	50.28	2.783E-12
	^{20}O	^{242}Cf	45.40	1.447E-13
	^{20}Ne	^{242}Cm	61.88	6.604E-19
	^{22}Ne	^{240}Cm	65.94	7.839E-17
	^{24}Ne	^{238}Cm	65.66	2.756E-16

Table 7.6. Calculated Q value and cluster formation probability for the decay of $^{270}110$ emitting various clusters.

Parent nuclei	Emitted cluster	Daughter nuclei	Q value (MeV)	Cluster formation probability, S
$^{270}110$	^{4}He	^{266}Hs	10.75	2.309E-01
			11.17	2.734E-01
			10.92	2.474E-01
			13.21	6.074E-01
			10.29	1.926E-01
			10.75	2.312E-01
	^{8}Be	^{262}Sg	24.46	3.411E-04
			20.64	4.374E-05
			21.42	6.571E-05
			21.75	7.819E-05
	^{10}Be	^{260}Sg	14.42	4.839E-06
	^{12}C	^{258}Rf	41.52	1.983E-07
			37.65	1.407E-08
			38.48	2.446E-08
			38.81	3.054E-08
	^{14}C	^{256}Rf	36.44	2.491E-08
	^{16}O	^{254}No	54.93	1.502E-12
	^{18}O	^{252}No	54.15	3.381E-12
	^{20}O	^{250}No	48.54	9.584E-14
	^{20}Ne	^{250}Fm	67.75	1.602E-18
	^{22}Ne	^{248}Fm	71.13	1.328E-16
	^{24}Ne	^{246}Fm	70.16	2.619E-16

Table 7.7. Calculated Q value and cluster formation probability for the decay of $^{272}110$ emitting various clusters.

Parent nuclei	Emitted cluster	Daughter nuclei	Q value (MeV)	Cluster formation probability, S
$^{272}110$	^{4}He	^{268}Hs	10.55	2.128E-01
			10.77	2.326E-01
			10.57	2.148E-01
			10.09	1.776E-01
	^{8}Be	^{264}Sg	19.93	3.062E-05
			20.61	4.345E-05
	^{10}Be	^{262}Sg	14.02	3.827E-06
	^{12}C	^{260}Rf	36.29	5.967E-09
	^{14}C	^{258}Rf	35.68	1.447E-08
	^{16}O	^{256}No	53.23	4.276E-13
	^{18}O	^{254}No	53.39	1.862E-12
	^{20}O	^{252}No	48.33	8.408E-14
	^{20}Ne	^{252}Fm	66.00	4.058E-19
	^{22}Ne	^{250}Fm	70.01	4.974E-17
	^{24}Ne	^{248}Fm	69.56	1.563E-16

Table 7.8. Calculated Q value and cluster formation probability for the decay of $^{278}112$ emitting various clusters.

Parent nuclei	Emitted cluster	Daughter nuclei	Q value (MeV)	Cluster formation probability, S
$^{278}112$	^{4}He	$^{274}110$	11.87	3.022E-01
			12.49	3.879E-01
			10.20	1.557E-01
			11.46	2.568E-01
			11.87	3.027E-01
	^{8}Be	^{270}Hs	22.52	7.427E-05
			20.31	2.363E-05
			21.70	4.829E-05
	^{10}Be	^{268}Hs	16.76	1.148E-05
	^{12}C	^{266}Sg	39.15	1.638E-08
	^{14}C	^{264}Sg	38.25	3.828E-08
	^{16}O	^{262}Rf	55.74	7.552E-13
	^{18}O	^{260}Rf	55.81	3.415E-12
	^{20}O	^{258}Rf	51.35	2.778E-13
	^{20}Ne	^{258}No	68.40	4.513E-19
	^{22}Ne	^{256}No	72.90	9.899E-17
	^{24}Ne	^{254}No	73.03	6.468E-16

7.3 Results and Discussion

In Figures 7.1 to 7.8 the solid line represents the average behaviour. From these plots it is clear that cluster formation probability decreases with mass of the emitted cluster up to A_2=20 and then increases and remains almost a constant. From the observed variation of cluster formation probability with mass of the cluster, we conclude that in exotic decays transition from cluster mode to fission mode takes place at A_2=20 [111]. This value is comparable with result of Shanmugam et al [113] based on cubic plus Yukawa plus exponential model (CYEM), according to whom the transition point is at A_2=16. These authors arrived at this value by comparing half life time values obtained for various clusters from their fission model (CYEM) with those values obtained from cluster model for parent nuclei in trans-tin region and found that deviation of the results become larger after A_2=16.

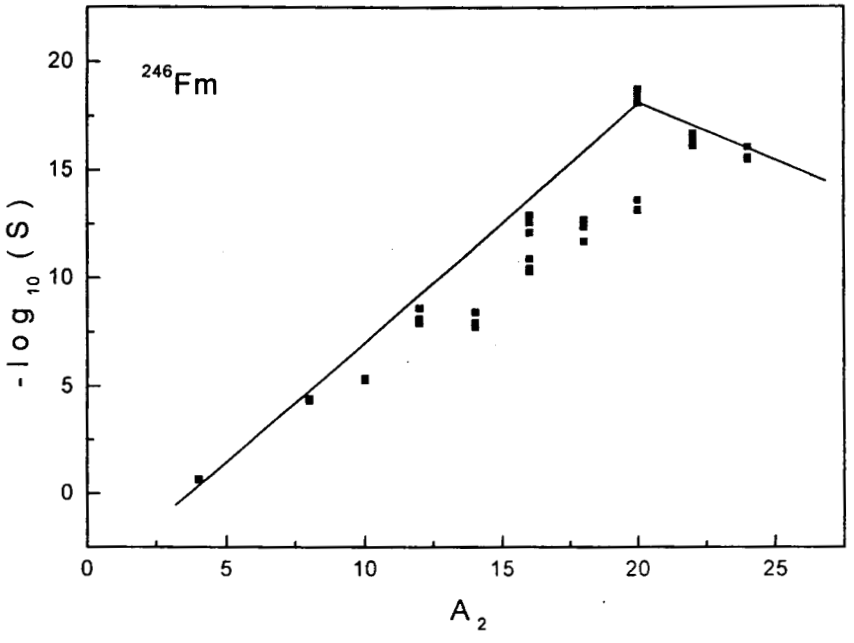

Fig. 7.1 Plot for $-\log_{10}(S)$ vs A_2 for the emission of various clusters from ^{246}Fm

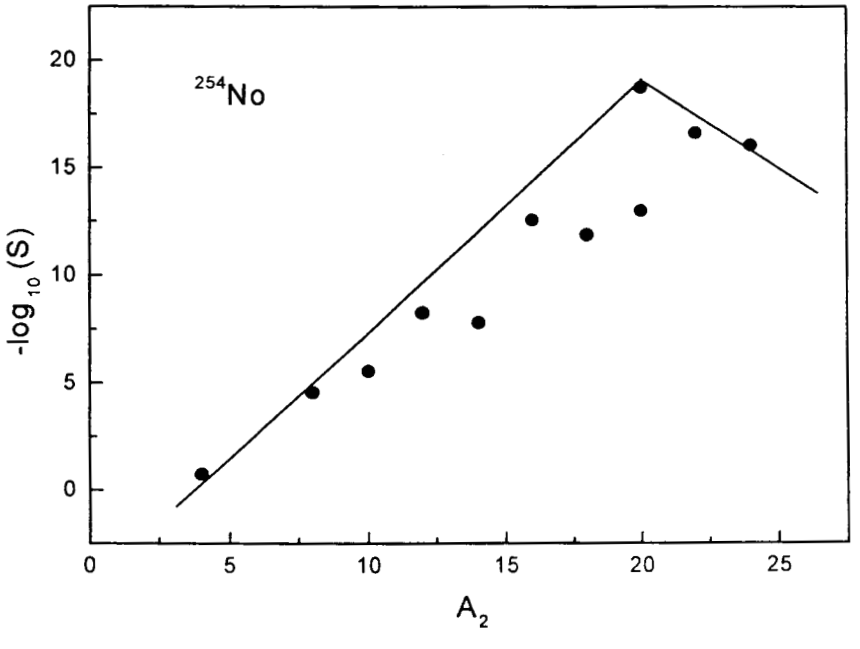

Fig. 7.2 Plot for $-\log_{10}(S)$ vs A_2 for the emission of various clusters from ^{254}No

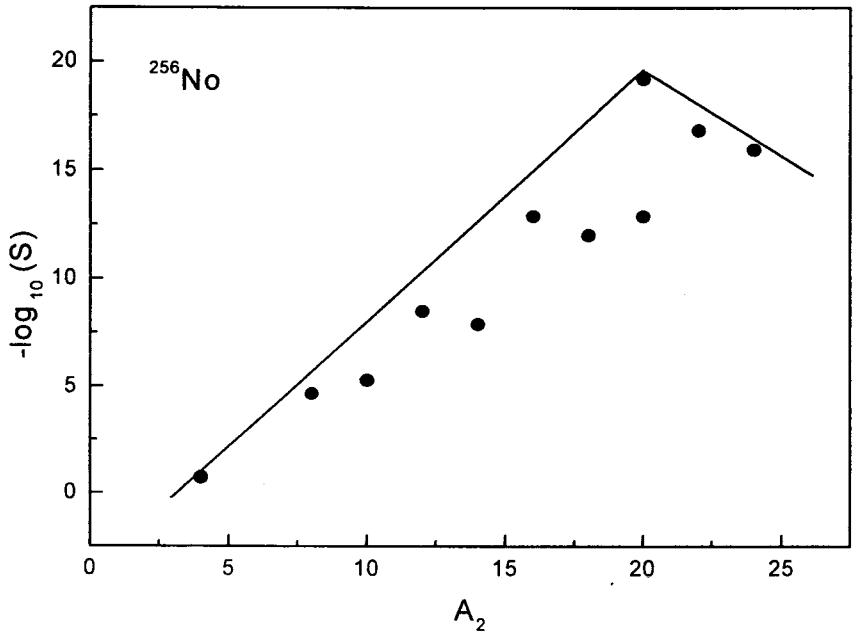

Fig. 7.3 Plot for $-\log_{10}(S)$ vs A_2 for the emission of various clusters from ^{256}No

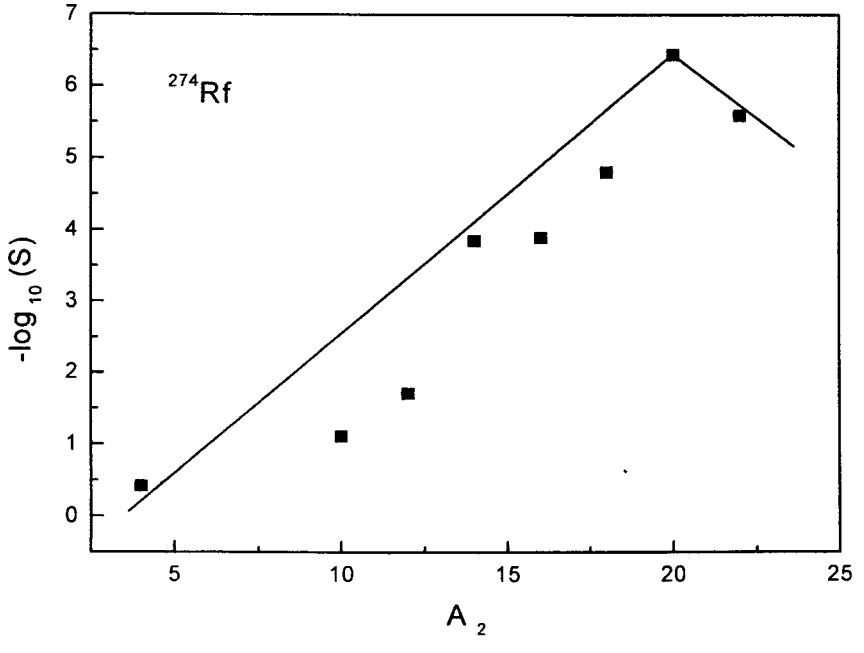

Fig. 7.4 Plot for $-\log_{10}(S)$ vs A_2 for the emission of various clusters from ^{274}Rf

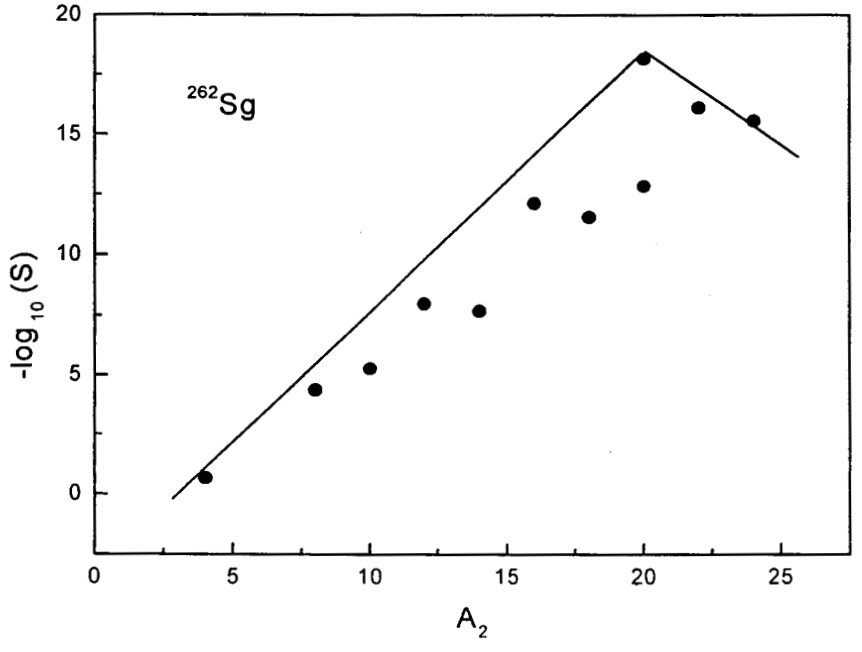

Fig. 7.5 Plot for $-\log_{10}(S)$ vs A_2 for the emission of various clusters from ^{262}Sg

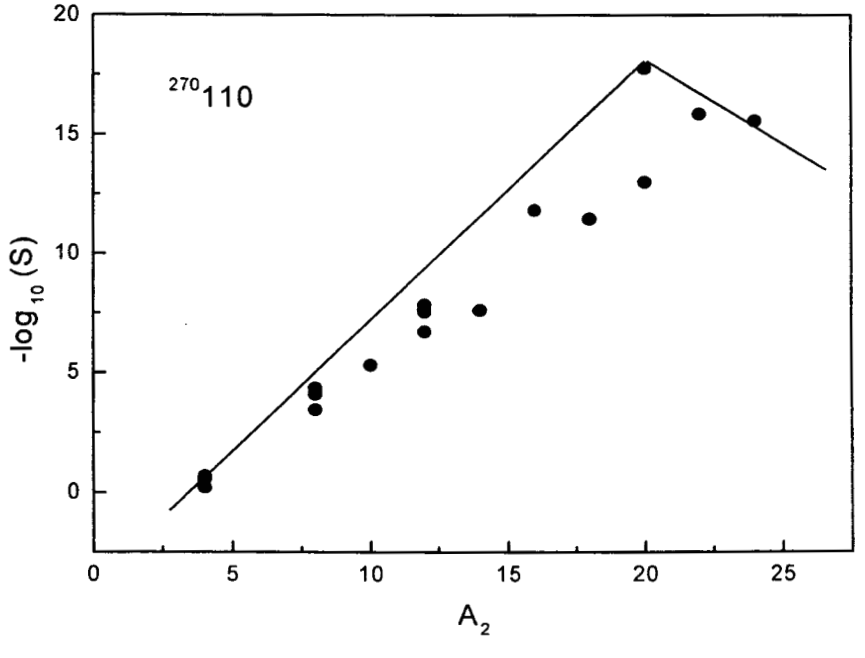

Fig. 7.6 Plot for $-\log_{10}(S)$ vs A_2 for the emission of various clusters from ^{270}110

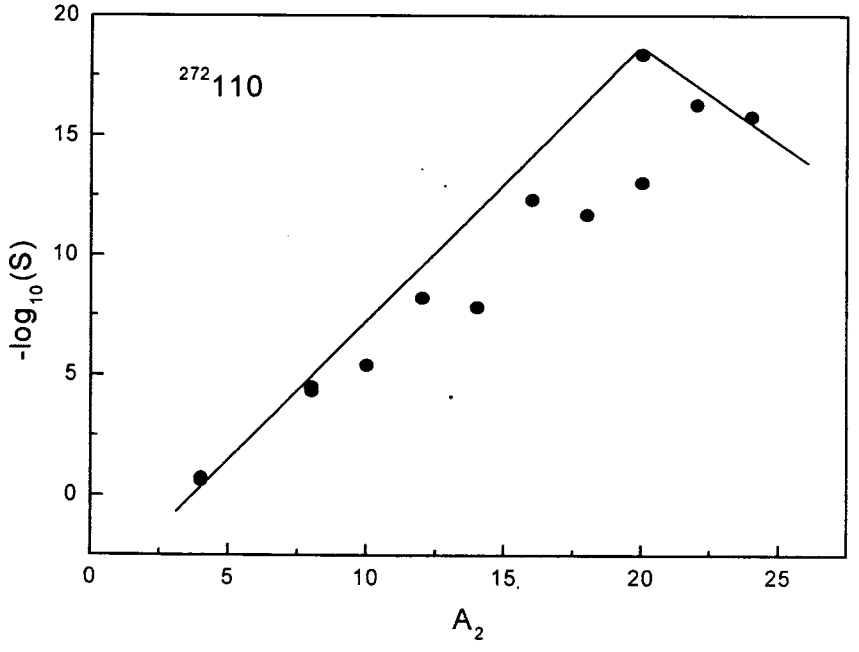

Fig. 7.7 Plot for $-\log_{10}(S)$ vs A_2 for the emission of various clusters from $^{272}110$

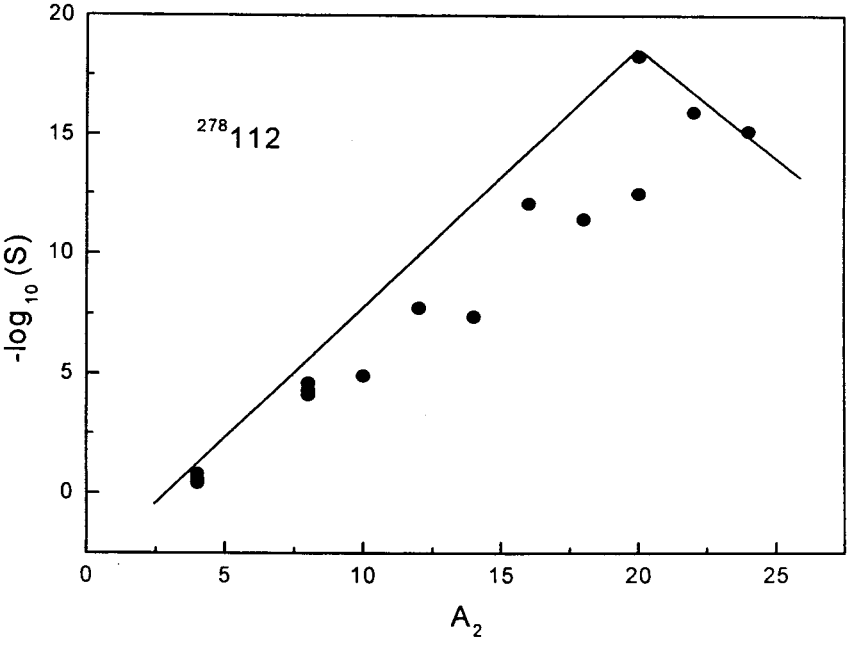

Fig. 7.8 Plot for $-\log_{10}(S)$ vs A_2 for the emission of various clusters from $^{278}112$

THEORETICAL STUDIES OF NUCLEAR STRUCTURE IN VIEW OF EXOTIC NUCLEAR DECAYS

Thesis submitted to the University of Calicut
in partial fulfilment of the requirements
for the Degree of

DOCTOR OF PHILOSOPHY

IN PHYSICS

By

K.P. SANTHOSH

DEPARTMENT OF PHYSICS
UNIVERSITY OF CALICUT

2002

CHAPTER 8

DECAY FROM EXCITED STATES OF PARENTS

Exotic decay from the ground state of superdeformed ^{76}Sr, ^{78}Sr and ^{80}Sr with estimated quadrapole deformation $\beta_2 = 0.35 - 0.44$ [114,115,116,117] and the decay from the excited states of these nuclei, which can be produced as compound system in heavy ion reactions are presented in this chapter.

8.1 Decay from the ground state

^{76}Sr, ^{78}Sr and ^{80}Sr are superdeformed nuclei, which can be produced in heavy ion reactions [118,119]. Due to such large ground state deformation, these nuclei are unstable against both fission and exotic decay processes. Asymmetric mass splitting is favoured for these nuclei as liquid drop fissility parameter $x = Z^2/50A$ is far less than Businaro-Gallone transition point [120,121]. ($x_{BG} = 0.396$ for $\ell = 0$, and this value decreases as ℓ value increases). Negative Q value for clusters with mass $A_2 < 12$ including α particle shows that these nuclei are stable against light clusters. Table 8.1, 8.2 and 8.3 give the half life times and other characteristics for ground state decay of ^{76}Sr, ^{78}Sr and ^{80}Sr respectively, emitting various clusters. Calculated half life time values show that these

nuclei are also stable against heavier clusters with mass $A_2 \geq 12$ since $T_{1/2} > 10^{80} s$. The reason for this kind of stability of ^{76}Sr is due to the stable deformed shell closure at $N = Z = 38$ which supports the earlier predictions [114,122] and for that of ^{78}Sr is due to the stable deformed shell closure at $Z = 38$ and the spherical/deformed shell closure at $N = 40$. It is found that ^{78}Sr is more stable than ^{76}Sr and ^{80}Sr is more stable than ^{78}Sr. The role of Q value is also reflected in the Tables 8.1 to 8.3. Smaller Q value results in smaller penetrability P (smaller decay constant λ). This makes ^{80}Sr more stable than ^{78}Sr and ^{76}Sr. Also neutron excess (2 more than $N = 40$ shell closure) is responsible for the extra stability of ^{80}Sr.

8.2 Decay of excited compound system

If a nucleus is formed in a heavy ion reaction, depending on the excitation energy and angular momentum, the excited compound nucleus undergo fission (also called fusion-fission), decay via cluster emission or result in resonance phenomena (dinuclear orbiting). The light compound system with $A \leq 42$ and the heavier one with $A \geq 64$ would go through orbiting and fission [123,124].

The barrier penetrability P for excited compound system is given as

$$P = \exp\left(-\frac{2}{\hbar}\sqrt{2\mu(V - Q_{eff})}dz\right) \tag{8.1}$$

where the effective Q value, $Q_{eff} = Q + E^*$ (8.2)

The excitation energy E^* is related to nuclear temperature θ in MeV [15] as given in equation 2.7

Tables 8.4 to 8.6 give the half life time and other characteristics for the decay of excited compound system $^{76}Sr^*$, $^{78}Sr^*$ and $^{80}Sr^*$ formed in heavy ion reactions. Figures 8.1 to 8.3 give the variation of half life time with nuclear temperature for various clusters for these compound systems. It is clear from these plots that the inclusion of excitation energy increases the decay rate (decreases $T_{1/2}$ value) considerably and these nuclei become unstable against decay.

Table 8.1. Calculated half life time and other characteristics for the decay of ^{76}Sr from its ground state.

Parent nuclei	Emitted cluster	Daughter nuclei	Q value (MeV)	Penetrability P	Decay constant λ	$\log_{10}(T_{1/2})$ Present	$\log_{10}(T_{1/2})$ PCM [17]
^{76}Sr	^{12}C	^{64}Ge	0.035	2.1969E-1329	2.1416E-1311	1310.5	1315.8
	^{16}O	^{60}Zn	4.53	2.1699E-111	2.6774E-91	90.41	87.15
	^{20}Ne	^{56}Ni	6.55	2.9174E-110	5.1811E-90	89.13	87.25
	^{24}Mg	^{52}Fe	7.87	4.0321E-116	8.5958E-96	94.91	96.02
	^{28}Si	^{48}Cr	9.92	1.3138E-109	3.5297E-89	88.29	87.62
	^{32}S	^{44}Ti	9.18	2.0994E-128	5.2195E-108	107.1	106.77
	^{36}Ar	^{40}Ca	10.69	1.8355E-117	5.3140E-97	96.12	95.97

Table 8.2. Calculated half life time and other characteristics for the decay of ^{78}Sr from its ground state.

Parent nuclei	Emitted cluster	Daughter nuclei	Q value (MeV)	Penetrability P	Decay constant λ	$\log_{10}(T_{1/2})$ Present	PCM [125]
^{78}Sr	^{16}O	^{62}Zn	2.89	4.6397E-155	3.6521E-135	134.28	137.37
	^{20}Ne	^{58}Ni	4.25	2.7325E-154	3.1488E-134	133.34	140.97
	^{24}Mg	^{54}Fe	7.16	1.3435E-125	2.6058E-105	104.43	114.29
	^{26}Mg	^{52}Fe	1.52	1.6549E-375	6.8134E-356	355.01	357.06
	^{28}Si	^{50}Cr	8.73	1.4069E-122	3.3264E-102	101.32	112.07
	^{30}Si	^{48}Cr	4.23	2.5132E-216	2.8792E-196	195.38	202.70
	^{32}S	^{46}Ti	7.13	3.4158E-158	6.5957E-138	137.02	147.56
	^{34}S	^{44}Ti	4.46	2.9158E-225	3.5219E-205	204.29	214.11
	^{36}Ar	^{42}Ca	5.76	3.9609E-194	6.1788E-174	173.05	184.32
	^{38}Ar	^{40}Ca	6.55	1.1123E-176	1.9731E-156	155.54	167.27

Table 8.3. Calculated half life time and other characteristics for the decay of ^{80}Sr from its ground state.

Parent nuclei	Emitted cluster	Daughter nuclei	Q value (MeV)	Penetrability P	Decay constant λ	$\log_{10}(T_{1/2})$ Present	$\log_{10}(T_{1/2})$ PCM [125]
^{80}Sr	^{16}O	^{64}Zn	0.55	5.5827E-436	8.3632E-417	415.92	415.90
	^{20}Ne	^{60}Ni	1.33	7.5674E-333	2.7289E-313	312.41	318.52
	^{24}Mg	^{56}Fe	4.35	3.2416E-184	3.8198E-164	163.26	177.20
	^{26}Mg	^{54}Fe	2.75	3.1732E-257	2.3635E-237	236.47	249.60
	^{28}Si	^{52}Cr	6.71	2.4776E-152	4.5026E-132	131.19	146.67
	^{30}Si	^{50}Cr	4.50	7.4669E-208	9.1001E-188	186.88	188.55
	^{32}S	^{48}Ti	4.31	3.2396E-230	3.7814E-210	209.26	223.60
	^{34}S	^{46}Ti	3.87	7.2582E-250	7.6072E-230	228.96	244.25
	^{36}Ar	^{44}Ca	1.51	2.9634E-469	1.2118E-449	448.76	462.48
	^{38}Ar	^{42}Ca	3.07	9.8580E-303	8.1961E-283	281.93	298.11

Table 8.4. Calculated half life time and other characteristics for the decay of excited compound system $^{76}Sr^{*}$. Nuclear temperature of the compound system is arbitrarily taken as θ=1.2MeV i.e. excitation energy $E^{*} = 10.96$ MeV.

Parent nuclei	Emitted cluster	Daughter nuclei	Q value (MeV)	Q_{eff} (MeV)	Penetrability P	Decay constant λ	$\log_{10}(T_{1/2})$ Present
$^{76}Sr^{*}$	^{12}C	^{64}Ge	0.035	10.995	1.4697E-28	4.5006E-08	7.19
	^{16}O	^{60}Zn	4.53	15.49	2.2170E-30	9.3536E-10	8.87
	^{20}Ne	^{56}Ni	6.55	17.51	5.5043E-38	2.6132E-17	16.42
	^{24}Mg	^{52}Fe	7.87	18.83	2.4517E-45	1.2505E-24	23.74
	^{28}Si	^{48}Cr	9.92	20.88	3.0776E-47	1.7404E-26	25.60
	^{32}S	^{44}Ti	9.18	20.14	3.7204E-56	2.0293E-35	34.53
	^{36}Ar	^{40}Ca	10.69	21.65	1.0747E-53	6.3015E-33	32.04

Table 8.5. Calculated half life time and other characteristics for the decay of excited compound system $^{78}Sr^{*}$. Nuclear temperature of the compound system is arbitrarily taken as θ=1.4MeV i.e. excitation energy $E^{*} = 15.59$ MeV.

Parent nuclei	Emitted cluster	Daughter nuclei	Q value (MeV)	Q_{eff} (MeV)	Penetrability P	Decay constant λ	$\log_{10}(T_{1/2})$ Present
$^{78}Sr^{*}$	^{16}O	^{62}Zn	2.89	18.48	9.7616E-22	4.9126E-01	0.149
	^{20}Ne	^{58}Ni	4.25	19.84	2.3124E-30	1.2437E-09	8.746
	^{24}Mg	^{54}Fe	7.16	22.75	1.4281E-32	8.7996E-12	10.90
	^{26}Mg	^{52}Fe	1.52	17.11	8.5724E-52	3.9719E-31	30.24
	^{28}Si	^{50}Cr	8.73	24.32	5.2023E-36	3.4327E-15	14.31
	^{30}Si	^{48}Cr	4.23	19.82	1.0816E-50	5.8047E-30	29.08
	^{32}S	^{46}Ti	7.13	22.72	1.9299E-46	1.1873E-25	24.77
	^{34}S	^{44}Ti	4.46	20.05	3.7094E-56	2.0138E-35	34.54
	^{36}Ar	^{42}Ca	5.76	21.35	2.7218E-54	1.5735E-33	32.64
	^{38}Ar	^{40}Ca	6.55	22.14	1.8558E-51	1.1126E-30	29.14

Table 8.6. Calculated half life time and other characteristics for the decay of excited compound system $^{80}Sr^*$. Nuclear temperature of the compound system is arbitrarily taken as θ=1.4MeV i.e. excitation energy $E^* = 16.02$ MeV.

Parent nuclei	Emitted cluster	Daughter nuclei	Q value (MeV)	Q_{eff} (MeV)	Penetrability P	Decay constant λ	$\log_{10}(T_{1/2})$ Present
$^{80}Sr^*$	^{16}O	^{64}Zn	0.55	16.57	1.8384E-26	8.2979E-06	4.922
	^{20}Ne	^{60}Ni	1.33	17.35	1.0448E-37	4.9156E-17	16.15
	^{24}Mg	^{56}Fe	4.35	20.37	3.4825E-39	1.9218E-18	17.56
	^{26}Mg	^{54}Fe	2.75	18.77	7.3066E-45	3.7149E-24	23.27
	^{28}Si	^{52}Cr	6.71	22.73	3.5898E-40	2.2101E-19	18.50
	^{30}Si	^{50}Cr	4.50	20.52	1.1990E-47	6.6640E-27	26.02
	^{32}S	^{48}Ti	4.31	20.33	1.7578E-54	9.6789E-34	32.85
	^{34}S	^{46}Ti	3.87	19.89	2.3482E-56	1.2650E-35	34.74
	^{36}Ar	^{44}Ca	1.51	17.53	3.1966E-70	1.5177E-49	48.66
	^{38}Ar	^{42}Ca	3.07	19.09	4.6441E-63	2.4012E-42	41.46

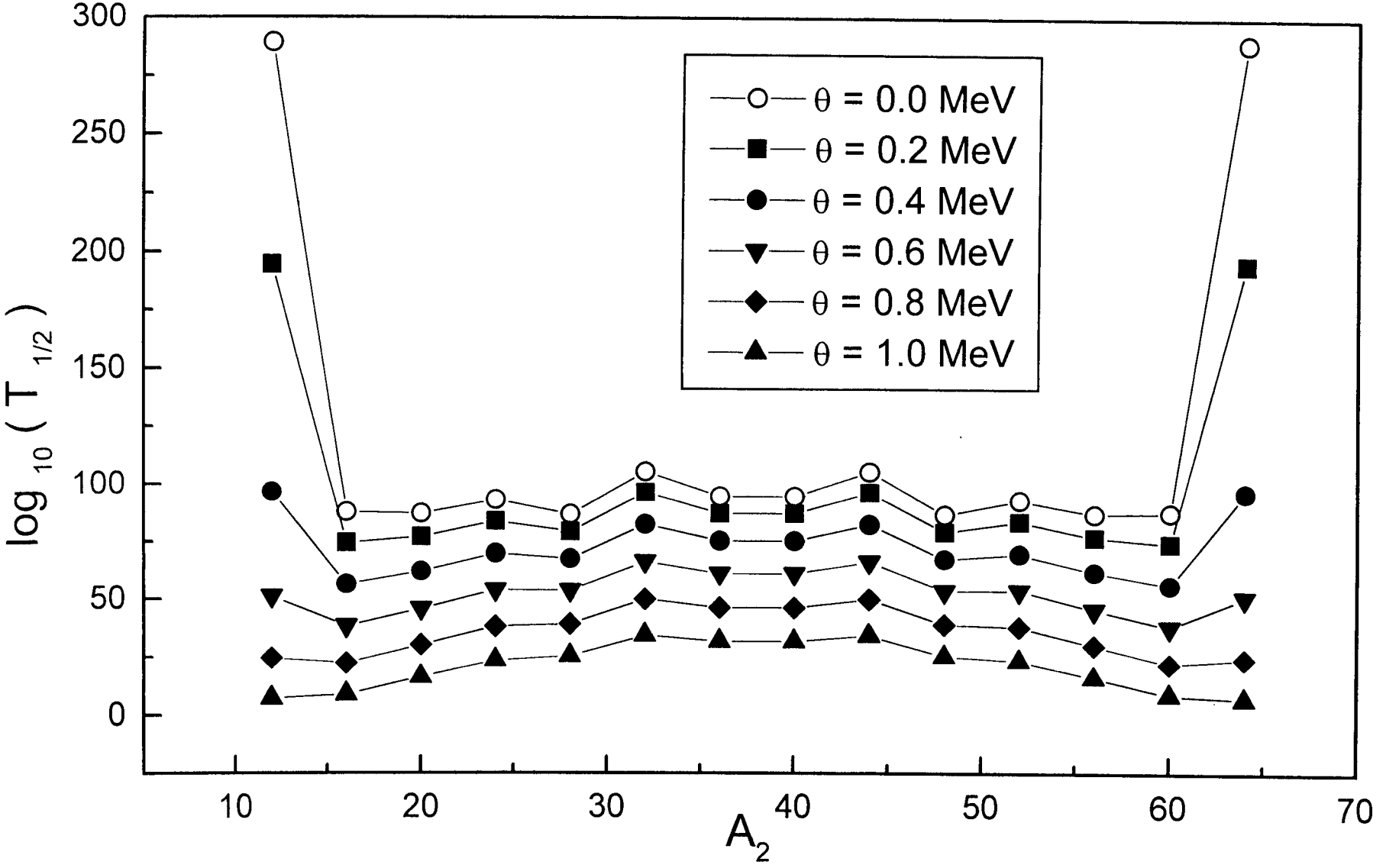

Fig. 8.1 Variation of half life time with temperature for various clusters from $^{76}Sr^{*}$

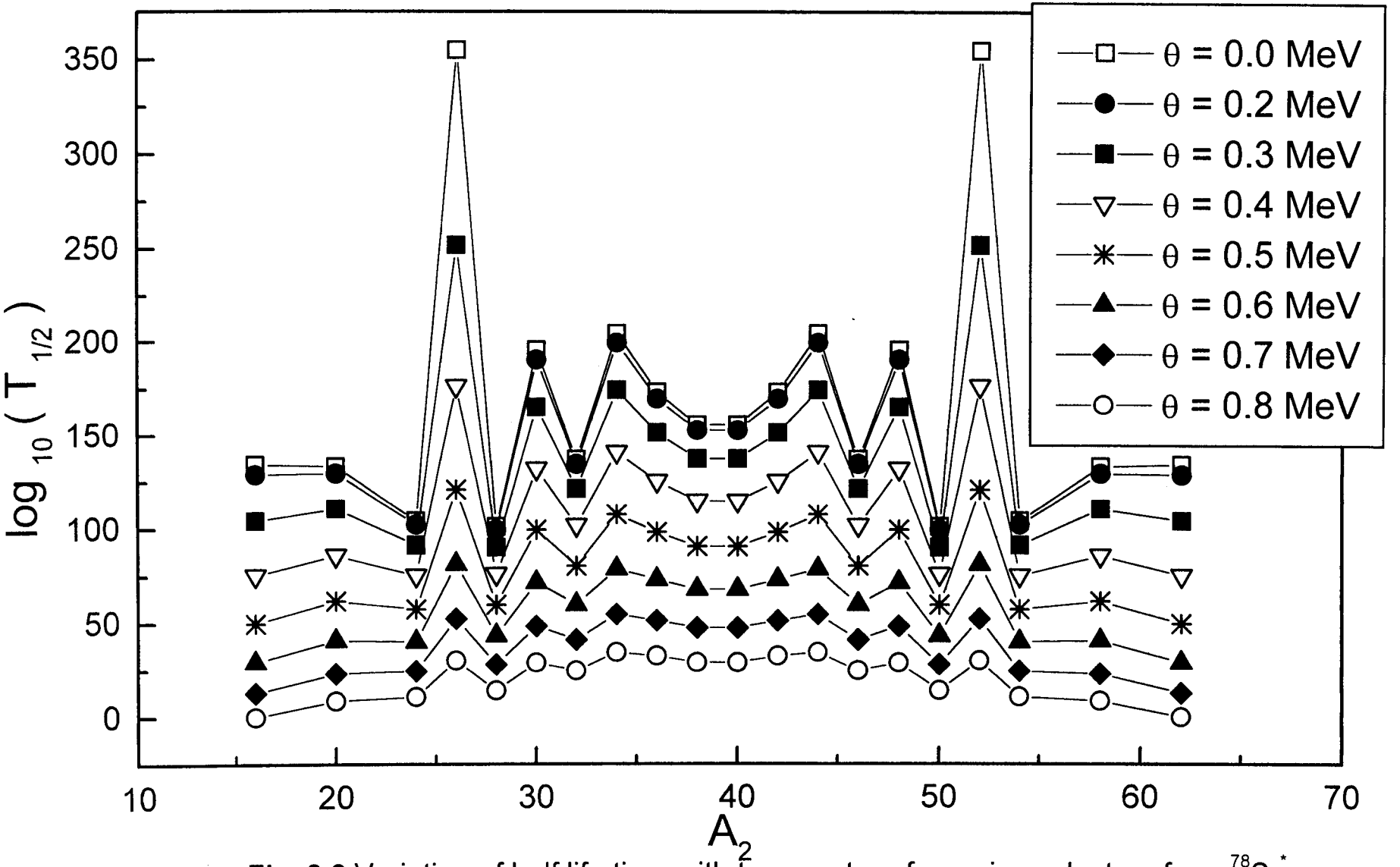

Fig. 8.2 Variation of half life time with temperature for various clusters from $^{78}Sr^{*}$

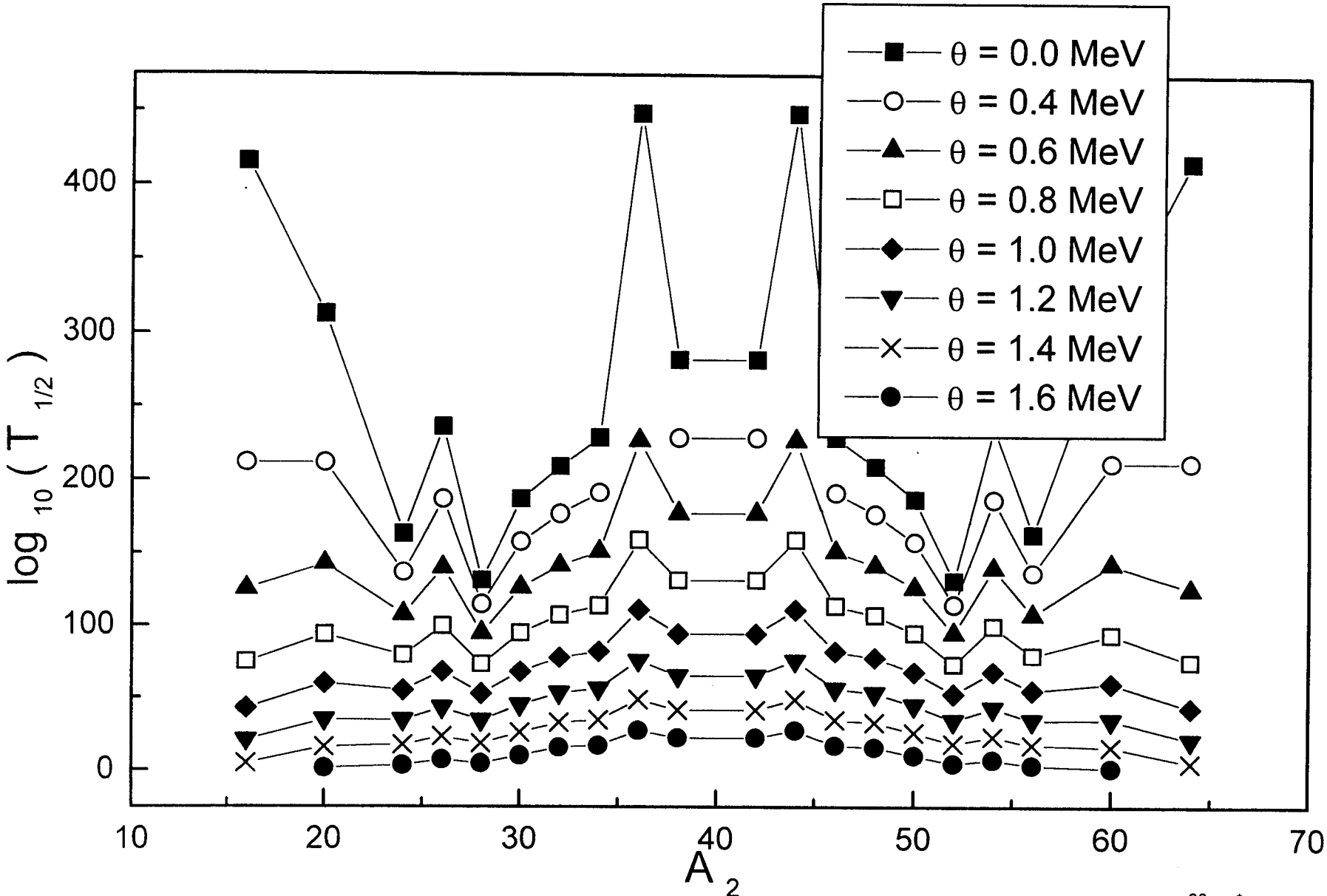

Fig. 8.3 Variation of half life time with temperature for various clusters from $^{80}Sr^{*}$

THEORETICAL STUDIES OF NUCLEAR STRUCTURE IN VIEW OF EXOTIC NUCLEAR DECAYS

Thesis submitted to the University of Calicut
in partial fulfilment of the requirements
for the Degree of

DOCTOR OF PHILOSOPHY

IN PHYSICS

By

K.P. SANTHOSH

DEPARTMENT OF PHYSICS
UNIVERSITY OF CALICUT

2002

CHAPTER 9

SYNTHESIS OF HEAVY AND SUPER HEAVY ELEMENTS

In this chapter we are presenting the theoretical studies carried out on the exotic decay of heavy nuclei ^{246}Fm, ^{254}No, ^{256}No, ^{258}Rf, ^{274}Rf, ^{262}Sg, ^{266}Hs, ^{270}110, ^{272}110, ^{278}112 and ^{302}120 emitting clusters ranging from ^{4}He to ^{32}S with a view to look for some measurable modes of decay which in turn may lead to the production of some other new heavy or super heavy nuclei as daughter. The main and the most observed decay from these heaviest systems is alpha decay. These heavy nuclei ($Z \geq 100$) can be produced in heavy ion "cold fusion" reaction with Pb as target. The target projectile combinations for cold synthesis of these heavy nuclei are given in Table 9.1.

Tables 9.2 to 9.12 give the half life times and other characteristics for the ground state to ground state decay of these heaviest systems. Figures 9.1 and 9.2 give the plot for $\log_{10}(T_{1/2})$ vs A_1, the mass of daughter nuclei. It is found that many of them are well within the present upper limit for measurements ($T_{1/2} < 10^{30}\,s$). This study also indicate that ^{274}110, ^{282}112, ^{284}112, ^{288}114, ^{290}114, ^{292}116, ^{294}116 and ^{298}118 are some super heavy nuclei that can be cold synthesized via exotic decay. When these heavy systems decay from excited state ie when excitation energies are included, $T_{1/2}$ values decrease

considerably. So in the form of daughter nuclei these heavy systems offer good possibility for the synthesis of other new heavy or super heavy nuclei.

Table 9.1. Target projectile combination for cold fusion reaction

Compound nuclei	Projectile nuclei	Target nuclei	Ref
^{246}Fm	^{40}Ar	^{206}Pb	[126]
^{254}No	^{48}Ca	^{206}Pb	[127]
^{256}No	^{48}Ca	^{208}Pb	[128]
^{258}Rf	^{50}Ti	^{208}Pb	[129]
^{274}Rf	^{58}Ti	^{216}Pb	[112]
^{262}Sg	^{54}Cr	^{208}Pb	[129]
^{266}Hs	^{58}Fe	^{208}Pb	[129]
$^{270}110$	^{62}Ni	^{208}Pb	[129]
$^{272}110$	^{64}Ni	^{208}Pb	[129]
$^{278}112$	^{70}Zn	^{208}Pb	[129]
$^{302}120$	^{94}Sr	^{208}Pb	[130]

Table 9.2. Logarithm of predicted half life time and other characteristics of ^{246}Fm decaying by emitting various clusters. For Q values masses are taken from [93,95,101].

Parent nuclei	Emitted cluster	Daughter nuclei	Q value (MeV)	Penetrability P	Decay constant	$\log_{10}(T_{1/2})$
^{246}Fm	^{4}He	^{242}Cf	8.506	2.38622E-22	9.32514E-02	0.871
			8.206	2.16394E-23	8.15824E-03	1.929
			8.376	8.56569E-23	3.29623E-03	1.323
	^{8}Be	^{238}Cm	16.14	5.61198E-47	2.79777E-26	25.39
			15.59	5.43267E-49	2.61608E-28	27.42
			15.78	3.28240E-48	1.60192E-27	26.64
	^{10}Be	^{236}Cm	10.09	4.29841E-84	1.24916E-63	62.74
			9.693	2.15606E-87	6.01740E-67	66.06
	^{12}C	^{234}Pu	30.51	1.45870E-50	1.23950E-29	28.75
			29.76	1.81063E-52	1.50073E-31	30.66
			27.96	2.46391E-57	1.91868E-36	35.56
	^{14}C	^{232}Pu	29.30	1.14326E-55	9.18758E-35	33.88
			28.66	1.56686E-57	1.23167E-36	35.75
			27.08	2.14662E-62	1.59438E-41	40.64
	^{16}C	^{230}Pu	19.92	5.58463E-95	3.02943E-74	73.36
			19.43	1.19569E-97	6.32658E-77	76.04
			18.04	8.5942E-106	4.22191E-85	84.22
	^{16}O	^{230}U	44.74	1.39432E-56	1.69912E-35	34.61
			42.23	3.54003E-62	4.07186E-41	40.23
			43.26	7.78990E-60	9.17811E-39	37.88
	^{18}O	^{228}U	44.42	1.97124E-58	2.37748E-37	36.47
			42.62	1.06111E-62	1.22793E-41	40.75
			41.69	5.38606E-65	6.09725E-44	43.06
	^{20}O	^{226}U	39.28	6.65567E-73	7.08841E-52	50.99
			38.00	1.13089E-76	1.16517E-55	54.77
			39.15	2.88196E-73	3.05950E-52	51.36
	^{20}Ne	^{226}Th	54.91	6.71230E-71	9.99329E-50	48.84
			53.08	6.34779E-75	9.13564E-54	52.88
			53.98	6.50497E-73	9.52128E-52	50.86
	^{22}Ne	^{224}Th	59.05	4.06423E-63	6.50291E-42	41.03
			57.58	3.36204E-66	5.24546E-45	44.12
			58.17	5.87737E-65	9.26336E-44	42.87
	^{24}Ne	^{222}Th	59.16	2.26802E-63	3.63462E-42	41.28
			57.84	2.92970E-66	4.59025E-45	44.18
			58.89	5.84731E-64	9.32755E-43	41.87
	^{24}Mg	^{222}Ra	69.88	4.28269E-74	8.11848E-53	51.93
			71.12	6.62350E-72	1.27595E-50	49.73

Table 9.3. Logarithm of predicted half life time and other characteristics of ^{254}No decaying by emitting various clusters. For Q values masses are taken from [93,95,101].

Parent nuclei	Emitted cluster	Daughter nuclei	Q value (MeV)	Penetrability P	Decay constant	$\log_{10}(T_{1/2})$
^{254}No	^{4}He	^{250}Fm	8.336	1.15087E-23	4.40760E-03	2.197
			8.230	4.79358E-24	1.81250E-03	2.580
			8.240	5.21018E-24	1.97242E-03	2.545
	^{8}Be	^{246}Cf	15.98	4.54312E-49	2.24245E-28	27.49
	^{10}Be	^{244}Cf	10.91	3.62005E-80	1.13749E-59	58.78
	^{12}C	^{242}Cm	30.47	1.45119E-52	1.23150E-31	30.75
	^{14}C	^{240}Cm	30.30	6.00861E-55	4.99349E-34	33.14
	^{16}O	^{238}Pu	45.15	4.55808E-58	5.60538E-37	36.09
	^{18}O	^{236}Pu	45.70	4.98739E-58	6.18856E-37	36.05
	^{20}O	^{234}Pu	41.34	5.07678E-70	5.69042E-49	48.09
	^{20}Ne	^{234}U	55.39	6.90037E-73	1.03631E-51	50.83
	^{22}Ne	^{232}U	59.96	2.93070E-64	4.76148E-43	42.16
	^{24}Ne	^{230}U	59.97	8.86437E-65	1.44001E-43	42.68
	^{24}Mg	^{230}Th	69.36	7.57219E-79	1.42271E-57	56.69
	^{26}Mg	^{228}Th	75.09	2.61830E-68	5.32512E-47	46.11
	^{28}Mg	^{226}Th	75.86	5.20278E-67	1.06894E-45	44.81
	^{28}Si	^{226}Ra	81.90	7.13663E-87	1.58300E-65	64.64
	^{30}Si	^{224}Ra	88.95	4.45558E-74	1.07335E-52	51.81
	^{32}Si	^{222}Ra	91.18	6.20234E-70	1.53159E-48	47.66
	^{34}Si	^{220}Ra	93.79	8.90947E-65	2.26305E-43	42.49
	^{32}S	^{222}Rn	94.06	1.46416E-94	3.72976E-73	72.27
	^{34}S	^{220}Rn	103.1	1.83927E-78	5.13309E-57	56.13

Table 9.4. Logarithm of predicted half life time and other characteristics of ^{256}No decaying by emitting various clusters. For Q values masses are taken from [93,95,101].

Parent nuclei	Emitted cluster	Daughter nuclei	Q value (MeV)	Penetrability P	Decay constant	$\log_{10}(T_{1/2})$
^{256}No	^{4}He	^{252}Fm	8.286	8.23279E-24	3.13408E-03	2.345
			8.580	8.76845E-23	3.45644E-02	1.302
			8.550	6.92612E-23	2.72066E-02	1.406
	^{8}Be	^{248}Cf	15.64	2.81099E-50	1.35796E-29	28.71
	^{10}Be	^{246}Cf	11.06	5.09652E-79	1.62344E-58	57.63
	^{12}C	^{244}Cm	29.79	3.17325E-54	2.63278E-33	32.42
	^{14}C	^{242}Cm	30.20	4.01867E-55	3.32872E-34	33.32
	^{16}O	^{240}Pu	44.07	2.67284E-60	3.20834E-39	38.33
	^{18}O	^{238}Pu	45.31	8.93097E-59	1.09876E-37	36.80
	^{20}O	^{236}Pu	41.58	3.17316E-69	3.57735E-48	47.29
	^{20}Ne	^{236}U	53.99	8.40330E-76	1.23012E-54	53.75
	^{22}Ne	^{234}U	59.35	2.39250E-65	3.84752E-44	43.26
	^{24}Ne	^{232}U	60.09	2.44522E-64	3.98019E-43	42.24
	^{24}Mg	^{232}Th	67.88	1.18862E-81	2.18559E-60	59.50
	^{26}Mg	^{230}Th	74.18	7.69114E-70	1.54528E-48	47.65
	^{28}Mg	^{228}Th	75.48	1.54677E-67	3.16199E-46	45.34
	^{28}Si	^{228}Ra	79.98	2.11502E-90	4.58142E-69	68.18
	^{30}Si	^{226}Ra	87.30	7.07114E-77	1.67184E-55	54.62
	^{32}Si	^{224}Ra	89.87	4.06875E-72	9.90291E-51	49.85
	^{34}Si	^{222}Ra	92.55	7.83127E-67	1.96288E-45	44.55
	^{32}S	^{224}Rn	91.37	1.94998E-99	4.82526E-78	77.16
	^{34}S	^{222}Rn	100.5	8.28574E-83	2.25429E-61	60.49

Table 9.5. Logarithm of predicted half life time and other characteristics of ^{258}Rf decaying by emitting various clusters. For Q values masses are taken from [93,95,101].

Parent nuclei	Emitted cluster	Daughter nuclei	Q value (MeV)	Penetrability P	Decay constant	$\log_{10}(T_{1/2})$
^{258}Rf	^{4}He	^{254}No	10.40	3.96966E-18	1.89673E+03	-3.43
			9.33	3.71853E-21	1.59394	-0.36
			9.20	1.47059E-21	6.21582E-01	0.047
	^{8}Be	^{250}Fm	18.50	3.31080E-42	1.89201E-21	20.56
	^{10}Be	^{248}Fm	13.00	5.40883E-69	2.02459E-48	47.53
	^{14}C	^{244}Cf	33.02	5.60038E-50	5.07204E-29	28.14
	^{18}O	^{240}Cm	46.58	8.08124E-59	1.02206E-37	36.83
	^{20}O	^{238}Cm	44.32	3.03098E-65	3.64224E-44	43.28
	^{22}O	^{236}Cm	39.41	2.51756E-80	2.68841E-59	58.41
	^{24}Ne	^{234}Pu	63.12	1.32476E-61	2.26510E-40	39.49
	^{28}Mg	^{230}U	80.92	2.27443E-61	4.98461E-40	39.14
	^{30}Mg	^{228}U	77.40	4.13004E-68	8.65740E-47	45.90
	^{34}Si	^{224}Th	97.50	1.10673E-62	2.92235E-41	40.38

Table 9.6. Logarithm of predicted half life time and other characteristics of ^{274}Rf decaying by emitting various clusters. Q values are taken from [112].

Parent nuclei	Emitted cluster	Daughter nuclei	Q value (MeV)	Penetrability P	Decay constant	$\log_{10}(T_{1/2})$
^{274}Rf	^{4}He	^{270}No	10.82	7.98296E-17	3.96835E+04	-4.76
	^{10}Be	^{264}Fm	26.98	2.25343E-22	1.75056E-01	0.597
	^{12}Be	^{262}Fm	21.95	5.80757E-35	3.55033E-14	13.29
	^{14}C	^{260}Cf	42.91	2.30833E-28	2.71672E-07	6.407
	^{16}C	^{258}Cf	40.26	2.59504E-33	2.84566E-12	11.39
	^{18}C	^{256}Cf	35.78	8.94123E-44	8.68636E-23	21.90
	^{20}O	^{254}Cm	58.16	9.19765E-35	1.45040E-13	12.68
	^{22}O	^{252}Cm	57.83	7.34256E-35	1.15056E-13	12.77
	^{24}Ne	^{250}Pu	74.61	1.13730E-38	2.29856E-17	16.48
	^{30}Mg	^{244}U	91.30	1.85464E-40	4.58588E-19	18.18
	^{36}Si	^{238}Th	107.5	7.93797E-42	2.30994E-20	19.48

Table 9.7. Logarithm of predicted half life time and other characteristics of ^{262}Sg decaying by emitting various clusters. For Q values masses are taken from [93,95,101]

Parent nuclei	Emitted cluster	Daughter nuclei	Q value (MeV)	Penetrability P	Decay constant	$\log_{10}(T_{1/2})$
^{262}Sg	^{4}He	^{258}Rf	9.646	6.19070E-21	2.74351	-0.59
			9.610	4.83443E-21	2.13446	-0.49
			9.700	8.94806E-21	3.98767	-0.76
	^{8}Be	^{254}No	18.70	4.27477E-43	2.46917E-22	21.45
			18.81	9.28489E-43	5.39491E-22	21.11
	^{10}Be	^{252}No	12.84	4.56408E-72	1.68775E-51	50.61
	^{12}C	^{250}Fm	34.40	2.91193E-47	2.78984E-26	25.40
	^{14}C	^{248}Fm	33.55	8.30115E-51	7.63869E-30	28.96
	^{16}O	^{246}Cf	50.27	1.00325E-52	1.37367E-31	30.70
	^{18}O	^{244}Cf	50.28	1.50894E-53	2.06000E-32	31.53
	^{20}O	^{242}Cf	45.40	1.64841E-65	2.02911E-44	43.53
	^{20}Ne	^{242}Cm	61.88	4.11068E-66	6.89683E-45	44.00
	^{22}Ne	^{240}Cm	65.94	5.09794E-59	9.10861E-38	36.88
	^{24}Ne	^{238}Cm	65.66	7.81358E-60	1.38975E-38	37.70
	^{24}Mg	^{238}Pu	77.51	4.89740E-71	1.02827E-49	48.83
	^{26}Mg	^{236}Pu	82.72	4.65350E-62	1.04260E-40	39.82
	^{28}Mg	^{234}Pu	82.87	1.06429E-61	2.38869E-40	39.46
	^{28}Si	^{234}U	91.49	3.10587E-78	7.69591E-57	55.95
	^{30}Si	^{232}U	97.50	5.70002E-68	1.50513E-46	45.66
	^{32}Si	^{230}U	98.30	2.58831E-66	6.89059E-45	44.00
	^{34}Si	^{228}U	99.19	2.68829E-64	7.22152E-43	41.98
	^{32}S	^{230}Th	103.9	3.64033E-87	1.02444E-65	64.83
	^{34}S	^{228}Th	111.2	9.80658E-75	2.95383E-53	52.37

Table 9.8. Logarithm of predicted half life time and other characteristics of ^{266}Hs decaying by emitting various clusters. For Q values masses are taken from [93,95,101].

Parent nuclei	Emitted cluster	Daughter nuclei	Q value (MeV)	Penetrability P	Decay constant	$\log_{10}(T_{1/2})$
^{266}Hs	^{4}He	^{262}Sg	10.00	1.28812E-20	5.91800	-0.93
			10.21	5.05947E-20	2.37328E+01	-1.53
			11.32	3.61582E-17	1.87966E+04	-4.43
			8.54	2.51851E-25	9.88145E-05	3.845
	^{8}Be	^{258}Rf	19.54	4.64442E-42	2.80334E-21	20.39
			18.14	2.31611E-46	1.29782E-25	24.73
	^{10}Be	^{256}Rf	15.14	6.18435E-62	2.69593E-41	40.41
	^{12}C	^{254}No	34.71	1.62290E-48	1.56887E-27	26.65
	^{14}C	^{252}No	36.10	8.91385E-47	8.82592E-26	24.89
	^{18}O	^{248}Fm	59.13	2.07106E-39	3.32507E-18	17.32
	^{20}O	^{246}Fm	48.06	5.75366E-62	7.49744E-41	39.97
	^{22}O	^{244}Fm	42.36	4.68844E-78	5.38138E-57	56.11
	^{24}Ne	^{242}Cf	68.61	2.34609E-57	4.36031E-36	35.20
	^{28}Mg	^{238}Cm	87.62	4.91791E-57	1.16705E-35	34.77
	^{32}Si	^{234}Pu	105.7	4.83616E-58	1.38480E-36	35.69
	^{34}Si	^{232}Pu	103.6	4.69108E-61	1.31606E-39	38.72

Table 9.9. Logarithm of predicted half life time and other characteristics of $^{270}110$ decaying by emitting various clusters. For Q values masses are taken from [93,95,101].

Parent nuclei	Emitted cluster	Daughter nuclei	Q value (MeV)	Penetrability P	Decay constant	$\log_{10}(T_{1/2})$
$^{270}110$	^{4}He	^{266}Hs	10.75	2.95008E-19	1.45646E+02	-2.32
			11.17	3.58154E-18	1.83799E+03	-3.42
			10.92	8.36077E-19	4.19457E+02	-2.78
			13.21	1.07863E-13	6.54628E+07	-7.98
			10.29	1.70368E-20	8.05418	-1.07
			10.75	3.02241E-19	1.49273E+02	-2.33
	^{8}Be	^{262}Sg	24.46	3.93038E-31	2.96968E-10	9.368
			20.64	2.22550E-40	1.41885E-19	18.69
			21.42	2.67996E-38	1.77323E-17	16.59
			21.75	1.88223E-37	1.26460E-16	15.74
	^{10}Be	^{260}Sg	14.42	1.79150E-67	7.43981E-47	45.97
	^{12}C	^{258}Rf	41.52	9.53419E-37	1.10251E-15	14.79
			37.65	3.96931E-44	4.16217E-23	22.22
			38.48	1.83951E-42	1.97142E-21	20.55
			38.81	8.19697E-42	8.86007E-21	19.89
	^{14}C	^{256}Rf	36.44	4.90734E-48	4.90469E-27	26.15
	^{16}O	^{254}No	54.93	6.92995E-49	1.03682E-27	26.83
	^{18}O	^{252}No	54.15	6.01504E-51	8.84376E-30	28.89
	^{20}O	^{250}No	48.54	1.10115E-63	1.44921E-42	41.68
	^{20}Ne	^{250}Fm	67.75	2.49065E-61	4.57517E-40	39.18
	^{22}Ne	^{248}Fm	71.13	9.63327E-56	1.85667E-34	33.57
	^{24}Ne	^{246}Fm	70.16	1.23681E-57	2.35059E-36	35.47
	^{24}Mg	^{246}Cf	84.57	5.06270E-66	1.15980E-44	43.78
	^{26}Mg	^{244}Cf	89.24	2.80675E-58	6.78410E-37	36.01
	^{28}Mg	^{242}Cf	88.87	1.25068E-58	3.01027E-37	36.36
	^{28}Si	^{242}Cm	99.92	1.58221E-72	4.28173E-51	50.21
	^{30}Si	^{240}Cm	105.4	1.89608E-63	5.41342E-42	41.11
	^{32}Si	^{238}Cm	105.9	4.11144E-62	1.17951E-40	39.77
	^{34}Si	^{236}Cm	106.4	9.70843E-61	2.79675E-39	38.39
	^{32}S	^{238}Pu	114.0	3.22924E-80	9.96993E-59	57.84
	^{34}S	^{236}Pu	120.8	4.49416E-69	1.47016E-47	46.67

Table 9.10. Logarithm of predicted half life time and other characteristics of $^{272}110$ decaying by emitting various clusters. For Q values masses are taken from [93,95,101].

Parent nuclei	Emitted cluster	Daughter nuclei	Q value (MeV)	Penetrability P	Decay constant	$\log_{10}(T_{1/2})$
$^{272}110$	^{4}He	^{268}Hs	10.55	9.34470E-20	4.52764E+01	-1.82
			10.77	3.68990E-19	1.82578E+02	-2.42
			10.57	1.08482E-19	5.26806E+01	-1.88
			10.09	4.97522E-21	2.30634	-0.52
	^{8}Be	^{264}Sg	19.93	2.66205E-42	1.63878E-21	20.63
			20.61	2.18169E-40	1.38896E-19	18.70
	^{10}Be	^{262}Sg	14.02	1.60403E-69	6.47654E-49	48.03
	^{12}C	^{260}Rf	36.29	7.32606E-47	7.40453E-26	24.97
	^{14}C	^{258}Rf	35.68	1.03952E-49	1.01729E-28	27.83
	^{16}O	^{256}No	53.23	7.88275E-52	1.14288E-30	29.78
	^{18}O	^{254}No	53.39	2.77390E-52	4.02116E-31	30.24
	^{20}O	^{252}No	48.33	4.97591E-64	6.52040E-43	42.03
	^{20}Ne	^{252}Fm	66.00	2.55552E-64	4.57307E-43	42.18
	^{22}Ne	^{250}Fm	70.01	1.45454E-57	2.75927E-36	35.40
	^{24}Ne	^{248}Fm	69.56	1.39098E-58	2.62098E-37	36.42
	^{24}Mg	^{248}Cf	82.53	2.88709E-69	6.45441E-48	47.03
	^{26}Mg	^{246}Cf	87.69	1.20349E-60	2.85838E-39	38.38
	^{28}Mg	^{244}Cf	87.93	4.88055E-60	1.16228E-38	37.76
	^{28}Si	^{244}Cm	97.54	3.43938E-76	9.08588E-55	53.88
	^{30}Si	^{242}Cm	103.6	4.16710E-66	1.16942E-44	43.77
	^{32}Si	^{240}Cm	104.6	5.30079E-64	1.50219E-42	41.66
	^{34}Si	^{238}Cm	105.6	8.79963E-62	2.51659E-40	39.44
	^{32}S	^{240}Pu	111.2	1.94919E-84	5.87117E-63	62.07
	^{34}S	^{238}Pu	118.7	4.19816E-72	1.34957E-50	49.71

Table 9.11. Logarithm of predicted half life time and other characteristics of $^{278}112$ decaying by emitting various clusters. For Q values masses are taken from [93,95,101].

Parent nuclei	Emitted cluster	Daughter nuclei	Q value (MeV)	Penetrability P	Decay constant	$\log_{10}(T_{1/2})$
$^{278}112$	^{4}He	$^{274}110$	11.87	4.47093E-17	2.43737E+04	-4.55
			12.49	1.09980E-15	6.31094E+05	-5.96
			10.20	2.21633E-21	1.03861	-0.18
	^{8}Be	^{270}Hs	22.52	1.01339E-36	7.04929E-16	14.99
			20.31	1.46382E-42	9.18369E-22	20.88
			21.70	8.73040E-39	5.85211E-18	17.07
	^{10}Be	^{268}Hs	16.76	2.87062E-58	1.38553E-37	36.70
	^{12}C	^{266}Sg	39.15	9.88109E-43	1.07740E-21	20.81
	^{14}C	^{264}Sg	38.25	9.85597E-46	1.03399E-24	23.83
	^{16}O	^{262}Rf	55.74	1.74332E-49	2.64673E-28	27.42
	^{18}O	^{260}Rf	55.81	5.89616E-50	8.93473E-29	27.89
	^{20}O	^{258}Rf	51.35	1.01306E-59	1.41045E-38	37.69
	^{20}Ne	^{258}No	68.40	8.91515E-63	1.65337E-41	40.62
	^{22}Ne	^{256}No	72.90	2.87795E-55	5.68486E-34	33.09
	^{24}Ne	^{254}No	73.03	4.66252E-55	9.22372E-34	32.88
	^{24}Mg	^{254}Fm	85.45	1.24895E-67	2.89095E-46	45.38
	^{26}Mg	^{252}Fm	91.13	2.85661E-58	7.05084E-37	35.99
	^{28}Mg	^{250}Fm	91.57	3.33139E-57	8.26195E-36	34.92
	^{28}Si	^{250}Cf	101.1	2.86172E-74	7.83346E-53	51.95
	^{30}Si	^{248}Cf	107.4	6.02470E-64	1.75207E-42	41.60
	^{32}Si	^{246}Cf	108.6	2.29774E-61	6.76048E-40	39.01
	^{34}Si	^{244}Cf	109.1	5.54505E-60	1.63778E-38	37.63
	^{32}S	^{246}Cm	115.1	1.01246E-82	3.15466E-61	60.34
	^{34}S	^{244}Cm	122.7	2.84065E-70	9.43947E-49	47.87

Table 9.12. Logarithm of predicted half life time other characteristics of $^{302}120$ decaying by emitting various clusters. For Q values masses are taken from [93,95,101].

Parent nuclei	Emitted cluster	Daughter nuclei	Q value (MeV)	Penetrability P	Decay constant	$\log_{10}(T_{1/2})$
$^{302}120$	4He	$^{298}118$	14.13	1.53131E-14	9.94088E+06	-7.15
			13.58	1.26042E-15	7.86382E+05	-6.05
	8Be	$^{294}116$	27.10	3.22398E-31	2.69886E-10	9.410
			26.03	1.97280E-33	1.58627E-12	11.64
			27.07	2.80555E-31	2.34599E-10	9.470
	^{10}Be	$^{292}116$	22.70	9.33235E-44	6.09967E-23	22.06
	^{12}C	$^{290}114$	44.44	2.21441E-39	2.74077E-18	17.40
			45.96	9.12912E-37	1.16855E-15	14.77
	^{14}C	$^{288}114$	46.10	5.17694E-37	6.54579E-16	15.02
	^{18}O	$^{284}112$	62.16	2.33931E-47	3.94820E-26	25.24
	^{20}O	$^{282}112$	60.24	3.85519E-51	6.29674E-30	29.04
	^{22}O	$^{280}112$	56.94	3.09103E-58	4.76902E-37	36.16
	^{34}Si	^{268}Sg	124.4	1.30993E-50	4.41462E-29	28.20

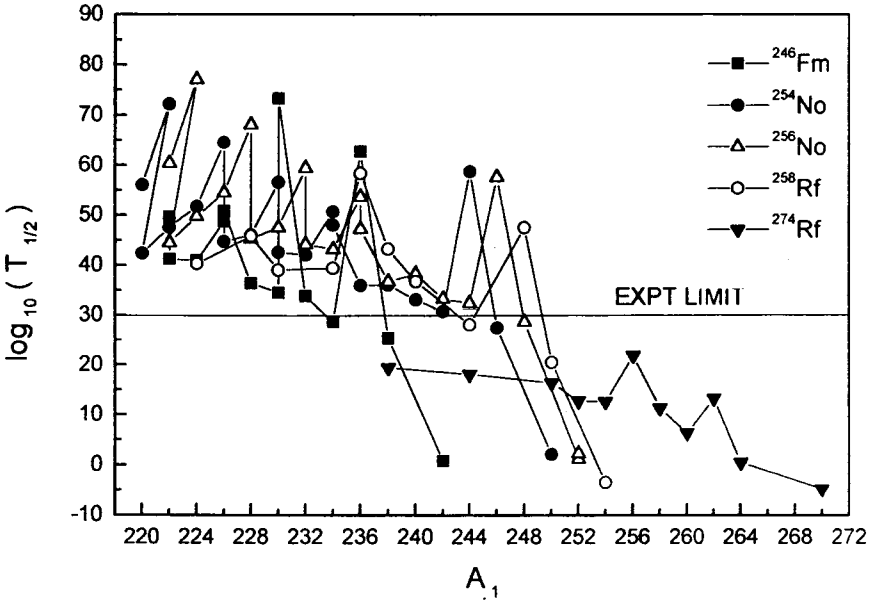

Fig. 9.1 Half life time for various clusters as a function of mass of the daughter nuclei.

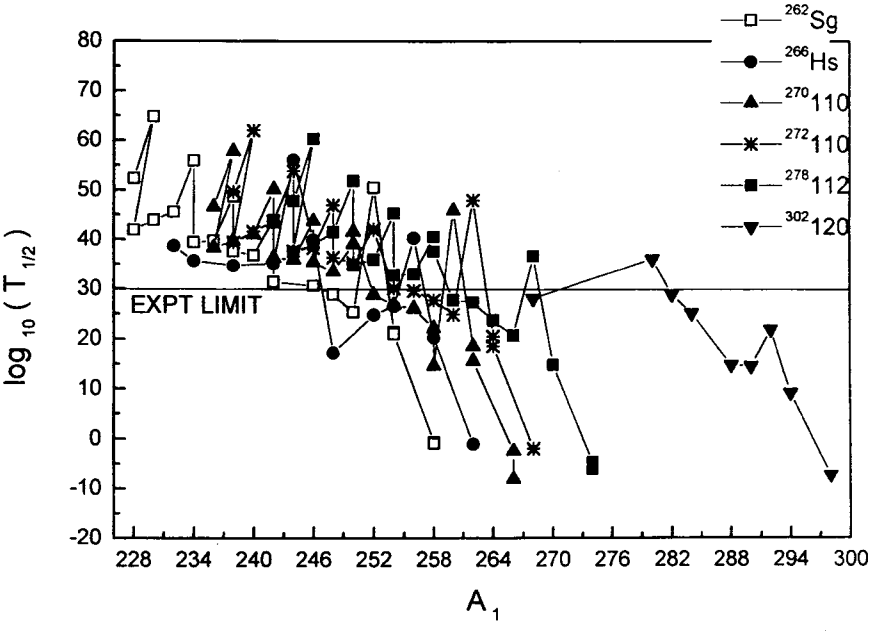

Fig. 9.2 Half life time for various clusters as a function of mass of the daughter nuclei.

THEORETICAL STUDIES OF NUCLEAR STRUCTURE IN VIEW OF EXOTIC NUCLEAR DECAYS

Thesis submitted to the University of Calicut
in partial fulfilment of the requirements
for the Degree of

DOCTOR OF PHILOSOPHY

IN PHYSICS

By

K.P. SANTHOSH

DEPARTMENT OF PHYSICS
UNIVERSITY OF CALICUT

2002

CHAPTER 10

SUMMARY AND CONCLUSIONS

The present thesis is an attempt to understand more on the exotic decay, the rare mode of decay intermediate between α emission and spontaneous fission. The common feature of this decay is that one of the nuclei always refers to spherically closed or nearly closed shell nucleus. The so far observed daughter nuclei in the exotic decay of naturally occurring radioactive nuclei are spherically closed shell ^{208}Pb or neighbouring nuclei. The only other nucleus experimentally searched for is ^{100}Sn daughter, in the exotic decay of ^{114}Ba produced in heavy ion reaction.

Chapter 2 gives a brief description of QMFT and the existing theoretical models, which are broadly classified as the fission model and the cluster model. Details of the present model are also given in this chapter, which is based on the potential barrier consisting of the Coulomb potential and the proximity potential. It is found that inclusion of proximity potential reduces the height of the barrier, which closely agrees with the experiments.

In chapter 3 the present model is applied to different cases of experimentally observed decay modes. It is found that the present model is able to reproduce the

experimental half lives and branching ratios reasonably well. In chapter 4 the exotic decay of neutron deficient Xe to Gd parents in trans-tin region emitting ^{4}He to ^{32}S was studied. Most of the decay half lives are well within the present upper limit for measurements. $T_{1/2}$ value is minimum for those decays leading to ^{100}Sn daughter which stress the role of doubly magic ^{100}Sn daughter in these decays. It is found that neutron excess in the parent nuclei slow down the exotic decay process. Geiger-Nuttall plots for all clusters from these parents are studied and are found to be linear. It is found that inclusion of proximity potential will not produce any deviation to the linear nature of these plots. Nuclear structure effects and shell effects are evident from the observed variation in slope and intercept of Geiger-Nuttall plots.

Exotic decay of neutron rich Ba to Gd parents emitting various clusters are also studied. In this case also it is found that $T_{1/2}$ has minimum value for those decays leading to doubly magic ^{132}Sn daughter compared with the neighbouring ones. This finding also reveals the role of doubly magic daughter in exotic decay. It is found that neutron proton asymmetry in parent and daughter is responsible for the reduced decay rate of these nuclei compared with their neutron deficient counterparts. The preference of non α like structures in the decay leading to ^{132}Sn and α like structure in the decay leading to ^{100}Sn point out the importance of asymmetry and symmetry of proton and neutron in the two cases respectively.

In chapter 5 we have modified the present model and made an attempt to study the effect of deformation β_2 and β_4 of parent and daughter on half life time, treating emitted cluster as spherical. When deformation effects are included half life time value is found to decrease and it is found that parent deformation alone will not produce any appreciable change. These findings are in gross agreement with the experiments.

We studied the fine structure (decay to the excited state of daughter) for some modes of decay and calculated the hindrance factor for ^{14}C transition from ^{223}Ra to various excited states of ^{209}Pb. The details are described in chapter 6. It is found that the transition to ground state is strongly hindered, while the one to first excited state is favoured. The transitions to second and third excited states are also hindered. Our findings are in good agreement with the experimental data. The fine structure from ^{223}Ra gives direct evidence on the presence of spherical component in the deformed parent nucleus.

Cluster formation probabilities are calculated within the fission model for 8 heavy nuclei and studied its variation with A_2, the mass of the emitted cluster. These are described in chapter 7. It is found that the cluster formation probability decreases with A_2 up to a value 20 and then increases and remains almost a constant. From the observed variation we conclude that the transition from cluster mode to fission mode take place at A_2=20 in exotic decay process.

Exotic decay of superdeformed ^{76}Sr, ^{78}Sr and ^{80}Sr nuclei in the ground state and formed in heavy ion reactions are studied in chapter 8. Our study shows that in the ground state these nuclei are stable against exotic decay. When these nuclei are formed as an excited compound system, depending on the excitation energy $T_{1/2}$ value decreases considerably and the nuclei become unstable against decay.

In the last chapter we studied the exotic decay of 11 heavy nuclei with $(Z \geq 100)$, which can be produced in heavy ion "cold fusion" reaction. Our study reveals that exotic decay of these heavy systems lead to the production of some other new heavy and super heavy nuclei as daughter.

THEORETICAL STUDIES OF NUCLEAR STRUCTURE IN VIEW OF EXOTIC NUCLEAR DECAYS

Thesis submitted to the University of Calicut
in partial fulfilment of the requirements
for the Degree of

DOCTOR OF PHILOSOPHY

IN PHYSICS

By

K.P. SANTHOSH

DEPARTMENT OF PHYSICS
UNIVERSITY OF CALICUT

2002

LIST OF PUBLICATIONS

Part of the work reported in this thesis has already has been published/accepted in various refereed Journals / Conference proceedings as listed below

Journals :-

1. Exotic decay in Ba isotopes via ^{12}C emission,

   K P Santhosh and Antony Joseph, *Pramana.J.Phys.* **55**, 375 (2000)

2. Exotic decay in Cerium isotopes,

   K P Santhosh and Antony Joseph, *Pramana.J.Phys.* **58**, 611 (2002)

3. ^{24}Ne radioactivity in Uranium isotopes,

   K P Santhosh and Antony Joseph, *Indian.J.Phys.* **76A** (2002) (in Press)

4. Exotic decay in proton rich Nd isotopes,

   K P Santhosh and Antony Joseph, *J.Phys.G: Nucl.Part.Phys.* (Revised and Sent)

5. Effect of parent and daughter deformation on half life time in exotic decay,

   K P Santhosh and Antony Joseph, *Pramana.J.Phys.* (Revised and Sent)

6. Exotic decay: Transition from cluster mode to fission mode,

   K P Santhosh and Antony Joseph, *Pramana.J.Phys.* (Revised and Sent)

7. Cluster radioactivity in Xenon isotopes,

   K P Santhosh and Antony Joseph, *Pramana.J.Phys.* (Communicated)

Symposia :-

1. Exotic decay of proton rich parents to ^{100}Sn,

   K P Santhosh and Antony Joseph in *Proceedings of Inter National Symposium on Nuclear Physics* (Mumbai, India, 2000) Vol **43B**, p 296

2. Cluster emission in Barium isotopes,

   K P Santhosh and Antony Joseph in *Proceedings of National Symposium on Radiation Physics* (Amritsar, India, 2001) p 338

3. ^{14}C cluster emission and fine structure in Radium isotopes,

   K P Santhosh and Antony Joseph in *Proceedings of National Symposium on Radiation Physics* (Amritsar, India, 2001) p 342

4. Fine structure in the radioactive decay of ^{231}Pa,

   K P Santhosh and Antony Joseph in *Proceedings of DAE-BRNS Symposium on Nuclear Physics* (Kolkata, India, 2001) Vol **44B**, p 82

5. Exotic decay of proton rich parents to ^{132}Sn,

   K P Santhosh and Antony Joseph in *Proceedings of DAE-BRNS Symposium on Nuclear Physics* (Kolkata, India, 2001) Vol **44B**, p 106

6. Transition from cluster mode to fission mode in exotic decay.

   K P Santhosh and Antony Joseph in *Proceedings of DAE-BRNS Symposium on Nuclear Physics* (Kolkata, India, 2001) Vol **44B**, p 108

THEORETICAL STUDIES OF NUCLEAR STRUCTURE IN VIEW OF EXOTIC NUCLEAR DECAYS

Thesis submitted to the University of Calicut
in partial fulfilment of the requirements
for the Degree of

DOCTOR OF PHILOSOPHY

IN PHYSICS

By

K.P. SANTHOSH

DEPARTMENT OF PHYSICS
UNIVERSITY OF CALICUT

2002

REFERENCES

[1] A Sandulescu, D N Poenaru and W Greiner, *Fiz.Elem.Chastits.At.Yadra* **11**, 1334 (1980); *Sov.J.Part.Nucl.* **11**, 528 (1980)

[2] R K Gupta and W Greiner in *Heavy Elements and related new phenomena* edited by R K Gupta and W Greiner (World Scientific Publication. Singapore, 1999) Vol **1**, p 536

[3] H J Rose and G A Jones, *Nature (London)* **307**, 245 (1984)

[4] J A Maruhn and W Greiner, *Phy.Rev.Lett.* **32**, 548 (1974)

[5] K H Ziegenhain, H J Lustig, J A Maruhn, W Greiner and W Scheid, *Fizika* **9** (Suppl 4) 559 (1977)

[6] J A Maruhn, W Greiner and W Schied in *Heavy ion collisions* edited by R.Bock(Amsterdam: North Holland, 1980) p 397

[7] H J Fink, W Greiner, R K Gupta, S Liran, J A Maruhn, W Scheid and O Zohni *Pro. Int. Conf. on Reaction between Complex Nuclei*, Nashville, TN, USA, 1974, (North Holland, Amsterdam) Vol **2,** p 21

[8] J A Maruhn and W Greiner, *Z. Phys.* **251**, 431 (1972)

[9] V M Strutinsky, *Nucl.Phys. A* **95**, 420 (1967)

[10] V M Strutinsky, *Nucl Phys. A* **122**,1 (1968)

[11] D R Inglis, *Phys.Rev.* **96**,1059 (1954)

[12] S T Balyaev, *K.Dan.vidensk.selsk.Mat.Fys.Medd.* **31**, No.11 (1959)

[13] W.Pauli in *Handbuch der Physik*, edited by H.Geiger and K.Sheel (Springer, Berlin, 1933) Vol **24**, Part I, p 120

[14] B Padolsky, *Phys.Rev.* **32**, 812 (1928)

[15] K J Le Couteur and D W Lang, *Nucl.Phys.* **13**, 32 (1959)

[16] A S Jensen and J Damgaard, *Nucl.Phys. A* **203**, 578 (1973)

[17] R K Gupta, M K Sharma, S Singh, R Nouicer and C Beck, *Phys.Rev.C* **56**, 3242 (1997)

[18] D N Poenaru, D Mazilu and M Ivascu, *J.Phys.G* **5**, 1093 (1979)

[19] D N Poenaru, M Ivascu and D Mazilu, *Comput.Phys.Commun.***19**, 205 (1980)

[20] D N Poenaru, M Ivascu, D Mazilu and A Sandulescu, *Rev.Roum.Phys.***25**, 55 (1980)

[21] W D Myers and W J Swiatecki, *Nucl.Phys.* **81**, 1 (1966) ; *Ark.Fys.* **36**, 343 (1967)

[22] H J Krappe and J R Nix in *Proceedings of the Smposium on Physics and Chemistry of Fission* (IAEA, Vienna, 1974) Vol **I**, p 159

[23] H J Krappe, J R Nix and A J Sierk, *Phys.Rev.C* **20**, 992 (1979)

[24] D N Poenaru, M Ivascu, A Sandulescu and W Greiner, *Phys.Rev.C* **32**, 572 (1985)

[25] Y J Shi and W J Swiatecki, *Nucl.Phys.A* **438**, 450 (1985)

[26] J Blocki, J Randrup, W J Swiatecki and C F Tsang, *Ann.Phys. (N.Y)* **105**,427 (1977)

[27] J Blocki and W J Swiatecki, *Ann.Phys. (N.Y)* **132**, 53 (1981)

[28] Y J Shi and W J Swiatecki, *Nucl.Phys.A* **464**, 205 (1987)

[29] G Shanmugam and B Kamalaharan, *Phys.Rev.C* **38**, 1377 (1988)

[30] H G de Carvalho, J B Martins and O A P Tavares, *Phys.Rev.C* **34**, 2261 (1986)

[31] D N Poenaru and M Ivascu, *J.Phys. (Paris)* **45**, 1099 (1984)

[32] P Moller, J R Nix and W J Swiatecki, *Nucl.Phys.A* **469**, 1 (1987)

[33] R Blendowske, T Fliessbach and H Walliser, *Nucl.Phys.A* **464**, 75 (1987)

[34] R Blendowske and H Walliser, *Phy.Rev.Lett.* **66**,1930 (1988)

[35] P R Christensen and A Winther, *Phys.Lett.* **65B**, 19 (1976)

[36] S S Malik and R K Gupta, *Phys.Rev.C* **39**, 1992 (1989)

[37] H Kroger and W Schied, *J.Phys.G* **6**, L85 (1980)

[38] M Greiner and W Schied, *J.Phys.G* **12**, L229 (1986)

[39] B Buck and A C Merchant, *Phys.Rev.C* **39**, 2097 (1989)

[40] B Buck, A C Merchant and S M Perez, *Nucl.Phys.A* **512**, 483 (1990)

[41] S A Gurvitz and G Kalbermann, *Phys.Rev.Lett.* **59**, 262 (1987)

[42] A Sandulescu, R K Gupta, W Greiner, F Carstoiu and M Horoi, *Int.J.Mod.Phys.E* **1**, 379 (1992)

[43] G R Satchler and W G Love, *Phys.Rep.* **55**, 183 (1979)

[44] G Bertsch, J Borysowicz, H Mc Manus and W G Love, *Nucl.Phys.A* **284**, 399 (1977)

[45] A J Sierk, *Phys.Rev.Lett.* **55**, 582 (1985)

[46] S Gales, E Hourani, M Hussonnious, J P Schapira, L Stab and M Vergnes, *Phys.Rev.Lett.* **53**, 759 (1984)

[47] W Kutschera, I Ahmad, S G Armatto III, A M Friedmann, J E Gindler, W Henning, T Ishii, M Paul and K E Rehm, *Phys.Rev.C* **32**, 2036 (1985)

[48] P B Price, J D Stevenson, S W Barwick and H L Ravn, *Phys.Rev.Lett.* **54**, 297 (1985)

[49] R P Henke and E V Benton, *U S Naval Radiobiological Defense Laboratory Report No.*USNRDL-Tr-122, 1967

[50] R L Fleischer, P B Price and R M Walker in *Nuclear Tracks in Solids: Principles and applications* (University of California Press, Berkely, 1975)

[51] P B Price, K J Moody, E K Hulet, R Bonetti, C Migliorino, *Phys.Rev.C* **43**, 1781 (1991)

[52] S W Barwick, P B Price and J D Stevenson, *Phys.Rev.C* **31**, 1984 (1985)

[53] S Wang, P B Price, S W Barwick, K J Moody and E K Hulet, *Phys.Rev.C* **36**, 2717(1987)

[54] R Bonetti, E Fioretto, C Migliorino, A Pasinetti, F Barranco, E Vigezzi and R A Broglia, *Phys.Lett.B* **241**, 179 (1990)

[55] L Brillard, A G Elayi, E Hourani, M Hussonnois, J F Le Du, L H rosier, L Stab, *C R Acad.Sci.Paris* **309**, 1105 (1989)

[56] M Hussonnois, J F Le Du, L Brillard, J Dalmasso and G Ardisson, *Phys.Rev.C* **43**, 2599 (1991)

[57] R Bonetti and A Guglielmetti in *Heavy Elements and related new phenomena* edited by R K Gupta and W Greiner (World Scientific Publication. Singapore, 1999) Vol **2**, p 643

[58] S P Tretyakova, A Sandulescu, V L Mikheev, D Hasegan, I A Lebedev, Yu S Zamyatnin, Yu S Korotkin and B F Myasoedov, *JINR Dubna Rapid Commun.* **13**, 34 (1985)

[59] M Paul, I Ahmad and W Kutschera, *Phys.Rev.C* **34**, 1980 (1986)

[60] K J Moody, E K Hulet, S Wang and P B Price, *Phys.Rev.C* **36**, 2710 (1987)

[61] P B Price, R Bonetti, A Guglielmetti, C Chiesa, R Matheoud, C Migliorino and K J Moody, *Phys.Rev.C* **46**, 1939(1992)

[62] S Wang, D Snowden Ifft, P B Price, K J Moody and E K Hulet, *Phys.Rev.C* **39**, 1647 (1989)

[63] K J Moody, E K Hulet, S Wang and P B Price, *Phys.Rev.C* **39**, 2445 (1989)

[64] S P Tretyakova, Yu S Zamyatnin, V N Kovantsev, Yu S Korotkin , V L Mikheev and G A Timofeev , *Z.Phys.A* **333**, 349 (1989)

[65] G Royer, *J.Phys.G: Nucl.Part.Phys.* **26**, 1149 (2000)

[66] A Guglielmetti, B Blank, R Bonetti, Z Janas, H Keller, R Kirchner, O Klepper, A Piechaczek, A Plochocki, G Poli, P B Price, E Roeckl, K Schmidt, J Szerypo and A J Westphal, *Nucl.Phys.A* **583**, 867c (1995)

[67] R Bonetti, C Chiesa, A Guglielmetti, C Migliorino, P Monti, A L Pasinetti and H L Ravn, *Nucl.Phys.A* **576**, 21 (1994)

[68] E Hourani, G Berrier Rosin, A Elayi, P Hofmann Rothe, A C Mueller, L Rosier, G Rotbard, G Renou, A Libe and D N Poenaru, *Phys.Rev.C* **52**, 267 (1995)

[69] E Hourani, L Rosier, G Berrier Rosin, A Elayi, A C Mueller, G Rappenecker, G Rotbard, G Renou, A Libe and L Stab, *Phys.Rev.C* **44**, 1424 (1991)

[70] D Weselka, P Hille and A Chalupka, *Phys.Rev.C* **41**, 778 (1990)

[71] R Bonetti, C Chiesa, A Guglielmetti, R Matheoud, C Migliorino, A L Pasinetti and H L Ravn, *Nucl.Phys.A* **562**, 32 (1993)

[72] R K Gupta and W Greiner, *Int.J.Mod.Phys.E* **3**, 335 (1994)

[73] R Bonetti, C Chiesa, A Guglielmetti, C Migliorino, A Cesana and M Terrani, *Nucl.Phys.A* **556**, 115 (1993)

[74] R Bonetti, C Chiesa, A Guglielmetti, R Matheoud, G Poli, V L Mikheev and S P Tretyakova, *Phys.Rev.C* **51**, 2530 (1995)

[75] R Bonetti, C Chiesa, A Guglielmetti, C Migliorino, A Cesana, M Terrani and P B Price, *Phys.Rev.C* **44**, 888 (1991)

[76] S P Tretyakova, A Sandulescu, Yu S Zamyatnin, Yu S Korotkin and V L Mikheev, *JINR Dubna Rapid Commun.* **17**, 23 (1985)

[77] S P Tretyakova, V L Mikheev, V A Ponomarenko, A N Golovchenko, A A Oglbin and V A Shigin, *JEPT Lett.* **59**, 394 (1994)

[78] A A Ogloblin, N I Venikov, S K Lisin, S V Pirozhkov, V A Pchelin, Yu F Rodionov, V M Semochkin, V A Shabrov, I K Shvetsov, V M Shubko, S P Tretyakova and V L Mikheev, *Phys.Lett.B* **235**, 35 (1990)

[79] A Sandulescu and W Greiner, *Rep.Prog.Phys.* **55**, 1423 (1992)

[80] Yu Ts Oganessian, V L Mikheev and S P Tretyakova, *JINR Dubna Report No.* E 7-93-57 (1993)

[81] Yu Ts Oganessian, A Lazarev, V L Mikheev, Yu A Shirokovsy, S P Tretyakova and V K Utyonkov, *Z.Phys.A* **349** , 341 (1994)

[82] A Guglielmetti, R Bonetti, G Poli, P B Price, A J Westphal, Z Janas, H Keller, R Kirchner, O Klepper, A Piechaczek, E Roeckl, K Schmidt, A Plochocki, J Szerypo and B Blank, *Phys.Rev.C* **52** ,740 (1995)

[83] A Guglielmetti, R Bonetti, G Poli, R Collatz, Z Hu, R Kirchner, E Roeckl, N Gunn, P B Price, B A Weaver and A J Westphal, *Phys.Rev.C* **56** , R2912 (1997)

[84] D N Poenaru, D Schnabel, W Greiner, D Mazilu and R Gherghescu, *At. Data. Nucl. Data. Tables* **48**, 231 (1991)

[85] D N Poenaru, W Greiner, K Depta, M Ivascu, D Mazilu D and A Sandulescu, *At.Data.Nucl.Data.Tables* **34**, 423 (1986)

[86] S Kumar, D Bir and R K Gupta, *Phys.Rev.C* **51**, 1762 (1995)

[87] G Shanmugam, G M Carmel Vigila Bai.and B Kamalaharan, *Phys.Rev.C* **51**, 2616 (1995)

[88] D N Poenaru, D Schnabel, W Greiner, D Mazilu and I Cata, *Report No* GSI-90-28 (1990)

[89] K P Santhosh and Antony Joseph, *Pramana.J.Phys.* **55**, 375 (2000)

[90] D N Poenaru, W Greiner and R Gherghescu, *Phys.Rev.C* **47**, 2030 (1993)

[91] S Kumar, R K Gupta, *Phys.Rev.C* **49**, 1922 (1994)

[92] Y Aboussir, J M Pearson, A K Dutta and F Tondeur, *Nucl.Phys.A* **549**, 155 (1992)

[93] P Moller, W D Myers, W J Swiatecki and J Treiner, *At.Data.Nucl.Data.Tables* **39**, 225 (1988)

[94] J Janecke and P J Masson, *At.Data.Nucl.Data.Tables* **39**, 265 (1988)

[95] P Moller and J R Nix, *At.Data.Nucl.Data.Tables* **39**, 213 (1988)

[96] S Liran and N Zeldes, *At.Data.Nucl.Data.Tables* **17**, 431 (1976)

[97] P E Haustein, *At.Data.Nucl.Data.Tables* **39**, 185 (1988)

[98] K P Santhosh and Antony Joseph, *Proceedings of National Symposium on Radiation Physics* (Amritsar, India, 2001) p 338

[99] D N Poenaru, W Greiner and E Hourani, *Phys.Rev.C* **51**, 594 (1995)

[100] K P Santhosh and Antony Joseph, *Pramana.J.Phys.* **58**, 611 (2002)

[101] A H Wapstra, G Audi and R Hoekstra, *At.Data.Nucl.Data.Tables* **39**, 281 (1988)

[102] K P Santhosh and Antony Joseph in *Proceedings of DAE-BRNS Symposium on Nuclear Physics* (Kolkata, India, 2001) Vol **44B**, p106

[103] K P Santhosh and Antony Joseph in *Proceedings of International Symposium on Nuclear Physics* (Mumbai, India, 2000) Vol **43B**, p 296

[104] P Moller and J R Nix, *Nucl.Phys.A* **361**, 117 (1981)

[105] S Rosenblum, *C.R.Acad.Sci.Paris* **188**, 1401 (1929)

[106] O Dumitresu, *Phys.Rev.C* **49**, 1466 (1994)

[107] M Hussonnois, J F Le Du, L Brillard and G Ardisson, *Phys.Rev.C* **42**, R 495 (1990)

[108] K P Santhosh and Antony Joseph in *Proceedings of National Symposium on Radiation Physics* (Amritsar, India, 2001) p 342

[109] K P Santhosh and Antony Joseph in *Proceedings of DAE-BRNS Symposium on Nuclear Physics* (Kolkata, India, 2001) vol **44B**, p 82

[110] R K Sheline and I Ragnarsson , *Phys.Rev.C* **43**, 1476 (1991)

[111] K P Santhosh and Antony Joseph in *Proceedings of DAE-BRNS Symposium on Nuclear Physics* (Kolkata, India, 2001) Vol **44B**, p108

[112] R K Gupta, S Singh, G Munzenberg and W Schied, *Phys.Rev.C* **51**, 2623 (1995)

[113] G Shanmugam and G M Carmel Vigila bai, *Pramana.J.Phys.* **53**, 443 (1999)

[114] R Bengtsson, P Moller, J R Nix and J Y Zhang, *Phys.Scr.* **29**, 402 (1984)

[115] C J Lister, A A Chishti, B J Varley, W Gelletly an A N James in *International Workshop on Nuclear Structure of the Zirconium region* (Bad Honnef) edited by J Eberth, R A Meyer and K Sistemich (Berlin : Springer, 1988) p 298

[116] C J Gross, J Heese, K P Lieb, C J Lister, B J Varley, A A Chihti, J H Mc Neill and W Gelletly, *Phys.Rev.C* **39**, 1780 (1989)

[117] R K Gupta, W Schied and W Greiner, *J.Phys.G* **17**, 1731 (1991)

[118] L G Sobotka, M A Mc Mahan, R J Mc Donald, C Signarbieux, G J Wozniak, M L Padgett, J H Gu, Z H Liu, Z Q Yao and L G Moretto, *Phys.Rev.Lett.* **53**, 2004 (1984)

[119] P M Evans, A E Smith, C N Pass, L Stuttge, B B Back, R R Betts, B K Dichter, D J Henderson, S J Sanders, F Videback and B D Wilkins, *Phys.Lett.B* **229**, 25 (1989); *Nucl.Phys.A* **526**, 365 (1991)

[120] U L Businaro and S Gallone, *Nuovo Cimento* **1**, 629 (1955)

[121] U L Businaro and S Gallone, *Nuovo Cimento* **1**, 1277 (1955)

[122] C Beck, D Mahboub, R Nouicer, T Matsuse, B Djerroud, R M Freeman, F Hass, A Hachem, A Morsad, M Youlal, S J Sanders, R Dayras, J P Wieleczko, E Berthoumieux, R Legrain, E Pollacco, Sl Cavallaro, E De Filippo, G Lanzano, A Pagano and M L Sperduto, *Phys.Rev.C* **54**, 227 (1996)

[123] S J Sanders, *Phys.Rev.C* **44**, 2676 (1991)

[124] N Aissaoui, F Haas, R M Freeman, C Beck, M Morsad, B Djerroud, R Caplar and A Hachem, *Phys.Rev.C* **55**, 516 (1997)

[125] R K Gupta, S Dhaulta, R Bonetti and W Scheid, *J.Phys.G: Nucl.Part.Phys.* **25**, 1089 (1999)

[126] G Royer and B Remaud, *Nucl.Phys.A* **444**, 477 (1985)

[127] Yu Ts Oganessian, V K Utyonkov, Yu V Lobonov, F S Abdulin, A N Polyakov, I V Shirokovsky, Yu S Tsyganov, S Iliev, V G Subbotin, A M Sukhov, G V Buklanov, A N Mezencev, O V Ivanov, K Subotik, R W Lougheed, K J Moody, M A Stoyer, M J Stoyer and J F Wild, *Proceedings of VI International Conference on Dynamical Aspect on Nuclear Fission* (Slovak Republic, Casta-Paperchichka, October 1988)

[128] A V Yeremin, V I Cheigin, M G Itkis, A P Kabachenko, S P Korotkov, O N Malyshev, Yu Ts Oganessian, A G Popeko, J Ronac, R N Sagaidak, M L Chelnokov, V A Gorshkov and A Yu Lavrentev, *Rapid.Comm.JINR* **6**, (92)-98

[129] S Hofmann, *Rep.Prog.Phys.* **61**, 639 (1998)

[130] R K Gupta, *Pramana.J.Phys.* **57**, 481 (2001)